Universiteit Gent
Faculteit Wetenschappen
Vakgroep Biologie
Evolutionaire Morfologie van Vertebraten

EVOLUTIONARY MORPHOLOGY OF THE EXTREMELY SPECIALIZED FEEDING APPARATUS IN SEAHORSES AND PIPEFISHES (SYNGNATHIDAE)

Part 1 - Text

Heleen Leysen

Thesis submitted to obtain the degree of Doctor in Sciences (Biology)

Academiejaar 2010-2011

Proefschrift voorgedragen tot het bekomen van de graad van Doctor in de Wetenschappen (Biologie)

Rector: Prof. Dr. Paul van Cauwenberge
Decaan: Prof. Dr. Herwig Dejonghe
Promotor: Prof. Dr. Dominique Adriaens

EVOLUTIONARY MORPHOLOGY OF THE EXTREMELY SPECIALIZED FEEDING APPARATUS IN SEAHORSES AND PIPEFISHES (SYNGNATHIDAE)

Part 1 - Text

Heleen Leysen

Thesis submitted to obtain the degree of Doctor in Sciences (Biology)

Academiejaar 2010-2011

Proefschrift voorgedragen tot het bekomen van de graad van Doctor in de Wetenschappen (Biologie)

Rector: Prof. Dr. Paul van Cauwenberge
Decaan: Prof. Dr. Herwig Dejonghe
Promotor: Prof. Dr. Dominique Adriaens

READING* AND EXAMINATION COMMITTEE

Prof. Dr. Luc Lens, voorzitter (Universiteit Gent, BE)

Prof. Dr. Dominique Adriaens, promotor (Universiteit Gent, BE)

Prof. Dr. Peter Aerts (Universiteit Antwerpen & Universiteit Gent, BE)*

Prof. Dr. Patricia Hernandez (George Washington University, USA)*

Dr. Anthony Herrel (Centre National de la Recherche Scientifique, FR)*

Dr. Bruno Frédérich (Université de Liège, BE)

Dr. Tom Geerinckx (Universiteit Gent, BE)

Dankwoord

Het schrijven van dit doctoraat was me niet gelukt zonder de hulp, raad en steun van een aantal mensen. Een woord van dank is hier dan ook gepast.

Allereerst wil ik Prof. Dr. Dominique Adriaens bedanken voor alles wat hij de afgelopen jaren voor mij heeft gedaan. Er zijn veel zaken die het goede verloop van een doctoraat bepalen en de invloed van de promotor is volgens mij een niet te onderschatten factor. Ik ben dan ook heel blij met Dominique als promotor, hij stond letterlijk dag en nacht klaar met goede raad, suggesties voor nieuwe technieken, nuttige artikels, correcties van manuscripten en hulp bij statistische verwerking. Ik wil hem bedanken voor zijn fenomenale kennis en expertise waaruit ik gretig heb kunnen putten en voor de vele interessante congressen en workshops waar hij me naartoe heeft laten gaan, maar vooral om me de kans te geven aan dit doctoraat te beginnen en om me te helpen het tot een goed einde te brengen. Echt heel erg bedankt!

Dit onderzoek maakt deel uit van 'het zeepaardjesproject', wat niet alleen financiële steun van het Fonds voor Wetenschappelijk Onderzoek (FWO) betekende, maar ook een zeer interessante en aangename samenwerking met het Labo voor Functionele Morfologie van de Universiteit van Antwerpen. Vooral Gert heeft me heel erg geholpen, zijn boeiende experimenten en onze discussies over hoe het hyoid nu toch precies werkt, zetten me telkens weer aan het denken. Ook Sam verdient een woord van dank voor zijn feedback en alle modelleringswonderen die hij heeft verricht. Prof. Dr. Peter Aerts wil ik bedanken voor zijn constructieve kritiek en enthousiasme tijdens de projectvergaderingen en op congres. Dr. Anthony Herrel ben ik dank verschuldigd voor het snel beantwoorden van mijn mailtjes en voor zijn interesse in het zeepaardjesonderzoek. Uiteraard was dit doctoraat niet mogelijk zonder zeepaardjes en zeenaalden, en dus bedank ik de derde partner van het project, de Koninklijke Maatschappij voor Dierkunde van Antwerpen en in het bijzonder Philippe Jouk, Zjef Pereboom en Peter Galbusera voor het bezorgen van de nodige specimens. Maar ook dank aan de Mariene Biologie voor de staalname van *Syngnathus rostellatus* en *S. acus*, Jos Snoeks van het Koninklijk Museum voor Midden Afrika voor het uitlenen van de *Microphis brachyurus aculeatus* specimens, Ronald Vonk van het Zoologisch Museum van Amsterdam voor toegang tot de collectie en David en Marcel voor hun hulp bij het kweken van *Hippocampus reidi*.

Het Instituut voor de Aanmoediging van Innovatie door Wetenschap en Technologie in Vlaanderen (IWT) ben ik erkentelijk voor het toekennen van een doctoraatsbeurs.

I also greatly appreciated the cooperation with Prof. Dr. Elizabeth Dumont. Her experience in the field of finite element greatly inspired me and I thoroughly enjoyed the FEM workshop at Amherst. I wish to thank her for all her assistance, advice and motivation. I am indebted to Prof. Patricia Hernandez for her expertise in

immunohistochemistry and her unfailing patience when introducing me into the basics of this technique. Although I wasn't able to incorporate immuno's in this dissertation, I am very grateful for everything she taught me.

Voor alle problemen met ophelderingen, kleuringen of verdunningen, voor histologische protocols, voor snijwerk, om te weten of mijn afval bij organische of anorganische zuren hoorde, voor het indienen van onkostennota's, voor hulp bij procite of endnote, om een bepaald product terug te vinden, voor de verzorging van het zeepaardjesaquarium en voor nog veel meer praktisch werk kon ik steeds bij Barbara en Joachim terecht. Hun kennis heeft me heel erg geholpen en onnoemelijk veel uren labowerk uitgespaard.
Ik kon ook steeds rekenen op het bewonderenswaardige geduld van Hilde, Miranda, Jeroen en Martin voor alle administratieve hulp, practicum-gerelateerde zaken, IT-problemen of onvindbare boeken en artikels. Bedankt!
Voor het maken van de CT-scans ben ik dank verschuldigd aan Prof. Dr. Luc Van Hoorebeke, Manuel, Matthieu, Loes, Prof. Dr. Nora De Clerck en Andrei.
Gerard wil ik bedanken voor zijn hulp bij de vormgeving. Niets dan lof voor absara!

Het werk van mijn Bachelorstudenten Anouck, Lien en Karen is dit onderzoek zeker ten goede gekomen en daarvoor wil ik hen graag bedanken. Ook de masterthesis van Marjolein, Karen en Annelies zijn van onschatbare waarde geweest, waarvoor dank.

Veel dank gaat naar mijn (ex-)collega's die me steeds met plezier naar de Ledeganck deden komen. Frank en Stijn, een vrolijker duo zal het lab volgens mij niet gauw meer kennen. Zij slaagden er zelfs in om een middagpauze in de resto gezellig te maken, wat toch een hele prestatie is. Natalie bedank ik voor haar bemoedigende woorden, toen ik nog een eiland met haar deelde en later via mail. Tom wil ik graag extra bedanken voor zijn niet aflatende behulpzaamheid bij het vinden van het juiste engels woord, bij het regelen van allerlei IWT- of andere administratieve dingen en bij het nalezen van teksten, maar ook bij het opeten van een tros pitloze druifjes of een fruittaart. Paul, bedank ik voor zijn hulp bij de morfometrische analyses, voor zijn nuchtere levenskijk en voor onze weddenschap die me tot lezen aanzet. Met Celine heb ik een lange, gemeenschappelijke weg afgelegd, samen thesis schrijven, samen IWT voorbereiden, samen naar congressen en workshops en samen practica begeleiden. Ik ben haar dankbaar voor haar zin voor relativering en om altijd klaar te staan met een helpende hand. Voor het oplossen van allerhande computerproblemen of statistische vraagstukken kon ik rekenen op Tim. Hij en Niels hebben samen, door hun optimisme en honger naar kennis mijn motivatie echt een stevige duw in de rug gegeven, meer dan ze beseffen. En Niels, ik kijk uit naar alle toekomstige 'weetjes van de dag'! Los van al de werkgerelateerde hulp wil ik Barbara en Joachim, die me geholpen hebben om me van bij het begin thuis te voelen in het lab, graag bedanken voor hun opgeruimdheid en voor de fijne babbeltjes tussen het werken door. Catherine wil ik bedanken omdat ze me heeft aangezet langer op het lab te blijven, voor de ontspanning daarbuiten en voor de prachtige muziek (La Meglio Gioventù! Elis Regina! Roby Lakatos! Frida! The Tolga Quartet!...) die het werk zeker heeft vergemakkelijkt. Met Annelies heb ik met veel

plezier een eiland, liefde voor Italië en ontroerende neefjes- en nichtjesverhalen gedeeld. Ik wil haar bedanken voor haar hulp bij het maken van reconstructies, uiteindelijk lukte het ons samen om de meest raadselachtige nevenverschijnselen van Amira op te lossen. Emilie ben ik veel dank verschuldigd voor de gezellige gesprekjes, de geweldig motiverende aansporingen in de laatste weken en voor onze gedeelde (zij het passieve) interesse voor fotografie. Eindelijk zal ze rustig kunnen werken zonder dat ik steeds over haar schouder meekijk. Soheil wist steeds interessante artikels, boeken en software op te sporen en heeft een niet te onderschatte bijdrage geleverd aan mijn kennis van Iran. Het beste lamsvlees van mijn leven at ik bij hem thuis, waarvoor dank. Also Fatemeh has made me enthusiastic about the Iranian culture by bringing delicious cakes and cookies to the lab. I would like to thank her for joining me through the last stressful weeks before the deadline. I thank Spyros for sharing his great taste in music with me and for never returning to the ARC after a meeting with Dominique, without dropping in on our office. I also own a lot of thanks to Mimi, I've always admired her cheerfulness, sense of perspective and perseverance and I loved attending the Montreal meeting together. I want to thank Aslı for being such a good friend and for the great time we had in Torino. Uiteraard wil ik ook graag alle andere mensen van op 't derde bedanken, voor de practicabegeleiding, gezellige middagpauzes, uitstapjes naar de Serli, filmavondjes en internationale culinaire ontdekkingen. Nu ik het opschrijf besef ik pas hoe hard ik dit allemaal zal missen!!

Bovendien is hier een hartelijke 'dankjewel' voor al mijn mede-bioloogjes op zijn plaats. Stijn, Patricia, Sasha en Greet wil ik bedanken voor de leuke intermezzo's en de heerlijke reizen. Ik hoop dat daar nog vaak een vervolg op komt! Ook Marjolein verdient veel dank voor het aanbrengen van het zeepaardjesonderwerp in het lab en voor alles wat we samen gedaan hebben. Vera, Loe & Sam, Stien & Wim, Mimi en de Italianen bedank ik voor de nodige ontspanning, voor het luisteren naar mijn geklaag, voor de vele etentjes, om af en toe te vragen hoe het nog met de zeepaardjes is en vooral om er op bepaalde momenten niet naar te vragen. Hanne en Barbara, de treinritjes Antwerpen-Gent zal ik steeds associëren met gezelligheid (en 'keneel'). Een betere woon-werkverplaatsing kan ik me niet inbeelden, super hard bedankt! Goedele, Aslı, Catherine, Stijn en Freija (en hun zetels en bedden) bedank ik om me van het Gentse leven na de laatste trein te laten genieten. Mijn huisgenoten, Nelles, Jasper, Annelies en Anton, verdienen ook een bedankje omdat ze zo'n aangenaam gezelschap waren om bij thuis te komen na een werkdag.

Jef, Ona, Bas, Toon, Boris, Renée, Oskar, Dunia, Leyla, Ziya en Sanaa, bedank ik niet omdat ze iets aan dit doctoraat hebben bijgedragen, maar gewoon omdat ze er zijn. Mijn broers en (toekomstige) schoonzussen wil ik ongelooflijk hard bedanken om me te verwennen met heerlijke maaltijden, leuke uitstapjes en reisjes en om me terug kleine zus te doen voelen. En tenslotte heel erg veel dank aan mijn ouders om me zelf mijn weg te laten kiezen en om me volledig te steunen bij elke beslissing die ik nam.

Heleen

Er gaat meer boven je pet dan eronder
Toon Hermans

TABLE OF CONTENTS

1 Introduction

This dissertation deals with the morphology of the specialized feeding apparatus of pipefishes and seahorses within an evolutionary context. Their remarkable head morphology forms the base of an interesting paradox between exceptionally short prey capture times on the one hand and severe hydrodynamic constraints on the other. That paradox is elaborated on in the present chapter, but first an introduction to the concepts of 'evolution' and 'specialization' is provided, before they are applied to pipefishes and seahorses.

1.1. ADAPTIVE EVOLUTION AND SPECIALIZATION

Long before the term 'evolutionary biology' existed, philosophers and scientists tried to explain the vast phenotypic variation present in nature. Many great minds agonized over the process that accounts for the enormous complexity and diversity of life. As early as in the sixth century BC, ancient Greeks like Anaximander and Empedocles developed the first theories involving transformation of organisms over time, what we now call evolution. Evolution is defined as the change in characteristics of living organisms between generations (Ridley, 1993). It explains life's diversity, which can be regarded as the response to

environmental diversity. At the same time, evolution accounts for the unity of life since all individuals, extinct and extant, are related through the process of descent with modification from common ancestors.

The theory of descent with modification, as originally formulated by Charles Darwin (1859) and Alfred Russel Wallace (1889), is essentially based on three concepts. Firstly, birth rates of several organisms are much higher than their environment can support (Kutschera & Niklas, 2004). To illustrate this, Darwin (1859) calculated that, starting with one pair of elephants and using a minimum rate of natural increase, in less than five centuries there would be as many as fifteen million elephants alive. He concluded that there must be a natural down-regulating mechanism for this overproduction and argued that it could be found in competition. Members of all species[1] are thought to compete with each other for access to resources of which the availability is limited. Darwin (1859) referred to this phenomenon as the struggle for existence. Secondly, living organisms display individual variation in phenotypic traits, which have a genotypic basis as was discovered in 1866 by George Mendel, to be rediscovered only in 1900 by Hugo de Vries. Darwin and Wallace both noted that certain character differences have an effect on an individual's ability to survive and reproduce. An organism in possession of such a trait has better chances in the struggle for life. And thirdly, the perceived variation appeared to be heritable and could thus be passed from generation to generation leading to similarly characterized offspring.

These three arguments combined allowed Darwin and Wallace to formulate the hypothesis of natural selection as the driving force for evolution. In short, it implies the increased probability of survival and reproduction of the members in a population best fitted to deal with the environmental factors, this is, survival of the fittest. The fitness of an individual in this context is defined as the relative contribution of its genotype to the next generation, relative to the contributions of other genotypes (Lawrence, 2005). A character that increases the fitness of an individual with respect to other individuals in the population is an adaptive trait (Bock, 2003). Hence, individuals that are better adapted to their environment have a better chance to reproduce and in turn, some of their offspring will likely possess the adaptive characters.

[1] a species is defined as a group of interbreeding natural populations that is reproductively isolated from other such groups (Mayr, 1996)

Occasionally an adaptation can be so extreme that it substantially changes (part of) the morphology of an animal, providing it with unique functional features. An example of this is the peculiar bill with overlapping upper and lower bill tips in crossbills (finches of the genus *Loxia*), which appears to be an adaptive trait to extract seeds from conifer cones with improved efficiency (Benkman, 1987; 1993; Edelaar *et al.*, 2005). Another illustration of an extraordinary phenotype is found in the great anteater (*Myrmecophaga tridactyla* L.), which belongs to the suborder Vermilingua. The anterior part of its cranium is elongated and the animal has a long, sticky tongue with small spikes, which can be protruded to a great extend and serves to catch ants and termites (Naples, 1999). Scale-eating cichlids (part of the tribe Perissodini) also exhibit a remarkable morphology. Their mouth is not longer directed rostrally, but is bent laterally (either left or right) due to asymmetry of the jaws, which makes it a very efficient tool for removing scales of the flank of other fish (Liem & Stewart, 1976; Stewart & Albertson, 2010).

Such traits are considered adaptive specializations, provided that they improve the performance of behaviours related to that morphology and hence grant individuals a fitness advantage in a given ecological setting (Ferry-Graham *et al.*, 2002). In a trophic context, adaptive specialists are more efficient at obtaining their preferred prey items than generalists. Therefore, crossbills, anteaters and scale-eating cichlids can be regarded as adaptive specialists. Usually, specialists occupy only a narrow ecological niche; they are limited to a restricted range of the available resources due to ecological, mechanical or evolutionary constraints (Dobzhansky, 1973; Ferry-Graham *et al.*, 2002). Trophic specialists, exploiting a limited dietary breadth, would be predicted to lack flexibility or versatility in their feeding strategies compared to generalists (Ralston & Wainwright, 1997). The feeding versatility of an individual is interpreted as its ability to modulate the kinematics of feeding structures in response to different food types (Sanderson, 1991). In consequence of the specialist's stereotypy, species that occupy a small niche could be more prone to extinction since they are less resilient to changes in environmental conditions. Hence, species appear to face a trade-off between selection for a broader ecological niche in order to cope with unfavourable abiotic factors and limited food availability on the one hand, and pressure towards a narrow niche with increased intake proficiency of a particular food type on the other hand.

1.2. SYNGNATHIDAE: A CASE OF EXTREME SPECIALIZATION

1.2.1. What are syngnathids?

Members of the family Syngnathidae (*i.e.* seahorses, pipefishes, pipehorses and seadragons) probably are the world's most unfish-like fish and in the past they have caused many taxonomists a serious headache. Even Linnaeus (1766) categorized seahorses and pipefishes in a division of the Amphibia (together with e.g. lampreys, sharks, rays, sturgeons and razorfish).

In fact, seahorses, pipefishes and their allies belong to the Teleostei, a group counting over 26,000 extant species (Fig. 1.1). This group includes 96% of all living fishes and is the most diversified group of vertebrates. Teleosteans occur in every freshwater, brackish and marine habitat (rivers, lakes and oceans) and some can even survive on land. They exhibit a large variety of locomotion behaviours (swimming, gliding, walking or staying immobile) and the teleost diet is extremely diverse (algae, zooplankton, worms, snails, insect larvae, clams, shrimps, amphibians, other fish, fry, scales, blood, faeces,...). In short, they have radiated into countless niches (Helfman *et al.*, 2009). Teleostean synapomorphies[2] include: the presence of a ventrocaudal process at the quadrate bone, the maxillary bones are mobile and enable upper jaw protrusion, coronoid bones are absent, there is a fusion between articular, angular and retroarticular bones in the lower jaw, the parietal bones are caudally distinctly broader than rostrally, the urohyal bone is formed as an ossification within the sternohyoideus tendon and there is a single, median vomeral bone that forms the roof of the mouth (Nelson, 2006; Wiley & Johnson, 2010). The Teleostei can be divided into four cohorts, namely the Osteoglossomorpha, Elopomorpha, Ostarioclupeomorpha (=Otocephala) and Euteleostei (Fig. 1.1A; Nelson, 2006).

The Euteleostei, or "true" teleosts, are by far the largest group within the Teleostei. Shared traits, *i.e.* presence of an adipose fin, nuptial breeding tubercles and a rostral membranous component to the first uroneural, are found in the

[2] a synapomorphy is a homologous character common to two or more taxa and is thought to have its origin in a single structure in their common ancestor (Lawrence, 2005)

basal euteleosteans and apparently have been lost in the more derived ones (Lauder & Liem, 1983). The Euteleostei consist of 28 orders and 346 families and comprise, among others, the Acanthomorpha (Fig. 1.1B). This group, also called the spiny-rayed fishes, is characterized by the presence of true fin spines in the dorsal, anal and pelvic fins instead of hardened segmented rays (Helfman *et al.*, 2009). Encompassing approximately 16,000 species in over 300 families (including cods, tunas, stonefishes, flatfishes, puffers and much more), they comprise over 60% of the extant teleosts and about one-third of all living vertebrates. Acanthomorph monophyly is supported by both morphological and molecular analyses (Nelson, 2006). The phylogeny of the Percomorpha, a clade within the Acanthomorpha, however, is problematic and currently under discussion (e.g. Lauder & Liem, 1983; Jamieson, 1991; Parenti & Song, 1996; Springer & Orrell, 2004; Smith & Craig, 2007; Smith, 2010). In this dissertation, the percomorphs are thought to encompass nine orders as shown in Fig. 1.1C (Nelson, 2006). This group contains over 13,000 mainly marine species that are characterized by the pelvic fin being attached to the cleithrum of the pectoral girdle and a rostral pelvic process that is ventrally displaced (Nelson, 2006; Helfman *et al.*, 2009).

Traditionally, pipefishes, seahorses and their allies are encompassed by the order Gasterosteiformes, but the systematic relationships among gasterosteiform fishes have been the subject of much discussion (see Wilson & Orr (submitted) for a review). According to the classification of Keivany & Nelson (2006) based on 110 informative osteological characters, the order is divided into three suborders: firstly the Hypoptychoidei, comprising only the family of the sand eels (Hypoptychidae), secondly the Gasterosteoidei, including the sticklebacks (Gasterosteidae) and the tubesnouts (Aulorhynchidae), and thirdly the Syngnathoidei to which families such as the seamoths (Pegasidae), armoured sticklebacks (Indostomidae), trumpetfishes (Aulostomidae) and pipefishes and seahorses (Syngnathidae) belong (Fig. 1.2; Keivany & Nelson, 2006). Recently, however, the monophyly of Gasterosteiformes has been questioned based on molecular phylogenetic research (Chen *et al.*, 2003; Smith & Wheeler, 2004; Dettai & Lecointre, 2005; Kawahara *et al.*, 2008). Although most of these molecular studies only include a few gasterosteiform representatives, making it difficult to evaluate the relationships of the order as a whole, Kawahara *et al.* (2008) analyzed members of all eleven families. They found support to place the

Indostomidae, Syngnathoidei (minus Indostomidae) and Gasterosteoidei together with the Hypoptychoidei in three separate clades within the Percomorpha and suggest a basal divergence (Fig. 1.3). According to this point of view, the Dactylopteroidei (flying gurnards) are classified as the sister group of the Syngnathoidei. The classification with Gasterosteoidei as the closest sister group of the Syngnathoidei, as suggested by Keivany & Nelson (2006), is followed here, since morphological analyses provide no alternative and the results of the molecular analyses are not consistent with each other.

Nevertheless, whether additional research confirms the tree proposed by Kawahara *et al.* (2008) or not, *Gasterosteus aculeatus* L. (three-spined stickleback) remains valid as a generalized percomorph out-group. Gasterosteiform fishes are characterized by an armour of plates that covers the body, the mouth is usually small, the pelvic girdle is never directly attached to the cleithra, they have only a limited number of branchiostegal rays and their gills are either reduced or modified (Lauder & Liem, 1983; Jamieson, 1991; Nelson, 2006). Besides that, many species have an uncommon locomotion, as for instance the shrimpfishes and razorfishes (family Centriscidae) that swim head-down with the dorsal edge of their razor-like body leading (Fig. 1.2; Helfman *et al.*, 2009) and the cleaner pipefish (*Doryrhamphus janssi* (Herald & Randall)) which is known to swim upside-down. Within this diverse order, differences in reproductive behaviour are numerous (e.g. Wilson *et al.*, 2001; Kawahara *et al.*, 2008). Some species, like sticklebacks, produce a glue-like substance that is used for building a nest out of plant material while male seahorses possess a pouch (this will be elaborated on later) (Nelson, 2006; Kawahara *et al.*, 2008). Gasterosteiform body size is also reasonably variable, ranging from less than 3 cm standard length (SL) in *Indostomus* species (Indostomidae) to over a meter SL in the genus *Fistularia* (Fistulariidae) (Nelson, 2006; Kawahara *et al.*, 2008). In total, the order of Gasterosteiformes covers eleven families, 71 genera and 278 species, the majority of which can be found in marine waters (Nelson, 2006).

The family of Syngnathidae is subdivided into two subfamilies: Syngnathinae (pipefishes, seadragons and pipehorses) and Hippocampinae (seahorses). Seadragons are relatively large fishes with a high, laterally flattened body covered by leafy appendages (Fig. 1.4D). Each of the two seadragon genera includes only one species: *Phyllopteryx taeniolatus* (Lacepède) (weedy seadragon) and *Phycodurus*

eques (Günther) (leafy seadragon). Pipehorses look like an intermediate form between pipefishes and seahorses, having a straight, horizontal body with a slightly tilted head and a prehensile tail (Fig. 1.4F; Kuiter, 2003; 2004). The genera *Solegnathus* and *Syngnathoides* and also the genera *Acentronura, Amphelikturus* and *Idiotropiscis* belong to the pipehorses, the latter three are sometimes referred to as pygmy pipehorses. All other members of the Syngnathinae subfamily are pipefishes. The Syngnathidae is by far the most speciose family of the Gasterosteiformes, with an estimated species number varying from 232 (Nelson, 2006) to over 320 (Kuiter, 2003). Numerous misidentifications, synonyms and even spelling mistakes have resulted in a taxonomic chaos. Especially among seahorses, species identification is problematic, since morphological differences between species are subtle and they are able to change colour and develop skin filaments on their body in order to camouflage themselves (Lourie *et al.*, 1999a; 2004; Murugan *et al.*, 2008; Sanders *et al.*, 2008). The subfamily Hippocampinae has recently been the subject of revision by Lourie and co-workers of the Project Seahorse (1999b, 2004). It consists of only one genus (*Hippocampus*) and Project Seahorse currently recognizes 38 species (http://seahorse.fisheries.ubc.ca, consulted on 16/02/2011) versus 54 valid species names according to Fishbase (Froese & Pauly, 2011). Within the syngnathid family a large morphological diversity exists: size, body shape, colour pattern, ornaments, body posture, fin arrangement and snout phenotype are all highly variable (Fig. 1.4). Nevertheless, there are some shared features, which will be discussed below.

Probably the most distinct syngnathid characteristic is the incubating area on the ventral side of the male body. This morphological structure can vary from an unprotected patch of skin onto which the brood is loosely attached, over one simple or two overlapping membranes on the trunk or tail, to a fully enclosed pocket-like pouch with a small aperture (Herald, 1959; Kornienko, 2001; Wilson *et al.*, 2001; Carcupino *et al.*, 2002; Kvarnemo & Simmons, 2004). The evolutionary trend towards increasing parental care corresponds fairly well to the prevailing molecular-based phylogeny of the family (Fig. 1.5; Wilson *et al.*, 2001; 2003; Helfman *et al.*, 2009; Wilson & Orr, submitted). The incubating area is associated with the syngnathid unique reproductive strategy: the female deposits the eggs in the pouch of the male where they are incubated. The male provides all post-fertilization parental care (e.g. protection, nutrition, osmoregulation and

ventilation) and fully developed, independent young are released from the pouch after a few weeks (Kornienko, 2001; Wilson *et al.*, 2001; Vincent & Giles, 2003; Foster & Vincent, 2004; Lourie *et al.*, 2004).

Instead of scales, the syngnathid body is covered with a complex of precisely arranged bony plates to protect them against predation. This armour, however rigid around the trunk, does not impede articulation of the separate segments in the caudal region. Especially in the tail of seahorses and pipehorses, that lacks a caudal fin, flexibility is high. The dorsoventral bending ability of the tail (it can curl even over 360°) is a rather unusual modification that makes it very efficient for grasping and holding on to objects (Hale, 1996; Bruner & Bartolino, 2008). Seahorses not only use their prehensile tail to anchor themselves to holdfasts, but it also has a function in courtship (entwining of tails) and male competition (tail wrestling) (Lourie *et al.*, 1999b).

Syngnathids exhibit great camouflage capacities. They can have a speckled colour pattern, weed-like appendages, skin filaments or warts that make them look like algae, seagrass or sticks (Kuiter, 2003). Combined with a slow, manoeuvring motion, enabled by undulation of their dorsal and pectoral fins, they fade almost completely with the surroundings (Consi *et al.*, 2001). This favours the ambush foraging strategy of syngnathids, they sit and wait until a prey, usually a small crustacean, comes close, which is then captured by a quick flick of the head (Foster & Vincent, 2004; Kendrick & Hyndes, 2005). The diet of syngnathids, being gape-limited suction feeders, comprises small crustaceans (mostly amphipods and copepods), other small invertebrates and fish fry (Payne *et al.*, 1998; Lourie *et al.*, 1999b; Teixeira & Musick, 2001; Woods, 2003; Foster & Vincent, 2004).

Although they individually have a very small home range, syngnathids are ubiquitous (Foster & Vincent, 2004). Most species occur in shallow temperate and tropical waters, especially in the Indo-West Pacific at the coast of Australia, South-East Asia and Japan (Lourie *et al.*, 1999b; Kuiter, 2003). Seahorses are almost exclusively marine (*Hippocampus capensis* Boulenger lives in estuaries), while pipefishes can be found in marine, brackish and even freshwater (Foster & Vincent, 2004). Their preferred habitat can consist of seagrasses, algae, corals, mangroves, *etc.*, which all offer protection from predators and a high prey density (Payne *et al.*, 1998; Lourie *et al.*, 1999b, Kendrick & Hyndes, 2003).

Despite the extensive interest in the reproductive strategies (e.g. Kvarnemo *et al.*, 2000; Carcupino *et al.*, 2002; Vincent & Giles, 2003; Poortenaar *et al.*, 2004), life history (e.g. Kanou & Kohno, 2001; Foster & Vincent, 2004), population dynamics (e.g. Teske *et al.*, 2003; Lourie *et al.*, 2005), aquaculture (e.g. Woods, 2003; Koldewey & Martin-Smith, 2010) and conservation (e.g. Goffredo *et al.*, 2004; Foster & Vincent, 2004; Scales, 2010) of syngnathids, little is known about most aspects of their phenotype. Many questions regarding their feeding behaviour, head morphology and possible adaptive traits to the specialized suction feeding remain unanswered. The few detailed anatomical studies that have been carried out date from the first half of the previous century or even before (e.g. McMurrich, 1883; Jungersen, 1910). Some of those studies do not deal with syngnathids exclusively, but superficially describe the cranium of a wide array of taxa (e.g. Gregory, 1933; de Beer, 1937) while others focus on the development of the skull (e.g. McMurrich, 1883; Kadam, 1958; 1961). Publications on myology or functional interpretation of the feeding apparatus are scarce. However, Branch (1966) supplies a reasonable description of the cranial osteology and myology of *Syngnathus acus* L. and he even makes suggestions about the feeding method based on his observations. Basic kinematical data on suction feeding events of *Hippocampus erectus* Perry and *Syngnathus floridae* (Jordan & Gilbert) is provided by Bergert and Wainwright (1997) and of *H. erectus* and *H. zosterae* Jordan & Gilbert by Colson *et al.* (1998), both in combination with a cursory morphological description of the head of the recorded species. Finally, Muller and Osse (1984) investigated the hydrodynamics of suction feeding in several fishes, including the snake pipefish (*Entelurus aequoreus* (L.)). All these studies form the foundation for the present doctoral research on evolutionary morphology of the syngnathid feeding apparatus.

1.2.2. Trophic specialization and constraints

The trade-off described above (Chapter 1.1), between selection for specialization on the one hand and trophic niche enlargement on the other, naturally also holds for members of the family Syngnathidae.

All syngnathids have an elongated, tubular snout with tiny terminal jaws that enables them to perform suction feeding. The length of the snout is highly variable, ranging from very short as in the mushroom-coral pipefish (*Siokunichthys nigrolineatus* Dawson) (Fig. 1.4E) to extremely elongate in for example the weedy seadragon (*Phyllopteryx taeniolatus)* (Fig. 1.4D). Having a snout with a very small diameter, seahorses and pipefishes are able to feed only on prey particles of limited size. Their morphology thus confines them to a diet of only small prey items from a broad range of available prey (Tipton & Bell, 1988; Teixeira & Musick, 1995; Woods, 2003; Kendrick & Hyndes, 2005). Hence syngnathids can be regarded as specialists (Ferry-Graham *et al.*, 2002). Their extreme phenotype (*i.e.* the slender snout) will only be selected for if it is associated with a fitness advantage (Ridley, 2003). Previous studies have shown that syngnathids exhibit high velocity and great precision when performing suction feeding (Muller & Osse, 1984; Bergert & Wainwright, 1997; de Lussanet & Muller, 2007). A general actinopterygian suction feeding event involves a rapid expansion of the buccal cavity, which results in a pressure difference between the inside of the cavity and the surrounding water. So when the jaws open, a water flow is generated that transports the prey into the mouth (e.g. Lauder, 1985). In seahorses and pipefishes this buccal expansion is preceded by a rotation of the head that positions the mouth close to the prey, a feeding mechanism known as pivot feeding (de Lussanet & Muller, 2007; Van Wassenbergh *et al.*, 2008). Prey intake time can be as little as 6 ms, ranking syngnathids among the fastest feeding teleosts ever recorded (Chapter 5.1; Muller & Osse, 1984; Bergert & Wainwright, 1997; de Lussanet & Muller, 2007). The elongated snout with small diameter increases the water flux rate in the mouth and thus enhances suction velocity. However, as mentioned before, the minute mouth aperture of syngnathids will directly constrain the size of prey that can be taken in. Moreover, the design of the head will likely influence the hydrodynamics of suction feeding. Elongation of the snout will increase the moment of inertia of the head during neurocranial elevation and drag forces will become more important with diminishing snout diameter. Hence, long-snouted species will need to generate more energy to both reach and suck in the prey.

The high level of cranial specialization is likely associated with a reduced functional versatility and could thus result in lower resilience when facing

environmental changes (Ralston & Wainwright, 1997; Adriaens & Herrel, 2009). In combination with anthropogenic threats (habitat loss and overexploitation) this might explain the vulnerable ecological status of Syngnathidae. Of the 71 syngnathid species registered in the IUCN Red List of Threatened Species, 10 are critically endangered, endangered or vulnerable, 20 are near-threatened or of least concern and for all 41 others there is insufficient data to assess the risk of extinction (IUCN, 2010). Their sparse distribution, low mobility, small home ranges, lengthy parental care, low fecundity and monogamy of some species severely reduce their chances to recover from ecological changes, making them susceptible to extinction (Foster & Vincent, 2004).

In order to understand the potential evolutionary origin and ecological implications of this unique phenotype, the extremely specialized cranial morphology of Syngnathidae is the focus of this study.

1.3. AIMS AND THESIS OUTLINE

1.3.1. Context and general aims

This doctoral study forms part of an integral Research Foundation Flanders (FWO) research project entitled "Functional consequences and ecological implications of extreme morphological specialization: design and function of the feeding apparatus in seahorses and pipefishes (Syngnathidae)" (project code G.0539.07). The project involves a partnership between the Research Group Evolutionary Morphology of Vertebrates at Ghent University (UGent), the Laboratory of Functional Morphology at the University of Antwerp (UA) and the Royal Zoological Society of Antwerp (KMDA).

The main aims of the project are to investigate the morphological and functional constraints of the syngnathid trophic system related to the extreme specialization, and to explore whether these constraints might partially explain the reduced ecological resilience of syngnathids. The core of this research project consists of the following three facets:

- A morphological analysis of the cranial diversity in syngnathids, which I carried out and is the subject of this dissertation (UGent).
- A functional analysis of feeding in syngnathids, performed by Gert Roos and Sam Van Wassenbergh (UA).
- An ontogenetic analysis of morphological and functional changes in the head of a syngnathid, an ongoing study started by me and Annelies Genbrugge, in collaboration with Gert Roos and Sam Van Wassenbergh (UGent and UA).

As the third party of the project, the KMDA contributed by supplying animals, both through CITES-regulated trade and established breeding programs.
The functional component of the research, being carried out at the University of Antwerp, focuses mainly on the dynamics and kinematics of the specialized suction feeding, the functional flexibility and versatility of the feeding apparatus and the effect of snout length variation on the performance (Roos, 2010).
This doctoral thesis is the collection of the results of the morphological analyses as part of the FWO project. The implications of snout elongation as depicted in the previous paragraph form the central theme of this research. The overall goal is to resolve the evolutionary pattern leading to the extreme morphological specialization of seahorses and pipefishes.

1.3.2. Thesis outline and specific aims

In total, this dissertation is divided into seven chapters.
The first (current) chapter starts with a short introduction to the concepts of 'evolution' and 'specialization'. A next paragraph provides background information on the phylogenetic position, general biology and specialized feeding apparatus of the family Syngnathidae as an introduction to these wonderful animals. The chapter concludes with the overall objectives of the research and the outline of the thesis.

In the second chapter the examined specimens, their origin and application are listed. Also the methods utilized are explained here, in order to avoid repetition in the following chapters. The additional chapters will only contain a concise material & methods section with reference to the second chapter. The last paragraph of this chapter includes some terminology used in the remainder of the dissertation.

The first results are given in the third chapter. A detailed morphological description of the feeding apparatus of a few syngnathid representatives is provided. The structural and functional interactions between the individual components in the head are examined in order to understand how seahorses and pipefishes are able to perform such exceptionally fast and powerful suction feeding. Two subdivisions are made. The first one focuses on the peculiar snout morphology of *Syngnathus rostellatus* Nilsson and *Hippocampus capensis* in a mere ontogenetical context and includes comparison with the generalized percomorph *Gasterosteus aculeatus* (Chapter 3.1). In particular, the following questions were addressed.

- Is snout elongation already present early in ontogeny?
- Which osteological components form part of the snout and how do they interact?
- What morphological changes contribute to an evolutionary shift towards snout elongation?

The second study evaluates the implications of snout elongation on the musculoskeletal structure by comparing the head morphology of several syngnathid species with varying snout length. It is hypothesized that changes in the snout length will alter the functional lever systems as to assure the same kinematical energy output (Chapter 3.2). The following questions were addressed.

- Does snout elongation affect the cranial musculoskeletal system?
- Is the syngnathid feeding apparatus a morphologically conserved entity (for example due to physical constraints)?
- What are the main morphological differences within the family?

The fourth chapter focuses on the morphological variation found within the syngnathid family. A geometric morphometric analysis is carried out to analyze

the intra- and interspecific shape variation in the head of several syngnathid species. By quantifying the amount of variation in the cranium, the hypothesis that specialization leads to a reduced morphological plasticity is tested. In addition, juvenile *Hippocampus reidi* Ginsburg are included in the analysis as to further elaborate on the developmental shape changes of the head. The following questions were addressed.

- What are the most prominent differences in the head shape of pipefishes *versus* seahorses, and are these differences related to relative snout length?
- Does relative snout length have an effect on the amount of intraspecific variation (*i.e.* are long-snouted species more constrained than short-snouted ones)?
- Is the developmental period after release from the pouch in seahorses characterized by important head shape changes?

In the fifth chapter, the results on the functional interpretation of the trophic morphology in syngnathids are presented. The chapter consists of two parts.
In the first part, a previously described planar four-bar model for suction feeding in syngnathids (Fig. 1.6; Muller, 1987) is evaluated. This integration of form and function is done in close collaboration with the University of Antwerp. Gert Roos and Sam Van Wassenbergh performed the kinematical analyses, whereas I provided a detailed morphological analysis of the individual components (linkages, joints and muscles) involved in the model (Chapter 5.1). The following questions were addressed.

- How does the syngnathid feeding apparatus work and how does it differ from a typical teleostean feeding sequence?
- How are syngnathids able to achieve these incredibly short prey capture times?
- Does the proposed theoretical four-bar mechanism (Fig. 1.6; Muller, 1987) reflect the feeding kinematics?

The second part concerns the mechanical stress exerted on the skull as a result of the fast and powerful suction feeding. The trophic apparatus needs to cope with high forces and pressures acting on it during feeding. Whether and how the length and the structure of the skeletal feeding apparatus influence the stress

distribution in the skull is the objective of this study (Chapter 5.2). The following questions were addressed.

- Where in the head does the stress caused by mechanical loading during suction feeding accumulate?
- Is there a relationship between snout length and stress distribution pattern in the syngnathid cranium?

All findings are discussed in chapter six. The obtained results are synthesized and integrated with data from the literature in an attempt to unravel the evolutionary pattern leading to the extremely specialized cranial morphology. In the first part, the role of the extensive parental care in the syngnathid evolution is considered. Next, the modifications of both the feeding apparatus and the feeding mode are discussed. Thirdly, evolutionary transitions within the family, such as the origin of the grasping tail and tilted head with respect to the body, are dealt with in a phylogenetic framework. The last part of the general discussion includes a concise conclusion.

And finally a synopsis, both in English and Dutch, covering all previously introduced chapters, is provided in the seventh chapter.

2 Material & methods

2.1. MATERIAL

The main part of this research was based on 76 specimens covering 14 syngnathid species (Table 2.1, 2.2, Fig. 2.1). Except for the specimens of *Syngnathus acus*, most specimens were also used in a geometric morphometric analysis, which included 368 specimens of 38 different species (Table 2.3). Among those was an ontogenetic series of *Hippocampus reidi*, with juveniles ranging in age between 1 and 65 days, used for an ontogenetic morphometric study in combination with the adults of *H. reidi*.

Selection of the species was based on systematic position within the existing phylogenetic framework (Fig. 1.5; Wilson & Orr, submitted), snout morphology (primarily regarding the level of snout elongation) and the availability of specimens.

As visible in table 2.1, many specimens were obtained through CITES-regulated commercial trade, but the specimens of *Hippocampus capensis* and *Hippocampus kuda* Bleeker were obtained from the Antwerp Zoo and the specimens of *S. rostellatus* and *S. acus* were caught on the Belgian continental shelf (North Sea) by the Marine Biology research group of the Ghent University. Of the specimens analyzed morphometrically, most belong to the collection of the Zoological Museum of Amsterdam, but the specimens of *Microphis brachyurus aculeatus*

(Bleeker) are part of the Royal Museum of Central Africa collection and some commercially obtained specimens were included as well (Table 2.3). Several juveniles were included in the research: *H. capensis* is bred at the Antwerp Zoo, the juvenile *H. reidi* are the offspring of seahorses held in a breeding facility at the research group (as is described under 2.2.1) and some of the caught *S. rostellatus* males were pregnant (Table 2.2).

Table 2.1 – Adult specimens used for the morphological studies with reference to the specific chapter(s) (between brackets) in which they are utilized. Abbreviations: AZ, Antwerp Zoo; C, commercial trade; CT, computed tomography; FEA, finite element analysis; HL, head length; NS, North Sea; SL, standard length.

species	SL (mm)	HL (mm)	origin	method
Corythoichthys intestinalis	120.2	16.1	C	CT-scanning (3.2)
Corythoichthys intestinalis	102.7	16.9	C	clearing and staining (3.2)
Corythoichthys intestinalis	117.6	16.4	C	clearing and staining (3.2)
Corythoichthys intestinalis	120.8	16.4	C	dissecting (3.2)
Corythoichthys intestinalis	136.2	18.2	C	dissecting (3.2)
Doryrhamphus dactyliophorus	103.5	25.4	C	CT-scanning, FEA, dissecting (3.2, 5.2)
Doryrhamphus dactyliophorus	91.2	23.6	C	serial sectioning, 3D-reconstructing (3.2)
Doryrhamphus dactyliophorus	105.1	25.0	C	clearing and staining (3.2)
Doryrhamphus janssi	102.7	22.6	C	serial sectioning (3.2)
Doryrhamphus janssi	105.6	24.5	C	dissecting (3.2)
Doryrhamphus janssi	81.5	16.4	C	clearing and staining (3.2)
Doryrhamphus janssi	90.8	19.5	C	clearing and staining (3.2)
Doryrhamphus melanopleura	41.6	11.6	C	clearing and staining (3.2)
Doryrhamphus melanopleura	56.5	13.2	C	CT-scanning, FEA, dissecting (3.2, 5.2)
Dunckerocampus pessuliferus	94.5	26.0	C	serial sectioning (3.2)
Dunckerocampus pessuliferus	112.3	30.1	C	dissecting (3.2)
Syngnathus acus	330.2	39.4	NS	serial sectioning
Syngnathus acus	332.4	43.4	NS	serial sectioning
Syngnathus acus	325.1	42.7	NS	clearing and staining
Syngnathus acus	350.1	45.8	NS	dissecting
Syngnathus acus	371.6	46.1	NS	dissecting
Syngnathus acus	311.3	38.7	NS	CT-scanning
Syngnathus rostellatus	126.2	14.8	NS	clearing and staining (3.1)
Syngnathus rostellatus	111.1	14.5	NS	clearing and staining (3.1)
Syngnathus rostellatus	111.5	13.0	NS	clearing and staining
Syngnathus rostellatus	97.9	12.2	NS	clearing and staining (3.1)
Syngnathus rostellatus	95.7	13.6	NS	staining
Syngnathus rostellatus	100.0	12.6	NS	staining
Syngnathus rostellatus	109.1	14.0	NS	staining
Syngnathus rostellatus	110.8	15.3	NS	CT-scanning, FEA (5.2)
Syngnathus rostellatus	93.8	13.5	NS	staining
Syngnathus rostellatus	105.0	13.0	NS	clearing and staining (3.1)
Syngnathus rostellatus	97.5	13.7	NS	staining
Syngnathus rostellatus	114.5	14.1	NS	dissecting
Syngnathus rostellatus	126.4	15.1	NS	dissecting
Syngnathus rostellatus	129.1	15.5	NS	dissecting
Hippocampus abdominalis	222.7	30.9	C	CT-scanning, FEA, dissecting (3.2, 5.2)
Hippocampus barbouri	141.4	25.5	C	CT-scanning
Hippocampus breviceps	50.7	9.8	C	CT-scanning
Hippocampus capensis	96.1	15.2	AZ	clearing and staining (3.1)
Hippocampus capensis	97.6	17.7	AZ	clearing and staining (3.1)
Hippocampus capensis	99.0	16.0	AZ	clearing and staining (3.1)
Hippocampus capensis	99.2	16.8	AZ	CT-scanning
Hippocampus capensis	133.0	19.4	AZ	clearing and staining
Hippocampus kuda	117.4	24.8	AZ	clearing and staining

(continued on next page)

species	SL (mm)	HL (mm)	origin	method
Hippocampus kuda	93.3	19.5	AZ	clearing and staining
Hippocampus kuda	94.6	19.2	AZ	clearing and staining
Hippocampus kuda	125.2	23.8	AZ	serial sectioning
Hippocampus reidi	117.2	23.8	C	clearing and staining (3.1, 3.2, 5.1)
Hippocampus reidi	113.5	21.4	C	clearing and staining (3.1, 3.2, 5.1)
Hippocampus reidi	103.5	24.0	C	serial sectioning, 3D-reconstructing (3.2, 5.1)
Hippocampus reidi	119.0	25.2	C	CT-scanning, FEA (3.1, 5.1, 5.2)
Hippocampus reidi	109.7	24.4	C	clearing and staining (3.1, 5.1)
Hippocampus reidi	113.7	23.8	C	dissecting (3.2)
Hippocampus reidi	138.1	28.3	C	dissecting (3.2)
Hippocampus reidi	152.8	32.2	C	dissecting (3.2)
Hippocampus reidi	123.9	25.5	C	CT-scanning, FEA (5.2)
Hippocampus zosterae	28.3	4.5	C	CT-scanning, serial sectioning
Hippocampus zosterae	29.0	5.3	C	CT-scanning, FEA, serial sectioning (3.2, 5.2)
Hippocampus zosterae	32.8	5.3	C	clearing and staining (3.2)

Table 2.2 – List of juvenile syngnathid species used for the morphological studies. Abbreviations: CT, computed tomography; dp, days post-release from pouch; HL, head length; pr, pre release from pouch; SL, standard length.

species	SL (mm)	HL (mm)	age	method
Hippocampus capensis	29.4	6.7	14 dp	clearing and staining
Hippocampus capensis	13.3	2.8	1 dp	clearing and staining (3.1)
Hippocampus capensis	13.6	2.9	2 dp	clearing and staining (3.1)
Hippocampus capensis	12.8	2.8	3 dp	serial sectioning, 3D-reconstructing (3.1)
Hippocampus capensis	14.0	3.2	4 dp	clearing and staining (3.1)
Hippocampus reidi	7.0	2.0	1 dp	serial sectioning, 3D-reconstructing (3.1)
Hippocampus reidi	7.2	2.1	1 dp	CT-scanning
Hippocampus reidi	7.5	2.3	1 dp	clearing and staining
Hippocampus reidi	6.0	1.8	1 dp	clearing and staining
Syngnathus rostellatus	11.0	1.8	pr[1]	clearing and staining (3.1)
Syngnathus rostellatus	14.5	2.3	pr[1]	clearing and staining (3.1)
Syngnathus rostellatus	11.3	2.2	pr[1]	clearing and staining (3.1)
Syngnathus rostellatus	11.4	1.9	pr[1]	clearing and staining (3.1)
Syngnathus rostellatus	13.1[2]	2.1	pr[1]	serial sectioning (3.1)
Syngnathus rostellatus	19.3	3.5	pr[1]	serial sectioning
Syngnathus rostellatus	25.5	4.8	pr[1]	serial sectioning

[1] The age of the specimens of *S. rostellatus* could not be determined since they were collected from the brood area of the sampled males.

[2] Standard length was estimated by interpolation based on the head length over standard length ratio of other specimens.

Table 2.3 – List of all 38 syngnathid species plus the juveniles of *Hippocampus reidi* used for the morphometric analysis. Abbreviations: AZ, Antwerp Zoo; B, bred at the research group; C, commercial trade; D, drawings (see chapter 4); HL, head length; NS, North Sea; RMCA, Royal Museum of Central Africa; SnL, snout length; st dev, standard deviation; ZMA, Zoological Museum of Amsterdam.

species	number of specimens	origin	mean (SnL/HL) ± st dev
Anarchopterus criniger	1	D	0.253
Anarchopterus tectus	1	D	0.250
Bryx dunckeri	1	D	0.265
Bryx randalli	1	D	0.337
Campichthys tricarinatus	1	D	0.315
Corythoichthys intestinalis	7	C+ZMA	0.469±0.019
Cosmocampus balli	1	D	0.359
Cosmocampus brachycephalus	1	D	0.271

(continued on next page)

species	number of specimens	origin	mean (SnL/HL) ± st dev
Cosmocampus hildebrandi	1	D	0.328
Doryichthys martensii	2	ZMA	0.347±0.013
Doryichthys retzii	6	ZMA	0.372±0.018
Doryrhamphus dactyliophorus	1	C	0.662
Doryrhamphus janssi	6	C	0.572±0.012
Doryrhamphus melanopleura	3	C	0.438±0.023
Dunckerocampus pessuliferus	2	C	0.649±0.083
Gasterotokeus biaculeatus	1	ZMA	0.539
Haliichthys taeniophorus	1	ZMA	0.569
Microphis brachyurus aculeatus	95	RMCA	0.578±0.012
Microphis caudocarinatus	1	D	0.420
Minyichthys inusitatus	1	D	0.238
Siokunichthys bentuviai	1	D	0.180
Syngnathoides biaculeatus	18	ZMA	0.553±0.026
Syngnathus parvicarinatus	1	D	0.278
Syngnathus rostellatus	15	NS	0.458±0.011
Syngnathus typhle	15	ZMA	0.483±0.038
Hippocampus abdominalis	5	C+ ZMA	0.390±0.024
Hippocampus barbouri	3	C	0.502±0.017
Hippocampus breviceps	2	C	0.424±0.014
Hippocampus capensis	4	AZ	0.338±0.022
Hippocampus guttulatus	29	ZMA	0.360±0.029
Hippocampus hippocampus	1	ZMA	0.328
Hippocampus histrix	5	ZMA	0.476±0.015
Hippocampus kuda	40	C+ ZMA	0.428±0.036
Hippocampus ramulosus	18	ZMA	0.354±0.032
Hippocampus reidi	12	C	0.426±0.026
Hippocampus reidi juveniles	54	B	0.442±0.028
Hippocampus spinosissimus	3	ZMA	0.375±0.028
Hippocampus trimaculatus	5	ZMA	0.496±0.006
Hippocampus zosterae	3	C	0.315±0.135

2.2. METHODS

2.2.1. Keeping live specimens

Specimens obtained from commercial trade (Bassleer Biofish, Belgium and De Jong Marinelife, the Netherlands) were kept in a 1.15 × 0.55 × 0.65 m aquarium (411 l). The tank had a 10 cm sandy bottom and live rock, a protein skimmer, two heating elements, two light bulbs with a photoperiod of 12 hours, a filter and a pump. Temperature was kept constant at 24° C and salinity at 32 ppt. The animals were fed defrosted *Artemia* or *Mysis* daily as syngnathids feed mainly on small crustaceans (Payne *et al.,* 1998; Foster & Vincent, 2004; Kendrick & Hyndes, 2005; Felício *et al.,* 2006; Karina *et al.,* 2006; Kitsos *et al.,* 2008).

The juvenile *Hippocampus reidi* specimens were obtained from successful

breeding in the lab. Juveniles that emerged from the male's pouch were immediately transferred to a smaller tank 0.35 × 0.20 × 0.25 m (17.5 l) at a temperature of 26° C. Water was partly refreshed three times a day and the juveniles were fed rotifers first and later *Artemia*, three times daily. Various males gave birth to in total nine litters of young, which were kept in separate aquaria. Mortality caused none of the juveniles to live over 94 days.

2.2.2. Sacrificing and fixation

Sacrificing was achieved by an overdose of MS 222 (tricaine methanesulfonate, Sigma Aldrich, St. Louis, MO) in accordance with the Belgian law on the protection of laboratory animals (KB d.d. November 14, 1993). Fixation was done in a 10% buffered and neutralized formalin solution.

2.2.3. Biometry

After sacrificing, small individuals were photographed using a digital camera (ColorView 8, Soft Imaging System GmbH Münster, Germany) mounted on an Olympus SZX-9 stereoscopic microscope (Olympus GmbH Hamburg, Germany) and driven by the software program analySIS 5.0 (Soft Imaging System GmbH Münster, Germany). Pictures of larger specimens were captured by means of a macroscopic digital camera (Sony DSC-F717 camera with Carl Zeiss Vario-Sonnar 9.7-48.5mm f/2-2.4 lens, Canon EOS 400D camera with Canon EF-S 18-55mm f/3.5-5.6or lens or Nikon D40X camera with 18-55mm f/3.5-5.6 GII AF-S DX NIKKOR lens). A scale bar was included in each picture and the specimens were oriented in a plane parallel to the camera, with maximal overlap of paired anatomical structures as to minimize orientational errors. For all specimens, freeware ImageJ 1.43u (Rasband W.S., US National Institutes of Health, Maryland) was used to measure standard length (SL), head length (HL) and snout length (SnL). Standard length of pipefishes was measured as described by FishBase (Froese & Pauly, 2011), *i.e.* the distance between the tip of the snout and the base of the caudal fin (Fig. 2.2A). In seahorses the situation is different since

they lack a caudal fin. Here standard length was defined according to the measuring protocol described by Lourie *et al.* (1999a;b) *i.e.* as the sum of head length, trunk length (TrL) and tail length (TaL) (Fig. 2.2B). For all specimens, head length was measured as the distance from the tip of the upper jaw to the base of the cleithral curvature just below the gill slit, and snout length as the distance between the tip of the upper jaw and the caudal margin of the nostril.

2.2.4. *In toto* clearing and staining

Clearing and staining of bone and cartilage with alizarin red S and alcian blue was done according to a slightly modified version of the protocol of Taylor & Van Dyke (1985) (Table 2.4). Adjustments include omission of the degreasing, final cleaning and guanine removal steps, limitation of cartilage staining to less than 12 hours as the acetic acid could decalcify bone, which makes alizarin red bone staining ineffective, and shortening of bleaching time to a few hours maximum. An Olympus SZX-7 stereoscopic microscope equipped with an Olympus SZX-DA drawing attachment was used to study and draw the bony and cartilaginous elements of the cranium. KOH 5% was used to completely disarticulate the suspensorium of some adult specimens, so all bones could be individually examined in detail.

Table 2.4 – Clearing and staining protocol modified from Taylor & Van Dyke (1985).

step	solution	duration
dehydration	50% alcohol	12h
	75% alcohol	12h
	96-100% alcohol	12h
	96-100% alcohol	12h
cartilage staining	9-30 mg alcian blue 8GX (Sigma) in 100 ml of 40% glacial acetic acid and 60% absolute alcohol	12h
neutralization	saturated borax ($Na_2B_4O_7.10H_2O$)	48h
bleaching	10% H_2O_2 in 0.5% KOH	0.5-6h
clearing	enzyme buffer: 0.45 g purified trypsin in 400 ml of 30% saturated borax	12h-...
bone staining	0.5% KOH in 0.1% alizarin red S (Sigma)	24h
further clearing	0.5-3% KOH	12h-...
preservation	25% glycerine + 75% 0.5% KOH	12h
	50% glycerine + 50% 0.5% KOH	12h
	75% glycerine + 25% 0.5% KOH	12h
	100% glycerine	storage

2.2.5. Dissecting

For the study of soft tissue structures, such as ligaments, tendons and muscles, dissections were performed. Visualization of muscle fibre orientation, origin and insertion sites was enhanced by the use of an iodine solution (Bock & Shear, 1972).

2.2.6. Serial sectioning

Serial histological cross sections of 14 specimens were made in order to study the detailed anatomy. Head or entire body was embedded in Technovit 7100 (Heraeus Kulzer Wehrheim, Germany) according to the Technovit 7100 User Instructions (Table 2.5). Next, semi-thin sections (2 or 5 µm) were cut using a Leica Polycut SM 2500 sliding microtome (Leica Microsystems GmbH Wetzlar, Germany) equipped with a wolfram carbide coated knife. Finally, slices were stained with toluidine blue, mounted on slides with either DPX or a xylene based mounting medium and covered.

Table 2.5 – Technovit 7100 User Instructions embedding protocol

step	solution	duration
vacuum fixation	10% buffered formalin	days-weeks
washing	tap water	8h
decalcification	Decalc (Histolab)	36h
washing	tap water	5h
dehydration	30% alcohol	12h
	50% alcohol	12h
	70% alcohol	12h
	96% alcohol (two times alcohol renewal)	12h
embedding	Technovit 7100 solution A	min. 24h
	Technovit 7100 solution A renewal	min. 48h
	add Technovit 7100 harder II	12h
	place in deep freezer	12h
polymerization	place at room temperature (check progress)	approx. 12h
	place in oven (approx. 40°C)	1h

2.2.7. Computed tomography scanning

CT-scans of one or more specimens of almost all species (with the exception of *Doryrhamphus janssi*, *Dunckerocampus pessuliferus* Fowler and *Hippocampus kuda*)

were made either at the Micro CT Research Group of the University of Antwerp (MCT; http://webh01.ua.ac.be/mct) or at the Centre for X-ray Tomography of Ghent University (UGCT; Masschaele *et al.*, 2007; http://www.ugct.ugent.be). The MCT group uses a SkyScan-1072 compact desktop system for non-destructive high resolution X-ray microscopy and microtomography (SkyScan Kontich, Belgium). At the UGCT, all specimens were scanned using the transmission tube head, at 100 kV tube voltage (except for one of the *H. reidi* specimens, which was scanned with the directional tube head at 80 kV tube voltage). For each individual between 500 and 1900 projections of between 500x500 and 1096x1096 pixels were recorded (1000 projections of 748x748 pixels for the *H. reidi*), with an exposure time between 1 s and 1.6 s per projection and covering 360 degrees. The raw data were processed and reconstructed using the in-house developed CT-software Octopus (Vlassenbroeck *et al.*, 2007).

2.2.8. Graphical 3D-reconstructing

Computer-generated 3D-reconstructions were made to visualize skeletal elements, using CT-data, and overall topography (*i.e.* bones, cartilage, muscles, ligaments, tendons, *etc.*), using histological sections. Images of the histological sections were captured using a digital camera (Colorview 8) mounted on a Reichert-Jung Polyvar light microscope (Reichert Depew, USA), controlled by the software program analySIS 5.0. The digital images of histological data were imported in the software package Amira (3.1, 4.1.0, 5.1.0 or 5.2.2; Visage Imaging, Berlin, Germany). Alignment of the histological sections and tracing of the elements was done manually by superimposition to get maximal overlap of all structures. Each element was rendered and separately smoothed. In some cases Rhinoceros 3.0 software (McNeel Europe SL Barcelona, Spain) was used for making images of all structures combined. For the CT-data, both software programs Amira 5.2.2 and myVGL 2.0.4 (Volume Graphics GmbH, Heidelberg, Germany) were used to generate volume rendered as well as surface rendered reconstructions of the cranial skeleton.

2.2.9. Geometric morphometric analysis

Geometric morphometrics are frequently used to qualify and quantify anatomical shape changes with an ontogenetic, phylogenetic or pathological basis. Especially landmark-based analyses provide an accurate description of these shape changes and in addition have the advantage of allowing a clear visualization, interpretation and communication of the results (Zelditch *et al.*, 2004).

Here, the landmark-based geometric morphometric analysis involved the use of the Thin Plates Spline freeware (tps; Rohlf, F.J., State University of Stony Brook, New York). First tpsUtil version 1.46 (Rohlf, 2010a) was used for construction of the tps-files. Landmarks (LM) were digitized on the pictures of the head with tpsDig2 version 2.16 (Rohlf, 2010b). The following 15 homologous landmarks were digitized (Fig. 2.3): (1) dorsorostral tip of premaxillary bone; (2) distal point of dentary bone; (3) ventrocaudal point of lower jaw below suspensorial articulation; (4) ventral point where snout is dorsoventrally at its narrowest; (5) dorsal point where snout is dorsoventrally at its narrowest; (6) base of mesethmoidal curvature; (7) caudal border of nostril; (8) operculo-hyomandibular articulation; (9) ventrorostral tip of sphenotic bone; (10) most dorsal point of skull at the level of the eye with respect to the line connecting LM1 with LM12; (11) most dorsal point of skull at the level of the braincase with respect to the line connecting LM1 with LM12; (12) base of cleithral curvature where the gill slit is situated; (13) dorsal point of pectoral fin base; (14) ventral point of pectoral fin base; and (15) ventrocaudal tip of preopercular bone. For all specimens, head length was calculated as the distance between LM1 and LM12, snout length as the distance between LM1 and LM7 and snout height as the distance between LM4 and LM5. The interlandmark distances were calculated using PAST version 2.03 (Hammer *et al.*, 2001).

Superimposition is used to remove all non-shape variation in the configurations of landmarks (*i.e.* variation in position, orientation and scale). Various superimposition methods exist, here the landmarks were submitted to a generalized Procrustes analysis (GPA), which superimposes landmark configurations using least-squares estimates for translation and rotation parameters (Adams *et al.*, 2004). The centroid of each configuration is translated to the origin, the sets of landmarks are rotated to minimize the squared

differences between corresponding landmarks and configurations are scaled to a common, unit size. TpsSmall version 1.20 (Rohlf, 2003) was used to confirm the fitness of the dataset for further statistical analysis. Next, for each specimen partial warps were computed in tpsRelw version 1.49 (Rohlf, 2010c) and submitted to a principal component analysis (PCA) resulting in relative warps (RWs) that summarize the variation among the specimens. Deformation grids were generated to visualize the shape variation and relative warp scores and centroid size were saved for further analyses.

One tps-file comprising all pipefishes and one for the seahorses were loaded in CoordGen6f (Sheets, 2000a) and TwoGroup6h (Sheets, 2000b), both part of the Integrated Morphometrics Package freeware (IMP; Sheets, H.D., Canisius College, Buffalo, New York). The (dis)similarity of pipefishes *versus* seahorses was determined by means of a Goodall's F test, which examines differences in mean shape between two groups relative to the shape variation found within the groups. It compares the Procrustes distance between the means of two samples to the amount of variation found in the samples. The probability that this F-score could have arisen by chance was tested by a Bootstrap resampling procedure (4,900 Bootstraps).

Finally, tpsRegr version 1.37 (Rohlf, 2009) was used to perform regression analyses between the obtained relative warp scores on the one hand and centroid size, log head length or snout length over head length (*i.e.* relative snout length) on the other hand.

Another tps-file was made, comprising only *Hippocampus reidi* specimens, both adult and juvenile. Identical landmarks were placed, a PC analysis was carried out and deformation grids were used to visualize shape changes. In order to detect important transformations during development, we wanted to plot head shape (*i.e.* relative warp scores) over age. Since we did not know the exact age of all specimens, head length was used as a proxy (correlation coefficient between age and head length is 0.93, based on ten *H. reidi* juveniles with age ranging between 1 and 65 days; Fig. 2.4).

2.2.10. Finite element analysis

Finite element analysis is a technique in which mechanical loading of a physical system is simulated in a model to investigate the resulting stress distribution. The finite element method allows estimation of stress distribution in objects of complex geometry for which no exact analytical solutions exist. It implies dividing the complex and irregularly shaped object into a large number of discrete, manageable elements connected to each other by nodes. The mesh, *i.e.* all the elements and nodes combined, needs to be assigned material properties that define the elastic behaviour of the model, such as Young's modulus and Poisson's ratio. Next, boundary constraints are applied to the mesh to anchor the model and the loading conditions are defined. Finally, the model is solved under the assigned material properties, boundary conditions and applied forces to obtain nodal displacements and then the resulting stresses. Although initially developed for engineering, the finite element method has started to find its way into biological analyses as well (e.g. Dumont *et al.*, 2005; Richmond *et al.*, 2005).

The raw CT-data of *H. reidi* and *H. zosterae* were processed to generate a continuous, 'water-tight' surface model using the software program Mimics 12 Materialise NV (Leuven, Belgium); for all other specimens Amira 5.1.0 or 5.2.2 was used. The operculum, branchial arches and post-cranial structures were removed. All of the models were simplified and initially smoothed in Amira 5.1.0.

Ideally the model of a fish head, having more degrees of freedom compared to a mammalian skull, would consist of several separate but articulating bony elements, including cartilaginous structures, suture morphology, connective tissue, ligamentous connections, *etc.* Not only will the complexity of such a system vastly increase the computational resources required to construct the finite element model and run the analysis, but unfortunately, many of the necessary data is lacking for syngnathids in particular and even for fishes in general. Since generating a model that accurately reflects the reality is impossible, an exploratory analysis was performed by making some simplifications, *i.e.* the cranium was modelled as a single unit, without taking sutures in the braincase and articulations between the functional components in the skull into account. The two suspensorio-neurocranial joints, the suspensorio-hyoid articulation, the lower jaw, the maxillary bones and the interopercular

bone were fused and treated as solid, immobile elements. Obviously, the results of these analyses must be interpreted cautiously, yet I feel that they still give a valuable estimation of the stress during suction feeding in syngnathid skulls.

To reduce the effects of model size, Rhinoceros 4.0 software (McNeel Europe SL Barcelona, Spain) was used to scale the reconstructions to the same braincase length, defined as the distance between the rostral border of the parietal bone and the occipital joint of the basioccipital bone

Geomagic Studio 10 GmbH (Stuttgart, Germany) was used to fine-tune the models, prepare them for solid meshing (*i.e.* fill artificial holes, repair intersecting triangles and adjust the aspect ratio of the triangles), and to reduce triangle number. The surface models were exported to Strand7 Pty Ltd (Sydney, Australia) and transformed into solid models.

Assigning material properties to the models was not straightforward since there is only data of two fish species available. Erickson *et al.* (2002) analyzed the pelvic metapterygia of *Polypterus* sp. and found a mean Young's modulus of 17.6±7.8 GPa and in a recent publication, Horton & Summers (2009) determined a Young's modulus for acellular bone in *Myoxocephalus polyacanthocephalus* (Pallas) of 6.48±0.31 GPa. Data concerning material properties of skull bones in fishes is lacking. Besides that, there is considerable variation in features like bone density, cortical thickness, direction of loading, microstructure, *etc.* between taxa, bones and even sites within bones. So even if the material properties of fish skull bones would have been examined, there is no guaranty that they would approximate the values of syngnathid skull bone properties. For example, Peterson & Dechow (2003) found that the elastic properties of some cranial bones in humans are more similar to those measured in long bones than to those of the mandible. Hence, an arbitrary Young's modulus of 20 GPa was chosen, which is the mean of a range of material properties of various bones in birds and eutherian mammals: 6.7-34.1 GPa (Currey, 1999). According to the same line of reasoning, the models were assigned with a Poisson's ratio of 0.3, based on various bones in actinopterygians, birds and eutherian mammals.

Constraints were applied to a few nodes at the occipital joints of the skulls and suction pressure was simulated by loading the suspensoria and rostral part of the neurocranium with a pressure of 20 kPa oriented inwards, towards the central, longitudinal axis of the cylindrical snout (Fig. 2.5). Because our goal was to

compare the relative magnitudes and patterns of stress among the models (not absolute stress magnitudes), we applied the same pressure to the snouts of all models based on measurements from within the buccal cavity of trumpetfish (20 kPa, Huskey & Quintero, 2006). Von Mises stress was used to describe the effect of the mechanical loading on the models. The Von Mises criterion is a formula for combining the principal stresses (acting in the x, y, and z directions) at a given point into an equivalent stress, or Von Mises Stress, which is then compared to the yield stress of the material. If the Von Mises stress exceeds the yield stress, then the material is considered to be at the failure condition. Hence, Von Mises stress is a good predictor of failure under ductile fracture (Nalla *et al.*, 2003). We predicted stress distributions in the skull models by means of linear finite element analysis.

2.3. TERMINOLOGY

According to Balon (1975), the larval period of fishes begins with the switch to exogenous feeding and lasts until the median fin fold is differentiated. The juvenile period is then defined as starting with complete differentiation of fins and ending with the onset of gamete maturation (Balon, 1975). Given the fact that the differentiation of the fins precedes the onset of exogenous feeding in syngnathids (Azzarello, 1990 and personal observation), a larval period is missing and newly released young are considered juveniles. Moreover, newborns resemble miniature adults in form (see chapter 3.1 and 6.1), as is confirmed for *Hippocampus kuda* (Choo & Liew, 2006). In the latter species, growth allometries after release from the brood pouch reflect typical teleostean juvenile growth and not larval growth (Choo & Liew, 2006). Therefore, the term juvenile is used instead of larva here. Although many authors refer to a larval stage and even a metamorphosis[3] inside the pouch, the latter cannot be excluded with the data

[3] defined by Lawrence (2005) as the transformation of one structure into another, most commonly referring to the radical change in form and structure undergone by some animals between embryo and juvenile stage

presented in this thesis (e.g. Choo & Liew, 2006; Forsgren & Lowe, 2006).

Throughout this dissertation, prey distance refers to the distance between the prey and the snout tip at the onset of prey capture, hence before head rotation (distance 6-8 on Fig. 5.2). Prey capture time is defined as the time necessary to suck in the prey.

The terminology of all muscles follows that of Winterbottom (1974). For the major part of the osteological components, the terminology proposed by Lekander (1949), Harrington (1955) and Arratia & Schultze (1990) is followed. Nevertheless, in some occasions another name, which seemed more correct or apt, is applied. The use of those terms is accounted for below.

The dentary and anguloarticular bones in *Syngnathus rostellatus* and *H. capensis* could be a fusion of several bones. In most teleosts, the dentary bone comprises the perichondral mentomeckelian, the dermal splenial and the dermal dentary bones, and should thus be named 'dento-splenio-mentomeckelium' according to the nomenclature of Lekander (1949). The anguloarticular bone is the fusion of the perichondral articular bone, the dermal splenial bones and the dermal angular bone; the 'angulo-splenio-articular'. However, whether this is also the case for syngnathids is not certain, because the absence of the preoperculo-mandibular canal may indicate the absence of the splenial bones. In the current deficiency of conclusive ontogenetic evidence to elucidate this, the terms 'dentary bone' and 'anguloarticular bone' are used here.

Kindred (1924) suggested there is a pterygoid bone in *Syngnathus fuscus* Storer, which would be a fusion of the ectopterygoid and the endopterygoid bones. According to Kadam (1961) the ectopterygoid and the endopterygoid bones ossify separately in *Nerophis* (species not stated), *Syngnathus serratus* (Temminck & Schlegel) and *Hippocampus* (species not stated). Bergert & Wainwright (1997) found both an ectopterygoid and an endopterygoid bone in *S. floridae*, and solely an ectopterygoid bone in *H. erectus*. In the species studied here we found no indications of an endopterygoid bone. As Kadam (1961) correctly pointed out, the bone that Kindred (1924) describes as the pterygoid bone consists of two separate

elements and one of them is indeed the dermal ectopterygoid bone. However, he did not notice that the bone he called the endopterygoid bone is perichondral, and therefore homologous to a metapterygoid bone. Bergert & Wainwright (1997) followed Kindred (1924) in identifying the metapterygoid bone of *S. floridae* as the endopterygoid bone. In addition, they did not mention the presence of a similar bone in *H. erectus*. Swinnerton (1902) stated that in *Gasterosteus aculeatus* the pterygoid bone takes up the position of both endopterygoid and ectopterygoid bones, however, only one centre of ossification is found. According to de Beer (1937) *G. aculeatus* possesses both an ectopterygoid and an endopterygoid bone, fused to form what he calls a pterygoid bone. We could not exclude a fusion between the ecto- and endopterygoid bone in the syngnathid species studied here. However, based on its topography, ventrolateral to the autopalatine and the metapterygoid bone, the syngnathid pterygoid bone is considered homologous to the ectopterygoid bone.

As Branch (1966) mentioned, the homology of the circumorbital bones has been unclear. Kindred (1924) and de Beer (1937) defined the metapterygoid bone of *S. fuscus* as "the intramembranous ossification dorsal to the quadrate, rostral to the symplectic and excluded from contact with the metapterygoid process of the palatoquadrate by the pterygoid". However, Kadam (1961), Branch (1966) and Patterson (1977) pointed out that this is not the metapterygoid bone, but the lacrimal bone. Jungersen (1910) identified the circumorbital bones as the posterior and anterior preorbital bones in *Syngnathus typhle* L. (which he called *Syphonostoma typhle*) because of their position lateral of the adductor mandibulae muscle. Gregory (1933) stated that *Phyllopteryx* possesses "a row of antorbital plates on the side of the oral tube", which he labelled as two metapterygoid bones. As previously mentioned, Kindred (1924) and de Beer (1937) maintained that the lacrimal bone in *S. fuscus* is the metapterygoid bone, although they correctly pointed out that the second infraorbital bone is a circumorbital bone. Kadam (1961) described the two bones of the suborbital chain in *Nerophis* as an anterior preorbital bone and a posterior suborbital bone and he remarked that in *Syngnathus* and *Hippocampus* there are two preorbital bones. The use of the terms preorbital and suborbital bones should be avoided as they only indicate the position of these bones relative to the orbit but do not say anything about their

homology (Daget, 1964). Therefore we use the terms antorbital bone and infraorbital bones, as e.g. in Lekander (1949), Nelson (1969) and Schultze (2008).

The term prevomeral bone is used by many authors (e.g. Gregory, 1933; de Beer, 1937; Harrington, 1955) instead of vomeral bone. Here, the latter is used, because of the homology with the vomeral bone in sarcopterygians (Schultze, 2008). The use of the terms parietal and postparietal bones as substitutes for the frontal and parietal bones is also based on the terminology of Schultze (2008), who provides evidence for absence of the mammalian frontal bones in actinopterygians.

3 Morphological description

3.1. MORPHOLOGY OF THE CHONDRO- AND OSTEOCRANIUM

Modified from:
Leysen H, Jouk P, Brunain M, Christiaens J, Adriaens D.
Cranial architecture of tube-snouted Gasterosteiformes (*Syngnathus rostellatus* and *Hippocampus capensis*)
Journal of Morphology 2010, 271:255-270.

Abstract

The long snout of pipefishes and seahorses (Syngnathidae, Gasterosteiformes) is formed as an elongation of the ethmoid region. This is in contrast to many other teleosts with elongate snouts (e.g. butterflyfishes) in which the snout is formed as an extension of the jaws. Syngnathid fishes perform very fast suction feeding, accomplished by powerful neurocranial elevation and hyoid depression. Clearly, suction through a long and narrow tube and its hydrodynamic implications can be expected to require certain adaptations in the cranium, especially in musculoskeletal elements of the feeding apparatus. Not much is known about which skeletal elements actually support the snout and what the effect of

elongation is on related structures. Here, we give a detailed morphological description of the cartilaginous and bony feeding apparatus in both juvenile and adult *Syngnathus rostellatus* and *Hippocampus capensis*. Our results are compared to previous morphological studies of a generalized teleost, *Gasterosteus aculeatus*. We found that the ethmoid region is elongated early during development, with the ethmoid plate, the hyosymplectic and the basihyal cartilage being extended in the chondrocranium. In the juveniles of both species almost all bones are formed, although only as a very thin layer. The elongation of the vomeral, mesethmoid, quadrate, metapterygoid, symplectic and preopercular bones is already present. Probably because of the long and specialized parental care, which enables the release of advanced developmental stages from the brooding pouch, morphology of the feeding apparatus of juveniles is already very similar to that of adults. We describe morphological features related to snout elongation that may be considered adaptations for suction feeding; e.g. the peculiar shape of the interhyal bone and its saddle-shaped articulation with the posterior ceratohyal bone might aid in explosive hyoid depression by reducing the risk of hyoid dislocation.

3.1.1. Introduction

Unlike other long-snouted teleosts (e.g., butterflyfishes, Chaetodontidae), the tubular snout of syngnathids is not formed by the extension of the jaws, but by an elongation of the region between the autopalatine bone and the lateral ethmoid bone, namely the ethmoid region. This snout with tiny terminal jaws enables pipefishes and seahorses to perform fast and powerful suction feeding. They approach their prey from below and a rapid neurocranial elevation positions the mouth close to the prey. Next an explosive expansion of the snout followed by lower jaw depression, causes water to flow into the mouth aperture (Chapter 5.1; Muller & Osse, 1984; Muller, 1987; de Lussanet & Muller, 2007). Suction feeding in pipefishes and seahorses is the fastest ever recorded in teleosts. Muller and Osse (1984) found that *Entelurus aequoreus* captured its prey in 5 ms, while Bergert and Wainwright (1997) recorded a time of 5.8 ms for *Hippocampus erectus* and 7.9 ms for *Syngnathus floridae*. De Lussanet and Muller

(2007) recorded capture times of 6-8 ms for *S. acus* and Roos *et al.* (chapter 5.1) recorded 5.77 ms for *H. reidi*. It was recently discovered that newborns are even faster (Van Wassenbergh *et al.*, 2009). However, having a long and narrow snout is not without hydrodynamic costs. For example, by increasing the length of the snout, the moment of inertia increases. Secondly, it implies that a large difference in pressure between the buccal cavity and the surrounding water must be created (Poiseuille's law). And finally, as the upper and lower jaws closing the mouth aperture are minute, the prey size is constrained. Hence, the hydrodynamic implications of suction feeding through a long, narrow tube can be expected to rely on special adaptations in the feeding apparatus, particularly of musculoskeletal components forming and acting upon the jaws and ethmoid region.

To understand to what degree structural specializations of the tubular snout can be related to this highly performant suction feeding, a detailed examination of the morphology is needed. Thus far, studies dealing with syngnathid morphology are scarce or lack great detail (McMurrich, 1883; de Beer, 1937; Kadam, 1958; 1961; Branch, 1966). To fill the gap in current knowledge, this study focuses on the detailed anatomy of the cranial skeletal system of *Syngnathus rostellatus* (Nilsson's pipefish) and *Hippocampus capensis* (Knysna seahorse). Special attention is paid to the snout morphology to understand which skeletal elements are in fact elongated and what effect this elongation may have on the cranial architecture. The study of juveniles is required for a better comprehension of interspecific differences, as well as the detailed anatomical nature of snout elongation. The highly derived syngnathid morphology is compared to that of a generalized teleost, namely *Gasterosteus aculeatus* (three-spined stickleback), based on the study of Anker (1974).

3.1.2. Brief material & methods

The four adults and five juveniles of *Syngnathus rostellatus* (126.2, 111.1, 97.9, 105.0, 11.0, 14.5, 11.3, 11.4 and 13.1 mm SL respectively), three adults and four juveniles of *Hippocampus capensis* (96.1, 97.6, 99.0, 13.3, 13.6, 12.8 and 14.0 mm SL respectively) and two adults and one juvenile of *H. reidi* (117.2, 113.5 and 7.0 mm

SL respectively) studied are presented in Table 2.1 and 2.2. Adult as well as juvenile specimens of all species (with exception of a juvenile *H. reidi*) were cleared and stained according to the protocol of Taylor and Van Dyke (1985). In the juveniles, bone staining was not very clear, so serial histological cross sections were used, which also enabled more precise detection of the skeletal elements. Graphical 3D-reconstructions of the chondrocranium of both *S. rostellatus* and *H. capensis* were generated. The specimen of *S. rostellatus* (13.1 mm SL) used for serial sectioning shows the hyoid in a resting position, whereas that of *H. capensis* (12.8 mm SL) had its hyoid depressed. For more information on specimens and protocols I refer to chapter 2.

3.1.3. Results

A. Juvenile cranium

Syngnathus rostellatus

The cartilaginous neurocranium consists of two parts that are separated by the eyes: the rostral ethmoid and the caudal otic capsule (Fig. 3.1). The ethmoid plate is long and narrow but becomes wider rostrally where it lies ventral to the rostral cartilage (Fig. 3.1A,B). More caudally the ethmoid plate bears a vertical ridge, *i.e.* the internasal septum, connected to the orbitonasal laminae, which enclose the orbitonasal foramina (Fig. 3.1A,B). Although the ethmoid plate and the septum are firmly fixed, histological differences among the cartilaginous elements suggests that the internasal septum is not formed as an outgrowth of the ethmoid plate. There is a clear difference in the size, shape and organization of their chondrocytes (Fig. 3.2D). The ethmoid plate is continuous with the trabecula communis, that lies medial to the orbits (Fig. 3.1B,C). Ventrally the otic capsule is provided with an articulation facet for the hyomandibular part of the hyosymplectic cartilage. Meckel's cartilage bears a ventral retroarticular process and articulates caudally with the pterygoquadrate part of the palatoquadrate cartilage, which is roughly L-shaped (Fig. 3.1A). The palatine part, which is completely separated from the pterygoquadrate part, lies laterally to the ethmoid plate (Fig. 3.1A). The largest cartilage element of the splanchnocranium is the hyosymplectic cartilage, which consists of a long, horizontal symplectic part, and

a shorter oblique hyomandibular part (Fig. 3.1A,C). At the ventrocaudal margin of the hyosymplectic cartilage lies the interhyal cartilage, articulating ventrally with the ceratohyal cartilage (Fig. 3.1C). Medial to the two ceratohyal cartilages lies one long basihyal and two shorter hypohyal cartilages (Fig. 3.1C).

Juveniles of *S. rostellatus* show the onset of ossification in most places, however, only a very thin layer of bone was observed (Fig. 3.2). Ventral to the ethmoid plate the dermal parasphenoid bone has already formed. This very long bone runs from the ethmoid region up to the posterior part of the otic region (Fig. 3.2D,F). Formation of the mesethmoid bone begins dorsal to the ethmoid plate and around the internasal septum (Fig. 3.2C). A thin bony sheet at the ventral end of the orbitonasal laminae is the precursor of the lateral ethmoid bone. Around the main part of Meckel's cartilage, the dentary bone is formed (whether this bone includes the mentomeckelian and splenial bones is uncertain due to the absence of canals, see chapter 2.3 for a discussion on the terminology; Fig. 3.2B). This bone bears a large ventral ridge and caudally encloses the anguloarticular bone (this could be fused with the splenial bones, but again no canals were observed, see chapter 2.3 for a discussion on the terminology), which is still poorly developed and only present on the lateral side of Meckel's cartilage (Fig. 3.2B). The retroarticular bone is visible as a small ossification of the ventrocaudal part of the Meckel's cartilage (Fig. 3.2B). In the upper jaw, both maxillary and premaxillary bones have appeared and are already fairly well developed. The former articulates with the rostral cartilage dorsally. The autopalatine bone is present but does not bear a clear maxillary or vomeral articulation facet yet (Fig. 3.2A). Ventral to the palatoquadrate cartilage the ectopterygoid bone is formed (Fig. 3.2A). This dermal bone shows a small horizontal part and a longer vertical one that meets the dorsal process of the quadrate bone. At the dorsal edge of the palatoquadrate cartilage, the small metapterygoid bone arises (Fig. 3.2C). The quadrate bone bears a dorsal process, as well as a ventromedial and ventrolateral wing. More caudally these wings enclose the cartilaginous hyosymplectic and the symplectic bone (Fig. 3.2C,E). The symplectic bone consists of both the ossification around the rostral part of the hyosymplectic cartilage and a dorsal crest on top of the perichondral part (Fig. 3.2E). The hyomandibular bone is formed caudally around the hyosymplectic cartilage and bears dorsal articulations with the neurocranium and opercular bone that remain

cartilaginous (Fig. 3.2F). The preopercular bone consists of both a short and long process. The long one covers the quadrate and symplectic bones rostrally and is also provided with a large lateral process (Fig. 3.2E). Its shorter oblique bar covers the hyomandibular bone caudally (Fig. 3.2F). All other elements of the hyoid arch, *i.e.*, basihyal, hypohyal, ceratohyal and interhyal cartilages, show the presence of a very thin sheet of bone (Fig. 3.2E,F). The hypohyal bones bear a ventrolateral and a ventromedial process, which surround the ceratohyal bones ventrally (Fig. 3.2E). Anterior and posterior ceratohyal bones are hard to distinguish from each other at this stage (Fig. 3.2E). Within the tendon of the sternohyoideus muscle, the urohyal bone has also arisen. The opercular bone is a thin but fairly large bony sheet, bearing a lateral process and articulating with the hyomandibular bone medially. None of the other opercular bones (interopercular, subopercular and suprapreopercular bones) and neither the branchiostegal rays are present yet.

Hippocampus capensis

For the chondrocranium of *H. capensis* (Fig. 3.3), we report only those features which differ from *S. rostellatus*.

The ethmoid plate of the cartilaginous neurocranium in *H. capensis*, is shorter and rostrally narrower than that of *S. rostellatus* (Fig. 3.3A,B). Caudal to the olfactory organs, the ethmoid plate widens and meets the orbitonasal laminae (Fig. 3.3A,B, 3.4D). It is also continuous with the trabecula communis, but in the seahorse the latter is much shorter and more robust (Fig. 3.3C). The otic capsule has a distinct position compared to that in *S. rostellatus*, namely dorsocaudal to the orbits. Hence, it does not lie on the same level as the ethmoid plate, but at an angle to the latter (otic capsule tilted about 34° up; Fig. 3.3A). At the ventral surface of the otic capsule, the articulation facet of the hyomandibular part of the hyosymplectic cartilage is much more prominent and it is laterally flanked by a spheno-pterotic ridge (Fig. 3.3A). Meckel's cartilage is more tapered rostrally compared to that of *S. rostellatus* (Fig. 3.3A). The symplectic part of the hyosymplectic cartilage is somewhat shorter in *H. capensis*. The hyomandibular part, however, is longer and more vertically orientated compared to that of the pipefish (Fig. 3.3A). In the seahorse, the shorter basihyal cartilage lies in front of the ceratohyal cartilages, which may be due to the hyoid being retracted (Fig. 3.3A,C).

Almost all bones are present in the juvenile *H. capensis* studied, except for the circumorbital bones (Fig. 3.4). The vomeral bone lies ventral to the ethmoid plate and becomes covered by the parasphenoid bone more caudally (Fig. 3.4A,B,D). The latter bears two rather large lateral wings that reach the ventral surface of the otic capsule. The dentary bone rostrally bears a small lateral process and has a well developed coronoid process. The anguloarticular bone and retroarticular bone are prominent and there is a ligamentous connection between the retroarticular bone and the slender interopercular bone that continues to run up to the posterior ceratohyal bone (Fig. 3.4C). The dorsal crest of the symplectic bone is larger in *H. capensis* compared to *S. rostellatus* (Fig. 3.4E). There is a large spine on the lateral surface of the preopercular bone and the ascending bar is oriented vertically instead of obliquely as in the pipefish (Fig. 3.4F). The bony sheets around the hypohyal and ceratohyal cartilages are well developed (Fig. 3.4F). In addition, the anterior and posterior ceratohyal bones are distinct from each other. In the seahorse, the urohyal bone is much shorter. The opercular bone has a convex shape and bears a prominent lateral process. Also the subopercular bone and branchiostegal rays are fairly well developed in juvenile *H. capensis*.

B. Adult cranium

Syngnathus rostellatus

The most distinctive character of the skull of *Syngnathus rostellatus* is the highly extended tube snout (Fig. 3.5). It is formed by the elongation of the vomeral, mesethmoid and the circumorbital bones of the neurocranium and of the quadrate, metapterygoid, symplectic, preopercular and interopercular bones of the splanchnocranium (Fig. 3.5A).

Both the maxillary and premaxillary bones are relatively small and toothless (Fig. 3.5A,B,D,E). The maxillary bone bears two cartilaginous processes dorsally: a rostral premaxillary one and a caudal one for the articulation with the vomeral bone. Below the latter process there is also a cartilaginous articulation surface for the autopalatine bone. The round rostral cartilage is situated mediocaudal to the maxillary bone and dorsal to the vomeral bone. Ventrally, the maxillary bone is triangularly shaped, covering the coronoid process of the dentary bone to which it is ligamentously connected. The slender premaxillary bone is rostrocaudally

flattened and tapers ventrally. It is provided with a dorsocaudal cartilaginous articulation head for the maxillary bone.

The vomeral bone is a long and narrow bone that broadens rostrally, forming an articulation with the autopalatine bone laterally and the maxillary bone rostrally (Fig. 3.5A,B,D,E). The hind part of the vomeral bone reaches the lateral ethmoid bones and is covered dorsally by the mesethmoid bone. More caudally, it is wedged in a fissure of the parasphenoid bone. The mesethmoid bone covers more than half the length of the snout and stretches out caudally, up to the parietal bones (Fig. 3.5A,B). The lateral ethmoid bone is a slim bone that separates the nasal opening from the orbits (Fig. 3.5A,B).

The parasphenoid bone is positioned rostrally between the dorsal mesethmoid bone and the ventral vomeral bone (Fig. 3.5A). It bears two lateral wings behind the orbits and fits into a wedge of the basioccipital bone caudally. In most specimens studied of *S. rostellatus* only two circumorbital bones are present, which seem to be homologous to an antorbitolacrimal and a second infraorbital bone (Chapter 2.3). Only one specimen has just one bone on its right side. In the individuals with two circumorbital bones, the large antorbitolacrimal bone caudally reaches the front end of the nasal opening, and covers a large part of the quadrate bone (Fig. 3.5A,B). Ventrally, the antorbitolacrimal bone shows one or several small indentations. The second infraorbital bone is much smaller and borders the ventral side of the nasal opening, as well as the anterior side of the orbits (Fig. 3.5A,B,C).

The large dentary bone of the lower jaw has a well developed coronoid process (Fig. 3.5A,C,D). Inside a cavity of the dentary bone, the smaller anguloarticular bone fits, which bears a distinctive cartilaginous articulation with the quadrate bone caudally (Fig. 3.5A,C,D). The retroarticular bone is very small, with a strong mandibulo-interopercular ligament connecting it to the interopercular bone (Fig. 3.5A,C,D).

In the adult stage, the autopalatine bone carries a prominent cartilaginous maxillary process, a smaller articulation condyle for the vomeral bone and a slender cartilaginous process caudally (Fig. 3.5A,B,D,E). There is no separate dermopalatine bone and as in most extant teleosts, it is probably fused to the autopalatine bone (Arratia & Schultze, 1991). The ectopterygoid bone is roughly triangularly shaped, with a vertical part running along the ascending process of

the quadrate bone and a horizontal part that is covered dorsally by the vomeral bone (Fig. 3.5A,B,D,E). This horizontal part shows a gap into which the cartilaginous process of the autopalatine bone fits, with a firm connection linking both bones. Lateral to the vomeral bone and behind the ectopterygoid bone lies the metapterygoid bone which tapers caudally and is covered by the upper rostral margin of the lacrimal bone (Fig. 3.5A,B). The quadrate bone, a long perichondral bone that stretches out caudally, is mostly covered by the metapterygoid bone rostrally and the two circumorbital bones caudally (Fig. 3.5A,B,C).

The hyomandibular bone articulates dorsally by a double condyle with the sphenotic bone and with the cartilaginous surface between the sphenotic, the prootic and the pterotic bones and it also bears a dorsocaudal opercular process. The symplectic bone is almost completely covered by the preopercular and circumorbital bones and forms the ventral border of the orbits (Fig. 3.5A). It bifurcates rostrally into two processes: a lower horizontal part that joins the quadrate bone, and a more dorsal oblique crest lying behind the upper margin of the second infraorbital bone.

The long horizontal process of the preopercular bone overlaps with the quadrate bone rostrally where it tapers (Fig. 3.5A,C). Medially the preopercular bone has two ridges: one supporting the symplectic bone and one for insertion of the levator arcus palatini muscle, which continues to run along this ridge and more caudally in a groove of the hyomandibular bone. Ventrally the preopercular bone has a cartilaginous differentiation where the cartilaginous head of the interhyal bone articulates. There is no articulation between the interhyal bone and the hyomandibular bone. The interopercular bone is covered by the preopercular bone and the quadrate bone, with an interoperculo-hyoid ligament connecting it to the posterior ceratohyal bone caudally (Fig. 3.5C). The interhyal bone, which is stout and small, is ventrally provided with a very firm, saddle-shaped joint for the posterior ceratohyal bone (Fig. 3.5A,C). The posterior ceratohyal bone has a small lateral process, close to the interhyal articulation (Fig. 3.5C). Onto this process, the interoperculo-hyoid ligament attaches rostrally and at its caudal base, the two branchiostegal rays are connected. There is a firm interdigitation between the posterior and anterior ceratohyal bone. Distally, there is a small triangularly shaped gap between the left and right anterior ceratohyal bones, just below the

very firm cartilaginous symphysis. The anterior ceratohyal bones are connected to the urohyal bone by a paired ceratohyal-urohyal ligament (Fig. 3.5C). The hypohyal bone is a small element that is firmly connected to the medial face of the anterior ceratohyal bone. Medial to the anterior ceratohyal bones and covered by the other elements of the hyoid lies the slender basihyal bone, which remains cartilaginous rostrally. The urohyal bone is a fairly long and slender bone that broadens somewhat rostrally where the ceratohyal-urohyal ligaments attach (Fig. 3.5C).

The opercular bone is large and has a convex lateral surface (Fig. 3.5A,B,C). There is just a tiny gill slit close to the cleithrum. The suprapreopercular bone is a small bone lying dorsorostrally to the opercular bone (Fig. 3.5A,B). The subopercular bone is sickle-shaped, covered by the ventral edge of the opercular bone. The two branchiostegal rays, which are long and slender, join the caudal margin of the opercular bone and reach up to the gill slit (Fig. 3.5A,C). There are no canals for the lateral line system present in any of the bones studied.

Hippocampus capensis

The premaxillary and maxillary bones look very similar to those in *S. rostellatus* (Fig. 3.6A,B,D,E). In *H. capensis*, however, they are more heavily built and the maxillary bone shows a more prominent convex curve when viewed rostrally. The rostral cartilage has a more elliptical shape instead of being round (Fig. 3.6E).

The dorsal part of the tube snout consists of the vomeral bone and the mesethmoid bone (Fig. 3.6B). The latter has a slightly bifurcated rostral end and covers approximately half the snout length. The lateral ethmoid bone is very distinct and has quite a large lateral process (Fig. 3.6A,B).

The parasphenoid bone stretches ventrally along the neurocranium and bends somewhat upwards in the otic region (Fig. 3.6A). The number of circumorbital bones in *H. capensis* is variable. In spite of this variability, some of them can be considered as homologous (antorbital, lacrimal and dermosphenotic bones) as indicated by Schultze (2008). The dermosphenotic bone is consistently present in all specimens observed. Variation was found at the level of all other circumorbital bones, including left right variation (e.g. one specimen, 97.6 mm SL, has an additional fourth circumorbital bone on its right side of which the homology is less obvious). Another specimen (99.0 mm SL) also seemed to have a fused

antorbitolacrimal bone, whereas separate bones were observed in others. The most common pattern observed is where the antorbital bone is the smallest, covering the quadrate bone and the metapterygoid bone (Fig. 3.6A,B). The lacrimal bone also covers the quadrate bone and is provided with a dorsorostral gap into which the metapterygoid bone fits (Fig. 3.6A,B). Finally, the second infraorbital bone covers the quadrate, the preopercular and a large part of the symplectic bones (Fig. 3.6A,B,C). Of the circumorbital bones, the most anterior one covers the next at its caudal end, so the antorbital bone covers the lacrimal bone, which in turn covers the second infraorbital bone.

The dentary bone is a short but solid bone (Fig. 3.6A,C,D). Ventrocaudally, the anguloarticular bone bears two ventral processes in between which the small retroarticular bone fits (Fig. 3.6A,C,D).

The autopalatine bone is a rather slender bone whereas the ectopterygoid bone is somewhat firmer compared to the one in *S. rostellatus* (Fig. 3.6A,B,D,E). The metapterygoid bone fits into a gap of the lacrimal bone caudally (Fig. 3.6A,B).

The two neurocranial condyles of the hyomandibular bone are larger and more distant from each other in the seahorse. In addition, the hyomandibular bone is provided with a lateral process that is firmly connected to the preopercular bone. The oblique fork of the symplectic bone present in the pipefish is larger in the seahorse and forms a dorsal plate upon the perichondral part. Only the caudal part, that borders the ventrorostral margin of the orbits, is visible in a lateral view (Fig. 3.6A). The preopercular bone has a short ascending process that forms the posterior margin of the orbits (Fig. 3.6A,C). The interopercular bone is much shorter compared to that in *S. rostellatus* (Fig. 3.6A,C). The interhyal, the anterior and posterior ceratohyal, the hypohyal and basihyal bones resemble those of *S. rostellatus* (Fig. 3.6A,C). The urohyal bone, which is more robust, has a rostral bifurcation with both processes connected to the anterior ceratohyal bone by ceratohyal-urohyal ligaments (Fig. 3.6C).

The opercular bone is higher and has a less rounded dorsocaudal edge (Fig. 3.6A,B,C). The suprapreopercular bone is absent. The two very thin and slender branchiostegal rays reach up to the caudal edge of the opercular bone (Fig. 3.6A,B,C). As in *S. rostellatus* the canals for the lateral line are absent in all bones studied.

3.1.4. Discussion

A. Aspects of snout elongation

As shown in Table 2.2, even though size ranges are similar, there is a difference in developmental stage between the juveniles of *Syngnathus rostellatus* (11.0-14.5 mm SL) and *Hippocampus capensis* (12.8-14.0 mm SL). Due to the different developmental stages of our specimens (*S. rostellatus* specimens had not left the brood pouch), we cannot link the morphological differences between the two species to differences in their developmental rate. However, this poses no problem for the main goal of this study, *i.e.* to show the relation between snout elongation and cranial morphology in an early developmental stage. Therefore, we will focus on the differences between both species, irrespective of their different developmental stages.

Both *S. rostellatus* and *H. capensis* have an elongated snout compared to *Gasterosteus aculeatus*. This elongation is restricted to the ethmoid region (vomeral, mesethmoid, circumorbital, quadrate, metapterygoid, preopercular, interopercular and symplectic bones). It appears to occur early in development, as observed in several Syngnathidae (e.g. *Hippocampus antiquorum* Leach (Ryder, 1881), *Syngnathus peckianus* Storer (McMurrich, 1883), *S. fuscus* (Kindred, 1921), *Hippocampus* (Kadam, 1958) and *Nerophis* (Kadam, 1961)). In *H. antiquorum* and *S. peckianus*, the ethmoid region is even elongated before the yolk sac is fully absorbed (Ryder, 1881; McMurrich, 1883).

A short comparison between some of these elements in syngnathids and the stickleback, as a generalized teleost representative without an elongated snout, is given here in order to understand the implications of snout elongation on cranial morphology in syngnathids (Fig. 3.7).

The vomeral bone stretches up to the lateral ethmoid bone in *S. rostellatus* and *H. capensis*, but in *Nerophis* it does not reach the nasal region (Kadam, 1961). According to Kadam (1961), this is a difference between the Gastrophori (syngnathids with the brood pouch rostral to anal fin: e.g. *Nerophis*) and the Urophori (brood pouch caudal to anal fin: e.g. *Syngnathus* and *Hippocampus*). Rostrally the vomeral bone provides an articulation with the maxillary bone, but there is no mesethmoid-premaxillary articulation present as there is in primitive teleosts (Gregory, 1933).

In *S. rostellatus* and *H. capensis* the quadrate bone consists of a perichondral ascending process and a membranous horizontal process. Whether or not this horizontal process is homologous to the one considered a teleostean synapomorphy by Arratia and Schultze (1991), could not be confirmed here. The process is much smaller on the quadrate bone in *G. aculeatus*, which is triangularly shaped with its apex dorsally (Anker, 1974). The ventrorostral corner of the quadrate bone provides the articulation with the lower jaw and ventrocaudally it bears a cartilaginous extension that lies lateral to the symplectic bone (Anker, 1974).

The preopercular bone in *S. rostellatus* and *H. capensis* is L-shaped. In the former the horizontal process is substantially longer than the vertical one, while in *H. capensis* the difference is less and in *G. aculeatus* the vertical process is the largest (Anker, 1974). Caudally, this vertical process meets the opercular bone in syngnathid species (Jungersen, 1910; Kindred, 1924; Kadam, 1961; Branch, 1966), but in *G. aculeatus* they only join each other dorsally (ventrally they are separated by an ascending process of the subopercular bone; Swinnerton, 1902; Anker, 1974).

In *G. aculeatus* the interopercular bone covers the subopercular bone caudally (Anker, 1974), but both lie well separated from each other in *S. rostellatus* and *H. capensis*.

The occurrence of an antorbital bone and lacrimal bone, followed by six infraorbital bones bordering the orbit (the first, third and sixth being the lacrimal, jugal and dermosphenotic bones, respectively), is a primitive feature of most teleosts (Reno, 1966; Nelson, 1969; Schultze, 2008). In the suborder Syngnathoidei other circumorbital bones besides the lacrimal bone are usually absent (Nelson, 2006), however, in syngnathids there are usually two to three infraorbital bones, which develop late (Kadam, 1961). In *S. rostellatus* and *H. capensis* the circumorbital bones are positioned in front of the orbit instead of around it. There is, however, a difference between those two species, as most specimens of the seahorse studied have an antorbital bone, a lacrimal bone (= first infraorbital bone) and a second infraorbital bone, whereas there are only two circumorbital bones present in almost all *S. rostellatus* specimens studied. Here, the posterior one corresponds to the second infraorbital bone. The anterior one is the largest one and appears to be a fusion between the antorbital bone and the

lacrimal bone. This hypothesis is supported by the absence of a separate antorbital bone, the bone being as large as and taking the place of both the antorbital bone and the lacrimal bone in *H. capensis*. In addition, there is a ventral indentation that could point out the incomplete fusion between the antorbital bone and the lacrimal bone. The formation of the antorbitolacrimal bone could be a structural advantage to strengthen the elongated snout laterally. During the fast elevation of the snout, large, ventrally oriented forces are expected to be exerted onto the dorsal part of the snout. In the case of an unfused antorbital bone and lacrimal bone, a possible bending zone between the two bones exists. The formation of an antorbitolacrimal bone could reduce the risk of bending and still allows lateral expansion of the snout. In *G. aculeatus* there are three separate circumorbital bones present (Swinnerton, 1902; de Beer, 1937; Anker, 1974).

B. Fast suction feeding adaptations

Syngnathid fishes are known to capture prey by an unusual feeding strategy known as pivot feeding (de Lussanet & Muller, 2007). They perform a rapid elevation of the head, which brings the mouth quickly close to the prey (Muller, 1987). Then, expansion of their long snout generates a fast water flow that carries the prey into the mouth. This increase in buccal volume is mainly achieved by a lateral expansion, instead of ventral expansion typical for most suction feeding fish (Roos *et al.*, 2009). The hyoid is known to play an important role in suspensorium abduction as well as in depression of the lower jaw (Roos *et al.*, 2009).

Seahorses and pipefishes are ambush predators; they sit and wait until a prey comes close to the mouth (Foster & Vincent, 2004). They are known to consume mainly small crustaceans such as amphipods and copepods (Foster & Vincent, 2004; Kendrick & Hyndes, 2005) and a recent study by Castro *et al.* (2008) showed that nematodes are also one of the main food items consumed in the wild. According to Kendrick and Hyndes (2005), the trophic specialization of these fishes can be explained by their extreme snout morphology (length and gape), their feeding behaviour and in the case of seahorses, their low mobility.

Syngnathids have a very small mouth aperture, severely limiting food particle size. The maxillary and premaxillary bones of *S. rostellatus* and *H. capensis* are rather small. Teeth, both oral and pharyngeal, are absent and prey is swallowed

whole (Lourie *et al.*, 1999b). *Gasterosteus aculeatus*, however, has a large, teeth-bearing premaxillary bone that is protrusible (de Beer, 1937; Alexander, 1967a; Anker, 1974; Motta, 1984; Nelson, 2006). Under the assumption that a long ascending process of the premaxillary bone is associated with a great amount of protrusion (Gosline, 1981; Motta, 1984; Westneat & Wainwright, 1989; Westneat, 2004), the lack of an ascending process in *S. rostellatus* and *H. capensis* indicates there is no upper jaw protrusion (Branch, 1966; Bergert & Wainwright, 1997). They do have a small rostral cartilage, dorsorostral to the ethmoid plate and medial to the maxillary bones. This rostral cartilage is not necessarily an adaptation to the powerful suction feeding but could rather be an ancestral feature also found in Percidae, Cichlidae, Atherinoidei, Gasterosteidae and others, where it assists in upper jaw protrusion (Alexander, 1967a; 1967b; Motta, 1984). Alternatively, the rostral cartilage in syngnathids could be involved in the fast rotation of the maxillary and premaxillary bones during mouth opening. Depression of the lower jaw induces a rostral swing of the maxillary bone, because of the firm primordial ligament running from the coronoid process to the maxillary bone. As a consequence of the connection between maxillary and premaxillary bones, both rotate rostrally. The mouth aperture is then laterally enclosed, resulting in a more circular gape, hence, a more rostrally directed water flow into the mouth might be generated as hypothesized by Lauder (1979; 1985) and experimentally shown by Sanford *et al.* (2009). Kindred (1921) and Kadam (1961) also found a rostral cartilage in *S. fuscus* and *Nerophis*, which is connected to the palatine cartilage with dense connective tissue. Kadam (1958) further mentions a rostral cartilage articulating with the premaxillary and maxillary bones in *Hippocampus*.

The lower jaw of *S. rostellatus* and *H. capensis* is similar to the one in *G. aculeatus*, but much shorter relative to their head length. The anguloarticular bone in the syngnathid species is more tightly fixed to the dentary bone, improving the rigidity of the lower jaw. This might facilitate abduction of the left and right lower jaws, observed during manipulation of specimens (Roos *et al.*, 2009). In the stickleback there is no fusion between the angular bone and articular bone. The angular bone also fits into a cavity of the dentary bone, but with a potential pivoting zone in between them (Anker, 1974). There is a saddle-like joint between the articular bone and the quadrate bone, as in *S. rostellatus* and *H. capensis*.

The metapterygoid bone is a perichondral ossification of the metapterygoid process of the palatoquadrate cartilage (Arratia & Schultze, 1991). In *G. aculeatus*, as in other general teleosts, the quadrate and the hyomandibular bones are connected by means of the metapterygoid bone, forming the suspensorium (Gregory, 1933; Anker, 1974). This is not the case in *S. rostellatus* and *H. capensis*, where there is no connection between the short metapterygoid and the hyomandibular bones. Neither is there a connection between the very rudimentary metapterygoid process of the pterygoquadrate part of the palatoquadrate cartilage and the hyosymplectic cartilage in the pipefish and seahorse juveniles.

The symplectic part of the hyosymplectic cartilage in S. *rostellatus* juveniles is very long compared to the hyomandibular part, with the angle between these two parts being obtuse. In *H. capensis*, both parts are almost equally long and they are perpendicular to each other. This arrangement looks very much like the one in *G. aculeatus* (Swinnerton, 1902; Kindred, 1924). Kadam (1961) describes the symplectic bone in *Nerophis* as a chondromembranous bone with a perichondral part, namely the ossification of the anterior region of the hyosymplectic cartilage, and an intramembranous part, which rises up from the perichondral part. The vertical plate bears a dorsorostral process and decreases gradually in height more caudally. This is also found in *S. rostellatus* and *H. capensis*.

At the 6.3-9.0 mm SL stage of *G. aculeatus*, where there is no ossification of the cranial cartilage yet, the hyomandibular part of the hyosymplectic cartilage already has the two-headed articulation with the neurocranium as seen in adults (Swinnerton, 1902; Kindred, 1924; de Beer, 1937; Anker, 1974). The dorsorostral condyle articulates in a socket formed by the sphenotic bone, the dorsocaudal condyle fits in a socket of the pterotic bone (Anker, 1974). In the juvenile syngnathids (*S. rostellatus*, *H. capensis* and *H. reidi*), there is only a single cartilaginous articulation. The hyomandibular bone in adult *S. rostellatus* and *H. capensis* is similar to the one in *G. aculeatus*; it also bears a double articular facet with the neurocranium, as in *H. reidi*. Dissection and manipulation of this double hyomandibular articulation in *S. rostellatus* and *H. capensis* proved that it is very firm. Strikingly, in *S. fuscus* (Kindred, 1924; de Beer, 1937), *Nerophis* (Kadam, 1961) and *S. acus* (Branch, 1966) only a single condyle is present, which is thought to

increase the freedom of movement of the hyomandibular bone (Kindred, 1924; Branch, 1966).

The connection between the suspensorium and the hyoid arch is provided by the interhyal bone. The general teleost articulation is a ball-and-socket joint, with a rod-shaped interhyal bone bearing a rounded head that fits into a facet of the suspensorium, allowing the interhyal bone to rotate in every direction with respect to the suspensorium (Anker, 1989; Aerts, 1991). The configuration in *G. aculeatus* is similar (Anker, 1974). This is not true for *S. rostellatus* and *H. capensis*, where the interhyal bone articulates with the preopercular bone dorsally and bears two articulation heads ventrally, in between which the posterior ceratohyal bone articulates. In that way, movement is more restricted to one in a rostrocaudal direction, resulting in a hyoid depression during the expansive phase of the suction feeding. The two heads of the hyomandibular bone in combination with the robust interhyal bone can be assumed to indirectly reduce the degrees of freedom between the hyoid and the neurocranium, hence contraction of the sternohyoideus muscle is expected to be translated in a more powerful hyoid depression. Fast hyoid rotation is thus possible with a reduced risk of disarticulation of the ceratohyal bone. In *S. peckianus* (McMurrich, 1883), *S. fuscus* (de Beer, 1937), *Nerophis* (Kadam, 1961), *S. acus* (Branch, 1966), *S. floridae* and *H. erectus* (Bergert & Wainwright, 1997) the interhyal bone is similar, but it is claimed to articulate with the hyomandibular bone instead of the preopercular bone.

Muller and Osse (1984) showed that high negative pressures will be reached in the gill cavity of the pipefish *Entelurus aequoreus* during prey capture. According to Osse and Muller (1980) the small gill slit and the strongly ossified gill cover are considered adaptations to the pivot type of feeding, characterized by a very fast neurocranial elevation (Muller & Osse, 1984; Muller, 1987; de Lussanet & Muller, 2007). The pressure in the opercular cavities is considered to be higher with increasing snout length, and a comparison between different syngnathid species showed that increasing snout length also results in a structurally more robust opercular bone (e.g. more ridges, greater curvature and thicker; Osse & Muller, 1980; Muller & Osse, 1984). In both, *S. rostellatus* and *H. capensis*, the gill slits are nearly closed by a firm sheet of connective tissue covered with skin with only a small aperture at the dorsocaudal tip. Their opercular bone is firm and thick and

has a convex surface which will help in withstanding medially directed forces. Comparison between the two species reveals that the opercular bone in the pipefish, which has a more elongated snout, is smaller, thicker and has a greater curvature, as expected.

The branchiostegal rays support the branchiostegal membrane, which closes the gill cavity ventrally. Among teleosts there can be more than twenty branchiostegal rays, but acanthopterygians almost never have more than eight (Gosline, 1967; Arratia & Schultze, 1990). In syngnathids the number of branchiostegal rays varies between one and three (McAllister, 1968). Here, in *S. rostellatus* and *H. capensis*, there are only two branchiostegal rays present on each side. As Gosline (1967) pointed out, the number of branchiostegal rays is related to the length of the hyoid bar. In syngnathids, the hyoid is relatively small, which might be associated with its lost function as a mouth bottom depressor (Roos *et al.*, 2009). A longer hyoid will have an increased moment of inertia resulting in hyoid depression at a lower velocity. In addition, the angle between the line of action of the sternohyoideus muscle and the hyoid will become less favourable as the hyoid length increases. Thus, the length of the hyoid bar is expected to be constrained and consequently, there will be less available space for attachment of the branchiostegal rays.

In both adult and juvenile *H. capensis* the braincase is tilted dorsally with respect to the ethmoid region so it is situated dorsocaudally to the orbita instead of caudally as in *S. rostellatus, S. fuscus* and *Nerophis* (all pipefishes; Kindred, 1921; Kadam, 1961). In the *H. reidi* juvenile (7.01 mm SL) this dorsal tilting of the otic capsule was also visible, although the tilt was less than the one in *H. capensis* juvenile (only about 20° up compared to 34° in the latter). In adult *H. capensis*, more or less the same tilt is observed (38° up). Kadam (1958) described the presence of a spheno-pterotic ridge at the base of the taeniae marginales (which he calls postorbital processes) in *Hippocampus* that appears to be missing in *Nerophis* (Kadam, 1961) and *S. fuscus* (Kindred, 1921). We also observed this ridge in *H. capensis* and *H. reidi*, but not in *S. rostellatus*. Apart from that, the hyosymplectic articulation socket mediocaudally to this ridge is more distinct in the *Hippocampus* species studied.

It is obvious that already at an early developmental age the juvenile feeding apparatus resembles that of adult *S. rostellatus* and *H. capensis*. This might be the result of the specialized parental care that enables the postponing of release from the brooding pouch until an advanced developmental state is reached. In the seahorse brooding pouch, oxygen is supplied through surrounding capillaries and the male prolactin hormone is secreted, inducing breakdown of the chorion to produce a placental fluid (Lourie *et al.*, 1999b; Carcupino *et al.*, 2002; Foster & Vincent, 2004). Lack of oxygen and endogenous energy is probably no longer a limiting factor and emergence from the pouch may be delayed, as in *Galeichthys feliceps* Valenciennes, an ariid mouth-brooder (Tilney & Hecht, 1993).

3.2. IMPLICATIONS OF SNOUT ELONGATION

Modified from:
Leysen H, Christiaens J,De Kegel B, Boone MN,
Van Hoorebeke L, Adriaens D.
Musculoskeletal structure of the feeding system
and implications of snout elongation in
Hippocampus reidi and *Doryrhamphus dactyliophorus*
Journal of Fish Biology, in press

Abstract

Syngnathids capture prey by means of high-velocity pivot feeding with suspensorium abduction and neurocranial elevation. The presence of adaptive evolutionary modifications in the cranial musculoskeletal system, related to this type of feeding, is assumed. It is hypothesized that the syngnathid trophic apparatus, being highly specialized, will show a conserved morphology among species; however, some structural variation related to variation in snout length is expected. A thorough morphological description of the feeding apparatus in a long-snouted seahorse and pipefish (*Hippocampus reidi* and *Doryrhamphus dactyliophorus*) revealed some specialized features that might be associated with

the fast and powerful suction feeding, like the two ligamentous connections between the lower jaw and the hyoid, the saddle joint of the latter with the suspensorium and the vertebro-pectoral fusion that articulates on three points with the cranium. Despite the conserved morphology of the feeding apparatus, some morphological differences were observed between the two species. For instance in *H. reidi* the orientation of the occipital joint is ventrocaudal, the sternohyoideus and epaxial muscles are more bulky and both have a short tendon. In *D. dactyliophorus*, on the other hand, the protractor hyoidei muscle is enclosed by the mandibulo-hyoid ligament, the sternohyoideus and epaxial tendons are long and a sesamoid bone is present in the latter. These features were compared to the condition in several other syngnathid species with a large range of snout lengths, in order to evaluate the implications of snout elongation on the musculoskeletal structure of the cranium. The arched path of the adductor mandibulae muscle and the greater rigidity of the lower jaw might be related to elongation of the snout since it yields an increased mechanical advantage of the lower jaw system and a reduced torque between the elements of the lower jaw during protractor hyoidei muscle contraction, respectively. Nevertheless, most observed features did not seem to be related to snout length.

3.2.1 Introduction

Pipefishes and seahorses are remarkable creatures. Their extended body is covered with an armour of bony plates instead of scales, they have independently moveable eyes and males have a special reproductive structure like a pouch or a brooding area, whether or not covered by overlapping membranes, to protect the eggs and young (e.g. Herald, 1959; Vincent & Sadler, 1995; Lourie *et al.*, 1999b; Wilson *et al.*, 2001; Kuiter, 2003; Nelson, 2006). In addition, seahorses are characterized by a grasping tail instead of a caudal fin, a vertical body axis and a tilted head (e.g. Lourie *et al.*, 1999b; 2004). The evolution to this upright body posture might be related to the Late Oligocene expansion of seagrass habitats since the vertical leaves serve as excellent camouflage for seahorses, favouring both ambushing prey and avoiding predation (Teske & Beheregaray, 2009), as well as a vertical body position has been suggested to increase the distance from which

a prey can be captured during suction feeding in seahorses (Van Wassenbergh *et al.*, 2011). Besides all this, syngnathids have a tubular snout, formed by the elongation of the ethmoid region (chapter 3.1). Within the family a large diversity in the snout morphology exists, ranging from very short-snouted species, like *Siokunichthys breviceps* Smith, to species with an extremely elongated snout, like *Phyllopteryx taeniolatus*. All syngnathid species studied thus far are known to perform fast and powerful suction feeding with that snout (e.g. chapter 5.1; Ryer & Orth, 1987; Bergert & Wainwright, 1997; de Lussanet & Muller, 2007; Van Wassenbergh *et al.*, 2008; Storero & González, 2009). In teleosts, suction feeding is the most common feeding pattern. It involves a fast enlargement of the oro-branchial cavity resulting in a pressure difference between the inside of that cavity and the surrounding water. When the jaws open, a water flow is created which will transport the prey into the mouth. The oro-branchial expansion can be generated in ventral, dorsal, lateral and rostral directions by hyoid depression, neurocranial elevation, suspensorial abduction and both maxillary protrusion and lower jaw depression, respectively (Lauder, 1983). In pipefishes and seahorses, however, the jaws are not protrusible (Branch, 1966; Bergert & Wainwright, 1997) and there is almost no ventral expansion of the buccal cavity by means of hyoid rotation (Roos *et al.*, 2009). Instead, the main buccal volume increase in syngnathids is achieved by rapid suspensorial abduction, induced by the depression of the hyoid and lower jaw, where neurocranial elevation positions the mouth close to the prey (Roos *et al.*, 2009). This type of feeding, where only the head and not the entire body is accelerated towards the prey, is called pivot feeding (de Lussanet & Muller, 2007) and is also found in some deepsea fishes and flatfishes (Tchernavin, 1953; Muller & Osse, 1984; Gibb, 1995; 1997).

Despite a large variation in the snout morphology (Kuiter, 2003), the feeding mechanism of syngnathids seems quite conserved. Hence, the question is what the best morphology, *i.e.* long or short snout, would be for optimal performance during this specialized type of suction feeding. Kendrick and Hyndes (2005) predicted that syngnathids with longer snouts would be able to attack prey from a greater distance and with greater speed than those with shorter snouts, and thus would be more successful at catching relatively fast moving prey. This prediction was confirmed by a dietary analysis of both short and long-snouted species; the latter had consumed a greater amount of mobile prey. Also de Lussanet and

Muller (2007) argued that the optimal snout length is a species-specific trade-off between a long snout on the one hand, which decreases the angle the head needs to rotate and hence the time to approach the prey, and a short snout on the other hand, which decreases the moment of inertia of the head resulting in faster prey intake. Roos *et al.* (submitted a) performed kinematical analyses of prey capture events in both a long- and a short-snouted pipefish, respectively *Doryrhamphus dactyliophorus* (Bleeker) and *Doryrhamphus melanopleura* (Bleeker). They noted that the total distance travelled by the snout tip during pivot feeding is larger in the long-snouted pipefish. This suggests that species with a long snout can attack prey from further away, so probably more elusive prey can be caught. On the other hand, short-snouted species showed lower prey capture times. Besides that, they also found that prey catching efficiency was substantially less in long-snouted pipefishes compared to the pipefishes with a short snout. Since a correct positioning of the mouth with respect to the prey is crucial, the observed difference in prey catching efficiency might be related either to the prey type used in the experiment, which could have been too small for the long-snouted *D. dactyliophorus* to allow accurate aiming, or to the larger distance between the snout tip and the eyes in the long-snouted pipefish (Roos *et al.*, submitted a). A more recent study (Roos *et al.*, 2011) shows that a large snout diameter improves volume increase and expansion time, but negatively effects maximal flow velocity. A long snout reduces both maximal flow velocity and suction volume, however, as mentioned before, the time to reach the prey is decreased.

Considering the highly specialized feeding strategy of syngnathids, *i.e.* the high-velocity pivot feeding with suspensorium abduction and neurocranial elevation, it can be assumed that this has been associated with adaptive evolutionary modifications in the cranial musculoskeletal system. In addition, more specialized species are generally thought to show a reduced morphological versatility since even the smallest deviation of one element of the complex integrated system can have an effect on the performance (Adriaens & Herrel, 2009). Hence, the hypothesis tested in this study is that the syngnathid trophic apparatus, being highly specialized, will show a conserved morphology to some degree but where existing structural variation can be related to variation in snout length. Also, since changes in the snout geometry will have an impact on functional lever systems (especially at the level of tendons, ligaments and their

attachments), differences are expected to be found that reflect compensations to sustain kinematic *versus* force efficiency in these lever systems. For example, elongation of the snout and with it that of the jaw closing adductor mandibulae muscle complex, is expected to be associated with a change in its musculoskeletal architecture. So, an arrangement of the jaw closure apparatus in the longer snouted species to assure the same kinematical efficiency is expected. The mechanical advantage of the lower jaw lever system is for instance increased by increasing the height of the coronoid process of the dentary bone (where the adductor mandibulae tendons attach), or by a more dorsocaudally orientated muscle's line of action with respect to the jaw articulation. Also, when the protractor hyoidei muscle contracts while the mouth is kept closed, it might induce some torque between the elements of the lower jaw. Long-snouted species likely generate higher strain levels in the muscle and therefore the interdigitation between the anguloarticular and dentary bones is expected to be more firm. Finally, when snout length increases, the moment of inertia during head rotation will increase as well, so a larger power output is needed to accomplish fast neurocranial elevation. This might be realised by a larger epaxial muscle mass or an improved power amplifying system, such as a longer epaxial tendon.
To validate these hypotheses, a thorough morphological description of the feeding apparatus in a long-snouted seahorse, *Hippocampus reidi*, and an extremely long-snouted pipefish (*D. dactyliophorus*) is presented, to establish morphological traits that could be associated with the specialized feeding type. These traits are compared among several other syngnathid species with a large range of snout lengths to determine the implications of snout elongation on the musculoskeletal configuration of the feeding apparatus.

3.2.2. Brief material & methods

All animals were obtained from commercial trade in accordance with the CITES requirements (Table 2.1).
Dissections were performed on three specimens of *H. reidi* (113.7 mm, 138.1 mm and 152.8 mm SL), one specimen of *D. dactyliophorus* (103.5 mm SL), one *Hippocampus abdominalis* Lesson specimen (222.7 mm SL), one *D. melanopleura*

specimen (56.5 mm SL), two specimens of *Corythoichthys intestinalis* Ramsay (120.8 mm and 136.2 mm SL), one *Doryrhamphus janssi* specimen (105.6 mm SL) and one *Dunckerocampus pessuliferus* specimen (112.3 mm SL).
Three specimens of *H. reidi* (117.2 mm, 113.5 mm and 109.7 mm L_S), one of *D. dactyliophorus* (105.1 mm SL), two of *C. intestinalis* (102.7 mm and 117.6 mm SL), one of *Hippocampus zosterae* (32.8 mm SL) one of *D. melanopleura* (41.6 mm SL) and two of *D. janssi* (81.5 mm and 90.8 mm SL) were cleared and stained for bone and cartilage according to the protocol of Taylor and Van Dyke (1985).
Serial histological cross sections of the head of a *H. reidi* (103.5 mm SL), a *D. dactyliophorus* (91.2 mm SL), a *H. zosterae* (29.0 mm SL), a *D. janssi* (102.7 mm SL) and a *D. pessuliferus* (94.5 mm SL) specimen were made.
CT-scans of another specimen of *H. reidi* (119.0 mm SL), the dissected *D. dactyliophorus* specimen (103.5 mm SL), the dissected *H. abdominalis* specimen (222.7 mm SL), a specimen of *C. intestinalis* (120.2 mm SL), the dissected *D. melanopleura* (56.5 mm SL) and the sectioned *H. zosterae* specimen (29.0 mm SL) were made and computer-generated 3D-reconstructions were generated to visualize musculoskeletal topography of the cranium. The 3D-reconstruction of *H. reidi* shows a slight distortion at the level of the snout, which is probably an artefact due to the alignment (Fig. 3.8). However, this does not impair the qualitative interpretations in this study.

3.2.3. Results

A thorough description of the head morphology of *H. reidi* and *D. dactyliophorus* is given as a representative pipefish and seahorse feeding apparatus, which is further used for a comparison with that of other syngnathids species. Special attention is paid to the structures that are expected to have undergone modifications related to differences in snout length, as hypothesized in the introduction. Next, comparison of those structures is made between several syngnathid species with varying snout length.

A. Morphological description of *Hippocampus reidi*

Both lower jaw halves of *H. reidi* consist of Meckel's cartilage, and the dentary, the anguloarticular and the retroarticular bones. The dentary bone (Fig. 3.8A, 3.9) is the largest element. It bears no teeth and roughly has a triangular shape when viewed laterally. The dorsocaudal prominent coronoid process is connected to the ventrolateral surface of the maxillary bone by means of the primordial ligament. Two of the adductor mandibulae muscle bundles, namely A1 and A2, attach onto the coronoid process (Fig. 3.8A, 3.9, all adductor mandibulae tendons were reconstructed together (t-A) and their different attachment sites were observed on dissections). A1 attaches by means of a slender bifurcated tendon, of which the dorsal part attaches onto the dorsomedial surface of the maxillary bone and the ventral part on the coronoid process of the dentary bone. The A1 muscle bundle (Fig. 3.9A) is situated in between the medial A3 and the lateral A2 and runs dorsal to the latter to the caudal edge of the symplectic bone where it attaches. The bundle A2 (Fig. 3.8B, 3.9A) is the most lateral one, with the longest tendon and the largest muscle mass. Fibres are orientated rostrocaudally and attach on the preopercular and hyomandibular bones. The A3 tendon attaches ventrally on the medial face of the dentary. The short and thin A3 muscle sheet is the most medial bundle of the muscle complex and attaches on the rostral margin of the symplectic bone. The muscle bundle is in all three cases much longer than the tendon in front of the muscle and they all run almost in a straight line. The dentary bone is provided with a tube-like cavity in which the tapering end of the anguloarticular bone fits. At the medial side of the dentary bone, the stout mandibulo-hyoid ligament (Fig. 3.8C, 3.9) attaches ventrocaudally, which is connected to the anterior ceratohyal bone. More rostrally and close to the dentary symphysis, there is a small attachment site of the thin protractor hyoidei tendon (Fig. 3.8C). The protractor hyoidei muscle (Fig. 3.8A, 3.8C, 3.9A, 3.10A) runs ventrally to the mandibulo-hyoid ligament and attaches to the posterior ceratohyal bone (see chapter 5.1 for a more detailed description of this muscle). The rostral tendon of the protractor hyoidei is covered dorsally by the intermandibularis muscle (Fig. 3.8C) connecting left and right dentary bones. The anguloarticular bone (Fig. 3.8A, 3.9) bears a rostral process enclosed by the dentary cavity and the angular part of the coronoid process stretches along the caudal margin of the dentary bone. The dentary and anguloarticular bones are

firmly fixed by connective tissue and form a single functional unit. Caudally, the anguloarticular bone forms a saddle-shaped cartilaginous articulation for the quadrate bone surrounded by strong ligaments. The retroarticular bone (Fig. 3.8A, 3.8C, 3.9) is a very small bone that is connected to the interopercular bone by means of a firm mandibulo-interopercular ligament.
Both the premaxillary and maxillary bones are reduced and toothless bones that articulate with each other dorsally. The premaxillary bone (Fig. 3.8A, 3.8B, 3.9) is a slender bone that has a somewhat wider head that tapers ventrally. Both premaxillary heads are ligamentously connected and a short ligamentous sheet connects the premaxillary bone to the maxillary bones rostrally. The maxillary bone (Fig. 3.8A, 3.8B, 3.9) is more robust with a broadening ventral part where the primordial ligament attaches. Dorsally at the maxillary heads a ligament attaches that runs to the autopalatine bone. In between the left and right maxillary bones, a rostral cartilage is situated, which is enclosed by a large ligament that runs to the vomeral bone. The maxillary bones articulate with the cartilage dorsally to the vomeral bone.

The suspensorium forms the lateral wall of the tubular snout and most elements are therefore elongated. The small autopalatine bone (Fig. 3.8A, 3.8B, 3.9B) is a slender bar with a thickened rostral end, situated in a horizontal plane lateral of the vomeral bone. Its ventral side fits into a dorsal groove of the ectopterygoid bone and both are firmly connected by means of connective tissue. The rostral part of the autopalatine bone extends from this groove and articulates cartilaginously with the ethmoid cartilage dorsal to the vomeral bone. This forms the rostral one of the two articulations that moveably connect the suspensorium to the neurocranium. Apart from the horizontal part that surrounds the ventral part of the autopalatine bone, the ectopterygoid bone (Fig. 3.8A, 3.8B, 3.9B) bears a tapering descending process. This process runs along the ascending perichondral part of the quadrate bone to which it is connected through a sheet of connective tissue. The medial surface of the ectopterygoid bone is connected to the lateral side of the vomeral bone by means of a ligament. The metapterygoid bone (Fig. 3.8A, 3.8B, 3.9B) is a plate-shaped bone with a tapering end, with its ventral edge covered by the circumorbital bones. Rostrally it surrounds the dorsolateral surface of the quadrate bone and caudally its ventrolateral end is

covered by the lacrimal bone to which it is strongly attached by means of connective tissue. The quadrate bone (Fig. 3.8, 3.9B) consists of two parts, *i.e.* an ascending perichondral one with the quadrato-mandibular articulation at its base and a large horizontal plate with a tapering end. The mandibular articulation is saddle-shaped with the lateral head larger and lying more rostrally compared to the medial one. Both processes are connected to the anguloarticular bone by means of stout ligaments. Laterally to the ascending process there is a longitudinal groove, which is closed on the lateral side by the circumorbital bones. In this groove lie the tendons of the adductor mandibulae muscle complex (Fig. 3.10B). The horizontal branch of the quadrate bone reaches the nasal cavity and has a convex shape when viewed rostrally. In the space thus medially created, lie the hyosymplectic cartilage and the symplectic bone, attached to the surface of the quadrate bone by means of connective tissue. Almost halfway the length of the quadrate bone its horizontal process starts tapering, with the preopercular bone lying ventrally. There is a slender ventral gap between the two bones and the ventral edge of the quadrate bone and the dorsal margin of the preopercular bone are firmly connected through a ligament. The symplectic bone (Fig. 3.9A) is rod-shaped and bears a plate-like, dorsal crest with a rostral process. The rod encloses the hyosymplectic cartilage but the rostral end remains free, as well as the caudal part where it is still fused with the hyomandibular part of the hyosymplectic cartilage. Rostrally the perichondral part is surrounded by the quadrate bone and more caudally by the preopercular bone. The plate-like dorsal crest of the symplectic bone closes the medial side of the cavity created by the circumorbital bones in which the adductor mandibulae muscle complex runs. The A1 and A3 bundles of the complex (Fig. 3.9A) attach on the caudal and rostral part of this dorsal crest of the symplectic bone, respectively. The dorsorostral end of the symplectic bone is connected to the mesethmoid bone through a large ligament. Caudally the symplectic bone has a dorsolateral ridge supporting the adductor arcus palatini muscle (Fig. 3.8B, 3.9A). This muscle has its origin along the ventrolateral side of the parasphenoid bone and inserts on the symplectic bone rostrally and on the hyomandibular bone caudally. At the caudal tip of the perichondral rod of the symplectic bone, a firm ligament attaches medially that runs to one of the processes of the interhyal bone. The ventral side of the preopercular bone is connected to the dorsal edge of the interopercular bone by

means of a long ligament, leaving enough space for depression of the interopercular bone. Bundle A2 of the adductor mandibulae muscle complex attaches on the medial face of the preopercular and hyomandibular bones. The hyomandibular bone (Fig. 3.9A) bears a dorsorostrally and a dorsocaudally oriented articulation head that fit respectively into a socket on the ventral surface of the sphenotic bone and in the cartilaginous surface between the sphenotic, the prootic and the pterotic bones. It also has a medial and a lateral wing forming a hollow space for the levator arcus palatini muscle and the dilatators operculi muscles (Fig. 3.9A). The dilatator operculi muscle consists of two bundles, a dorsal one and a ventral one. The ventral bundle of the dilatator operculi muscle inserts medially on the dorsorostral edge of the opercular bone and has its origin on the lateral surface of the medial wing of the hyomandibular bone. It is covered by the dilatator operculi dorsalis muscle that originates at the suture of the lateral wings of the parasphenoid bone with the sphenotic bone and inserts on the dorsal process of the opercular bone by means of a tendon. For a more thorough description of the preopercular and hyomandibular bones in *H. reidi*, see chapter 5.1.

The hyoid arch consists of the interhyal, the anterior and posterior ceratohyal, the hypohyal and the basihyal bones. Although strictly not part of it, the urohyal bone is also closely associated with the hyoid. The interhyal bone (Fig. 3.8A, 3.8C, 3.9A) provides the articulation between the suspensorium and the other elements of the hyoid, which form a rigid unit. The posterior ceratohyal bone (Fig. 3.8A, 3.8C, 3.9A) has an irregular shape with a smooth dorsal surface that articulates in between the two heads of the interhyal bone. The very small attachment site of the tendon of the hyohyoideus abductor muscle that runs to the first of the two branchiostegal rays is situated at the caudal surface of the posterior ceratohyal bone. The bone tapers ventrally where there is a firm synchondrosis with the anterior ceratohyal bone. The anterior ceratohyal bone (Fig. 3.8A, 3.8C, 3.9A) has a somewhat triangular shape with a small but firm symphysis between the left and right bones close to their distal apices. Just dorsal of the symphysis, the very much reduced hypohyal bones lay together with the small basihyal bone. They are all strongly attached to the anterior ceratohyal bone and are almost incorporated by it (not visible on figures). The urohyal bone (Fig. 3.8A, 3.8C, 3.9A)

is a small, blunt bone, measuring less than the total hyoid length. The short tendon of the sternohyoideus muscle (Fig. 3.8A, 3.8C, 3.9A) encloses the urohyal bone almost entirely at its caudal tip. It is a very large muscle, which incorporates its tendon entirely (Fig. 3.10C). More details about the hyoid of *H. reidi* can be found in chapter 5.1.

The ethmoid bones form the dorsal surface of the snout and with the exception of the lateral ethmoid, they are all elongated. The narrow vomeral bone (Fig. 3.8A, 3.8B, 3.9) broadens rostrally where it articulates with the maxillary bones ventrally. Dorsally it is connected to a rostral part of the ethmoid cartilage that articulates with the autopalatine. Caudally it reaches the lateral ethmoid bone and is covered by the mesethmoid bone and the parasphenoid bone dorsally. The mesethmoid bone (Fig. 3.8A, 3.8B, 3.9A) interdigitates with the lateral ethmoid bones caudally. The parasphenoid bone (Fig. 3.8A) connects the ethmoid region with the occipital region of the skull. Along the major part of its length the adductor arcus palatini muscle originates (Fig. 3.9A). At the caudal margin of the muscle attachment, the parasphenoid bone bears two lateral wings, just behind the eyes. From there and caudally, the bone is bent upwards and fits into a cavity of the basioccipital bone.
The lateral wall of the snout is covered by a series of circumorbital bones (Fig. 3.8A, 3.8B). They are very variable in number and shape. In the reconstructed specimen there are three bones on the right side, which could be considered homologous to the antorbital, the lacrimal and the second infraorbital bones. On the left side, however, there are four circumorbital bones, of which the homology is somewhat problematic. The orbit is bordered by the lateral ethmoid bones rostrally, the parietal bone dorsally, the sphenotic bone caudally and the parasphenoid bone medially. The parietal bone (Fig. 3.8A, 3.8B, 3.9A) is the largest bone of the neurocranium, interdigitating with the mesethmoid bone mediorostrally and the lateral ethmoid bones laterorostrally. Caudal to the eyes, it has a suture with the prootic bone, the sphenotic bone, the pterotic bone, the epioccipital bone and the supraoccipital bone. Together with the latter, the parietal bone covers almost the entire neurocranial roof.
The otic region comprises the sphenotic, the prootic, the pterotic and the posttemporal bones. The sphenotic bone (Fig. 3.8A, 3.8B) has a small lateral spine

and a well developed postorbital process. From the ventral tip of this process, the levator arcus palatini muscle originates (Fig. 3.9A). The sphenotic bone forms ventrally, at the suture with the prootic bone, one of the two articulation sockets for the hyomandibular bone. The prootic bone is situated ventrally and interdigitates with all surrounding bones. At the ventral surface of the prootic bone, the adductor operculi muscle has its origin and attaches on the dorsomedial crest of the opercular bone. The levator operculi muscle (Fig. 3.9A) originates from the ventral surface of the prootic, the pterotic and basioccipital bones, and attaches along the dorsal edge of the opercular bone at the base of the dorsomedial crest. The pterotic bone (Fig. 3.8A, B) is provided with a cartilaginous socket in which the caudal articulation head of the hyomandibular bone articulates. Apart from this ventral component, the pterotic bone also has a large lateral component that fits in between the sphenotic, parietal, epioccipital and posttemporal bones. The posttemporal bone (Fig. 3.8A, 3.9A), which also bears a lateral spine, covers the neurocranium laterocaudally. There is no postparietal bone.

All the elements of the occipital region are connected to each other by serrated sutures. The supraoccipital bone (Fig. 3.8A, 3.8B, 3.9A) is wedged in between the left and right parietal bones rostrally and its caudal tapering end touches the corona (*i.e.* the first postcranial bony plate). It has an ascending profile so the neurocranium is higher than wide when viewed caudally. At the centre of the supraoccipital caudal surface, the supracarinalis muscle (Fig. 3.9A, 3.10D) attaches which runs to the neural arch of the first vertebra and to the second postcranial bony plate. It consists of a left and a right muscle bundle whose fibres are merged and hence are hard to separate. Lateral of the supracarinalis muscle attachment, the well-developed epaxial muscle attaches by means of two large, but short tendons (Fig. 3.10D). The epioccipital bone (Fig. 3.8A, 3.8B) lies medially to the posttemporal bone and laterally to the supraoccipital bone. It is surrounded by the parietal and pterotic bones rostrally and the exoccipital caudally. The exoccipital bone (Fig. 3.8A, 3.8B) flanks the occipital joint and the foramen magnum laterally. It covers the largest part of the caudal neurocranial surface and is ligamentously connected to the dorsorostral tip of the cleithrum. The basioccipital bone (Fig. 3.9A) bears the occipital joint and stretches out in between the left and right exoccipital and pterotic bones ventrally where it

interdigitates with the parasphenoid bone. The occipital joint has a ventrocaudal orientation, contributing to the angle between the head and the body in the seahorse. Synchondroses remain present, for instance in between the prootic and sphenotic bone and at the border of the basioccipital bone.

The interopercular bone (Fig. 3.8A, 3.8C, 3.9A) is a plate-like bone that lies ventrally in the snout, medially to the preopercular bone. It is connected to the latter, the lower jaw and the hyoid by means of ligaments described earlier. The subopercular bone (Fig. 3.8A, C) is a small and very thin bone ventromedial to the opercular bone to which it is connected by means of connective tissue. The opercular bone (Fig. 3.8A, B, C) is a large, convexly shaped bone that tapers at its dorsocaudal edge. Its ventrocaudal margin is rounded with the two slender branchiostegal rays running along the edge. In between the insertions of the dilatator operculi and adductor operculi muscles, there is a small cartilaginous hyomandibular articulation laterally. The attachment of the levator operculi muscle (Fig. 3.9A) can be found along the dorsal margin of the opercular bone. This straight dorsal edge follows the lateral ridge of the neurocranial floor and caudally the tapering end covers the medial cleithrum where there is a small gill slit.

B. Morphological description of *Doryrhamphus dactyliophorus*

The description of the cranium of *D. dactyliophorus* will be limited to those features in which it differs from *H. reidi*.

The dentary bone (Fig. 3.11A, 3.11C, 3.12) has a somewhat more complex shape. It is longer than wide and is provided with a prominent lateral crest that gives the rostral end a concave profile when viewed frontally. The coronoid process is less developed. The adductor mandibulae muscle complex (Fig. 3.11A, 3.12) consists of only two muscle bundles; a ventral one, thought to be homologous to the A2[4], and a dorsal one, probably homologous to A3[5], that attach both with a very long tendon onto the coronoid process of the dentary bone. The A1 bundle was not

[4] Homology is based on similar attachment sites as the A2 bundle in *Hippocampus reidi* and on the lack of a division inserting on the maxillary bones, characteristic for A1.

[5] Homology is based on the identical origin as the A3 bundle in *Hippocampus reidi* and on the ventral position of the muscle with respect to A2. However, the insertion on the coronoid process of the dentary bone, uncommon for A3, might point to a secondary division of A2 instead.

found. The fusion with the anguloarticular bone (Fig. 3.11A, 3.11C, 3.12B) seems to be more firm compared to the seahorse, as well as it has a larger process forming the posterior part of the coronoid process. The tendon of the protractor hyoidei muscle (Fig. 3.11C, 3.12A) attaches further away from the symphysis between the left and right dentary bone. The muscle is interrupted by dense connective tissue three times. Strikingly, the fibres of the protractor hyoidei muscle are enclosed by the heavily built mandibulo-hyoid ligament (Fig. 3.10E, 3.11C), leaving only the rostral and caudal bifurcating ends free.
The premaxillary and maxillary bones are identical to the ones in *H. reidi*, except for the dorsomedial process of the maxillary bone being smaller in *D. dactyliophorus* (Fig. 3.11A, 3.11B, 3.12).

The suspensorio-neurocranial articulation is a hinge joint consisting of two small projections of the autopalatine bone (Fig. 3.11A, 3.11B, 3.12B) with a cartilaginous part of the vomeral bone in between. The horizontal part of the ectopterygoid bone (Fig. 3.11A, 3.11B, 3.12B) in *D. dactyliophorus* is provided with a large laterorostral process that is absent in *H. reidi*. Caudally there is a slender groove into which the palatoquadrate cartilage and the perichondral part of the quadrate bone are situated and the ectopterygoid bone meets the metapterygoid bone dorsocaudally. As all other bones of the suspensorium, the metapterygoid bone (Fig. 3.11A, 3.11B) in this pipefish is much more elongated compared to *H. reidi*. Besides that, the most prominent difference is that the metapterygoid bone in the former has a dorsal part and a lateral part at an almost perpendicular angle to each other so that the cross section of the snout has a rectangular appearance, compared to a more circular shape in the seahorse (Fig. 3.10F). Unlike the quadrate bone in *H. reidi*, the one in *D. dactyliophorus* has no clear differentiation between the ascending perichondral part and the horizontal plate since both parts are almost similar in height (Fig. 3.11). The tendons of the adductor mandibulae muscle complex lie rostrally in a furrow of the quadrate bone that is laterally closed by the lacrimal bone and the metapterygoid bone (Fig. 3.10F). More caudally the tendons run dorsally in the snout. Somewhat more than halfway its length, the quadrate bone starts to taper and the caudal third covers the hyosymplectic cartilage and the symplectic bone laterally whereas it is covered itself by the preopercular bone. The horizontal, medial groove of the

preopercular bone (Fig. 3.11), in which the caudal end of the quadrate bone and the symplectic bone lies, bulges outwards on its lateral side. The A2 muscle of the adductor mandibulae complex (Fig. 3.12A) attaches on the medial surface of the preopercular bone and caudally on the dorsal crest of the symplectic bone. Caudally the dorsal margin of the preopercular bone curves outwards, forming the rounded border of the orbit and interdigitating with the ventrocaudal part of the second infraorbital bone. There is no preopercular spine. The perichondral part of the symplectic bone (Fig. 3.11A, 3.12A) in *D. dactyliophorus* is much longer with respect to the plate-like part, compared to the situation in the seahorse. Furthermore, the vertical plate is provided with a prominent dorsolateral crest that interdigitates with the dorsomedial part of the second infraorbital bone and that separates the ventral adductor mandibulae muscle complex from the dorsal adductor arcus palatini muscle. Bundle A3 of the adductor mandibulae muscle (Fig. 3.12A) attaches rostrally on the dorsal crest as in *H. reidi*. The hyomandibular bone (Fig. 3.12A) is blunter than the one in *H. reidi*. The medial and lateral wings of the seahorse, in between which the levator arcus palatini muscle and dilatator operculi muscles run, are here obliquely orientated, resulting in a rather ventrolateral and a dorsomedial wing. The connection with the preopercular bone is very tight as the hyomandibular bone is provided with several lateral protrusions that interdigitate with the preopercular bone. Apart from that, the hyomandibular bone and its ligament and muscle attachments are similar to those in *H. reidi*.

The shape and ligament configuration of the interhyal bone (Fig. 3.11A, 3.11C) is similar in the two species. The posterior ceratohyal bone (Fig. 3.11A, 3.11C, 3.12A) in *D. dactyliophorus* shows a lot of indentations and protrusions. The medial ones form the interdigitating parts with the anterior ceratohyal bone, ensuring a firm connection. Laterally there is a knob-like process that is also present in the seahorse but it is larger in the pipefish. The interoperculo-hyoid ligament and the tendon of the protractor hyoidei muscle attach, respectively, rostrally and just ventrally to this process. At the caudal surface, ventral to its cartilaginous head, the tendon of the hyohyoideus abductor muscle (Fig. 3.11C, 3.12A) originates. This muscle runs along with the branchiostegal rays before it attaches, so it does not attach on the rostral tip of the branchiostegals but

somewhat more caudally. Rostrally the fused branchiostegal rays are ligamentously attached to the posterior ceratohyal bone. The anterior ceratohyal bone (Fig. 3.11A, 3.11C) has the same, somewhat triangular, shape as in *H. reidi* but is spinier. The apices of the left and right bones do not diverge very much and the symphysis is located at the level of the apices, so more distal compared to the seahorse. The hypohyal bones are quite large and situated at the most dorsal half of the anterior ceratohyal bone, almost at the level of the mandibulo-hyoid ligament attachment (not visible on figures). In *H. reidi* the basihyal bone is really tiny, in *D. dactyliophorus* it is a long and slender ossification around the even longer cartilaginous basihyal rostrally. The urohyal bone (Fig. 3.11A, 3.11C, 3.12A) is long; more than three times the hyoid length. The sternohyoideus muscle (Fig. 3.11A, 3.11C, 3.12A) is not as large as that in *H. reidi*, and the well developed tendon is not incorporated by the muscle (Fig. 3.10G).

As mentioned before, the ethmoid region of *D. dactyliophorus* is much more elongated compared to that in *H. reidi*. The vomeral bone consists of a central rod with two lateral wings (Fig. 3.11A, 3.11B). Once covered by the mesethmoid bone caudally, the wings disappear whereas the central part of the vomeral bone runs up to the end of the lateral ethmoid bone. Rostrally the mesethmoid bone (Fig. 3.11A, 3.11B) tapers whereas in *H. reidi* its rostral end bifurcates. Both vomeral and mesethmoid bones show a low dorsal crest along their entire length, in the seahorse this crest is only present in the mesethmoid bone at the level of the nasal cavities. Rostrally, at the level of the parietal bones, the parasphenoid bone (Fig. 3.11A) lies in between the dorsal mesethmoid bone and the ventral vomeral bone. The caudal end of the parasphenoid bone is not bent dorsally as in the seahorse, but it does also fit in a cavity of the basioccipital bone.
In *D. dactyliophorus* there are only two circumorbital bones: a very small lacrimal bone and a large second infraorbital bone (Fig. 3.11A, 3.11B). The lacrimal bone covers the tendons of the adductor mandibulae muscle complex and the ascending process of the quadrate. Dorsally it is partially enclosed by the metapterygoid bone that separates the two infraorbital bones from each other. The second infraorbital bone (Fig. 3.10F) has an almost horizontal part and a vertical one dorsally similar to the metapterygoid bone. It covers the adductor mandibulae tendons and the metapterygoid bone rostrally and the adductor

mandibulae muscle caudally. The horizontal part interdigitates both with the symplectic bone and with the preopercular bone caudally where it forms part of the border of the orbit. In all *D. dactyliophorus* specimens studied, the number and shape of the circumorbital bones is the same. The preorbital part of the parietal bone (Fig. 3.11A, 3.11B, 3.12A) is larger in the pipefish than in the seahorse and the former does not have a spine. The spine of the sphenotic bone (Fig. 3.11A) is also absent but apart from that, there are almost no differences. The adductor operculi muscle does not originate from the prootic bone but from the pterotic bone (Fig. 3.12A). The posttemporal bone (Fig. 3.11A, 3.11B) is spineless but shows a prominent ridge. In *D. dactyliophorus* the postparietal bone is also missing.

The supraoccipital bone (Fig. 3.10H, 3.11A, 3.11B, 3.12A) has a biconcave profile in cross section where it is provided with clear attachment sites for the postcranial muscles. The supracarinalis muscle consists of a separate left and right bundle that attach directly in the concave indentations of the supraoccipital bone. These bundles run to the neural arch of the first vertebra (not reconstructed) where they attach by means of a very small tendon. Together with the epioccipital bone (Fig. 3.11A, 3.11B), the supraoccipital bone encloses a cavity for the very solid tendon of the slender epaxial muscle. Interestingly, within the tendon, a very long bony rod is embedded. The rostral part of the tendinous tissue is in fact a short, but firm ligament that connects the supraoccipital bone to this sesamoid bone. More caudally the ventrolateral surface of the sesamoid bone is covered by the epaxial muscle and its tendon. The dorsal components of both the epioccipital bone and the exoccipital bone (Fig. 3.11A, 3.11B) are larger in the pipefish, left and right bones even interdigitate with each other medially, ventral to the supraoccipital bone. The occipital joint, formed by the basioccipital bone (Fig. 3.12A), is oriented caudally so that the cranium and vertebral column lie on the same axis.

C. Other syngnathid species

For purposes of comparison with other pipefishes and seahorses only those features that might be related to snout elongation are treated.

Hippocampus zosterae (Fig. 3.13A) is a short-snouted seahorse. The articulation between autopalatine and vomeral bone involves less cartilage than the one in *H.*

reidi. The dentary and anguloarticular bones interdigitate rather loosely and the coronoid process is low with respect to the length of the lower jaw long axis. The adductor mandibulae tendons are much shorter than the muscle bundles and the protractor hyoidei muscle, which is not enclosed by the mandibulo-hyoid ligament, attaches mediorostrally on the dentary. The hyoid is a very solid structure with a firm ceratohyal symphysis. As is the case in *H. reidi*, the urohyal length is less than the hyoid length and the sternohyoideus muscle is of substantial size. There is no sesamoid bone in the short epaxial tendon and the epaxial muscle is well developed.

In *H. abdominalis* (Fig. 3.13B), a seahorse with intermediate snout length, the anguloarticular and dentary bones are not very firmly interdigitated and the dentary bone is provided with a high coronoid process. The adductor mandibulae muscle complex runs approximately in a horizontal line caudally and only about a fourth of its length consists of just tendon. The anterior part of the vomeral bone broadens somewhat and at its rostral end it articulates with the autopalatine bone by means of a point articulation. Like the other seahorses, the urohyal bone of *H. abdominalis* is shorter than the hyoid and no epaxial sesamoid bone is present. However, the protractor hyoidei muscle is enclosed by the firm mandibulo-hyoid ligament for almost its entire length, similar to the situation in *D. dactyliophorus*. The protractor hyoidei tendon attaches on the ventromedial surface of the dentary bone, rostral to the mandibulo-hyoid ligament attachment site. Somewhat more caudally, the ligament incorporates the muscle and only the caudal third of the protractor hyoidei muscle is left free. Here, the left and right bundles diverge and run ventral to the ligament to respectively the posterior and anterior ceratohyal bone, where they attach. The sternohyoideus and epaxial muscles are both well developed and have short tendons.

Corythoichthys intestinalis (Fig. 3.13C) has a short but very slender snout. Its skull bones are covered with many small indentations, especially at the level of the braincase, the opercular bone and caudally on the preopercular bone. The vomeral bone is very slim and provides a simple articulation with the autopalatine bone rostrally. Also the dentary bone is slender and its rostral part is bent upwards to almost the same height as the well developed coronoid process.

The anguloarticular bone is fairly well attached to the dentary bone. The protractor hyoidei muscle and mandibulo-hyoid ligament run separately to the posterior and anterior ceratohyal bones, respectively. The length of the adductor mandibulae tendons is small in comparison to the muscle length. The symphysis between left and right anterior ceratohyal bones is large, taking up almost half of the total hyoid length. The urohyal bone is long, being more than two times the hyoid length, and has a small bifurcation caudally. The sternohyoideus and epaxial muscles are smaller than the ones in *H. reidi*, but their tendons are not as long as in *D. dactyliophorus*. Nevertheless, *C. intestinalis* has a long and slender ossified rod within the tendon of the epaxial muscle. However, the ligamentous part that connects the supraoccipital bone with this rod is shorter than in *D. dactyliophorus*. Like all pipefishes, *C. intestinalis* has a caudally oriented occipital joint, with no angle between the head and the body.

In *D. melanopleura* (Fig. 3.13D), also a short-snouted pipefish, the snout and maxillary bones are covered with small protuberances. The occipital joint, which has a caudal orientation, is elliptically shaped and quite broad. The lower jaw in *D. melanopleura* has a fairly solid connection between the separate elements and a relatively high coronoid process. The protractor hyoidei muscle is not enclosed by the mandibulo-hyoid ligament in *D. melanopleura*. The tendons of the sternohyoideus and the epaxial muscle are all relatively long. The two muscles also have a smaller diameter than the muscles of the seahorses. *Doryrhamphus melanopleura,* like *D. dactyliophorus* and *C. intestinalis*, has a long and slender sesamoid bone within the tendon of the epaxial muscle. The urohyal bone is long, exceeding the hyoid three times in length, and the caudal bifurcation is large, almost reaching the cleithrum.

The cranium of the long-snouted *D. janssi* and *D. pessuliferus* is quite similar to the one in *D. dactyliophorus*. The lower jaw of *D. janssi* looks like the one in *D. dactyliophorus*, with a low coronoid process and robust connection between dentary and anguloarticular bone. However, the mandibulo-hyoid ligament does not enclose the protractor hyoidei muscle. In *D. pessuliferus* the lower jaw interdigitation is also firm and in addition, the protractor hyoidei muscle is enclosed by the mandibulo-hyoid ligament. In both species, the part of the

adductor mandibulae complex that consists of solely tendon is approximately half the total length and the muscle runs dorsally in the snout. The hinge-joint between the autopalatine and the vomeral bone found in *D. dactyliophorus* is a simple point-joint in these two species here. All three species have a very long urohyal bone, but in both *D. pessuliferus* and *D. janssi*, it is a forked, very slender rod. In the latter the urohyal bone keeps running in between the hypaxial muscle bundles even well beyond the pectoral fin, reaching a length of over six times the hyoid length, which is almost as long as the entire snout. In *D. pessuliferus* the urohyal length is only somewhat more than two times the hyoid length. Their sternohyoideus muscle, which is not very large, has a well developed tendon, similar to the situation found in *D. dactyliophorus*. Both *D. pessuliferus* and *D. janssi* possess a long and slim sesamoid bone in the long epaxial tendon.

3.2.4. Discussion

Pipefishes and seahorses are pivot feeders; they capture prey by means of a rapid dorsorotation of the head in combination with an equally fast expansion of the buccal cavity. Syngnathid pivot feeding starts with hyoid rotation, which is followed by neurocranial elevation (both movements are coupled in a four-bar mechanism; chapter 5.1; Muller, 1987; Van Wassenbergh *et al.*, 2008). Next, the mouth is opened, the snout is expanded and the prey is sucked in after only 6 ms approximately (Bergert & Wainwright, 1997; de Lussanet & Muller, 2007; Roos *et al.*, 2009). The specialized feeding strategy is hypothesized to be associated with morphological modifications and innovations of the feeding apparatus, especially with respect to the snout. Therefore, the morphology of the main cranial elements will be discussed in a functional context first. In the next part of the discussion, the structural variation in the cranium of all studied syngnathids is considered in an attempt to assess the implication of variation in snout length on the head morphology.

A. Specialized feeding strategy

The studied syngnathid species all have a fused dentary and anguloarticular bone, as well as a saddle-shaped quadrato-mandibular joint and a firm but mobile

dentary symphysis. The hyoid configuration resembles the one of the lower jaw in having a solid synchondrosis between the anterior and posterior ceratohyal bones, a saddle-shaped interhyo-ceratohyal articulation and a strong and flexible ceratohyal symphysis. Besides the special lower jaw and hyoid morphology, the maxillary bones are much reduced in size and the pectoral girdle is immovably connected to the vertebrae. Although these traits are not necessarily syngnathid synapomorphic characters, they might be related to the pivot feeding. These features and their assumed role during suction feeding are elaborated on, based on the morphology of *H. reidi* and *D. dactyliophorus*.

All three elements of each lower jaw half (dentary, anguloarticular and retroarticular bones) function as a single unit that articulates by means of a saddle joint with the suspensorium. This type of articulation permits only rotation in a sagittal plane, resulting in mouth opening and closing. Theoretically, lower jaw depression can be accomplished in three different ways: (1) the mandibulo-hyoid ligament translates hyoid rotation into mouth opening, (2) the mandibulo-interopercular and interopercular-hyoid ligaments form a second coupling between hyoid rotation and lower jaw depression, and (3) contraction of the protractor hyoidei muscle will also open the mouth (note that an opercular four-bar mechanism for depressing the lower jaw (e.g. Anker, 1974; Westneat, 1990; Hunt von Herbing *et al.*, 1996b; Van Wassenbergh *et al.*, 2005) is not functional in syngnathids since there is no connection between the opercular and interopercular bones). In what follows, these three lower jaw depressing mechanisms are discussed in more detail.

(1) The very well developed mandibulo-hyoid ligament attaches medially on the dentary bone, ventrorostral to the quadrato-mandibular articulation (so below the axis of rotation) and runs to the anterior ceratohyal bone. These attachment sites differ from the general actinopterygian configuration of such a mandibulo-hyoid ligament, where it connects the retroarticular process of the lower jaw with the posterior ceratohyal bone (e.g. *Oncorhynchus mykiss* (Walbaum) (Verraes, 1977), *Polypterus senegalus* Cuvier, *Lepisosteus oculatus* Winchell and *Amia calva* L. (Lauder, 1980a; Lauder & Norton, 1980), *Ateleopus japonicus* Bleeker (Sasaki *et al.*, 2006)). Verraes (1977) suggested that in *Gasterosteus aculeatus* (which belongs to the same order as the Syngnathidae; Nelson, 2006) the hyalo-mandibular ligament described by Anker (1974) is not homologous to the mandibulo-hyoid ligament of

other fishes. The mandibulo-hyoid ligament is then absent or it could have become split up in a separate mandibulo-interopercular and interoperculo-hyoid ligament (Stiassny, 1996). This might also be true for syngnathids, since the attachment sites of the mandibulo-hyoid ligament resemble the ones of the hyalo-mandibular ligament in *G. aculeatus*. An argument supporting this hypothesis is the above mentioned mandibulo-interopercular and interoperculo-hyoid ligaments being also present in syngnathids.

(2) The mandibulo-opercular ligament connects the retroarticular bone to the interopercular bone, which is in its turn connected to the ceratohyal posterior by means of the interoperculo-hyoid ligament. Obviously these three ligaments (mandibulo-hyoid, mandibulo-interopercular and interopercular-hyoid) will couple hyoid to lower jaw depression.

(3) There is also the possibility of jaw depression through contraction of the protractor hyoidei muscle. When the mouth of *H. reidi* is closed, the line of action of the protractor hyoidei muscle lies dorsal to the quadrato-mandibular joint, so contraction will not result in lower jaw depression, but instead the muscle will probably be strained and elastic energy will be stored (similar to the catapult mechanism in the epaxial muscle of syngnathids (Van Wassenbergh *et al.*, 2008)). Both *H. reidi* and *D. dactyliophorus* specimens used for the 3D-reconstructions have their hyoid and lower jaw depressed, but the mandibulo-hyoid ligament does not seem to be fully extended, as it is curved ventrally along the hyoid. This could suggest that the ligament contributes only to the initial phase of mouth opening, resulting in a lowering of the dentary (and thus also of the protractor hyoidei tendon attachment site) until the muscle line of action shifts to below the lower jaw articulation. Further lower jaw depression could then be the consequence of a sudden release of the strain energy stored in the protractor hyoidei muscle-tendon system. The mandible would then rotate further ventrally due to its own inertia, causing the slack status of the mandibulo-hyoid ligament. The tendinous interruptions of the protractor hyoidei muscle would be especially beneficial since tendons are better suited for storing elastic strain energy than muscle tissue is (Alexander & Bennet-Clark, 1977).

The mouth is closed again through the contraction of the adductor mandibulae complex, in combination with the rotation of the hyoid to its resting position

and the relaxation of the mandibular ligaments and protractor hyoidei muscle. Lower jaw adduction is also accomplished by contraction of the intermandibularis muscle that attaches close to the dentary symphysis and perhaps indirectly by contraction of the adductor arcus palatini muscle, which will adduct the suspensoria (the latter muscle might also be responsible for the initial locking of the cranial four-bar system prior to neurocranial elevation (Roos *et al.,* submitted b)).

Syngnathids do not have a typical teleostean hyoid configuration with a ball and socket joint between the interhyal and the hyomandibular bones. Instead, the interhyal bone has a rounded dorsal head that articulates with the preopercular bone and two large ventral processes that form a saddle-shaped articulation with the posterior ceratohyal bone. As in the lower jaw, this type of joint will limit the translational and rotational degrees of freedom of the articulation and may facilitate muscle action to be transferred strictly unto hyoid depression. This may reduce the risk of dislocation during fast and powerful hyoid depression, powered by the contraction of the sternohyoideus muscle. At first, all elements of the hyoid will rotate as a single rigid unit with respect to the preopercular bone. However, at a certain angle, this rotation seems to become restrained and from that point on, the interhyal bone remains immobile and the posterior ceratohyal bone starts articulating with respect to it. The angle over which the hyoid turns during suction feeding is more than 90°. Hence, once beyond the point of 90°, there is no direct contribution of hyoid depression to buccal volume increase through a lowering of the buccal floor (Roos *et al.*, 2009). Indirectly, however, hyoid depression does contribute to oral expansion via suspensorial abduction, which is the main cause of buccal volume increase (Roos *et al.*, 2009). When the hyoid is protracted, the two anterior ceratohyal bones lay at an angle with respect to each other in a way that both hyoid bars and the symphyseal hinge axis do not fall in the same plane. Contraction of the sternohyoideus muscle will therefore not only result in hyoid depression, but also in rotation of the hyoid bars at their symphysis (Aerts, 1991). This rotation will move left and right hyoid outwards along their long axis, hence, the suspensoria will be abducted. This might be aided by contraction of the levator arcus palatini muscle.

In all species studied, the maxillary bones are very much reduced and premaxillary bones are toothless. Their contribution to the buccal volume

increase during suction will not be substantial, nor are they used for grasping the prey since prey is exclusively caught by means of suction. Given the absence of an ascending process of the premaxillary bone, no real protrusion of the upper jaw seems possible. However, the configuration does allow rotation of both maxillary bones with respect to the vomeral bone. When the lower jaw depresses, the maxillary bones swing rostrally due to the primordial ligament that connects the ventral surface of the maxillary bone to the coronoid process of the dentary bone. This rostral swing could help closing the mouth opening laterally, giving it a more circular gape, which creates a more rostrocaudally oriented water flow (Alexander, 1967c; Lauder, 1979; 1985; Aerts & Verraes, 1987). The medially situated rostral cartilage, also found in *Gasterosteus aculeatus* (Anker, 1974) and for example in cyprinodontiform fishes (Hernandez *et al.*, 2009), could be a reminiscent feature that translates the rotation of the maxillary bones into movement of the premaxillary bones, similar to the kinethmoid in cyprinid fishes (Harrington, 1955; Alexander, 1966; 1967a; Motta, 1984; Hernandez *et al.*, 2007).
There is a small overlap between the cleithrum of the pectoral girdle on the one hand and both exoccipital and posttemporal bones on the other hand (a supracleithrum is absent). Since the pectoral girdle is firmly attached to the vertebral column, this overlap forms two extra articulations (left and right) between the cranium and the vertebro-pectoral complex, besides the occipital joint. These three articulation points all lay on the same axis, so fast neurocranial elevation with a reduced risk of dislocation is possible. In most actinopterygians, the pectoral girdle consists of a relatively small scapulacoracoid (or a scapula and coracoid) that supports the fin and is attached to the cleithrum, which is connected to a series of other dermal bones including the posttemporal one (Gosline, 1977; Starck, 1979; McGonnell, 2001). Unlike the situation in syngnathids, in most actinopterygians there is no connection between the girdle and the vertebral column and most elements of the shoulder girdle articulate with each other, resulting in a very mobile structure (Gosline, 1977). In *G. aculeatus*, there is a supracleithrum that is movably connected to the posttemporal bone rostrally and to the cleithrum caudally (Anker, 1974). In addition, a small costa and connective tissue provides the connexion between the cleithrum and the transverse process of the first vertebra (Anker, 1974). This situation, *i.e.* the reduced mobility compared to the typical actinopterygian

configuration, may be regarded as the plesiomorphic condition to the syngnathid configuration. On the supraoccipital bone, the supracarinalis muscle and the tendon of the epaxial muscle attach. The epaxial muscle and its tendon are involved in a power-amplifier system, which makes the extremely high-velocity rotation of the head in syngnathids possible (Van Wassenbergh *et al.*, 2008). The supracarinalis muscle is connected to the first vertebra and might also be associated with neurocranial elevation during suction feeding.

B. Variation related to snout length

The morphology of the lower jaw and hyoid, as previously described, is very similar in all studied species, regardless of their snout phenotype. This conservative morphology is precisely what was expected in these high performance suction feeders, as even a tiny change in the complex integrated system could have a negative effect on the feeding performance (Adriaens & Herrel, 2009). However some variation related to differences in snout length was expected, since an elongation of the snout is thought to influence the efficiency of the mechanics of the lever systems in the head.

Increase in snout length implies there has to be an elongation of either the adductor mandibulae tendon or muscle complex. Since powerful jaw closure is not required in suction feeding, elongation of the tendon instead of the muscle is energetically more efficient. An additional advantage of tendon over muscle elongation is that tendinous tissue occupies less space. This is reflected in the jaw muscle morphology of the species with the longest snouts: in *D. dactyliophorus, D. janssi* and *D. pessuliferus* the tendons of the adductor mandibulae are all very long, with approximately half of the distance between origin and insertion being covered by tendon alone. Besides that, elongation of the adductor mandibulae complex is expected to be associated with changes in the coronoid height, onto which the muscle attaches, or in the muscle line of action to maintain kinematic efficiency. The angle between the axis connecting the jaw joint with the attachment site of the adductor mandibulae muscle on the coronoid process (*i.e.* the in-lever arm) and the line of action of the muscle will decrease with increasing snout length. This will reduce the mechanical advantage of the lever system. The mechanical advantage increases with elongation of the in-lever arm, hence, a higher coronoid process is hypothesized to be present in long-snouted

species. The coronoid process is low with respect to the length of the lower jaw in both short- and long-snouted species (*D. dactyliophorus, D. janssi, C. intestinalis* and *H. zosterae),* whereas others (*H. reidi, H. abdominalis, D. melanopleura and D. pessuliferus*) have a relatively high coronoid process. Therefore, the hypothesis does not hold true. However, the path of the adductor mandibulae muscle is more arched in the long-snouted pipefishes (*D. dactyliophorus* and *D. pessuliferus*), and the muscle is at the snout tip ventrally supported by a ridge of the quadrate that probably prevents it from lowering during contraction. Hence, the muscles line of action at the level of the attachment site on the dentary is orientated more dorsally. This will likely result in an increased angle with the in-lever arm and could hence increase the mechanical advantage of the lower jaw lever system.

If the protractor hyoidei muscle is strained prior to mouth opening, as suggested in the first part of the discussion and based on kinematic data (Roos *et al.*, 2009), torque might be induced between the separate elements of the lower jaw. This could be more of an issue in long-snouted species, since more elastic strain energy can be stored in the long protractor hyoidei muscle and its tendon. Therefore, an increase in the amount of interdigitation and ligamentous connection between the anguloarticular and dentary bones with increasing snout length was hypothesized. In seahorses, the dentary-anguloarticular interdigitation ranged from loosely (*H. zosterae*) over intermediate (*H. abdominalis*) to rather firm (*H. reidi*) with increasing snout length, supporting the hypothesis. Also, all long-snouted pipefishes seem to have a tighter connection between the elements of the lower jaw than some shorter snouted species do, like *C. intestinalis* and *Syngnathus rostellatus* (chapter 3.1). However, another short-snouted pipefish, *D. melanopleura,* has quite a firmly interdigitated lower jaw as well.

The sternohyoideus muscle is confluent with the hypaxial muscle, which plays an important role in the coupling of hyoid rotation and neurocranial elevation (chapter 5.1; Muller, 1987; Van Wassenbergh *et al.*, 2008). Before prey capture, the epaxial and hypaxial muscles contract and tension is built up in both tendons (Van Wassenbergh *et al.*, 2008). This energy is suddenly released when the four-bar mechanism is unlocked, resulting in powerful movements of the hyoid and head. Snout elongation will increase the moment of inertia of the head, hence, a larger power output is needed to overcome this during head rotation. It is therefore hypothesized that the epaxial and sternohyoideus muscles of a long-

snouted syngnathid will either have a larger cross section or a longer tendon to, respectively, generate extra force and store extra energy for head rotation. In all seahorses, regardless of their snout length, both epaxial and sternohyoideus muscle have a short tendon and a large diameter. On the other hand, all pipefishes, with exception of *C. intestinalis*, have slender but very long sternohyoideus and epaxial tendons and muscles. Thus, no trend of either increase or decrease in tendon length or muscle diameter with increasing snout length was observed. Yet, there appears to be a phylogenetic pattern (pipefishes *versus* seahorses) in head rotation technique. The long tendon and small diameter of the sternohyoideus muscle in the pipefishes seems beneficial for generating the required power. In the seahorses, the large muscle cross section may indicate that the main power for head rotation is generated by muscle contraction (as opposed to release of stored strain energy). Potentially, the bent neck in the seahorses prevents the optimal functioning of the elastic recoil mechanism in the sternohyoideus and hypaxial muscles as found in pipefishes. However, *C. intestinalis* seems to have an intermediate configuration, with rather short tendon lengths and larger epaxial and sternohyoideus muscles. The similarity with seahorse muscle morphology might be related to their trophic behaviour, sit-and-wait feeding strategy rather than active pursuit of the prey, as in other pipefishes. Kinematical data of the path travelled by the mouth during feeding also shows a convergence between seahorses and *Corythoichthys intestinalis* (Van Wassenbergh *et al.*, 2011). Besides that, a recent phylogeny (Teske & Beheregaray, 2009) suggests a closer relationship between *Corythoichthys* and *Hippocampus* species than for instance between the latter and the genus *Syngnathus*.

Finally, the articulation between the autopalatine bone and the ethmoid cartilage at the level of the vomeral bone is merely a point articulation in *H. reidi*. However, in *D. dactyliophorus* the autopalatine bone is provided with two small lateral processes in between which the vomeral bone articulates, thus forming a hinge joint. This configuration permits motion with only one rotational degree of freedom, which might reduce the risk of dislocation during suspensorial abduction. The extremely long snout in *D. dactyliophorus* may then explain the necessity for such a stronger joint, as torque forces exerted on the snout may be more substantial during snout abduction. None of the other syngnathids (*H.*

zosterae, H. abdominalis, D. melanopleura, C. intestinalis, D. janssi and *D. pessuliferus*) have the same hinge-like articulation between autopalatine and vomeral bones.

Apart from the hypothesized differences, some other features are worth mentioning. One of those is the mandibulo-hyoid ligament that encloses the protractor hyoidei muscle entirely, thus forming a sheath for the muscle. This striking configuration is found in both long- and short-snouted pipefishes (*D. dactyliophorus, D. pessuliferus* and *C. intestinalis)* and in *H. abdominalis*, but it is absent in the others (*D. janssi, D. melanopleura, H. reidi* and *H. zosterae).* Hence, it is not related to snout length, neither is it characteristic for pipefishes. The functional advantage of this configuration, however, remains unclear.

An interesting finding related to the epaxial muscle is the presence of a long sesamoid bone embedded into its very firm tendon in all pipefishes studied. Usually, sesamoid bones are formed in tendons that pass over a joint where they protect the tendon from damage and where they could improve the mechanical efficiency of the related muscle (Sarin *et al.*, 1999; Hall, 2005). Mineralisation of an energy-storing tendon would be a bad thing since it would significantly reduce the elasticity (Currey, 2010). This loss of potential strain energy storage capacity will negatively affect the epaxial catapult performance. Potentially, the elastic energy necessary for the power enhancement is stored in the small but firm epaxial ligament connecting the supraoccipital bone with the tendon bone. The fact that this ligament is shorter in the two pipefishes with a short snout supports this hypothesis since less strain energy is required for pivot feeding in short-snouted species as the moment of inertia is lower. The epaxial sesamoid bone is found in none of the seahorses. Again, this might be explained by the seahorse's tilted head, due to which the epaxial tendon is curved. The presence of a long and rigid element within this tendon would probably impede force transfer, since the curved line of action of the epaxial muscle would not correspond to the straight long axis of the sesamoid bone. Still, the epaxial sesamoid bone is not a pipefish specific character, since it was not found in *S. rostellatus* (chapter 3.1). More comparative morphological and kinematic analyses will be required before any conclusions can be made on the functional significance of the presence or absence of this sesamoid bone.

Also, a prominent phylogenetic difference in urohyal length was observed. The seahorses studied here all have a short urohyal bone, with a length of less than

the hyoid length and lacking a bifurcation. In the pipefishes the urohyal bone is very much elongated with respect to the hyoid length (to even over six times as long in *D. janssi*). Of all pipefishes, the urohyal bone was shortest in *S. rostellatus,* with a length of about twice that of the hyoid (chapter 3.1). The urohyal length does not seem to be correlated with snout length as both short-snouted and long-snouted pipefishes have a very long urohyal bone. With the exception of *D. dactyliophorus* and *S. rostellatus*, the pipefish urohyal bone has a bifurcating caudal end, which can be small, as in *C. intestinalis,* or well developed, as in *D. melanopleura* and *D. pessuliferus,* or it can consist of two exceptionally long and slender diverging rods, as in *D. janssi*. Analogous to the epaxial sesamoid bone, the absence of an elongated urohyal in seahorses may be related to the tilted position of the head with respect to the body (making the distance along a straight line between the hyoid and the pectoral girdle too short).

In conclusion, some variation in lower jaw rigidity and adductor mandibulae muscle line of action was found, which could be snout length specific. However, most striking features, like the mandibulo-hyoid ligament enclosing the protractor hyoidei muscle, the presence of an epaxial sesamoid bone and the elongation of the urohyal bone in some pipefishes or the well developed sternohyoideus muscle in seahorses, could not be explained by variation in snout length. These traits may rather be associated with different power generating strategies, namely storage and release of elastic energy *versus* pure muscle force. However, similarity of certain features might also be associated with phylogenetic relatedness of the species; possibly not all shared traits have a purely functional base (see also discussion of chapter 4).

4 Morphological variation

Modified from:
Leysen H, Roos G, Adriaens D.
Morphological variation in pipefish and seahorse head shape in relation to snout length and developmental growth
Journal of Morphology, submitted

Abstract

The feeding apparatus of Syngnathidae, with its elongate tubular snout and tiny, toothless jaws, is highly specialized for performing fast and powerful pivot feeding. In addition, the prolonged syngnathid parental care probably enables the juveniles to be provided with a feeding apparatus that resembles the one in adults, both in morphology and function. In this study a landmark-based geometric morphometric analysis was carried out on the head of syngnathid representatives in order to (1) examine to what degree pipefish shape variation is different from that of seahorses; (2) determine whether the high level of specialization reduces the amount of intraspecific morphological variation found within the family; and (3) elucidate whether or not important shape changes occur in the seahorse head during post-release ontogeny. We found that (1) there is a significant shape difference between pipefish and seahorse head shape: the main differences concern snout length and height, position and orientation of

the pectoral fin base and height of the head and opercular bone. We hypothesize that this might be related to different prey capture kinematics (long snout with little head rotation *versus* short snout with large head rotation) and to different body posture (in line with the head *versus* vertical with a tilted head) in pipefishes and seahorses; (2) both pipefishes and seahorses showed an inverse relation between relative snout length and intraspecific variation and although pipefishes show a large diversity in relative snout elongation, they are more constrained in terms of head shape; and (3) the head of juvenile *Hippocampus reidi* specimens still undergoes gradual shape changes after being expelled from the brood pouch. Ontogenetic changes include lowering of the snout and head but also differences in orientation of the preopercular bone and lowering of the snout tip.

4.1 Introduction

The family Syngnathidae consists of pipefishes, seadragons, pipehorses and seahorses, all having a tubular snout with tiny, terminal, toothless jaws. The snout can be extremely elongate, up to a snout length of almost two thirds of the total head length as in the weedy seadragon (*Phyllopteryx taeniolatus*). In most animals jaw morphology, mouth shape and dentition type can provide a quite accurate idea about the preferred prey type and feeding strategy. The shape of a fish skull, consisting of over 30 moveable bony elements and more than 50 muscles (Lauder, 1983), reflects the individual's diet and prey capture mechanism to a great extent (Gerking, 1994; Delariva & Agostinho, 2001; Ferry-Graham *et al.*, 2001a; Palma & Andrade, 2002). Dietary influences on head morphology (or *vice versa*) are particularly evident in trophic specialists, who exploit a limited dietary breadth with respect to the available prey types in their habitat (Sanderson, 1991). These species have highly specific feeding demands and their head usually is characterized by specific adaptations which make the feeding apparatus well-suited for their diet (e.g. jaw asymmetry and specialized dental morphology in scale-eating cichlids (Liem & Stewart, 1976; Takahashi *et al.*, 2007; Stewart & Albertson, 2010)).

The syngnathid feeding apparatus and feeding strategy are highly specialized (see chapter 3.2 and 5.1). Seahorses and pipefishes approach their prey ventrally, or

they sit and wait until a prey passes above the snout. Than the head rapidly rotates dorsally to position the mouth close to the prey and almost at the same time, a fast buccal expansion creates a water flow that transports the prey into the mouth (Van Wassenbergh *et al.*, 2008). It is shown that a syngnathid suction feeding event is performed with great precision and at high speed (Muller & Osse, 1984; Bergert & Wainwright, 1997; de Lussanet & Muller, 2007). The rate of the incoming water is increased by the small diameter of the snout, hence suction velocity is enhanced. Prey intake time is as little as 6 ms, making syngnathids among the fastest feeding teleosts ever recorded (Chapter 5.1; Muller & Osse, 1984; Bergert & Wainwright, 1997; de Lussanet & Muller, 2007). Due to the tiny mouth aperture and narrow snout, the syngnathid diet consists solely of small prey items (mostly crustaceans) (Tipton & Bell, 1988; Teixeira & Musick, 1995; Woods, 2003; Foster & Vincent, 2004; Kendrick & Hyndes, 2005). We already noted the similarities between pipefishes and seahorses (the long and slender snout with small toothless jaws at the tip), but there are also some noticeable differences. Pipefishes (subfamily Syngnathinae) are characterized by a long, cylindrical body and a narrow head without spines, whereas seahorses (subfamily Hippocampinae) have an upright body axis with a prehensile tail and a high, tilted head usually with spines and a corona (*i.e.* the first nuchal plate with a crown-like process on top). In this study we are interested in the variation in syngnathid head shape and we address three different questions. First, we investigated whether pipefishes and seahorses occupy a distinct part of the syngnathid morphospace, or whether their head shape is spread over a continuum of shapes with transitional forms in between the typical pipefish and seahorse morphotypes.

Another interesting aspect is the hypothesis that the trophic apparatus in specialists is well-adapted to the prevailing circumstances. Hence, only a small deviation of one element of the specialized and complexly integrated feeding system may result in reduced functional performance of the whole system (Adriaens & Herrel, 2009). Consequently it is expected that a specialized organism will show a less versatile feeding system morphology and hence a reduced amount of intraspecific variation. So our second question is whether this can be generalized for syngnathids: does the high level of specialization influence the amount of morphological variation found within the family? Long-snouted

species are expected to be able to catch a prey from a greater distance and have shorter prey capture times (Muller & Osse, 1984; Kendrick & Hyndes, 2005; de Lussanet & Muller, 2007). Analysis of the syngnathid stomach content has demonstrated that long-snouted species consume more prey items that are relatively more mobile, compared to short-snouted species (Kendrick & Hyndes, 2005). Hence, long-snouted syngnathids can be regarded as trophically more specialized and they are therefore expected to show a reduction in morphological variation with respect to shorter snouted syngnathids.

Thirdly, not only their feeding apparatus and strategy makes syngnathids an interesting study object, they are particularly well known for their remarkable parental care. Normally, newly hatched larval fishes are not fully developed yet, however their feeding apparatus must be operational by the time the yolk sac is resorbed. Often this critical period is accompanied by a dietary shift during development so that in early stages feeding can occur in a different way and on different prey items than after the transition to juvenile and adult feeding. This can involve intense morphological transformations during ontogeny (e.g. the ventral shift of the mouth in the suckermouth catfish *Ancistrus* cf. *triradiatus* described by Geerinckx *et al.* (2005) or the radical transformation from tapetail to whalefish as recently discovered by Johnson *et al.* (2009), which consists of a major increase in jaw length among other things). In syngnathids, however, this metamorphosis does not take place (at least not after release from the pouch): newly born seahorses are known to be provided with an adult feeding apparatus and prey capture kinematics (Van Wassenbergh *et al.*, 2009). This similarity is facilitated by the prolonged parental care in seahorses and pipefishes; embryos hatch in a special brood area on the male body where they are nourished and protected (Lourie *et al.*, 1999b; Carcupino *et al.*, 2002; Foster & Vincent, 2004). Release of the young into the free world is delayed until an advanced developmental stage has been reached; likely the incredible investment of seahorse parents in their offspring has extended the developmental phase in the pouch (Chapter 3.1 and Foster & Vincent, 2004; Dhanya *et al.*, 2005; Van Wassenbergh *et al.*, 2009). All elements of the external skeleton in juvenile pipefishes and seahorses are present and they are capable of independent feeding at the moment of release from the pouch (Kornienko, 2001; Foster & Vincent, 2004). Therefore it is plausible that all great morphological transformations will

take place during the period in the brood pouch. The only changes that are likely to occur after being expelled from the pouch will be the result of differential relative growth patterns (allometries) since the relative snout length of newly released seahorses is much smaller compared to the one of adults. Traditional morphometric research has demonstrated that there are some gradual ontogenetic changes in relative head and snout dimensions. Choo and Liew (2006) noted a decrease in head length, head height, snout length and snout height in relation to standard length in *Hippocampus kuda,* with snout length and height increasing relatively to head length and height. Other allometries were observed by Roos *et al.* (2010) in *H. reidi,* where snout length increased and snout height decreased relative to head length. However, potential subtle differences in head shape (e.g. position of the corona, orientation of the opercular bone, steepness of the mesethmoidal curvature) rather than changes in head dimension could not be discovered with the applied linear measurements. Detection of these shape changes within a coordinate system requires a detailed geometric morphometric analysis. The final question of this research is whether or not juvenile seahorses still show a period with substantial morphological transformations after release from the brood pouch.

The previously mentioned questions were addressed by quantifying the morphological variation in the cranium of a broad range of syngnathid representatives. First we examined to what degree pipefish shape variation is different from that of seahorses. We performed a landmark-based geometric morphometric analysis on the external head of a large number of syngnathid representatives and expected it to yield a clear separation of the two subfamilies, due to the prominent differences in head height and tilting among other things. Secondly, we examined whether syngnathid shape variation is constrained in relation to relative snout length, either at an inter- or intraspecific level. For this part, our predictions are based on the previously formulated assumption that a high level of specialization is associated with a reduction of morphological variety. If this hypothesis holds true, a long-snouted pipefish or seahorse species, being more specialized than a short-snouted one, will show a reduced level of intraspecific morphological variation. For the same reason, at an interspecific level, we expected pipefishes, which can have extremely elongated snouts and thus are trophically more specialized, to be morphologically more constrained

than seahorses. To test this hypothesis at an intraspecific level, a regression analysis between the relative average snout length of a species and the variance of the shape variables of that species as a proxy of intraspecific variation was carried out. For the hypothesis at an interspecific level, we compared both subfamilies in terms of their variance. Finally, we investigated the hypothesis that syngnathids do not experience extensive ontogenetic shape changes from the moment they are released from the pouch because important morphological transitions have likely occurred during the period of parental care.

4.2. Brief material & methods

In total 368 specimens of 38 different species were analyzed morphometrically (Table 2.3). This includes 54 juvenile specimens of *Hippocampus reidi*, ranging in age between 1 and 65 days, which were used for the ontogenetic study in combination with the adults of *H. reidi*. Animals were sacrificed and fixed as described in chapter 2.2.2 and the right side of the head of all animals was photographed (see chapter 2.2.3).

The geometric morphometric analysis involved the use of the Thin Plates Spline freeware (tps; Rohlf, F.J., State University of Stony Brook, New York) as explained in chapter 2.2.9 and figure 2.3.

The range of snout lengths in our sample did not adequately reflect the diversity in relative snout length known to exist in the pipefish subfamily; it lacked short-snouted pipefishes. For example, species like *Siokunichthys bentuviai* Clark and *Anarchopterus* (Dawson) have a relative snout length of respectively about 0.180 and 0.250 (measurements made on drawings by Dawson in Kuiter, 2003), which is even shorter than the relative snout length of the seahorse species with the shortest snout in our analysis, *Hippocampus zosterae*. Therefore, drawings of the lateral side of the head of 11 short-snouted species and one long-snouted species (*Microphis caudocarinatus* (Weber)) made by Dawson (1978; 1983; Kuiter, 2003) were added to the original dataset (Table 2.3). These drawings did not include a scale bar, hence for analyses relying on size factors (e.g. regression between centroid size and relative warp scores) the drawings were left out. The use of the dataset without the drawings is clearly mentioned throughout the results.

We carried out the same analyses without LM2, because its position (on the distal point of the dentary bone) is expected to be dependent on the gape (Fig. 2.3). In specimens with a depressed lower jaw LM2 will be located more ventrorostrally compared to its position in fishes with a closed mouth. Omitting LM2 allowed us to assess the consequences of this potential error.

Another tps-file was made for the ontogenetical analysis (see chapter 2.2.9).

For those species represented in the analysis by more than ten specimens, the species variance was calculated using the following formula:

$$\sum_j \frac{{d_{ij}}^2}{(n_i - 1)}$$

with d_{ij} the Euclidean distance of all RW scores that together explain over 95% of the total variation of the j^{th} specimen in species i to the RW scores of the species consensus, and n_i the number of specimens in species i. The species variance is a measure of how much each specimen within a species deviates from the species consensus; the larger the variance, the more divers that species is. Hence, it is a reflection of the morphological intraspecific variation of a species.

The same formula was used to determine a measure for interspecific variation for pipefishes and for seahorses respectively, only the overall subfamily consensus was used instead of the species consensus and all species variances were summed for each subfamily. The previously mentioned formula is calculated analogous to the partial disparity described by Foote (1993), but it has the number of specimens in a subgroup (n_i-1) in the denominator rather than the total number of specimens of all subgroups combined (N_i-1). In this way, the proxy for intraspecific variation is less susceptible to differences in subgroup size.

4.3. Results

A. Overall shape variation

Firstly, no differences between the results with or without LM2 were observed, hence the dataset including LM2 was used because it allowed us to interpret lower jaw length (distance between LM3 and LM2).

In addition, we could prove that simplification of a picture by a drawing did not affect the placing of landmarks since the results after adding the drawings were as expected: the short-snouted species all cluster together near the *Doryichthys* species, which are also short-snouted, and the long-snouted pipefish *Microphis caudocarinatus* could be found closer to the other long-snouted species (Fig. 4.1).
As expected, the Goodall's F test showed that there is a significant difference between pipefishes and seahorses (F-score = 713.03; df = 26.00, 7800.00; p-level < 0.0001; Bootstrap p-level = 0.0002).
The first and second relative warp scores are plotted to visualize the shape differences (Fig. 4.1). The first axis of the relative warp plot (RW1), which explains 75.08% of the total variation, separates pipefishes from seahorses. Positive scores of the RW1 (*i.e.* pipefish morphotype) mainly reflect a vast decrease in head height with respect to the consensus (ventral shift of LM10 and LM11) and a dorsal displacement of the shortened pectoral fin base (dorsal shift of LM13 and LM14). In addition, they reflect a dorsoventral shortening of the opercular bone (shortening of the distance between LM15 and LM8), an increase in snout length (caudal displacement of LM6 and LM7) and a dorsoventral lowering of the snout and lower jaw (dorsal shift of LM2, LM3 and LM4). Specimens at the other extreme (*i.e.* seahorse morphotype) have a large and very high head (dorsorostral shift of LM10 and dorsocaudal shift of LM11), a dorsoventrally enlarged opercular bone (dorsal shift of LM8 in combination with the ventral displacement of LM15), a relatively short but high snout (convergence of LM1-5 with LM6-7 together with a ventral displacement of LM3, LM4 and LM15) and an elongated and ventrally displaced pectoral fin base (ventrorostral shift of LM13 and even more so for LM14) compared to the consensus configuration.
The shape changes represented by the second relative warp axis, which explains 10.02% of the total shape variation, also reflects variation in snout height (dorsoventral shift of LM1 and LM5), snout length (divergence or convergence of LM5 and LM6) and head length (rostrocaudal movement of LM8 and LM15 together with rostrocaudal movement of both LM13 and LM14), but all to a lesser degree compared to RW1. Besides that, RW2 represents variation in a rostrocaudal pectoral fin base displacement (shifts in LM13 and LM14 position

along the long axis of the head) and in the orientation of the opercular bone (rostrocaudal movement of LM8 with respect to LM15).

B. Shape variation and snout dimensions

The regression analysis (of the dataset without the drawings) showed that less than 3.5% of the total shape variation was explained by either centroid size or log head length, indicating that the obtained RW scores are independent of size. On the other hand, 65.32% of the overall variation is explained by differences in relative snout length. Of all relative warps, the first is the only one that is correlated with relative snout length (a correlation coefficient of 0.89). Hence, these results confirm that one of the main differences between the pipefish and seahorse morphotype is their relative snout length, as was already evident from the comparison of deformation grids along RW1. Also, the first relative warp axis is significantly negatively correlated with relative snout height (a correlation coefficient of -0.92).

Four pipefish and four seahorse species are represented in the analysis by more than ten specimens and thus their species variance was calculated as a proxy for intraspecific shape variation as described earlier (Table 4.1). Both pipefish and seahorse subfamilies seemed to show an inverse relation between relative snout length and intraspecific variation, so the morphological variation of long-snouted species is likely to be more constrained than that of short-snouted species (Fig. 4.2). However, with only four data points in each group, there was not sufficient statistical support for this trend. Another thing that can clearly be noted is that almost each seahorse species shows a higher amount of intraspecific variation than the pipefishes. This was also found on an interspecific level, overall variation was lower for pipefishes ($4.86\ 10^{-3}$) than for seahorses ($7.78\ 10^{-3}$).

Table 4.1 – List of the four pipefishes and four seahorses for which the intraspecific variation was calculated

species	number of specimens	mean (SnL/HL) ± st dev	intraspecific variation
Syngnathus rostellatus	15	0.458±0.011	1.46E-03
Syngnathus typhle	15	0.483±0.038	3.55E-03
Syngnathoides biaculeatus	18	0.553±0.026	1.59E-03
Microphis brachyurus aculeatus	95	0.578±0.012	0.96E-03
Hippocampus reidi	12	0.426±0.026	3.39E-03
Hippocampus ramulosus	18	0.354±0.032	8.33E-03
Hippocampus guttulatus	29	0.360±0.029	8.03E-03
Hippocampus kuda	40	0.428±0.036	6.94E-03

It is obvious from the plot of RW1 *versus* RW2 scores (Fig. 4.1) that the seahorse specimens are scattered all around the graph whereas the space occupied by the pipefishes is more stretched along an axis as if not all possible positions in the syngnathid morphospace could be occupied. This difference was quantified by performing a linear regression between RW1 and RW2 (accounting for the most prominent shape changes), resulting in a correlation coefficient of R^2=0.61 (p-level<0.0001) for pipefishes compared to R^2=0.08 (p-level<0.0001) for seahorses. This proves again that seahorses show a higher level of interspecific variation and that pipefishes all follow a similar morphological pattern. The pipefish morphospace is best described as an ellipse with the long axis primarily explaining differences in relative snout length, but also in snout height, rostrocaudal position of the pectoral girdle, head height and opercular height. This trend probably depends greatly on the selection and number of specimens and species in the analysis.

C. Ontogenetic scaling

The adult *Hippocampus reidi* specimens are well separated from the other age classes by a combination of the first and second relative warp axis, explaining, 40.25% and 16.75%, respectively, of the total shape variation (Fig. 4.3). Apparently, even after 65 days, changes in head shape still occur. Ontogenetic shape transitions from a one day old stage to adult involve a reduction of the obtuse angle between the rostral edge of the opercular bone and the snout to an almost right angle (dorsorostral shift of LM8 and to a lesser degree of LM15), dorsoventral lowering of the snout tip (ventral displacement of LM1 with respect to LM5) and tilting of the pectoral fin base (dorsocaudal shift of LM13 and even more of LM14), besides a dorsoventral lowering of the head with respect to its length (ventral displacement of LM10 and LM11) and a dorsoventral compression of the snout (dorsal shift of LM3, LM4 and LM15) (Fig. 4.3). To evaluate the presence of different stages or inflexion points in the ontogeny, we plotted head length (as a measure of age) over relative warp scores. Although there are changes in head shape during post-release development, no clear trend in head shape over time could be established (Fig. 4.4).

4.4. Discussion

An important remark is that some of the variation found might be caused by phylogenetic non-independency. Related species might share the same traits due to shared ancestry. To control for phylogenetic relatedness in comparative analyses, a fully resolved phylogeny is required. Unfortunately a tree including all pipefish and seahorse genera is currently not available. Hence, the results of this geometric morphometric analysis need to be interpreted carefully.

A. Pipefish *versus* seahorse shape variation

Both subfamilies are morphologically clearly separated from each other, suggesting a bimodal distribution in head shape on subfamily level instead of a morphological continuum (Fig. 4.1). The main differences between the pipefish and seahorse head shape are snout length and height, position and orientation of the pectoral fin base and height of the head and opercular bone. The short-snouted pipefishes cluster at the left hand side of the pipefish morphospace, as expected since the first relative warp axis, separating pipefishes (+RW1) from seahorses (-RW1), is highly correlated with snout length (Fig. 4.1). However, they do not occur more to the left in the plot than *Hippocampus zosterae,* yet the relative snout length of some of them is smaller. This confirms that RW1 reflects more than just relative snout length, as elaborated on in the results.

The first relative warp axis is correlated positively with snout length and negatively with snout height. When relative snout length is plotted over relative snout height for all syngnathids studied, linear regression yields a negative slope (slope=-0.3794, R^2=0.81, p-level<0.0001). Hence an increase in relative snout length results in a decrease of relative snout height and this relation is more pronounced in pipefishes (slope=-0.3134, R^2=0.67, p-level<0.0001) compared to seahorses (slope=-0.1982, R^2=0.36, p-level<0.0001). In pipefishes, absolute snout height does not vary much over a wide range of snout lengths, so long-snouted pipefishes tend to have a relatively narrow snout. De Lussanet and Muller (2007) have determined that the optimal snout length of syngnathids is inversely related with snout cross-section. If it can be assumed that natural selection would favour an optimal snout length, our results confirm the hypothesis of de Lussanet and Muller (2007). They stated that a long snout is advantageous since it minimizes

the angle over which the head must be turned and hence reduces the time to reach the prey (de Lussanet and Muller, 2007). However, a longer snout implicates a larger striking distance, which may reduce striking success (Roos *et al.*, submitted a). Moreover, an increased snout length implies a higher total moment of inertia, which negatively influences the angular acceleration of head rotation. Reduction of the cross-sectional area of the snout decreases the total moment of inertia and compensates for the longer snout. This is confirmed by our analysis. Muller & Osse (1984) reasoned that the velocity and acceleration of the water relative to the mouth opening increases with increasing snout length, hence faster prey can be caught. Roos *et al.* (2010) established this experimentally since they found that the snout length in both juvenile and adult *H. reidi* approaches the optimal length for a given width, in order to minimize the time to reach prey. Apparently, long-snouted species only require limited head rotation in comparison with a short-snouted species that requires a large excursion of the head to overcome the same distance. In addition, the increase in cranial rotation performance by snout elongation is opposed to the associated reduction in suction performance (Roos *et al.*, 2011). Improvement of the efficiency of the two different aspects of pivot feeding, *i.e.* head rotation *versus* suction performance might be reflected in pipefish *versus* seahorse morphology. Seahorses have an upright posture and in rest their head is at an acute angle with their body. During head rotation of a feeding strike, the supraoccipital bone slides under the corona (thus producing the characteristic clicking sound (Colson *et al.*, 1998)). Pipefishes, on the other hand, have their head in line with their body at the beginning of a prey capture event. Manipulation of cleared and stained specimens (*D. dactyliophorus, S. rostellatus* and *C. intestinalis*) showed that from a certain angle, further head rotation is mechanically impeded. Either the cranio-vertebral joint morphology limits neurocranial elevation or the supraoccipital bone or the epaxial bones (very long and slender ossifications within the tendon of the epaxial muscle in some pipefishes, see chapter 3.2) are pushed against the first nuchal plate (no sliding was observed in pipefishes). Muller & Osse (1984) suggest a mechanical limitation of head rotation by the ligament connecting the supraoccipital bone with the cleithrum (which they refer to as the plate formed by the fused pectoral radials and dorsal vertebral processes). We presume that the seahorse configuration might allow for a greater rotation of the head with

respect to the body compared to the pipefish situation. If this hypothesis holds, seahorses do not need to have an extremely elongated snout to overcome the prey-mouth distance as a vast amount of cranial rotation would suffice to reach the prey. A recent study by Van Wassenbergh *et al.* (2011) proved that the bent trunk orientation of seahorses improves feeding performance by increasing the strike distance. A typical pipefish body orientation, on the other hand, appears to be beneficial by increasing strike velocity. Another reason to assume improved head rotation performance with an increase in tilting of the head is the large insertion site for the well-developed epaxial muscle, which plays a crucial role in neurocranial elevation, on the high supraoccipital bone in seahorses. Experimental support for the hypothesis is found in kinematical data: neurocranial elevation in adult *Hippocampus reidi* reaches 31° (Chapter 5.1) and even as much as 40° in juvenile *H. reidi* (Van Wassenbergh *et al.*, 2009), *versus* a rotation of only about 20° in *Syngnathus leptorhynchus* Girard (Van Wassenbergh *et al.*, 2008) and rotation does not exceed 10° in *Doryrhamphus dactyliophorus* or *D. melanopleura* (Roos *et al.*, submitted a). However, Bergert and Wainwright (1997) found a neurocranial elevation of 29° in *S. floridae*, equal to what they recorded for *Hippocampus erectus*, which shows that our hypothesis cannot be generalized for all syngnathids. A comparative study of the supraoccipital-nuchal plate morphology and mechanics that will help resolve this is called for.

Other morphological differences between pipefish and seahorse heads, *i.e.* ventral position of the pectoral fin base and opercular bone higher than long in the latter, might also be explained as a consequence of the head tilting in seahorses. The pectoral girdle is attached to the vertebral column so the ventral displacement of the pectoral fin base observed in our deformation grids, actually represents a shift of the entire body from a caudal position to a ventrocaudal one with respect to the head. At the same time, by tilting the head with the pectoral girdle immovably fixed to the vertebral column, the distance between the caudal margin of the preopercular bone and the rostral tip of the cleithrum is reduced leaving only little space for the gills in rostrocaudal direction. This might have caused the branchial chamber in seahorses to expand more in a dorsoventral direction hence the height of the opercular bone exceeds its length (the opposite is the case in pipefishes).

We demonstrated the existence of several differences in the head shape of pipefishes and seahorses, yet they evolved from the same ancestor. The oldest fossils of the family date 50 Myr back and morphologically resemble modern pipefishes (Teske *et al.*, 2004; Teske & Beheregaray, 2009). It would be interesting to see where in the syngnathid morphospace the most recent common ancestor, from which pipefishes and seahorses diverged from each other, will plot. According to a recent publication by Teske and Beheregaray (2009) pipehorses of the genus *Idiotropiscis* can be regarded as the extant evolutionary link between seahorses and pipefishes. These seahorse-like pipefishes swim horizontally but their head is tilted ventrally over an angle of about 25° with respect to the body (Kuiter, 2004). Based on pictures, the head of *Idiotropiscis* species seems to stand midway between the one of pipefishes and seahorses in terms of snout and head dimension. Hence, it is expected to show other transitional features as well, for instance in the position of the pectoral fin and the shape of the opercular bone. A future geometric morphometric analysis that includes one of the three *Idiotropiscis* species might yield elucidating results with respect to syngnathid evolution.

B. Shape variation and snout length

We hypothesized that there would be a greater amount of morphological variation within a short-snouted species *versus* within a long-snouted one (intraspecifically) and also in seahorses compared to pipefishes (interspecifically). As explained before, the expectation that long-snouted species would be morphologically more constrained follows from the experimentally based assumption that they are more specialized. Support for syngnathids with a long snout being more specialized was found in gut contents analyses. The diet of long-snouted syngnathids consists of a higher number of mobile prey compared to what is ingested by short-snouted species (Franzoi *et al.*, 1993; Kendrick & Hyndes, 2005). This suggests that a long snout enables a species to capture prey from a greater distance and in a shorter time, as argued by Muller and Osse (1984) and de Lussanet & Muller (2007), and was later demonstrated by Roos *et al.* (submitted a). Hence long-snouted syngnathids can be confidently regarded as trophic specialists.

Our preliminary results on intraspecific variation are within our expectations: for both pipefishes and seahorses there is an indication of a negative relationship between relative snout length and degree of intraspecific variation. In other words, the more specialized a species (longer snout), the more morphologically constrained it is (reduced variation). However we must be careful when drawing conclusions from these results as we only looked at four different species for each subfamily and also because both the correlation coefficient and the slope in pipefishes are small (R^2=0.26, slope=-0.0102). Adding another species might change the observed relationship between pipefishes and seahorses. For future research, it will be interesting to include other species, both short-snouted ones (for instance *H. zosterae* and *Siokunichthys bentuviai*) and long-snouted species (*D. dactyliophorus* and *H. barbouri* Jordan & Richardson) to see if the present inverse relation still stands.

On an interspecific level, seahorses show a higher degree of variation compared to pipefishes. However, we must note that the average relative snout length of the four pipefish species is higher than that of the four seahorse species. Since we saw that long-snouted species are morphologically more constrained than short-snouted ones, the difference in interspecific variation (*i.e.* pipefishes having less variation than seahorses) is possibly the result of our selection of long-snouted pipefishes *versus* shorter snouted seahorses. Nevertheless, if we look at the distribution of all specimens, both long- and short-snouted ones, in the plot of RW1 *versus* RW2 scores (Fig. 4.1), we see that the morphospace occupied by seahorses is smaller compared to the pipefish morphospace. Hence, the diversity in relative snout shape is larger for pipefishes than for seahorses. Yet, the fact that the pipefish specimens have an elliptical distribution in the plot suggests that they are more constrained in terms of cranial morphology since all specimens follow a similar allometric pattern. Although some further investigation is needed, for now we can conclude that the level of interspecific variation in seahorses probably is higher than in pipefishes.

Studies dealing with the effect of specialization on morphological diversity are scarce. Holliday & Steppan (2004) investigated how hypercarnivory (specialization to a meat-only diet) affects morphological variation in mammalian carnivores. They found that hypercarnivores show significantly lower morphological diversity than their primitively non-hypercarnivorous sister

groups, which probably is related to functional constraint. These findings support our observation within syngnathids.

A methodological consideration might be the fact that in these analyses specimens belonging to the 'species' *H. guttulatus* Cuvier, *H. kuda* and *H. ramulosus* Leach were used. These 'species' are known to be species complexes and they encompass various morphotypes. Lourie *et al.* (1999b) do not even recognize *H. ramulosus* as a separate species but rather as a synonym of *H. guttulatus*. Currently, there is no alternative to using these species complexes as they have not been revised yet. The use of the invalid species name *H. ramulosus* should be avoided, however, the seahorse identification key (Lourie *et al.,* 2004) often does not yield one unambiguous species name but rather various possible solutions. Hence, here the assignment of specimens to the species complexes is preferred over the use of unidentifiable specimens. Furthermore, this complication of seahorse identification does not take the edge of the results of the geometric morphometric analysis. For the calculation of the RW scores, the variation among specimens (and not groups) is calculated hence whether a specimen belongs to species A or species B will not change its position on the RW1 versus RW2 plot. On an intraspecific level, it might be so that what we consider now as one species in fact are several, which could reduce the amount of intraspecific variation for the separated species compared to what we have found here. However, there is no reason to assume that breaking down the species complex into separate species will affect the intraspecific variation differently for long- *versus* short-snouted species. Hence, in the absence of taxonomical clarification, we do not consider the use of species complexes an issue.

C. Shape variation and ontogenetic scaling

No evidence of saltatory development was found that could contradict the hypothesis that in syngnathids complex morphological changes and ontogenetic modifications takes place during the extended period of parental care in the brood pouch and not afterwards. In many other fish, freshly hatched embryos possess a yolk sac for endogenous nutrition. The yolk sac will be depleted at the transition to active feeding; a period characterized by the development of the jaw

apparatus and hence changes in head shape. In syngnathids, there is no larval period and metamorphosis is absent or occurs in the brood pouch, so the feeding apparatus is already fully developed before emerging (Kornienko, 2001; Choo & Liew, 2006). This is consistent with the findings for *Syngnathoides biaculeatus* (Bloch), *Hippocampus kuda* and *H. reidi*, where the newborns resemble miniature adults with a completely functional feeding apparatus and a fully absorbed yolk sac (Dhanya *et al.*, 2005; Choo & Liew, 2006; Roos *et al.*, 2011). Another reason to expect little change is the fact that prey capture events in juvenile seahorses are observed to be even faster than in adults, 2.5 ms compared to 5 ms (Van Wassenbergh *et al.*, 2009 and chapter 5.1). To ensure the success of the incredibly rapid pivot feeding, the combined movement of all elements involved in the feeding apparatus (lower jaw, hyoid, neurocranium, suspensorium and operculum) is required. The slightest deviation of one element from its normal path might cause a reduction in performance. So, juvenile seahorses are expected to be highly constrained, not only morphologically but also kinematically.

Still the juveniles differ from the adults; among the main allometric shape changes are lowering of the snout and head with respect to snout length, but also a different orientation of the preopercular bone and of the snout tip. Roos *et al.* (2010) noticed a transition from short and broad snouts to long and narrow ones during the development of *H. reidi*. This supports our findings that the head of juvenile seahorses still undergoes gradual shape changes after release from the brood pouch. Reynolds number of the juvenile's environment is relatively low and therefore the escape response of the (even smaller) prey items will be limited (Larsen *et al.*, 2008; Roos, 2010). High-velocity head rotation for a fast approach of the prey is thus no necessity; on the other hand, powerful suction is required to set the viscous fluid into motion. A feeding apparatus with a short and broad snout is beneficial for optimizing suction performance and is hence typically found in juvenile syngnathids.

Probably the allometric shifts in buccal cavity shape, changes in the orientation of the opercular bone and lowering of the snout tip will have an effect on the hydrodynamics of suction feeding. The high efficiency of the feeding mechanism in juvenile *H. reidi* can most likely only be assured if along with these morphological changes the kinematics of prey capture were also altered to a certain degree. Indeed, ontogenetic changes in the snout dimension of *H. reidi*

appear to have an influence on suction feeding capacity and on cranial rotation performance (Roos *et al.*, 2011).

5 Functional interpretation

5.1. KINEMATICS OF THE FEEDING APPARATUS

Modified from:
Roos G*, Leysen H*, Van Wassenbergh S, Herrel A, Jacobs P, Dierick M, Aerts P, Adriaens D.
Linking morphology and motion: A test of a four-bar mechanism in seahorses.
Physiological and Biochemical Zoology 2008, 82:7-19.
* authors with equal contribution

Abstract

Syngnathid fishes possess a highly modified cranium characterized by a long and tubular snout with minute jaws at its end. Previous studies indicated that these species are extremely fast suction feeders with their feeding strike characterized by a rapid elevation of the head accompanied by a rotation of the hyoid. A planar four-bar model is proposed to explain the coupled motion of the neurocranium and the hyoid. Because both neurocranial elevation and hyoid rotation are crucial for the feeding mechanism in previously studied Syngnathidae, a detailed evaluation of this model is needed. In this study, we present kinematic data of the feeding strike in the seahorse *Hippocampus reidi*. We combined these data with a

detailed morphological analysis of the important linkages and joints involved in rotation of the neurocranium and the hyoid and we compared the kinematic measurements with output of a theoretical four-bar model. The kinematic analysis shows that neurocranial rotation never precedes hyoid rotation, thus indicating that hyoid rotation triggers the explosive feeding strike. Our data suggest that while neurocranium and hyoid initially (first 1.5 ms) behave as predicted by the four-bar model, eventually, the hyoid rotation is underestimated by the model. Shortening, or a posterior displacement of the sternohyoideus muscle (of which the posterior end is confluent with the hypaxial muscles in *H. reidi*), probably explains the discrepancy between the model and our kinematic measurements. As a result, while four-bar modelling indicates a clear coupling between hyoid rotation and neurocranial elevation, the detailed morphological determination of the linkages and joints of this four-bar model remain crucial in order to fully understand this mechanism in seahorse feeding.

5.1.1. Introduction

Suction feeding is present in most vertebrate groups, including frogs (Dean, 2003), salamanders (Elwood & Cundall, 1994), turtles (Van Damme & Aerts, 1997) and even mammals (Bloodworth & Marshall, 2005). However, suction feeding is ubiquitous in some groups, such as teleost fish (Muller & Osse, 1984; Lauder, 1985) and elasmobranchs (Wilga *et al.*, 2007). The kinematics of suction feeding have been studied and compared between a wide variety of fish (e.g. Carroll & Wainwright, 2003; Gibb & Ferry-Graham, 2005; Van Wassenbergh *et al.*, 2005). Among the fish species studied, a striking variation in head morphology can be found, ranging from the asymmetrical morphology found in flatfish (Gibb, 1997) to the more general laterally compressed percomorph morphology in largemouth bass (Svanbäck *et al.*, 2002) to the extremely elongated upper and lower jaw found in long-jawed butterfly fish (Ferry- Graham *et al.*, 2001a). However, despite these great differences in cranial morphology, all these species have converged behaviourally to perform suction feeding.

According to Lauder (1985), prey capture through suction is characterized by four phases: preparation, expansion, compression and recovery. During the

preparation phase, the buccal cavity is compressed and consequently the buccal volume is decreased. In the subsequent expansion phase, the mouth opens quickly through hyoid rotation or through the coupling between the lower jaw, the interopercular bone and the operculum. After mouth opening, the suspensorium abducts laterally and the cranium rotates dorsally. Because of this rapid expansion of the head, the volume in the buccal cavity increases rapidly, subsequently sucking in the prey with the surrounding water. To ensure a continuous posterior flow of water, the expansion movement must proceed from the front to the back of the head. This is often termed the rostrocaudal expansion sequence and is observed in all suction-feeding teleosts studied to date (e.g. Lauder, 1985; Carroll & Wainwright, 2003; Gibb & Ferry-Graham, 2005; Van Wassenbergh *et al.*, 2005). During the compression phase, the mouth of the fish closes, the suspensorium adducts and the hyoid elevates, together decreasing the volume of the buccal cavity. Finally, the opercular and branchiostegal valves open, allowing the sucked water to flow out of the buccopharyngeal cavity through the gill arches. In the last phase, the recovery phase, all the skeletal elements return to their original position.

One of the most extreme cranial morphologies in teleost fish is undoubtedly found in syngnathid fishes. These fish are characterized by an elongated tubular snout with minute jaws at its end. Despite this peculiar feeding morphology, it is unclear whether they have converged on the general teleost suction-feeding pattern as mentioned above. However, it is known that seahorses and pipefish use suction to capture their prey (Muller, 1987; Bergert & Wainwright, 1997; de Lussanet & Muller, 2007; Van Wassenbergh *et al.*, 2008). Moreover, their feeding strike is characterized by a very fast rotation of the hyoid and a rapid elevation of the head. Prey capture times within 6 ms are recorded, making them among the fastest suction-feeding vertebrates (Bergert & Wainwright, 1997; de Lussanet & Muller, 2007; Van Wassenbergh *et al.*, 2008). To execute such extremely rapid movements, Muller (1987) suggested a need for power amplification. More recently, Van Wassenbergh *et al.* (2008) verified that the rapid elevation of the head is probably accomplished by elastic recoil of the tendons of the epaxial muscles.

Muller (1987) also postulated a mechanical linkage between the elevation of the neurocranium and the rotation of the hyoid and described a four-bar linkage

model by which the rapid dorsal rotation of the neurocranium could power the expansion of the oropharyngeal cavity and cause explosive suction. The proposed four-bar model consists of the ceratohyal-interhyal complex, the sternohyoideus-urohyal complex, the neurocranium-suspensorium complex and the pectoral girdle (Fig. 1.6). If this four-bar linkage is kept in a locked position and accompanied by active muscle contraction, elastic energy could potentially be stored and later released. In pipefish, it was originally hypothesized and later demonstrated (Muller, 1987; Van Wassenbergh *et al.,* 2008, respectively) that the hyoid is kept in a locked position while the epaxial and hypaxial muscles contract. Through shortening of the muscles, the tendons of the epaxial muscles lengthen and could store elastic energy. A small deviation of the hyoid from its stable position could then trigger the release of previously stored elastic energy, resulting in very fast movements of the head and the hyoid.

In spite of these hypotheses, our understanding of these extremely fast movements is limited because of the relative low temporal resolution of the recordings of the suction event in previous studies (200–400 frames per second [fps], Bergert & Wainwright, 1997; 1,000 fps, de Lussanet & Muller, 2007; but 2,000 fps, Van Wassenbergh *et al.,* 2008). However, to test the proposed four-bar system, a quantitative analysis of the movements of the cranial elements during the strike is essential. Additionally, a detailed study of the spatial topography and morphology of the joints and linkages of the proposed four-bar system is crucial for our understanding of the functioning of the system.

In this study, we examined the feeding kinematics and cranial morphology in the seahorse species *Hippocampus reidi*. Quantification of the movements of the cranial elements during prey capture combined with a detailed 3D-analysis of the morphology of the linkages in the proposed four-bar system based on serial histological sections and CT-scanning allows us to test the validity of the model proposed by Muller (1987). Moreover, these data can provide insight on how the extreme suction performance of these animals is achieved.

5.1.2. Brief material & methods

Different *Hippocampus reidi* specimens were used for the morphological analyses and the collection of kinematic data.

A. Morphology

Three specimens (117.2, 113.5 and 109.7 mm SL; Table 2.1) were cleared and stained according to the protocol of Taylor and Van Dyke (1985). On one of them, dissections were performed on the hyoid for a clearer view of the articulation facets. Serial histological cross sections (5 µm) of the head of a fourth specimen (103.5 mm SL) were made. The fifth *H. reidi* (119.0 mm SL) was scanned at the modular micro-CT setup of Ghent University using the directional tube head, at 80 kV tube voltage. Next, computer-generated 3D-reconstructions were made based on CT-data and histological sections to visualize overall morphology. For more details on methods, procedures or protocols, see chapter 2.2.

Only those muscles, tendons, ligaments and cartilaginous elements related to the hyoid were reconstructed (see chapter 3.2 for the complete reconstructions). The 3D-reconstruction, using the histological data, shows a slight distortion at the level of the snout (Fig. 5.1C), which is probably an artefact due to the alignment. Only serial sections of the cranial skeleton were used, so the cleithrum was not fully reconstructed (see Fig. 3.8 for a complete reconstruction).

B. Kinematics

Two days before a planned filming session, we stopped feeding the animals. During the recording sessions, animals were placed in a smaller tank (0.3 m × 0.2 m × 0.05 m) with a scale bar attached to the tank. At the time of the experiments, five animals were fed small crustaceans attached to the outflow of a pipette.

Movements of several cranial elements were quantified during prey capture by means of lateral view high-speed video recordings. The video recordings were made using a Redlake Imaging MotionPro digital camera (Redlake, Tucson). Four arrays of eight each red ultra bright LEDs were used for illumination. Sequences were filmed at 2,000 fps with a shutter time of 0.2 ms. Only videos in which the head was oriented perpendicular to the lens of the camera were retained for further analysis, thus eliminating correction for parallax. A total of 14 recordings

from five individuals were used, namely three videos of four individuals and two of one individual.

Eight landmarks were digitized (Fig. 5.2) frame by frame using Didge software (A. Cullum, Creighton University, Omaha, NE): (1) the tip of the nose spine, just anterior of the eye; (2) the tip of the snout posterior to the maxillary bones; (3) the symphysis of the ceratohyal bones; (4) the distal tip of the ventrolateral spine on the pectoral girdle; (5) the tip of the process on the second nuchal plate; (6) the proximal tip of the premaxillary bone; (7) the distal tip of the dentary bone; and (8) a distinct point on the prey that could be tracked down during the whole sequence (e.g. the eye).

Based on the X and Y coordinates of these landmarks, five variables were calculated: (a) mouth opening (distance 6–7); (b) hyoid angle (angle between 1–2 and 3-p, p being the coordinate of the centre of the interhyal bone, of which the position was first determined based on a CT-scan and subsequently recalculated for each time step based on the position of the neurocranium landmarks 1–2); (c) neurocranial elevation (angle between 1–2 and 4–5); (d) cleithrum to hyoid distance (distance 3–4); and (e) prey distance (distance 6–8).

In order to reduce digitation noise, the kinematic profiles were filtered using a fourth-order low-pass zero phase shift Butterworth filter with a cutoff frequency of 500 Hz and velocities and accelerations were calculated through numerical differentiation of the smoothed displacement profiles. The maximal displacements, velocities and accelerations of each variable were measured as well as the time needed to reach maximal displacements. Time 0 was defined as the image before the first visible movement.

C. Four-Bar Model

The coupling between the rotation of the neurocranium and the hyoid was evaluated by calculating the output of the planar four-bar system described by Muller (1987). The following landmarks were defined as the joints in the four-bar system (Fig. 5.2): (p) the centre of the interhyal bone; (q) the point of articulation of the neurocranium and the vertebral column–pectoral girdle complex; (r) the mediorostral tip on the cleithrum near the origin of the sternohyoideus muscle (s); and the symphysis of the ceratohyal bones. CT-scan image reconstructions were used to determine the positions of these four-bar joints relative to the

digitized landmarks on the high-speed video images (Fig. 5.2). The coordinates of p and q were calculated with respect to a frame of reference defined by two points moving with the neurocranium (landmarks 1–2; Fig. 5.2). Similarly, the coordinate of r is calculated with respect to landmarks 4–5 (Fig. 5.2). Finally, because the coordinate of s at time t = 0 corresponds to a digitized coordinate (landmark 3; Fig. 5.2), the initial configuration of the four-bar system at t = 0 is set.

From this moment on, the distances of pq, ps, rs and qr are kept constant. The neurocranium-suspensorium bar qp was chosen as the fixed bar (*i.e.* the frame). The time-dependent change in the angle between pq and qr equalled the change in the measured neurocranial elevation angle and was used as input motion. The formulas presented in Aerts and Verraes (1984) were used to calculate the resultant rotation of the hyoid with respect to the frame under the four-bar conditions described above. Because the in vivo measured hyoid angle (angle 1–2 to 3-p, Fig. 5.2) is also available, the four-bar model prediction can be compared with this angle for each time step sampled in the kinematic analysis.

In order to visualize the spatial configuration of the model components before and after neurocranial elevation, the following procedure was executed. Based on the 3D-reconstruction of the CT-data, 3D-coordinates (bilateral where possible) were retrieved using Amira 4.1.0 software from a selection of 23 articulation points and skeletal reference points (Fig. 5.3). The coordinates were then imported into Rhinoceros 3.0 software to construct a simplified model of those structures involved in the hyoid rotation and neurocranial elevation: (1) mandibulo-quadrate articulation; (2) mandibular symphysis; (3) premaxillary symphysis; (4) rostral tip of the vomeral bone; (5) distal tip of the nose spine; (6) articulation between the supraoccipital bone and the corona (*i.e.* the first nuchal plate); (7) distal tip of the dorsocaudal process on the corona; (8) distal tip of the process on the second nuchal plate; (9) articulation between the neurocranium and the first vertebra; (10) articulation between the neurocranium and the pectoral girdle; (11) distal tip of the ventrolateral spine on the pectoral girdle; (12) tip of the angle formed between the dorsal horizontal arm of the pectoral girdle and the vertical arm; (13) rostral point of the pectoral complex (formed by the cleithrum and several plates of the bony armour); (14) caudal tip of the urohyal bone; (15) symphysis of the ceratohyal bones, (16) articulation between posterior

ceratohyal bone and interhyal bone; and (17) articulation between interhyal and preopercular bones.

D. Statistics

In order to statistically determine whether a difference in timing exists between cranial rotation, hyoid rotation and mouth opening, a contingency table (Fisher's exact test) was used. Data from feeding sequences in which movements occur at the same time frame were omitted from the contingency table. In case a temporal distinction occurs, the contingency table tests whether or not this difference in timing is significant. Note, however, that this statistical test does not rule out that the actual movements might occur at exactly the same instant. This separation of the data set was used only for this specific statistical analysis.
To compare our measurements with the predicted values of the model, a paired t-test was used at each time frame to determine at which instant the predicted and the measured values statistically differ. In addition, a least squares regression analysis was used to investigate whether a strong correlation exists in our kinematic data between the angles of hyoid rotation and cranial rotation during the feeding sequence.

5.1.3. Results

A. Morphology

The following description based on the histological data was confirmed on *in toto* cleared and stained specimens.
The hyomandibular bone bears three cartilaginous articulation heads: two dorsally for the sphenotic bone and the cartilaginous surface between the sphenotic, the prootic and the pterotic bones respectively and a laterocaudal rounded condyle for the opercular bone (Fig. 5.1A,C). Both the opercular and neurocranial processes are surrounded by ligaments. A lateral and a medial wing on the hyomandibular bone form a groove in which the levator arcus palatine muscle lies dorsally and the preopercular bone interdigitates with the ventral side of the lateral wing. The hyomandibulo-sphenotic ligament is connected to the distal tip of the lateral wing and a ligament connected to the parasphenoid bone

attaches on the medial wing. Along its medial length, the hyomandibular bone is provided with a tendinous attachment of the adductor arcus palatine muscle. Ventrorostrally, there is a synchondrosis between the hyomandibular bone and the symplectic bone (Fig. 5.1A). A firm ligament runs between the hyomandibular and the interhyal bones. The hyomandibular bone in *Hippocampus reidi* is not connected to the metapterygoid or interhyal bones, as it usually is in teleosts (Gregory, 1933; Harrington, 1955; Rojo, 1991). According to Jungersen (1910) the contact between the metapterygoid and the hyomandibular bones is lost in the families Centriscidae, Aulostomidae, Solenostomidae and Syngnathidae, whereas Anker (1974) showed that it is still present in *Gasterosteus aculeatus*.

The preopercular bone is a very long L-shaped dermal bone (Fig. 5.1B). Its horizontal branch stretches out rostrally and is attached to the quadrate and the interopercular bones through ligaments. Caudally, the vertical branch is tightly connected to the lateral face of the hyomandibular bone through an interdigitation and connective tissue. Medially, it bears a ridge that supports the symplectic bone along its length and the levator arcus palatini muscle fits into a longitudinal groove (Fig. 5.1A). Laterally, it bears a spine. The levator arcus palatini muscle inserts tendinously mediocaudally onto the preopercular bone. The articulation with the interhyal bone is situated ventrally where the horizontal and vertical branches meet. Ligaments attached to the ventral surface of the preopercular bone enclose the joint for the interhyal bone. The preopercular bone supports the snout laterally and forms a large part of the suspensorium.

The perichondral interhyal bone is small, solid and bears a lateral and a medial head ventrally (Fig. 5.4). Dorsocaudally, the rounded cartilaginous surface forms a condyle that fits into the socket joint of the preopercular bone. In between the lateral and medial process of the interhyal bone, a saddle joint is formed where the posterior ceratohyal bone articulates. The lateral process bears ligaments that run to the posterior ceratohyal and preopercular bones, while massive ligaments from the symplectic and the hyomandibular bones attach onto the medial head dorsally and ventrally, respectively. Ligaments from both processes thus enclose the joint cavity between the interhyal and the posterior ceratohyal bones. The plane of the articulation facet between the preopercular bone and the interhyal

bone is oriented obliquely. The orientation of the long axis of the interhyal bone runs from ventromedially to slightly dorsolaterally (Fig. 5.1A).

The perichondral posterior ceratohyal bone is very irregularly shaped. Apart from the caudal saddle-shaped facet, which articulates in between the two processes of the interhyal bone, two heads are present on the proximal part of the posterior ceratohyal bone: a lateral one and a ventral cartilaginous one (Fig. 5.4). The interoperculo-hyoid ligament, connecting the interopercular bone with the posterior ceratohyal bone, attaches rostral to this lateral process. The slender tendon of the protractor hyoidei muscle runs ventral to the interoperculo-hyoid ligament and attaches on the lateral side of the posterior ceratohyal bone (Fig. 5.1B, 5.4A). Its lateral border supports the two slender branchiostegal rays. At its distal end, the posterior ceratohyal bone bears a thin, tapering process that interdigitates with the anterior ceratohyal bone. Apart from this interdigitation, there is a firm synchondrosis and a ligamentous connection between the anterior and posterior ceratohyal bones.

The anterior ceratohyal bone that incorporates the small hypohyal bone is larger than the posterior one and is more or less triangularly shaped (Fig. 5.4). The apex of the triangle is situated rostrally, where there is a small but very firm medial symphysis composed of connective tissue between the distal end of the left and right anterior ceratohyal bones. More proximally, a ligament connects the latter with the very small cartilaginous basihyal bone. Ventrally, at the apex, a ligament running to the urohyal bone attaches (Fig. 5.1, 5.4A). The mandibulo-hyoid ligament runs from the dentary bone as a single unit along the snout. When it reaches the hyoid, it separates into three parts. All parts attach together medially in a cavity of the anterior ceratohyal bone. Caudally, the anterior ceratohyal bone bears several slender processes in between which the long rod of the posterior ceratohyal bone fits.

The urohyal bone is a small, more or less cylindrical bone. Rostrally, it bears a thin dorsomedial ridge, giving the urohyal bone a triangular shape at its front in cross section (Fig. 5.4). A short and stout ligament attaches on both sides of the ridge and runs to the anterior ceratohyal bone. The tendon of the sternohyoideus muscle encloses the urohyal bone caudally (Fig. 5.1).

The large cleithrum forms the majority of the pectoral girdle. In lateral view, it is roughly comma-shaped, with a bigger dorsal part and a rostrally bent ventral part

(Fig. 5.1B). The dorsal component is flattened laterally except for a medial branch that interdigitates firmly with the processus transversus of the first vertebra (Fig. 5.1A). Laterally, this part is mostly covered by the dorsocaudal edge of the opercular bone. There is also a dorsocaudal interdigitation with the second nuchal plate, which lies posterior to the corona. Rostrally, a solid ligament runs from the rostral tip of the cleithrum to the caudal end of the exoccipital bone. This tip fits between the caudal end of the posttemporal bone laterally and the exoccipital bone medially, forming the articulation between the pectoral girdle and the neurocranium. A ligamentous connection with the posttemporal bone, which forms part of the neurocranium in *H. reidi*, is lacking. The ventral part of the cleithrum is bifurcated, with a medial branch contacting the scapulacoracoid and a lateral branch running ventrally, where it interdigitates with the bony armour forming some sort of pectoral complex (Fig. 5.1C). As such, the medial and lateral branches enclose a heart-shaped cavity into which the sternohyoideus muscle and pectoral fin musculature lie. These two branches fuse more caudally and form a bony sheet dorsal to the muscles.

The protractor hyoidei muscle is generally considered to be embryologically formed by the fusion of the intermandibularis posterior and the anterior interhyoideus muscle (Winterbottom 1974), but see Geerinckx and Adriaens (2007) for a discussion of possible misinterpretations on the true nature of this muscle. In *H. reidi*, however, both parts can still be clearly distinguished from each other because they are well separated by a tendinous connection (Fig. 5.1C). Rostrally, two short tendons are connected to the medial face of the left and right dentary bones, ventral to the anterior intermandibularis muscle (connecting the two dentary bone). The posterior intermandibularis part starts as two individual bundles of fibres fusing almost halfway along their length when reaching the tendinous connection. Fibres of both the posterior intermandibularis and the anterior interhyoideus muscle run in a longitudinal direction. Although not visible on the reconstruction, the serial sections show that along its entire length, the anterior interhyoideus consists of two bundles separated in the middle by a thin layer of connective tissue. More caudally, the bundles diverge, giving the muscle its typical X shape. Attachment by a long and slender tendon occurs on the lateral face of the posterior ceratohyal, just ventral to attachment of the interoperculo-hyoid ligament (Fig. 5.1B, 5.4A).

The sternohyoideus muscle inserts rostrally on the urohyal bone by a firm tendon that caudally splits into two and continues to run in between the fibres (Fig. 5.1). The muscle is enclosed by ventral bony plates of the body and partly by the lateral and medial branch of the cleithrum nearly along its entire length. More caudally, the bony armour extends laterally, with the pectoral fin musculature being situated dorsally. The site of origin of the sternohyoideus muscle is the cleithrum, the scapulacoracoid and the ventral bony plates onto which the muscle attaches through a layer of connective tissue. The two large and firm bundles of the sternohyoideus muscle course ventrorostrally and unite rostrally. Caudally they join the fibres of the hypaxial muscle.

B. Kinematics

During the preparatory phase, the animal approaches its prey relatively slowly. Next, the expansion phase is characterized by a fast rotation of the hyoid and a rotation of the head and snout. The mouth starts to open a few milliseconds later (Table 5.1; Fig. 5.5). Cranial elevation causes the mouth opening to be positioned in close proximity to and directed towards the prey, which is finally sucked into the mouth. After prey capture, a relatively long period is needed to restore the original configuration of the skeletal elements (Fig. 5.5).

The cranium starts to elevate 0.14 ± 0.08 ms (mean ± SE) after the onset of hyoid rotation (Table 5.1; Fig. 5.6A). In eight of the 14 analyzed sequences, feeding began with hyoid rotation. In six sequences, hyoid rotation and neurocranial elevation started at the same video image. Therefore, the onset of neurocranial elevation did not precede the onset of hyoid rotation in any of the sequences. Consequently, in the eight sequences where a clear temporal distinction between both movements is present, the onset of hyoid rotation is significantly earlier than the onset of neurocranial elevation (Fisher's exact test, $P = 0.04$). This result was supported by preliminary data based on videos recorded at 8,000 fps.

The onset of mouth opening takes place 0.11 ± 0.01 ms after the onset of neurocranial elevation (and thus 0.25 ± 0.07 ms after the onset of hyoid rotation). The onset of cranial elevation preceded the onset of mouth opening in 10 of the 14 sequences. In the four remaining sequences, the onsets of neurocranial elevation and mouth opening occurred at the same video image. Consequently, the onset of neurocranial elevation is significantly earlier on average than the

onset of mouth opening (Fisher's exact test, P = 0.02) in 10 videos where a clear temporal distinction was apparent. Mouth opening reaches a peak value of 0.27 ± 0.16 cm 3.50 ± 0.28 ms after the beginning of hyoid rotation.

The prey is sucked in 2.00 ± 0.16 ms after the mouth reaches its maximum gape (5.50 ± 0.44 ms after the onset of hyoid rotation). Next, the hyoid reaches its peak excursion of 68.45° ± 4.32° 17.29 ± 1.58 ms after the onset of hyoid rotation. The neurocranium is the last element reaching its peak elevation of 31.10° ± 2.13° 18.46 ± 1.59 ms after the onset of hyoid rotation. During the entire feeding strike, there exists a strong correlation between the cranial elevation and the hyoid rotation (correlation test, N = 51, R^2 = 0.99, P < 0.01).

The duration of the expansion phase (which begins with the onset of hyoid rotation and ends with the beginning of mouth closing) is 5.77 ± 0.66 ms. The compression phase (which is defined here as starting at the onset of mouth closing and ending when the mouth is fully closed) lasts much longer, with a duration of 415.74 ± 48.20 ms. The final recovery phase (which begins at the moment the jaws are fully closed and ends at the time all skeletal elements have acquired their original position) has a duration of 168.23 ± 36.27 ms. The total duration of the feeding sequence (from one frame before the onset of hyoid rotation until the end of the recovery phase) is 598.73 ± 25.12 ms, on average.

Table 5.1 - Summary kinematics of the prey capture event in *Hippocampus reidi* (N = 14). SE, standard error.

Variable	Mean	SE
Peak hyoid rotation (°) [1]	68.45	4.32
Peak velocity hyoid rotation (°/s)	29.85×10^3	2.42×10^3
Peak acceleration hyoid rotation (°/s²)	23.22×10^6	1.84×10^6
Onset hyoid rotation (ms)	0.50	0.00
Time to peak hyoid rotation (ms)	17.29	1.58
Time to peak velocity hyoid rotation (ms)	1.29	0.07
Time to peak acceleration hyoid rotation (ms)	0.50	0.00
Peak cranial elevation (°) [1]	31.10	2.13
Peak velocity cranial elevation (°/s)	13.88×10^3	976.77
Peak acceleration cranial elevation (°/s²)	10.36×10^6	709.71×10^3
Onset cranial elevation (ms)	0.64	0.08
Time to peak cranial elevation (ms)	18.46	1.59
Time to peak velocity cranial elevation (ms)	1.36	0.06
Time to peak acceleration cranial elevation (ms)	0.50	0.00
Peak mouth opening (mm) [1]	2.70	0.16
Peak velocity mouth opening (m/s)	1.58	0.12
Peak acceleration mouth opening (m/s²)	1.22×10^3	116.53
Onset of mouth opening (ms)	0.75	0.07
Time to peak mouth opening (ms)	3.50	0.28
Time to peak velocity mouth opening (ms)	1.21	0.09
Time to peak acceleration mouth opening (ms)	0.46	0.04

(continued on next page)

Variable	Mean	SE
Peak shortening pectoral girdle - ceratohyal tip (mm) [1]	1.05	0.18
Peak velocity shortening pectoral girdle - ceratohyal tip (m/s)	55.12	8.45
Peak acceleration shortening pectoral girdle - ceratohyal tip (m/s^2)	70.24×10^3	7.80×10^3
Onset of shortening pectoral girdle - ceratohyal (ms)	0.82	0.19
Time to peak shortening pectoral girdle - ceratohyal tip (ms)	12.80	0.25
Time to peak velocity shortening pectoral girdle - ceratohyal tip (ms)	0.54	0.18
Time to peak acceleration shortening pectoral girdle - ceratohyal tip (ms)	0.20	0.05
Duration of prey capture (ms)	5.50	0.44
Prey distance at time 0 (mm)	6.71	0.53
Peak velocity prey (m/s)	0.27	0.06
Peak acceleration prey (m/s^2)	190.37	57.62
Time to peak velocity prey (ms)	5.10	0.86
Time to peak acceleration prey (m/s^2)	4.00	0.91

[1] Calculated as the difference between the value at time 0 ms and the maximum value.

C. Four-Bar Model

The hyoid angle calculated through the four-bar model reaches a maximum peak of 88.99° ± 5.29° (mean ± SE) after 18.46 ± 1.49 ms. The measured hyoid angle is on average 10.99° larger, while the timing of peak excursion differs only by 1.17 ms (Fig. 5.6B). During the first 1.50 ms, the measured hyoid angle statistically shows no difference from the predicted hyoid angle (t-test, $t = 1.514$, $df = 13$, $P = 0.154$). After this initial phase, the predicted angle started to underestimate the measured hyoid angle significantly (t-test, $t = 3.034$, $df = 13$, $P < 0.01$ after time = 2.00 ms) and finally ends at 91.08% of the measured angle (Fig. 5.6B). This pattern is consistently observed for each individual feeding sequence analyzed.

The morphological analysis confirms that the neurocranium and the suspensorium can be represented as a single unit (as assumed in the four-bar model) articulating with the following structures: the pectoral girdle, the vertebral column, the ceratohyal bones (through the interhyal bone) and the lower jaws (Fig. 5.7). The upper jaws articulate with the neurocranium, but with respect to the four-bar linkage system, they can be considered as mechanically coupled to the neurocranial unit. The degrees of freedom between the neurocranium, pectoral girdle and vertebral column are reduced because the vertebral column is immovably connected to the pectoral girdle. As such, the pectoral girdle can be considered to be part of the postcranial skeletal unit. This also implies that the postcranial skeletal unit articulates with the neurocranium with three joints: two for the pectoral girdle and one for the first vertebra. All three joints show a topography where they are well aligned (so the vertebral articulation is lining up with the axis between the left and right pectoral articulation).

As neurocranial rotation must occur around the axis going through the three neurocranial joints, its elevation is coupled to a posterior displacement of the supraoccipital crest with respect to the nuchal plates. As the second nuchal plate is strongly connected to both the pectoral girdle and the neural spine of the first vertebra, a posterior rotation of the supraoccipital crest must be compensated for by a sliding or tilting action of the corona, with respect to the second nuchal plate and/or the neurocranium. At this point, it cannot be discerned whether this movement involves one or both actions, but the model does suggest that a forward movement of the corona with respect to the supraoccipital crest occurs (indicated by the shortened distance of the bar connecting the supraoccipital crest and the distal tip of the process on the corona; Fig. 5.7B).
Using the image of a feeding *H. reidi* at maximal neurocranial elevation, where the depressed hyoid bars could clearly be observed, the model could only be fitted properly if the interhyal bones were rotated forward (thus contrary to what would be expected for hyoid rotation). Observations of dissected specimens also indicated the interhyal bone to be directed rostrally when the hyoid is depressed. Whether or not the interhyal bone is also directed rostrally at the onset of neurocranial elevation could not be determined based on the model (Fig. 5.7).

5.1.4. Discussion

A. Comparison with Other Teleosts

A comparison of the kinematics of the feeding strike of *Hippocampus reidi* with the rostrocaudal expansion sequence of typical suction feeding teleosts reveals differences in the timing of the movements of the skeletal components. When there was a clear temporal distinction, the hyoid (and not the mouth, as observed for typical teleost suction feeders; see, e.g. Lauder, 1985; Carroll & Wainwright, 2003; Gibb & Ferry-Graham, 2005; Van Wassenbergh *et al.*, 2005) in *H. reidi* is the first component of the cranial system that is set in motion. However, in six of a total of 14 sequences, hyoid rotation and cranial elevation occur at the same time frame; therefore, we cannot statistically justify whether or not a difference in timing exists. In those cases where our temporal resolution was adequate and the two behaviours showed temporal separation, hyoid movements always preceded

cranial rotation. Considering the very fast movements, this apparent overlap in timing could be caused by the low temporal resolution of the recordings. Therefore, further analyses using higher temporal resolution are needed to confirm this finding and test its generality. The mouth is directed to the prey via cranial elevation, which occurs just after the onset of hyoid rotation. Cranial elevation thus appears to be used for positioning the mouth opening towards the prey rather than contributing to mouth opening (also found in clariid catfish; Van Wassenbergh *et al.*, 2006a), which also differs from the typical teleost pattern (e.g. Lauder, 1985). Prey capture occurred within 5–6 ms, which makes *H. reidi* one of the fastest suction feeders to date, comparable with the reported prey capture times of antennariid anglerfish (Grobecker & Pietsch, 1979).

B. Kinematics and Morphology Related to the Four-Bar System

The four-bar linkage proposed by Muller (1987) consists of the neurocranium-suspensorium complex, the hyoid, the sternohyoideus-urohyal complex and the vertebral column–pectoral girdle complex. In *H. reidi*, the articulation between the suspensorium and the hyoid is provided by the interhyal bone. In a generalized teleost, this small bone is usually rod-shaped and bears a rounded head that fits into a facet of the suspensorium, forming a ball-and-socket joint (Anker, 1989; Aerts, 1991). This configuration permits the interhyal bone to rotate in every direction with respect to the suspensorium (unless restricted by the suspensorium itself). In *H. reidi*, however, the interhyal bone is reduced to only the ball of the ball-and-socket joint, which bears two distinct ventral processes (Fig. 5.4). The posterior ceratohyal bone, forming a rigid unit with the anterior ceratohyal bone, articulates in between these heads. The two heads of the interhyal bone reduce the degrees of freedom between the hyoid and the suspensorium. Thus, movements are largely confined to a sagittal plane going through the long axis of the interhyal bone. This movement is very important for hyoid rotation during the expansion phase of suction feeding (Aerts, 1991). The morphological specialization of the interhyal bone does suggest that this bone and its movements play an important role in the suction-feeding mechanism and cannot be neglected.

The hyoid bar and the sternohyoideus-urohyal complex are connected through a ligament that runs from the ventral apex of the anterior ceratohyal bone to the

dorsomedial ridge of the urohyal bone (Fig. 5.1, 5.4A). The attachment of this ligament is the position where the force is applied during sternohyoideus contraction. As the distance between the attachment and the rotation centre (the articulation with the interhyal bone) is maximal, the moment arm and, as a consequence, the moment of force will be large as the hyoid becomes depressed (and thus the angle between the hyoid and the sternohyoideus muscle becomes more favourable). Caudally, the tendon of the sternohyoideus muscle encloses the urohyal bone. Surprisingly, several figures in Muller (1987) show a working line of the sternohyoideus muscle forming an angle with the urohyal bone. This is in contradiction to his previous definition of the sternohyoideus-urohyal complex, which comprises the sternohyoideus muscle and the urohyal bone as a single bar. Also, anatomically, this is impossible, because the urohyal bone in teleosts typically ossifies within the tendon of the sternohyoideus muscle and will therefore always be positioned in the working line of this muscle (and thus in the line through the tendon; de Beer, 1937; Patterson, 1977).

Our comparison between the results of the four-bar system (Muller, 1987) and the observed kinematics show good agreement during the first 1.5 ms of the feeding strike (Fig. 5.6B). After the initial 1.5 ms, the trajectories start to diverge and a clear difference between the two movement profiles becomes apparent. Given the above morphological considerations, this is most likely caused by shortening of the sternohyoideus-urohyal "bar" (rs in Fig. 5.2). Indeed, calculating the distance between the hyoid and the tip of the cleithrum shows an average shortening of 1.54 mm. A second possible explanation of the discrepancy between the four-bar model and the measured kinematics (Fig. 5.6B) is abduction of the hyomandibular bone; because this implies a lateral (outward) displacement of the interhyal joint, the projected length of the ceratohyal bones on the dorsoventral plane (*i.e.*, the four-bar plane) will decrease. However, calculating the distance between the hyoid tip and the interhyal bone in the dorsoventral plane never showed a significant decrease during the phase of rapid neurocranial elevation. Therefore, it appears that defining the sternohyoideus-urohyal complex as a bar of constant length and not suspensorium abduction is responsible for the underestimation of the actual rotation of the hyoid. It should also be noted that given the functional continuum of the sternohyoideus and the hypaxial muscles

in *H. reidi* (chapter 3.2), hypaxial muscle shortening may contribute to the observed decrease in length between the hyoid tip and the cleithrum tip.

Due to the immobile connection between the pectoral girdle and the vertebrae, the pectoral girdle and vertebral column should be considered a single mechanical unit (at least with respect to the four-bar linkage system). This simplification has also been made by Muller (1987); he eliminates the movable connection between the pectoral girdle and neurocranium and continues to work with the vertebra-neurocranium articulation. This configuration seems to indicate a strengthened but mobile connection between neurocranium and vertebral system by this pectoral-vertebral ankylosis[6], as the neurocranio-vertebral articulation lies onto the axis connecting the left and right pectoral articulations with the neurocranium. From a mechanical point of view, any deviation from this axis would be prone to cause a dislocation during extensive neurocranial elevation.

According to Bergert and Wainwright (1997), the components of the Muller four-bar linkage model are the hyomandibular bone, the ceratohyal bone, the sternohyoideus muscle together with the urohyal bone and the pectoral girdle. They give a description of the *Hippocampus erectus* skull, with the hyomandibular bone covering the preopercular bone and articulating with the interhyal bone (Bergert & Wainwright, 1997). However, this configuration cannot be found in *H. reidi*, *Hippocampus capensis*, or *Hippocampus kuda*.

C. Final Conclusion

In conclusion, our morphological and kinematic data clearly show an important coupling between the hyoid rotation and neurocranial elevation in *H. reidi*, as suggested by Muller's four-bar mechanism (1987). However, our results do reveal a significant difference between the model and the observed kinematics near the end of the neurocranial elevation phase, which points out that the model does not entirely describe the actual movements during a feeding strike in *H. reidi*. Because the sternohyoideus muscle runs through the pectoral girdle and is confluent with the hypaxial musculature, modelling the sternohyoideus-urohyal complex as a bar of constant length is not appropriate. Our data show that the

[6] an ankylosis is the union of two or more bones thus forming a single unit

extreme performance of the feeding system in seahorses is made possible by a series of morphological specializations of the cranial system.

5.2. MECHANICAL STRESS DISTRIBUTION IN THE FEEDING APPARATUS

Modified from:
Leysen H, Dumont ER, Brabant L, Van Hoorebeke L, Adriaens D.
Dealing with stress in the feeding apparatus of seahorses and pipefishes
Zoological Journal of the Linnean Society, submitted

Abstract

Pipefishes and seahorses (Syngnathidae) are extremely fast suction feeders, with prey capture times of less than 6 ms. These fast strikes are likely to result in large and rapid pressure drops in the buccal cavity. The high pressure gradients that occur during suction feeding imply heavy mechanical loading on the cranium, thus the feeding apparatus is thought to experience high amounts of stress. By means of a finite element analysis (FEA), we investigated where stress accumulates under strong suction pressure and whether there is a difference in the distribution of craniofacial stress between long- and short-snouted species. We predicted that high stress concentrations would occur at the articulations and in the cartilaginous regions of the cranium. We also predicted that, given the same pressure, the skulls of long-snouted species exhibit lower stress levels than

the skulls of short-snouted species, since the former are thought to be structurally better adapted to deal with high suction pressures. The results partially support our first hypothesis: except for *Doryrhamphus dactyliophorus* (whose uncharacteristic stress pattern we could not adequately explain), all models show peak stress concentrations at the articulations (e.g. suspensorio-neurocranial articulation) and cartilaginous regions (e.g. mesethmoid-parietal transition). On the other hand, the relationship between snout length and patterns of stress distribution was more difficult to assess. We did not find a simple relationship between snout length and the magnitudes of stress predicted by the FEA. In an attempt to explain this, we evaluated our methodology by assessing the effect of hyoid position and model construction on the stress distribution.

5.2.1. Introduction

Among teleosts, the most widespread method of prey capture is suction feeding (Lauder, 1980b; 1983; Muller & Osse, 1984; Lauder, 1985; Carroll *et al.*, 2004). Suction feeding involves a powerful expansion of the oral cavity that generates a negative pressure within the head relative to the ambient pressure. This pressure gradient draws water with the prey into the mouth to fill the added space and equalize the pressure (e.g. Alexander, 1969; Lauder, 1985; Sanford & Wainwright, 2002). Buccal expansion can be accomplished by maxillary protrusion, depression of the lower jaw, lateral abduction of the suspensoria, neurocranial elevation and depression of the hyoid (Alexander, 1969; Lauder, 1983).

Pipefishes and seahorses (Syngnathidae) are extremely fast suction feeders, with prey capture times of less than 6 ms (Chapter 5.1; Muller & Osse, 1984; Bergert & Wainwright, 1997; de Lussanet & Muller, 2007). Explosive cranial kinematics, such as extremely rapid accelerations of skeletal elements and high suction forces, are generated during the powerful suction feeding of these fishes. A syngnathid feeding strike is characterized by a very fast depression of the hyoid and an almost simultaneous neurocranial elevation. Mouth opening starts only after the hyoid has rotated 80°. Both lower jaw halves and hyoid bars push the suspensoria outwards while depressing, thus producing the main buccal volume

increase in syngnathids (Chapter 5.1; Roos *et al.*, 2009). Svanbäck *et al.* (2002) demonstrated that an increase in velocity of buccal expansion results in an increasing magnitude of suction pressure in largemouth bass. These large pressure gradients may result in heavy mechanical loading of the cranium during suction feeding. The fast strikes in syngnathids probably also produce large and fast pressure drops. Suction pressure has not yet been measured in syngnathids, but Muller and Osse (1984) demonstrated that pipefishes like *Entelurus aequoreus* (snake pipefish) perform suction feeding with almost permanently closed opercular valves (the gill slits are very small), therefore high negative pressure is built up inside their buccal cavity. Osse and Muller (1980) argued that the domed opercular bone, the lobed gills, the small gill slits and reduced number of branchiostegal rays are related to the high negative pressure experienced during suction feeding. Because of this pressure, a great amount of mechanical force is thought to be exerted onto the skull bones, especially onto those comprising the snout; these are actively abducted and thus create the suction pressure. This force can be assumed to result in high levels of stress in the feeding apparatus.

One of the goals of this study is to determine where stress accumulates under the assumed high pressure generated during suction feeding in seahorses and pipefishes. Given the fact that cartilaginous tissue has a high fluid content, it is capable of resisting high compressive pressure and is more compliant than bone (e.g. Herring, 1993; Lieberman *et al.*, 2001; Hall, 2005). Applying force to a non-fixed element will cause it to move instead of being stressed. The articulating bones in the skull in syngnathids will probably first translate force into motion when exposed to suction pressure and hence will experience less mechanical stress. In addition, presence of articular cartilage in joints is believed to prevent load concentrations (Mori *et al.*, 2010). We modelled the cranium as a single, immobile element and assigned it the material properties of bone, including the cartilaginous zones. Precisely because our models do not contain cartilage to dissipate stress and do not allow movement of articulating elements, we predict stress to be concentrated at those regions of the models where stress would be reduced in the real skulls (*i.e.* articulations, symphyses and cartilaginous zones). A finite element analysis (FEA) on 3D-models based on the cranium of several syngnathid species was performed to elucidate this.

We also investigated a hypothesis based on Poiseuille's law, which states that the volumetric flow rate of water through a tube is proportional to the radius of the tube to the fourth power and to the pressure difference between the two ends of the tube, but inversely proportional to the length of the tube and the dynamic fluid viscosity. In other words, to obtain the same water flow through a short, broad tube as through a long, narrow one, a larger pressure difference is needed in the latter. Translating this to syngnathid snouts, we expect species with a long and/or narrow snout having to generate a larger pressure difference by means of buccal expansion to achieve the same water flow as short-snouted species. Roos *et al.* (submitted a) observed that the distance to the prey when the head reaches its maximal rotation (*i.e.* the distance that needs to be overcome by suction) is much longer in a long-snouted species (*D. dactyliophorus*) compared to a short-snouted one (*D. melanopleura*). Therefore, long- and narrow-snouted species will have to withstand more stress because of the higher forces and faster accelerations of cranial elements needed to realize the high suction pressure. We wanted to assess the implications of snout elongation on the distribution of stress in the skull by comparing the stress patterns between long-snouted and short-snouted syngnathids. We hypothesize that, when exposed to the same pressure, the location of peak stress will be similar among species, but that the long-snouted species (for example *Doryrhamphus dactyliophorus* and *Hippocampus reidi*) will exhibit lower levels of stress than the short-snouted ones (for example *D. melanopleura* and *H. zosterae*). This is based on the assumption that the skulls of long-snouted species exhibit morphological adaptations that enable them to withstand relatively higher suction pressures. So, when the same pressure is applied to the cranium of a short- and a long-snouted species, the skull of the latter is expected to be less stressed since its structure would be stronger.

By comparing different species, not only the effect of snout length but also differences in snout morphology have to be taken into account. Factors such as variation in bone thickness, presence or absence of indentations or spines, overlap between bony elements and pure bone geometry could influence the patterns of stress distribution. We tried to exclude these factors by constructing two artificial seahorse models. We started with a long-snouted model (*H. reidi*) and shortened the snout until it had the same length as the snout in a short-snouted seahorse (*H. zosterae*) in the first model, and the snout length of a species

with an intermediate snout length (*H. abdominalis*) in the second. In this way we constructed three models (the natural *H. reidi*, the artificial *H. zosterae* and the artificial *H. abdominalis* models) with the same head morphology that differ only in snout length. As a consequence, any morphological adaptations in the head of the long-snouted *H. reidi* model for withstanding high suction pressure are present in both artificial models as well. Hence, when applying the same amount of pressure to the models, we expect to see identical stress patterns, except for slightly higher concentrations in the longer-snouted model due to the larger surface area unto which the pressure is applied.

5.2.2. Brief material & methods

A. Specimens

We used three pipefish species (genus *Doryrhamphus* and *Syngnathus*) and three seahorse species (genus *Hippocampus*) in this study. Adult specimens of *D. dactyliophorus* (103.5 mm SL), *D. melanopleura* (56.5 mm SL), *H. abdominalis* (222.7 mm SL), *H. reidi* (119.0 mm, 123.9 mm SL) and *H. zosterae* (29.0 mm SL) were obtained from commercial trade (Table 2.1, 5.2). The specimen of *S. rostellatus* (110.8 mm SL) was caught on the Belgian continental shelf (North Sea).

Table 5.2 – Overview of the constructed models, their surface area and some biometrics of the specimens scanned. The *H. reidi* depressed and protracted models are generated with CT-data of two different specimens. HL, head length; SL, standard length; SnL, snout length.

model	surface area (mm^2)	SL (mm)	HL (mm)	SnL (mm)	HL/SnL
Doryrhamphus dactyliophorus	298.3	103.5	25.4	16.6	1.5
Doryrhamphus melanopleura	263.5	56.5	13.2	5.8	2.3
Syngnathus rostellatus	224.8	110.8	15.3	7.4	2.1
Hippocampus abdominalis	358.2	222.7	30.9	11.8	2.6
Hippocampus reidi depressed	340.0	119.0	25.2	11.0	2.3
Hippocampus reidi protracted	384.7	123.9	25.5	10.4	2.5
Hippocampus zosterae	300.0	29.0	5.3	1.8	2.9
Hippocampus abdominalis artificial[1]	315.2	-	-	8.8	-
Hippocampus zosterae artificial[1]	276.3	-	-	5.9	-

[1] model generated with CT-data of *H. reidi* depressed

B. Constructing models

In total, nine models were made for this analysis: a model of each of the six species, two artificial seahorse models and a *H. reidi* model with the hyoid protracted (Table 5.2). For the *H. reidi* models, CT-data of two *H. reidi* specimens were used: one with the hyoid protracted (used for the *H. reidi* protracted model and the two artificial models) and one with a depressed hyoid (for the *H. reidi* depressed model). CT-scans and models were made as explained in chapter 2.2.7 and 2.2.10.

Dumont *et al.* (2009) demonstrated that if the goal of a comparative FEA study is to identify differences in stress magnitudes that stem solely from differences in model shape, then the ratios of applied force to model surface area must be held constant. In this analysis we chose not to completely eliminate the effect of size, since one of the aims is to determine the relationship between relative snout length and stress. Instead we scaled the models to equal braincase length (see chapter 2.2.10).

In addition to modelling different species, we created two artificial models with different levels of snout elongation in Rhinoceros 3.0 McNeel Europe (Barcelona, Spain). Starting with the original *H. reidi* model, the part of the snout between the ectopterygoid bone and the lateral ethmoid bone was compressed until it had the same length as the short snout in *H. zosterae* (Fig. 5.8). This model will be called the '*H. zosterae* artificial model'. Next, we constructed another model with the same hind part of the skull and the same jaws as the original *H. reidi* model, but this time we decreased snout length to approximate the intermediate length of the snout in *H. abdominalis*. This model will be referred to as the '*H. abdominalis* artificial model'.

We also reasoned that the outcome of the FEA might be influenced by the orientation of the hyoid since not all models had the hyoid in the same position. Hence, scans of a second *H. reidi* specimen, with its hyoid protracted, were made and a model was constructed which we could then compare with the original *H. reidi* model with its hyoid depressed. To distinguish between both *H. reidi* models one is called the '*H. reidi* protracted model', the other the '*H. reidi* depressed model'.

C. Finite element analysis

The finite element analysis was carried out as described in chapter 2.2.10 and figure 2.4. Since the stress magnitude differs vastly between the various models, different colour scales are used in figures 5.9 and 5.10 in order to avoid a limited range of colouring in the models with highest and lowest stress levels. This way, emphasis is laid on the (dis-)similarity in the stress distribution and comparison between the models is facilitated.

5.2.3. Results

A. Stress distribution in pipefishes and seahorses

Figure 5.9 illustrates the von Mises stress during simulated suction feeding. Peak stress values occur at the occipital joint where boundary constraints (both against displacement and rotation) were applied in order to anchor the model, this artefact can be ignored. In each of the seahorse models stress is concentrated at the articulation between the autopalatine bone and the neurocranium, in the hyoid and in the lateral wall of the snout. Some elevated stress is also found at the mesethmoid-parietal border. Lowest stress is present in the braincase, at the supraoccipital bone and at the spines on the lateral ethmoid, preopercular, parietal, sphenotic and posttemporal bones. In the *H. reidi* model high levels of stress are also present at the hyomandibulo-sphenotic joint, whereas the maxillary bones show very little stress (Fig. 5.9A). Stress is concentrated in the *H. abdominalis* model at the ventral border of the quadrate bone (where there is an indentation) and at the transition of the very slender vomeral bone to the mesethmoid bone (Fig. 5.9B). There is also stress in the lateral part of the snout and at the two suspensorio-neurocranial articulations (*i.e.* the hyomandibulo-sphenotic and autopalatine-vomeral joint). However, in the *H. zosterae* model, little stress accumulates at the level of the hyomandibulo-sphenotic articulation, especially compared to the amount of stress in the lateral wall of the snout (Fig. 5.9C). On the other hand, the contact zone between the hyoid and the suspensorium does experience a lot of stress. Within the seahorses, the *H. abdominalis* model, with an intermediate snout length, exhibits highest levels of stress, even up to five times the stress magnitude in the other two species. Stress

values are lower in the model of the long-snouted *H. reidi* and lowest in the short-snouted *H. zosterae* model (mark the different colour scales in figure 5.9).
The pipefish models show more diverse patterns in stress values. The pattern of stress distribution in the *S. rostellatus* and *D. melanopleura* models is quite similar but differs from the situation in the *D. dactyliophorus* model. In the former two, highest stress concentrations are found at the lower jaw symphysis and rostral to the nostrils, but also at the caudal suspensorio-neurocranial articulation and at the ventral border of the orbit (Fig. 5.9E,F). The dorsal and lateral surface of the braincase shows the lowest stress levels. The model of *S. rostellatus* also exhibit high stress at the attachment of the hyoid to the suspensoria, and almost no stress in the hyoid symphysis or in the parasphenoid bone. The stress in the *D. melanopleura* model is concentrated at the hyoid symphysis and at the autopalatine-vomeral articulation. Conversely, in the *D. dactyliophorus* model, the stress accumulates in the roof, floor and lateral walls of the braincase, the hyomandibulo-sphenotic articulation and around the orbit (Fig. 5.9D). The hyoid and the rostral part of the snout with the jaws exhibit very low stress. Comparing the three pipefish species, stress levels are lowest in the *S. rostellatus* model which has an intermediate snout length. Stress magnitudes are on average almost double in the model of short-snouted *D. melanopleura* and by far the highest in the extremely long-snouted *D. dactyliophorus* model (mark the different colour scales in figure 5.9).

B. Stress distribution in the artificial models

The stress distribution patterns of the *H. reidi* depressed and the artificial models are very similar, with peak stress concentrations at the hyoid symphysis, the hyomandibulo-sphenotic joint and the rostral articulation between the suspensorium and neurocranium (Fig. 5.10). Also the lower jaw and other parts of the hyoid besides the symphysis are prone to some stress, yet the models exhibit almost no stress at the maxillary bones and the braincase. In addition, the stress in the snout is transmitted in an almost identical manner; all three models show high amounts of stress laterocaudally in the snout and at the dorsorostral edge at the autopalatine-vomeral articulation. The laterorostral surface of the snout and ventrorostral edge of the orbit experience lowest stress. A minor difference between the models involves the stress concentration at the mesethmoid-parietal

border in the *H. reidi* and *H. zosterae* artificial models that seems to be missing in the *H. abdominalis* artificial model. This high similarity was expected since the three models all share the same morphology.
Again according to our expectations, the overall stress level in the models increases with increasing snout length. The artificial model of *H. zosterae* experiences very small amounts of stress, whereas the *H. reidi* model is subject to much higher levels and the *H. abdominalis* model shows intermediate stress values (mark the different colour scales in figure 5.10).

5.2.4. Discussion

A. Stress distribution in pipefishes and seahorses

We wanted to analyze where in the skull the stress would be concentrated, when loaded as expected during suction feeding. Our prediction was that the largest stress concentrations would occur at the level of the articulations, symphyses and cartilaginous zones in the cranium. This hypothesis is based on the assumption that these areas disperse or absorb the stress in the actual cranium. Since the skull was modelled as a single, immovable element with material properties of bone, the assumed stress absorption by the articulations and cartilaginous regions as such cannot be detected in our FEA results. Hence, the stress peaks that might be found at the articulations, symphyses and cartilaginous regions of the model will probably be much lower in reality. This hypothesis is more or less supported by the obtained results: apart from the models of *D. dactyliophorus* and *H. zosterae*, all models show elevated levels of stress at both suspensorio-neurocranial articulations. Again with the exception of *D. dactyliophorus*, peak stress concentrations were present at the lower jaw symphysis and hyoid symphysis, as expected. However, in *H. zosterae* and *S. rostellatus* no elevated stress concentration was found in the hyoid symphysis, which might be explained by the protraction of the hyoid, as we will explain further. Most models also have a stress accumulation at the mesethmoid-parietal transition just before the eye, which is a region comprising a lot of cartilage.
The cranium of *D. dactyliophorus* experiences much higher stress levels than the other skulls and also shows an inverted stress pattern with peak concentrations

in the braincase and lowest stress at the rostral part of the snout. We could not adequately explain these findings.

We can also compare the differences in stress distribution between a typical pipefish cranium and a typical seahorse. The most prominent difference between them is the deeper braincase of seahorses, but as we only applied loads to the suspensorium, not much stress was exerted on the braincase itself. However there are other differences between the two groups. In pipefishes the braincase is in line with the long axis of the snout (and of the entire body) whereas seahorses have a tilted braincase with respect to the snout (Chapter 3.1). This tilt can be quite large. An angle of around 40° between the long axis of the snout and the dorsal profile of the braincase is present in the seahorse species studied, whereas in these pipefishes this angle ranges between 15° and 25° (see also Fig. 5.9). Stress tends to increase at abrupt geometric transitions in the model, like at the level of the acute angle between the mesethmoid and parietal bones. We expected this effect to be more pronounced in seahorses than in pipefishes. Yet we did not find substantially higher stress levels in the mesethmoid-parietal transition of seahorses. Perhaps this can be accounted for by specific features of the geometry of the skull. We found that the mesethmoid bone bears a dorsomedial ridge in seahorses, thus allowing a better transmission of the stress within the bone. This could explain the lower than expected stress levels at the mesethmoid-parietal transition. Another difference between pipefishes and seahorses is the presence of spines and a higher supraoccipital bone in the latter. It has been suggested that the spines make seahorses less attractive as prey (Lourie *et al.*, 1999b). We noted that the spines and distal part of the supraoccipital bone experience almost no stress in any of the seahorses; hence, stress reduction might be an additional advantage of the spines.

B. Effect of snout length on stress distribution

We were also interested in the effect of snout elongation on the cranial stress distribution in seahorses and pipefishes. We expected that for a given mechanical loading, the longer the snout, the lower the stress would be, as the skull of long-snouted species is thought to be structurally better adapted to cope with higher mechanical loads. However, the model with the longest snout was not the least stressed, neither among the seahorses nor among the pipefishes. Moreover, we

did not find a trend in stress concentration (increasing or decreasing) from long-snouted species through intermediate forms to short-snouted species. This suggests that there is no simple relation between snout length and amount of stress expected to be caused by suction. A probable explanation is that the observed stress level is the result of the combination of snout length with the geometry of the bones forming the snout. The previously mentioned dorsomedial crest on the mesethmoid bone in seahorses could be an example. In the seahorses we also found that the lateral bones of the snout of *H. abdominalis* are much thinner on a cross section relative to the snout diameter, when compared to *H. reidi* and *H. zosterae*. This might account for the accumulation of stress in the lateral wall of the snout in the former and could explain why the level of overall stress exceeds that of the long-snouted *H. reidi*.

In order to separate the effect of snout elongation from the influence of snout morphology (*i.e.* bone geometry), we compared the results of the two artificial models with those of the natural model of *H. reidi*. The initial hypothesis was that these three models would be similar in stress pattern since they vary only in snout length; any morphological adaptation that enables them to withstand high pressure is present in all three of them. However, we expected to see a gradual increase in stress levels with increasing snout length, because the surface area to which the load is applied increases as well. All models seem to transmit the loads in a similar way: the stress distribution pattern is almost identical and when shortening the snout of *H. reidi* to the snout length of *H. abdominalis* (intermediate snout length) the stress levels were reduced and even more so for a snout length of *H. zosterae* (short snout length) (Fig. 5.10). So, in the absence of morphological differences, we found changes in stress levels related to relative snout length.

Based on the first analysis, we could not confirm our hypothesis that a long-snouted species encounters less stress because it has a stronger structure. Three reasons come to mind why this might be. First, long-snouted species might not have to generate higher suction pressure during feeding than short-snouted species and hence no structural reinforcement is needed. This can be rejected with fair certainty based on Poiseuille's law and Muller and Osse's (1984) finding that pressure in the opercular cavity increases with increasing snout length. A second possibility is that long-snouted species do experience high levels of

pressure but they do not exhibit morphological adaptations to withstand the increased stress. If this were true, the long-snouted syngnathids in our analysis should be more stressed than the short-snouted ones. We did not observe this pattern in comparisons among species, but it was present in the comparison of the artificial models. The fact that the artificial models varied only in snout length clearly demonstrates that the morphology of the cranium does have an influence on how stress is transmitted. Third, long-snouted species might have a cranium that is adapted to diminish stress during suction feeding in a way that we could not detect with our methodology (e.g. perhaps there is more cartilage in highly stressed regions). Although a recent morphological study found no prominent features that could be related to variation in relative snout length (Chapter 3.2), it might be an interesting avenue to pursue this more thoroughly on a histological level in the future.

C. Biological relevance of the results

Validation of the results of a finite element analysis requires a comparison between the results of the FEA and *in vivo* or *in vitro* data on bone strain in the modelled structures (Ross, 2005). Unfortunately, there are no experimental data on bone strain in the cranium of Syngnathidae, nor is it currently feasible given the size of these skulls. In absence of validation, we consider our comparison of stress patterns between the different models to be reliable, but absolute stress values are not. Still, we identified a few possible methodological limitations of our setup. Most notably, the position of the hyoid and simplification of the models and the forces acting upon them during suction might influence the FE outcome.

A possible source of inaccuracy could be the position of the hyoid in the constructed models: in the *H. zosterae, S. rostellatus* and *D. melanopleura* models the hyoid is protracted whereas the other models show a depressed hyoid. In order to test whether the position of the hyoid might influence the stress distribution pattern, we compared the *H. reidi* depressed model with the *H. reidi* protracted one (Fig. 5.11). The pattern of stress distribution is quite similar in both models, only the mesethmoid bone, the lateral surface of the snout and hyoid-suspensorium articulation are subject to more stress in the model with the hyoid protracted. This finding falls within our expectation since the protracted

hyoid does not have only one contact point at the articulation with the suspensorium, but is modelled continuously with the rest of the skull along almost the entire hyoid bars. Thus, a more firm connection between left and right suspensorium is formed in the model with its hyoid protracted, which reduces the flexibility of the suspensoria and could explain the observed increase of stress in the snout and mesethmoid bone when applying an inward pressure on the suspensoria in the model. On the other hand, the higher levels of stress at the hyoid symphysis observed in the model with the depressed hyoid make sense, since at this point the pressure of left and right side converges. The outcome of the hyoid test corresponds with our previous observations that *H. zosterae* (hyoid protracted) experiences more stress in the snout whereas *H. reidi* and *H. abdominalis* (hyoid depressed) have high stress accumulations at the hyoid symphysis (Fig. 5.9A-C). Hence, the differences between the three seahorse models might be partially related to changes in the position of their hyoid.

By constructing the skull as a single unit, we ignored the presence of sutures and articulations. This is especially important since sutures are known to be less stiff and experience higher sutural strains than bone (Herring & Teng, 2000; Rayfield, 2005; McHenry *et al.*, 2006). In this context, previous research has shown that the morphology of sutures is related to the type of deformation to which they are most resistant. As such, interdigitated sutures appear to be correlated with compression whereas abutting sutures usually are subject to tensile stress (Herring & Teng, 2000; Markey *et al.*, 2006; Markey & Marshall, 2007). Articulating elements transmit mechanical loading differently than fused elements, since cartilaginous articulations can function as stress absorbers. Unfortunately, analyzing the cranium as a solid unit instead of as an assembly of individual parts is necessary to reduce the complexity of constructing the model and to bring the processing of the analysis to a manageable level. By neglecting the effects of material anisotropy and heterogeneity, muscle force, neurocranial elevation and suture morphology, we assume that these factors affect all the species of our study in the same way (McHenry *et al.*, 2006). As techniques of modelling muscle forces, bony articulations and kinematics are being developed for finite element analyses, we look forward to adding those techniques to the analyses described here. In the present study, overall head shape and relative size

are the only substantial differences among the models and therefore explain all the differences we observe among them.

6 General discussion

A thorough insight into an animal's morphology is vital for understanding complex processes associated with its development, performance (e.g. locomotion, respiration, feeding, *etc.*) and evolutionary history. In this dissertation, a thorough morphological description of the musculoskeletal head in Syngnathidae is provided first. Secondly, the shape variation in the syngnathid head and the functional implications of the feeding apparatus are studied. In this chapter, these results are discussed in an ontogenetic, functional (with respect to feeding) and evolutionary context. The role of the complex parental care, the modifications of the feeding apparatus and the evolutionary patterns towards and within the family are dealt with.

6.1. ONTOGENETIC MORPHOLOGY

Syngnathids are known for their extreme parental care. The eggs, deposited by the female, are attached to the male's body where they are fertilized (e.g. Herald, 1959; Vincent *et al.*, 1995; Drozdov *et al.*, 1997; Pham Tchi Mi *et al.*, 1998; Kornienko, 2001; Wilson *et al.*, 2001; Vincent & Giles, 2003; Foster & Vincent,

2004; Lourie *et al.*, 2004; Ripley & Foran, 2009). In the incubating area of the male, the eggs can be loosely attached to the ventral surface of the body (e.g. *Entelurus, Nerophis*), separated from each other by a spongy mass (e.g. *Solegnathus, Doryrhamphus*), covered by a membrane either in combination with protective plates or not (e.g. *Syngnathus, Microphis*) or enclosed by a sealed brood pouch (e.g. *Hippocampus*) (Fig. 1.5; Herald, 1959; Kornienko, 2001; Wilson *et al.*, 2001; Carcupino *et al.*, 2002; Kvarnemo & Simmons, 2004). In the seahorse's pouch, small cups are formed on the incubating area in which the eggs, and later the embryos, are enveloped by epithelial tissue (Foster & Vincent, 2004). The male provides the embryos with all post-fertilization parental care until the yolk is completely absorbed. With increasing evolutionary complexity of brood area, the amount of parental investment in terms of nutrition and oxygenation is thought to increase (Carcupino *et al.*, 2002). The brood pouch of seahorses can be thought of as a pseudo-placenta for the embryos, having an osmoregulatory, aerative and nutritive function (Kornienko, 2001; Foster & Vincent, 2004; Stölting & Wilson, 2007). Also in *Syngnathus* pipefishes (e.g. *S. fuscus, S. floridae, S. scovelli* (Evermann & Kendall) and *S. abaster* Risso) parental nutrient provision, oxygenation and osmotic protection has been demonstrated (Drozdov *et al.*, 1997; Kornienko, 2001; Carcupino *et al.*, 2002; Ripley & Foran, 2009). The supply of oxygen and endogenous energy enables a delay of emergence from the brooding structure. From the moment of parturition (*i.e.* release from the brooding area), the syngnathid young are completely independent and receive no assistance or protection from their parents (Vincent *et al.*, 1995; Kornienko, 2001; Foster & Vincent, 2004; Van Wassenbergh *et al.*, 2009). The size and relative degree of development of newborn syngnathids might be related to the degree of differentiation of the incubation area exhibited by the male. Species provided with a pouch-like structure (e.g. *Syngnathus acus, S. typhle, S. acusimilis* Günther and *S. abaster*) appear to have larger young of a more advanced developmental stage compared to species that simply attach the embryos to their body surface (*Nerophis lumbriciformes* (Jenyns), *N. ophidion* L. and *Entelurus aequoreus*) (Monteiro *et al.*, 2003; Silva *et al.*, 2006). The release of well developed juveniles was also seen in other fish with unusual parental care. For example, in the white barbel (*Galeichthys feliceps*), an ariid mouth-brooder, embryos are ventilated and nourished in the adult buccal cavity. Hence, release from the mouth is postponed,

resulting in a total incubation period of almost double the pre-hatching period (Tilney & Hecht, 1993). A similar strategy is used in most haplochromine cichlids (Goodwin *et al.*, 1998; Salzburger *et al.*, 2005).

One of the consequences of the long and intense parental care and associated release of offspring at advanced developmental stages from the incubating area, is the great similarity of the head morphology of newly released young to that of adults (e.g. Azzarello, 1990; Dhanya *et al.*, 2005; Choo & Liew, 2006; Silva *et al.*, 2006). The osteology of early juveniles was elaborated on in chapter 3.1. From this study, it appears that in the newborns of *S. rostellatus, H. capensis* and *H. reidi* almost all bones are formed, although only as very thin layers. The bones that were not yet completely formed are the antorbital, two or three infraorbital bones (for discussion on circumorbital bone homology, see chapter 2.3) and some opercular bones in *S. rostellatus*. In *H. reidi*, the aforementioned bones only start to develop after 29 days (Reyserhove, 2008). This corresponds to the observed late onset of development of the circumorbital bones in other syngnathids (Kadam, 1961), which is also the case in other teleosts such as some Perciformes (*Sparus aurata* L.; Faustino & Power, 2001) and some Siluriformes (*Clarias gariepinus* (Burchell), *Ancistrus* cf. *triradiatus* Eigenmann and *Corydoras aeneus* (Gill); Adriaens & Verraes, 1998; Geerinckx *et al.*, 2007; Huysentruyt *et al.*, 2011). The absence of the inter-, sub- and suprapreopercular bones in *S. rostellatus* can be related to the fact that the studied specimen had not yet reached the free-living stage. However, in *H. reidi*, the interopercular bone, as well as the vomeral and retroarticular bones, are also not fully developed until 25 days post-release (Reyserhove, 2008). In *H. kuda* some minor developmental changes were observed after being expelled from the pouch as well (Choo & Liew, 2006). Only after four days did the cheek spines start to appear and coronary spines were not completely developed until the ninth day post-parturition. Another important difference between early juvenile and adult morphology concerns the single cartilaginous hyomandibulo-neurocranial articulation in juvenile syngnathids, whereas in adults the hyomandibular bone bears a double articular facet with the neurocranium (Chapter 3.1).

Overall, however, these osteological differences between early juveniles and adults are small. Van Wassenbergh *et al.* (2009) did show that not only the

skeletal elements but also all the muscles, ligaments and tendons involved in pivot feeding are present in newborn *H. reidi* juveniles, which seemed to be true for *H. capensis* as well (Thielemans, 2007). Perhaps even more importantly, we saw that the elongation of the snout occurs early in development of *S. rostellatus*, *H. capensis* and *H. reidi* (Chapter 3.1), which is also true for several other syngnathids (e.g. *H. antiquorum* (Ryder, 1881), *S. peckianus* (McMurrich, 1883), *S. fuscus* (Kindred, 1921), *Hippocampus* (species not stated, Kadam, 1958), *Nerophis* (species not stated, Kadam, 1961), *S. scovelli* and *H. zosterae* (Azzarello, 1990)). Also some of the specialized morphological features in the feeding apparatus that might be considered adaptations to the remarkable pivot feeding in syngnathids are already present in juveniles. An example can be found in the cartilaginous interhyal, which is very similar in form to the bony element in adults. Both have a double articulation head for the ceratohyal bone and a rounded surface for the articulation with the preopercular bone.

In some fishes, such as eels (e.g. Tesch, 2003; van Ginneken & Maes, 2005) and flatfishes (e.g. Geffen *et al.*, 2007), the free-living larva is shaped unlike the adult and undergoes a profound metamorphosis to produce the juvenile. This substantial change in morphology is often associated with a transition from freshwater to marine environment or with the settlement of planktonic larvae when they develop into benthic juveniles in marine fishes (Rose & Reiss, 1993). In many cases metamorphosis is accompanied by developmental alterations in feeding behaviour and habitat (Helfman *et al.*, 2009).

Syngnathids do experience a dietary shift. Prey size increases ontogenetically, likely since larger prey yield an advantage in terms of energy supply and subsequently growth. This ontogenetic shift in diet is related to a developmental increase in mouth gape, as is the case in other fish (e.g. Werner & Gilliam, 1984; Cook, 1996; Hunt van Herbing, 1996a). In addition, at least some syngnathids also undergo a transition from a pelagic to a benthic environment (Monteiro *et al.*, 2003; Foster & Vincent, 2004). Despite these behavioural changes during development, no real metamorphosis takes place. Only an increase in growth rate at the time of these shifts was observed in *H. kuda* (Choo & Liew, 2006). Dhanya *et al.* (2005) also found that newborn *Syngnathoides biaculeatus* only differ from adults in relative snout length and colour. Choo & Liew (2006) performed several body measurements on *H. kuda* juveniles and noticed that head length, snout

length and snout height (which they call snout depth) increase over developmental time. However, when comparing the increase in head length with the one in snout length, the increase in snout length is relatively larger compared to overall head growth. A similar comparison, but this time between head length and snout height, showed that snout height increases more slowly than head length. In other words, newly born *H. kuda* young have a shorter and relatively less high snout than older juveniles. A study on *H. reidi* yielded the same results, juveniles with short and broad snouts develop into long and narrow snouted adults (Roos *et al.*, 2010). The geometric morphometric analysis of chapter 4 revealed that the ontogeny of the same species also involves allometric changes of the snout height and head height with respect to snout length, as well as changes in the orientation of the preopercular bone and lowering of the snout tip. All these results show that syngnathid post-parturition development is characterized by gradual shape changes, and no major transformations occur.

As stated, newly released syngnathids closely resemble miniature adults. The median fin fold, which is a larval characteristic according to Balon (1975), has differentiated into the dorsal, anal and caudal fins long before parturition and thus before the transition to exogenous feeding (chapter 2.3; Azzarello, 1990). Hence before being expelled from the pouch, pipefish and seahorse young have already transformed into juveniles (whether or not by means of a metamorphosis) and most morphological differentiation takes place inside the pouch (Choo & Liew, 2006). As in other fish, the absence of a true larval stage can be related to the extreme reproductive strategy in syngnathids (Balon, 1979; 1984; Kolm & Ahnesjö; 2005). Elimination of the larval stage is generally accepted as an important ecological and evolutionary phenomenon (Balon, 1984) and may therefore have played a crucial role in evolution towards a specialized feeding apparatus (Huysentruyt, 2008).

Prolonging the embryonic period in syngnathids increases the available time for anatomical structures in the trophic apparatus to develop, as active feeding becomes necessary only later in ontogeny. Pipefishes and seahorses give birth to young with a feeding system appropriately configured for self-sufficiency (e.g. Linton & Soloff, 1964; Azzarello, 1990; Pham Tchi Mi *et al.*, 1998; Kornienko, 2001; Foster & Vincent, 2004; Teske *et al.*, 2005; Van Wassenbergh *et al.*, 2009).

Not only is the trophic system completely developed at birth, as is apparent from the previous paragraphs, but it is also fully functional, resembling the adult feeding apparatus both in form and function. Hence, the postponed onset of exogenous feeding in syngnathids enables the direct development of the adult phenotype without a transitional larval stage (Balon, 1979; 1986). This direct development saves the costs of additional functional remodelling of the trophic apparatus and in addition it increases the survival chances of the young because the vulnerable free-living larval stage, characterized by high mortality, is avoided (Balon, 1986).

Juvenile pivot feeding strikes are kinematically similar to those in adults and start with a very fast rotation of the hyoid followed by neurocranial elevation and finally mouth opening (Van Wassenbergh *et al.*, 2009). Prey capture in newly released *H. reidi* juveniles occurs twice as fast as an adult feeding sequence (2.5 ms compared to 5.5 ms) and the velocity of head rotation is over two times as high (exceeding 30,000°s^{-1} as opposed to less than 14,000°s^{-1}) (Chapter 5.1; Van Wassenbergh *et al.*, 2009). The period of steady improvement of prey capture performance during ontogeny, as typically found in other fishes (e.g. Drost, 1987; Coughlin, 1994; Reiriz *et al.*, 1998; Warburton, 2003), appears to be absent in *H. reidi* newborns (Van Wassenbergh *et al.*, 2009). However, prey capture success is low in newborn seahorses relative to adults, which might be related to the location of the centre of rotation of the head. In adults the centre of rotation is positioned close to the eyes, hence the eyes will remain practically immobile during neurocranial elevation, facilitating visual predation. Juveniles on the other hand, have their centre of rotation further away from the eye, which might negatively affect visual acuity (Roos *et al.*, 2010). Therefore, the gradual changes in head and snout dimension during development of the juveniles probably helps increasing prey capture success.

In many cases, significant ontogenetic alteration in shape and proportion almost certainly yields functional change as well (Emerson & Bramble, 1993). A clear example of the effect of allometrical growth on function is found in the mouth-opening mechanism in the generalized cichlid *Haplochromis elegans* Trewavas (Otten, 1982; Liem, 1991; Emerson & Bramble, 1993). In early stages, mouth opening is caused by contraction of the protractor hyoidei muscle (geniohyoideus in Otten, 1982). However, during development the articulation between lower

jaw and suspensorium becomes displaced so that the muscle line of action runs dorsal to the articulation. Hence, contraction of the protractor hyoidei muscle no longer results in mouth opening. Concurrently with the change in position of the suspensorial articulation, an alternative lower jaw depression mechanism is developed, *i.e.* the opercular mouth opening system (Otten, 1982).

So far, no such kinematical transition or shift in the sequence of movements of skeletal elements was observed in post-release development of syngnathids. Neither is there a period of ram feeding preceding the definitive adult suction feeding, as found in the young (both larvae and juveniles) of many other fish (e.g. Liem, 1991; Coughlin, 1994; Cook, 1996). The finding that the function of the cranial structures remains similar throughout syngnathid ontogeny is likely related to the lack of substantial shape changes (Choo & Liew, 2006).

However, in all fishes the allometric increase in head and snout dimensions will also change the size and shape of the buccal cavity. In a suction feeding event, it is the sudden increase in buccal volume that generates suction pressure, which eventually will cause the prey to be transported into the mouth. Hence the dimension and shape of the buccal cavity undoubtedly plays an important role in suction feeding hydrodynamics. For example, flow patterns during expansion are reasoned to be substantially affected by the size or shape of the buccal cavity (Drost *et al.*, 1988; Van Wassenbergh *et al.*, 2006b; Roos *et al.*, 2011).

The size and shape of the mouth opening is also thought to play a crucial role in prey capture. Suction feeders with a small gape are able to produce a high-velocity water flow and prey can thus be sucked in from a greater distance (Alexander, 1967c; Cook, 1996). Adult peak gape size is smaller than the one in juveniles with respect to their snout length, so it can be reasoned that adults have a gape morphology that is hydrodynamically advantageous for generating suction (Cook, 1996). The relatively larger gape in juveniles might be related to reducing viscosity, which plays a more important role in the larval fish environment than in the adult one (chapter 4.4; Webb & Weihs, 1986; Hunt von Herbing & Keating, 2003). Roos *et al.* (2011) found that there is a difference in feeding performance between short and broad snouted juveniles on the one hand and long and narrow snouted adults on the other. While juveniles are able to draw a high amount of water towards and inside the mouth and have a short expansion time, adults perform best in terms of cranial rotation, thus minimizing the time to reach prey

(Roos *et al.*, 2011). This difference reflects a trade-off that will be elaborated upon in chapter 6.2.

In short, the evolution of the highly specialized feeding apparatus likely has benefited from the extended period of parental care, since time available for development of the remarkable morphology is thereby increased.

6.2. FUNCTIONAL MORPHOLOGY

Throughout this dissertation, it has been established that the syngnathid head looks quite unlike the head of a generalized teleost. Among the most substantial differences are: (1) the elongation of those suspensorial and neurocranial bones forming the tubular snout (*i.e.* the quadrate, preopercular, symplectic, metapterygoid, vomeral and mesethmoid bones), (2) the reduced, toothless premaxillary and maxillary bones, (3) the bones of each lower jaw half being fixed to each other, (4) the short hyoid, (5) the peculiar shape of the interhyal bone, with its two articulation heads ventrally forming a saddle joint, (6) the loss of the connection between lower jaw and opercular bone, (7) the large, strongly ossified opercular bone, and (8) the reinforced cranio-vertebral articulation involving the pectoral girdle being fixed to the vertebral column. It is not surprising that these morphological features affect the kinematics of suction feeding in syngnathids. For example, due to the small mouth opening and the long buccal cavity, only a small expansion of the snout is required to generate a high-velocity water flow (Osse & Muller, 1980; Muller & Osse, 1984; Bergert & Wainwright, 1997; Roos *et al.*, 2009).

Syngnathids approach their prey by means of a very fast dorsorotation of the head, a feeding technique known as pivot feeding (de Lussanet & Muller, 2007; Roos *et al.*, 2009; submitted a; submitted b). In order to investigate whether the modifications of the feeding apparatus can be related to the specialized pivot feeding, a thorough description of a typical syngnathid feeding sequence and the role of the muscles involved in this complex feeding system will be given, based

on observations of live animals, results from chapters 3.1, 3.2, 5.1 and the publication by Roos *et al.* (2009). All times subsequently mentioned are expressed with respect to hyoid rotation, since time = 0 ms is defined as one video recording frame prior to the onset of its movement (see Fig. 5.5).

As in most suction feeding teleosts, a syngnathid prey capture event consists of four phases: the preparation, expansion, compression and recovery phases (Lauder, 1985).

In the preparatory phase, the prey is slowly pursued either by swimming up to it or, for syngnathids with a prehensile tail, by stretching the body towards the prey while grasping onto a holdfast. Prior to a feeding strike, the head is positioned suitably for prey capture and tilted ventrally, without losing visual focus on the prey. The head depression is probably caused by contraction of the sternohyoideus muscle that inserts on the urohyal bone (and indirectly, to the ceratohyal bones) and is partly confluent with the hypaxial muscles. Activity of the protractor hyoidei muscle (connecting the dentary bone with the ceratohyal posterior bone) is required to make sure the entire cranium and not only the hyoid rotates. To counter the action of the protractor hyoidei muscle on the lower jaw and hence prevent the mouth from opening, the adductor mandibulae muscle, which originates from the dentary and maxillary bones and inserts onto the preopercular, hyomandibular and symplectic bones, probably contracts as well.

The expansive phase starts with hyoid rotation and not mouth opening as usually is the case in teleosts (Lauder, 1985). Neurocranial elevation follows shortly after (0.4 ms) as both movements (neurocranium and hyoid rotation) are coupled (Fig. 5.5). Muller (1987) described a four-bar linkage, consisting of the hyoid, the neurocranium-suspensorium complex, the pectoral girdle and the urohyal bone together with the sternohyoideus muscle (Fig. 1.6). Although Muller's model did not entirely fit the kinematical data of Roos *et al.* (chapter 5.1) due to shortening of the sternohyoideus-urohyal bar, a biomechanical coupling between the movements of the hyoid and neurocranium does exist. Prior to the feeding strike, the hyoid is protracted lying in between the left and right suspensoria and in line with the urohyal-sternohyoideus bar. The epaxial and hypaxial muscles contract while the hyoid is kept in place, thus straining their long tendons. The elastic

energy stored in these tendons will then be rapidly released once the hyoid deviates from its locking position, resulting in a sudden neurocranial elevation. By means of such elastic recoil, the limitations of muscle performance can be circumvented (e.g. Alexander & Bennet-Clark, 1977; Aerts, 1998; Zack *et al.*, 2009). Accelerations are achieved that exceed the output of normal muscle contraction and power is amplified, provided that the energy is released in a shorter time span. The presence of this power amplification mechanism was experimentally proven for *Syngnathus leptorhynchus* (Van Wassenbergh *et al.*, 2008). Muller (1987) proposed the protractor hyoidei to be involved in triggering the system. Given the attachment of the protractor hyoidei muscle on the hyoid ventral to the articulation with the suspensorium, this would imply continuous contraction of the muscle during the storing of elastic energy to keep the hyoid immobile. Relaxation of the muscle would cause hyoid depression and hence dorsal rotation of the head. Recently, Roos *et al.* (submitted b) suggested suspensorial abduction to trigger the mechanism, based on the observation that hyoid rotation is only possible if the lateral snout walls are abducted (de Lussanet & Muller, 2007). It is therefore reasoned that contraction of the adductor arcus palatini muscle, which originates from the parasphenoid bone and inserts on the symplectic and hyomandibular bones, keeps the suspensoria adducted and the four-bar mechanism locked. When the muscle relaxes, a small widening of the snout enables hyoid rotation, which consequently releases the stored energy.

Comparison of pipefishes with seahorses showed that the sternohyoideus, hypaxial and epaxial muscles are much more massive in seahorses whereas the epaxial and hypaxial tendons are much longer in pipefishes (Chapter 3.2). I hypothesized that in pipefishes the elastic energy storage mechanism is favoured over muscle contraction for generating the power needed to elevate the neurocranium, whereas in seahorses the well developed muscle bundles indicate the opposite (Chapter 3.2). A kinematical analysis of pivot feeding in newborn seahorses (*Hippocampus reidi*) carried out by Van Wassenbergh *et al.* (2009) shows that the angular velocity of both head and hyoid rotation is incredibly fast. Their inverse dynamic analysis suggests that the elastic recoil system must already be present to power these prey capture movements (Van Wassenbergh *et al.*, 2009). Pipefishes and seahorses are both pivot feeders, with quite similar feeding behaviour and the same power amplifier system, however, the muscles thought to

deliver the highest fraction of total suction power (i.e. epaxial and hypaxial muscles) are very different in morphology. In seahorses, the short tendons and bulky epaxial and sternohyoideus muscles seem not ideal for storage and release of elastic energy. Electromyographical (EMG) research to analyze muscle activity prior to visible movement might help determine how these muscles generate the required power. The long tendons and relatively small epaxial and hypaxial muscle diameter of pipefishes clearly reflect the elastic recoil mechanism. Yet, elongate sesamoid bones were found in the epaxial tendon of some pipefishes (*Doryrhamphus dactyliophorus, D. melanopleura, D. janssi, Dunckerocampus pessuliferus* and *Corythoichthys intestinalis*) (Chapter 3.2). Their presence seems quite puzzling since a bone inside a tendon is not likely to increase the elastic properties of the tendon. However, if the power amplification is not impeded, then it might prevent the tendon from rupturing during contraction of the muscles.

The main function of neurocranial rotation is to position the mouth close to the prey, in addition to expanding the buccal cavity ventrocaudally. As the neurocranium articulates with the vertebro-pectoral complex, rotation will move the neurocranium away from the fixed pectoral girdle.

Hyoid depression will not substantially contribute to a ventral expansion of the buccal cavity, unlike in other fish, for two reasons. First, the hyoid is only covered by a thin layer of skin that does not expand much when the hyoid retracts. The second reason is that the angle over which the hyoid turns during suction exceeds 90°, hence from 90° on, the buccal floor is elevated instead of depressed. This was confirmed empirically by taking X-ray images of an expanded *Hippocampus reidi* head with a barium solution in the mouth cavity (Roos *et al.*, 2009). No fluid was found in the ventral space created by hyoid depression. Therefore the hyoid is thought to have lost its role in expanding the buccal cavity ventrally. However, hyoid rotation plays an important role in lower jaw depression and suspensorial abduction. When the sternohyoideus muscle contracts, the hyoid not only rotates caudally, but also pushes the preopercular bones outwards, thus widening the snout. The exact mechanism of this abduction remains unclear, but it might be the result of a twist of the hyoid bars along their long axis. The shape and orientation of the hyoid symphysis allows an increase of the angle between the long axes of the hyoid bars during hyoid rotation, hence

the suspensoria will be pushed outwards. This kind of twist will only be possible if the symphysis functions as a hinge joint and if the hyoid turns as a whole (including the interhyal bone) about its preopercular articulation, since the saddle-shaped joint between interhyal and ceratohyal posterior bone restricts movements other than those in a rostrocaudal plane (see chapter 3.1).

At 0.7 ms, mouth opening starts (Fig. 5.5). The mouth can be opened in three ways. First, as mentioned briefly before, contraction of the protractor hyoidei muscle will result in lower jaw depression. A second and a third mouth opening mechanism can be found in the ligamentous coupling between the lower jaw and the hyoid: the mandibulo-hyoid ligament on the one hand and the mandibulo-interopercular and interoperculo-hyoid ligaments on the other hand. Due to these linkages, rotation of the hyoid will result in opening of the mouth. A ligamentous connection between the lower jaw and the maxillary bones (primordial ligament) translates lower jaw depression into a rostral swing of the maxillary bones. This way the mouth is laterally closed resulting in a more circular gape which is known to reduce drag (Alexander, 1967c; Lauder, 1979; 1985; Bergert & Wainwright, 1997).

When the mouth is closed in *H. reidi*, the line of action of the protractor hyoidei muscle lies dorsal to the lower jaw articulation (Chapter 3.2). Contraction will therefore elevate the lower jaw instead of depressing it, indicating that the muscle does not play a crucial role in the initial phase of mouth opening. Branch (1966) goes one step further and states that the protractor hyoidei muscle is superfluous in the mouth opening mechanism, but is needed for protraction of the hyoid. He based his statement on the observation that cutting the protractor hyoidei muscle in a sacrificed *Syngnathus acus* specimen had no effect on depression of the lower jaw, as contraction of the sternohyoideus muscle is transmitted by the ligaments. I found that the protractor hyoidei muscle is enclosed by the mandibulo-hyoid ligament in *D. dactyliophorus, D. pessuliferus, C. intestinalis* and *H. abdominalis* (Chapter 3.2). Contraction of the muscle and the ligament is likely not coupled as they are separated from each other by a small circular cavity.

Kinematical data showed that lower jaw depression is only initiated after the hyoid has rotated over 80° (Roos *et al.*, 2009). This signifies either that the ligaments can only generate sufficient tension to open the mouth after

substantial hyoid rotation, or that mouth opening is counteracted during the first 80° of hyoid rotation. If so, then this counteracting is probably achieved by means of adductor mandibulae muscle contraction. The delay of mouth opening can be considered an advantage, as it avoids initiation of suction feeding when the prey is not yet within reach.

Another mouth opening mechanism often found in teleosts is the opercular linkage, which translates dorsocaudal movement of the opercular bone, caused by contraction of the levator operculi muscle (attaching ventrally on the braincase), through retraction of the interopercular bone and the mandibulo-interopercular ligament to depression of the lower jaw (e.g. Anker, 1974; Lauder, 1985; Westneat, 1990; Hunt von Herbing *et al.,* 1996a; Westneat, 2004; Van Wassenbergh, 2005). This system is not functional in syngnathids since a mechanical link between the opercular and interopercular bones is missing. The high sub-ambient pressures in the opercular cavity during suction feeding might be associated with reduction of the size of the gill slit and to strengthening of the operculum (Osse & Muller, 1980; Muller & Osse, 1984). This reinforcement likely also implies a limitation of opercular mobility; hence the loss of opercular elevation and coupled lower jaw depression seems beneficial. The absence of a levator operculi muscle in some pipefishes, e.g. *D. dactyliophorus* (Chapter 3.2) and *Syngnathus acus* (Branch, 1966) is very likely related to the decoupling of the lower jaw and the opercular bone.

During the first milliseconds of the expansive phase, the volume of the buccal cavity is actually reduced by means of a lateral compression of the head. This is probably a consequence of contraction of the adductor arcus palatini and the adductor operculi muscles (connecting the opercular bone to the prootic bone), resulting in a medial movement of the suspensorium and operculum, respectively. At 1.5 ms, the small gill slits open and next, around 2 ms, the snout starts to expand at the level of the lower jaws, which is brought about by the abducing force component of lower jaw depression that pushes the quadrate bones outwards. This is rapidly (2.5 ms) followed by a dilatation of the more posterior part of the snout, caused by hyoid depression (over 90°) and potentially aided by contraction of the levator arcus palatini muscle that has its origin on the sphenotic bone and its insertion on the hyomandibular and preopercular bones. The resulting suspensorial abduction causes the main expansion of the buccal cavity.

At 2.6 ms after the start of the expansive phase, peak gape is achieved (Fig. 5.5), followed by the neurocranium reaching its maximal rotation (3.6 ms). Very soon after that, the prey starts to move in the direction of the mouth opening (4.0 ms). At 4.8 ms the opercula are widened by means of the dilatator operculi (insertion on the opercular bone, origin on the hyomandibular, parasphenoid and sphenotic bones) and hyohyoideus abductor muscles (originating from the ceratohyal posterior bone and inserting on the first branchiostegal ray). The gill slits are sealed by the branchiostegal membrane and the two slender branchiostegal rays just prior to the prey being sucked in (5.7 ms).
In syngnathids, the compression phase is characterized by the start of mouth closure, which is accomplished by contraction of the adductor mandibulae muscle complex. The different bundles of this muscle elevate the lower jaw and also retract the maxillary bones to their more caudal position. The maximal buccal expansion is generated, moving the prey further through the snout (14.3 ms). At 19.6 ms, peak hyoid rotation is reached, after which the hyoid is protracted again by contraction of the protractor hyoidei muscle. Also the suspensorium starts to adduce by contraction of the adductor arcus palatini muscle, aided by contraction of the intermandibularis muscle (connecting left and right dentary bones) that pulls both lower jaw halves together. The mouth is not fully closed until about 420 ms. Due to contraction of the adductor operculi muscle, which causes an inward movement of the opercular bone and pulls the branchiostegal rays together, water is passed over the gills and expelled through the tiny branchial openings.
During the recovery phase all elements return to their original position. The neurocranium is completely depressed and the hyoid is protracted again. This phase lasts until approximately 600 ms after initiation of prey capture, sometimes longer.

Comparison between the kinematics of the syngnathid pivot feeding and those of a general teleost suction feeding event reveals the following: (1) movement of cranial elements in syngnathids does not proceed in a rostrocaudal sequence starting with mouth opening, followed by hyoid depression and finally head rotation. However, lateral expansion does follow the rostrocaudal wave typical for many aquatic suction feeders (see Bishop *et al.*, 2008 and references within).

The lower jaws abduct first, next the hyoid bars push the suspensoria outwards and lastly the opercula widen. (2) Buccal volume increase is mainly caused by lateral snout abduction, there is a certain amount of caudal expansion due to neurocranial elevation and no rostral or ventral expansion (absence of maxillary protrusion and lowering of the buccal floor). (3) Neurocranial elevation is substantial and is used to position the mouth close to the prey. (4) An opercular mouth opening mechanism is absent.

So the syngnathid trophic apparatus does not only diverge from a general teleost in its morphology, but also in function. The pivot feeding technique yields exceptionally short prey capture times, with large forces, velocities and accelerations involved. Hence, the cranial morphology is likely determined by mechanical demands associated with this type of feeding. The finite element analysis that simulated suction pressure in the cranium of several seahorses and pipefishes confirmed this. Highest stress magnitudes were found in those regions expected to be able to withstand high amounts of compressive stress (*i.e.* cartilage and articulations). Also, head morphology is found to affect the stress distribution generated during feeding. However, no simple relation was found with relative snout length. Nevertheless, snout length and diameter will probably influence prey capture performance. The family of Syngnathidae consists of species with many different degrees of snout dimension, yet all syngnathids recorded so far exhibit the same pivot feeding strategy. This raises the question what the most favourable snout length is for carrying out pivot feeding, or more specifically, whether snout elongation is related to an increase in feeding performance.

In theory, an elongate snout is beneficial because it decreases the head rotation angle to bridge a certain distance between the snout tip and the prey (Kendrick & Hyndes, 2005; de Lussanet & Muller, 2007). Prey can therefore be attacked from further away and, as the predator does not need to approach its prey closely to initiate a feeding strike, it will be less likely to be detected and has a greater chance to capture the prey (Flynn & Ritz, 1999; Kendrick & Hyndes, 2005). Also, long-snouted species should be able to achieve a higher angular velocity of the head, provided that the mass to be rotated is minimized (Muller & Osse, 1984). Consequently, species with a long snout are able to capture more rapidly

swimming prey (Franzoi *et al.*, 1993; Kendrick & Hyndes, 2005; Oliveira *et al.*, 2007). Besides that, a small gape allows the fish to be more selective in the uptake of prey (Branch, 1966). On the other hand, feeding through a long and slender tube is thought to entail several physical constraints. Firstly, with increasing snout length, the moment of inertia during head rotation increases as well (de Lussanet & Muller, 2007). To compensate for this, the cross-sectional area of the snout must be minimized, however a small gape is unfavourable for the capture of large prey and thus a tiny mouth opening limits syngnathids to consume only small prey items. Secondly, a long snout also increases the distance between the eye and the prey and given that syngnathids are visual predators, this might reduce the performance in terms of accurate aiming and positioning of the snout tip relative to the prey (Roos *et al.*, submitted a). Thirdly, the longer the snout, the larger the sub-ambient pressure in the buccal cavity must be to create the same flow velocity as in shorter snouted species (Poiseuille's law). Finally, the total buccal volume increase is expected to be smaller and expansion time longer in long-snouted species, which will negatively affect suction performance (Roos *et al.*, 2011).

Some experimental analyses on the relation between snout length and prey type or prey capture performance have been carried out. A comparison between the feeding kinematics of the long-snouted pipefish *D. dactyliophorus* and the short-snouted *D. melanopleura* showed that both species capture prey by means of the same stereotypical pivot feeding kinematics, but differences in certain aspects of the feeding strike could be observed (Roos *et al.*, submitted a). The long-snouted species turns its head over a larger angle to bring its mouth close to the prey, hence a larger distance is covered. In addition, *D. dactyliophorus* is able to generate a higher velocity of the mouth during head rotation, thus minimizing the time to reach the prey. A dietary study showed that long-snouted syngnathids consume more elusive prey from a wide range of available prey types than short-snouted species, confirming the short times to reach prey (Kendrick & Hyndes, 2005). The short-snouted *D. melanopleura*, however, captured its prey in less time and had a higher success rate, likely due to the smaller distance between eyes and mouth (Roos *et al.*, submitted a). Successful prey capture appears to depend greatly on adequate positioning of the snout tip relative to the prey.

A resemblance with butterflyfishes (Chaetodontidae) can be observed as this family also encompasses both short- and long-jawed species. Their remarkable feeding apparatus consists of elongated premaxillary bones and lower jaw that are not fused to form a tube, which differs from syngnathids where the bones of the ethmoid region form an elongated snout. Although bearing teeth, the long-jawed butterflyfishes (*Chelmon rostratus* (L.), *Forcipiger flavissimus* Jordan & McGregor and *Forcipiger longirostris* (Broussonet)) capture their prey by means of a combination of suction and ram feeding (Ferry-Graham *et al.*, 2001a). The prey is approached by swimming or by protruding the long and slender jaws towards it. Ferry-Graham *et al.* (2001a) demonstrated that the chaetodontid with the longest jaws (*F. longirostris*) initiated its feeding strike from a greater distance compared to other (shorter jawed) butterflyfishes, indicating that a lot of ram was performed to catch the prey. Besides that, the diet of this high-performance species is known to be exclusively comprised of elusive prey. Another study, in which kinematical data of five chaetodontid species was analyzed, revealed that the two short-jawed species never missed a strike whereas several failed attempts at prey capture were observed in the long-jawed butterflyfishes (Ferry-Graham *et al.,* 2001b). These findings are similar to the observations in long-snouted syngnathids, that rotate their head over a greater angle (i.e. initiate a prey capture event from further away), consume more highly mobile prey and have lower feeding success rate compared to short-snouted species. Both examples support the statement by Gibb & Ferry-Graham (2005) that as individuals of a species become more specialized in catching elusive prey, this will be reflected in modification of their suction feeding ability, either by changing their prey capture kinematics or their feeding apparatus morphology.

All this suggests that no optimal snout length exists for performing pivot feeding. Rather, there seems to be a trade-off between favouring the performance of head rotation and maximizing suction performance (Roos *et al.*, 2011). These different strategies are reflected in either a long snout with a small diameter and a high angular velocity to decrease the time to reach prey on the one hand, or shortening of the snout, thus increasing the suction volume and the velocity of the water flow on the other hand. The developmental shift from short- and broad-snouted juveniles to longer and more slender snouted adults could be related to this (see

chapter 6.1 and Roos *et al.*, 2010). The trade-off might explain the large morphological diversity in relative snout dimension present in Syngnathidae.

6.3. EVOLUTIONARY MORPHOLOGY

A significant amount of research has been carried out to resolve the phylogeny of the Percomorpha in general and the Gasterosteiformes in particular (e.g. Johnson & Patterson, 1993; Chen *et al.*, 2003; Miya *et al.*, 2003; Smith & Wheeler, 2004; Dettai & Lecointre, 2005; Miya *et al.*, 2005; Nelson, 2006; Keivany & Nelson, 2006; Kawahara *et al.*, 2008; Wilson & Orr, submitted). In spite of this, affinities are still not very well understood. As mentioned in the introduction (Chapter 1), the monophyly of the order Gasterosteiformes, as established based on morphological studies (Fig. 1.2; Johnson & Patterson, 1993; Nelson, 2006; Keivany & Nelson, 2006), is recently disputed by molecular data (Fig. 1.3; Chen *et al.*, 2003; Smith & Wheeler, 2004; Dettai & Lecointre, 2005; Kawahara *et al.*, 2008). According to the latter, the order should be divided into three groups, which are thought to have diverged early in Percomorph evolution. The first group consists of the Indostomidae, whose phylogenetic position has always been controversial (McAllister, 1968; Johnson & Patterson, 1993; Britz & Johnson, 2002; Nelson, 2006; Kawahara *et al.*, 2008) being placed within the Gasterosteoidei (Britz & Johnson, 2002; Takata & Sasaki, 2005; Nelson, 2006), in the suborder Syngnathoidei (Keivany & Nelson, 2006) or nested within another order, Synbranchiformes (Kawahara *et al.*, 2008). The second clade comprises the former suborder Gasterosteoidei and the third group encompasses the suborder Syngnathoidei (Kawahara *et al.*, 2008). According to this vision, the Syngnathoidei cluster together with the Dactylopteridae (flying gurnards), however morphological data does not support this sister taxon relationship (Johnson & Patterson, 1993).

Although the Gasterosteiformes remain a problematic clade and further analyses, both morphological and molecular (perhaps using nuclear instead of mitochondrial gene data), are needed to resolve the interrelations within the

clade, the previously described inconsistency does not affect the results of this dissertation. *Gasterosteus aculeatus* (three-spined stickleback), used as representing the ancestral condition for a comparison with *Syngnathus rostellatus* and *Hippocampus capensis* in chapter 3.1, might not be a sister group species of the Syngnathidae, but it remains a generalized percomorph in both points of view, and is therefore still suitable as an out-group. The results of this comparison are already briefly discussed in chapter 6.2.

The first evidence of Syngnathidae in the fossil record dates back to the Middle Eocene (ca. 50 Mya) (Patterson, 1993; Teske *et al.*, 2004). These ancestors resemble extant pipefishes, both having the head in line with the body, a tubular snout with a small mouth and bony plates covering the body (Teske & Beheregaray, 2009). The transition from pipefish to seahorse morphology (*i.e.* the upright body axis with the tilted head in combination with the prehensile tail) is not represented in the fossil record that is hence inadequate to elucidate all evolutionary patterns within the family. The only known seahorse fossils were found in Marecchia in Italy (ca. 3 Mya) and recently in Tunjice in Slovenia (ca. 13 Mya) (Teske *et al.*, 2004; Žalohar *et al.*, 2009). Due to these findings and the fact that seahorses have a cosmopolitan distribution, meaning that divergence of the genus *Hippocampus* from the other syngnathids should have occurred before the complete closure of the Tethyan seaway, the origin of seahorses is thought to be at least 20 Mya (Casey *et al.*, 2004; Žalohar *et al.*, 2009). A close affinity between seahorses and pipefish of the genus *Syngnathus* has been established based on molecular data (Wilson *et al.*, 2001; Wilson & Rouse, 2010). The obtained phylogeny corresponds surprisingly well with the relationships proposed by Herald (1959), which he inferred from studying brood pouch morphology within the Syngnathidae (Fig. 1.5). Wilson *et al.* (2001; 2003) state that the extremely rapid diversification of the brooding structures might be the driving force behind the evolution of the family. The attachment of eggs and embryos to the male body is thought to be derived from nest building and guarding behaviour of male ancestors (Baylis, 1981). From gluing organic material together to build a nest, as observed in the three-spined stickleback, it may be only a small step to gluing embryos on the body surface.

Recently, another molecular phylogeny (Teske & Beheregaray, 2009) contradicts the close relationship between *Syngnathus* pipefishes and seahorses, indicating *Idiotropiscis* pygmy pipehorses, *i.e.* seahorse-like pipefishes that swim horizontally (Kuiter, 2004), to be the sister taxon of seahorses. These pipehorses can be considered as the living evolutionary link between pipefishes and seahorses. Separation between the pipehorse and the seahorse lineages occurred during the Late Oligocene (ca. 25-28 Mya; hence much earlier than the first known seahorse fossil) and is suggested to be brought about by habitat association (Teske & Beheregaray, 2009). Tectonic events in the Western Pacific Ocean during this geological period resulted in the increase of shallow-water areas dominated by seagrass beds. Fragments of seagrasses were found together with the seahorse fossils in the Tunjice Hills, giving an indication of the ancestral habitat (Žalohar *et al.*, 2009). The seahorses' vertical body posture greatly benefitted by this vegetation since seagrasses provide better camouflage compared to algal reefs (Teske & Beheregaray, 2009). Also presently, seahorses occur abundantly in this habitat because seagrasses form adequate holdfasts and are usually associated with high concentrations of copepods and other important syngnathid prey items (Tipton & Bell, 1988; Foster & Vincent, 2004; Vizzini & Mazzola, 2004; Curtis & Vincent, 2005; Murugan *et al.*, 2008; Scales, 2010). Similar to the upright seahorse body, the selective pressure towards a more cryptic morphology might also have led to the evolution of fleshy appendages in seadragons (Wilson & Rouse, 2010).
Apart from the highly specialized brood pouch as a key innovation of the family or the ecologically based selection for evolution from pipefish to seahorse, the biomechanics of prey capture might also have been a driving force. In chapter 4, the geometric morphometric analysis yielded some differences in general head morphology between pipefishes and seahorses. The most important modifications that characterize the transition from a pipefish to a seahorse include a more ventral position of the pectoral fin, a decrease in snout length and an increase in snout, head and opercular heights. I reasoned that all these differences could be related to the tilted head of seahorses, either directly (e.g. displacement of the pectoral fin along with the body) or indirectly (as a consequence of head rotation). The tilting of the head with respect to the body is suggested to allow a greater degree of head rotation in seahorses (Chapter 4). Hence, a larger distance to prey could be spanned without having to increase the

snout length. If the prey is in front and above the mouth, rotation of the head over a large angle will bring the tip of the snout closer to the prey along the dorsoventral axis, however, it increases the distance to the prey along the rostrocaudal axis. So, in order to suck in the prey, a larger water volume has to be put into motion, which requires more energy. To overcome this problem, the snout tip can be positioned somewhat ventrorostral to the prey before the strike, as modelled in Fig. 5.7B (note the position of the mouth with respect to the outflow of the pipette). However, this might increase the risk of detection by the prey and subsequently trigger an escape response. Alternatively, the entire head can be moved anteriorly during rotation, which is subtly visible in Fig. 5.7A (also note the more posterior position of the mouth at the onset of neurocranial elevation in the video frame compared to the model). This anterior movement of the mouth was also observed by Van Wassenbergh *et al.* (2011). High speed recordings of prey intake in combination with modelling of the head rotation showed that a more pronounced angle between head and body, as in seahorses, is associated with an anterior translation of the head, in addition to its rotation. This way, the mouth moves towards the prey, which can thus be captured from further away. On the other hand, mathematical modelling suggests that a head in line with the body, as in pipefishes, favours higher velocities of the mouth during head rotation (Van Wassenbergh *et al.*, 2011). The tilted head of seahorses is considered to act in the same way as the elongation of the snout observed in many syngnathids. They both increase the prey distance, enlarge the space in which prey can be captured and therefore a larger number of food items might be caught (Van Wassenbergh *et al.*, 2011). Roos *et al.* (2011) found that the time to reach prey is decreased by increasing snout length during ontogeny. Apparently, time to reach prey can also be minimized by head rotation in combination with anterior movement of the mouth as in seahorses. Perhaps this explains the absence of extremely long-snouted seahorses. The seahorse with the longest snout is *Hippocampus histrix* Kaup (Lourie *et al.*, 2004), which has a snout length of about half its head length. Interestingly, the snout of the two fossil seahorse species found in Slovenia (*H. sarmaticus* and *H. slovenicus*), also measures half the length of the head (Žalohar *et al.*, 2009). Pipefishes such as *Doryrhamphus dactyliophorus* and *Dunckerocampus pessuliferus*, however, have a much more elongate snout, measuring over 65% of the head length.

During a seahorse feeding strike, the anterior displacement of the mouth is not always accomplished by swimming towards the prey, but by stretching the body towards it, while keeping the tail wrapped around a holdfast. Hence, the evolution to an increasingly bent head might be associated with the loss of the caudal fin and the tail becoming prehensile. Choo & Liew (2006) observed some vestigial caudal fin rays in newly born *Hippocampus kuda* that disappear after a few days, confirming the secondary loss of the caudal fin during evolution. Given the pipehorse morphology, being a pipefish-like body with a seahorse-like tail, it is likely that the origin of the grasping tail and the associated sit-and-wait feeding behaviour preceded that of the tilted head in combination with anterior translation of the mouth (Van Wassenbergh *et al.*, 2011). Kinematical analysis of prey capture in *Idiotropiscis* pipehorses might yield interesting results for understanding the evolutionary pattern that has led to the seahorse morphology and feeding strategy.

6.4. General conclusion

This dissertation focuses on the remarkably specialized feeding apparatus of the Syngnathidae. As in many evolutionary morphological studies, the research started with questions such as 'What does it consist of?', 'How does it work?', and 'Why does it look the way it looks?'. These questions seemed especially interesting for syngnathids since their head looks so unusual with the tubular snout and small jaws. Prey capture is incredibly fast and yet the advantages of the morphology are not immediately apparent given the hydrodynamic limitations. Hence, a research project was initiated with central aim to elucidate the evolutionary pattern that has led to the extreme morphological specialization of Syngnathidae.

In the first place, the results of this dissertation yield a number of structural features that probably are related to the pivot feeding. An example of this is the interhyal bone that deviates greatly from the typical teleostean rod-shape in bearing two articulation heads for the hyoid. The saddle joint thus formed,

constrains hyoid movement other than rotation in the sagittal plane. Apart from this and other modifications, the syngnathid head is also characterized by coupling events. The most important of these is found in the four-bar system that links hyoid rotation to neurocranial elevation and at the same time works as a power amplifier. Also a decoupling is observed as the opercular mouth opening mechanism is lost. These morphological traits are highly conserved among the family: they could be demonstrated in all studied species.

The family is characterized by a large morphological variation with regard to snout dimensions. The initial assumption was that species with a longer snout are more specialized for catching elusive prey, which was demonstrated by a dietary analysis (Kendrick & Hyndes, 2005). By means of a preliminary geometric morphometric analysis it was established that long-snouted syngnathids have a reduced intraspecific variation in terms of their head shape, as expected for a specialized morphology. However, a kinematical study proved that pipefish with a long snout do not necessarily perform faster pivot feeding than short-snouted species (Roos *et al.*, submitted a). Moreover, when looking at the syngnathid phylogeny (Fig. 1.5), there is no evolution towards a more elongate snout since the longest-snouted species are found in the *Phyllopteryx* and *Doryrhamphus* genera and not among seahorses (*Hippocampus*), which are considered as phylogenetically the most derived syngnathids. This suggests the presence of a trade-off rather than a straightforward evolutionary trend. A long snout is favoured to increase the angular velocity of head rotation and to minimize the time to reach prey, whereas a short snout is advantageous for increasing suction volume and velocity (Roos *et al.*, 2011).

Finally, the exceptional reproductive strategy and prolonged parental care very likely played an important role in the evolution of the feeding apparatus, since they allow the release of fully independent juveniles that resemble adults both in form and function.

Perhaps most importantly, the results of this dissertation highlight that Syngnathidae, with their highly specialized feeding apparatus, extraordinary development and unequalled performance, establish conclusive proof for the incredible capabilities of natural selection and evolution.

7 Summary & samenvatting

7.1. SUMMARY

This PhD thesis deals with the evolution of the specialized head morphology in Syngnathidae, a family among the bony fishes that comprises pipefishes, seahorses, seadragons and pipehorses. A detailed morphological description of the feeding apparatus of several syngnathid representatives forms the core of this research. Besides that, other aspects like morphological variation within the family, performance of the trophic system and mechanical loading during prey intake are thoroughly studied. The following summary provides a clear overview of the main results and conclusions of each chapter and presents answers to the research questions as formulated in chapter 1.3.2.

In the first chapter some general concepts like 'evolution', 'natural selection' and 'specialization' are illustrated. An introduction to the biology of Syngnathidae follows, in which their taxonomical position, reproduction, complex parental care and external morphology are discussed briefly. Next, the scientific problem of the study is described. The feeding apparatus is extremely specialized in this family. All representatives have a tubular snout with small, terminal jaws. Yet, the length and diameter of the snout is variable among species. Prey is captured by

means of head rotation, which positions the mouth close to the prey, followed by an increase of the buccal cavity volume. This expansion generates a sub-ambient pressure and hence a water flow towards the mouth is created. This type of feeding is known as pivot feeding. Prey intake is very fast (prey capture times are less than 6 ms), however, suction feeding by means of a long and slender snout also implies hydrodynamic constraints (such as more drag due to suction through a narrow tube and a high moment of inertia caused by rotation of a head with a long snout). This paradox renders the trophic apparatus in Syngnathidae a very interesting research topic. The objective of this doctoral research is to unravel the evolutionary pattern behind the extreme morphological and functional specialization.

Chapter two provides an overview of the studied material and the applied methods. First, a list of the chosen species is given with reference to the origin of the specimens and what they were used for. In a second part, the techniques that are used throughout the research are explained in depth. Detailed protocols for the clearing and staining of the specimens and for the histological sectioning are presented, as well as the applied methods for measuring, dissecting, CT-scanning and graphical 3D-reconstructioning. The geometric morphometric and finite element analyses are elaborated on a little more. The chapter closes with a clarification of various controversial terms.

The third chapter deals with the morphology of the feeding apparatus in Syngnathidae and is divided in two parts.
In the first part, the structure of the cranium of a pipefish (*Syngnathus rostellatus*) and that of a seahorse (*Hippocampus reidi*) is placed into an evolutionary context by comparison with the head morphology of a stickleback (*Gasterosteus aculeatus*). In addition, morphology of the juvenile head around the time of release from the pouch is described. Elongation of the snout in the cartilaginous skull is situated at the level of the ethmoid region, with the ethmoid plate, the hyosymplectic cartilage and the basihyal cartilage being extended. With exception of the circumorbital and some opercular bones, all cranial bones are already formed in the juveniles, albeit solely as a thin layer of bone. This close resemblance with the adult head is probably associated with the extended brood period and parental

care. Due to this, emergence of the young from the pouch can be delayed until an advanced developmental stage is reached. Apart from that, the results show that the adult snout is made up by the elongated vomeral, mesethmoid, quadrate, metapterygoid, symplectic and preopercular bones. Some morphological features that can be regarded as evolutionary adaptations to the specialized feeding type are the reduced maxillary and toothless premaxillary bones, the firmly connected bones of the lower jaw, the robust operculum and the saddle-shaped joint between the interhyal and ceratohyal posterior bone.
The second part of this chapter focuses on the effect of snout elongation within the family, both on an osteological and a muscular level. An exhaustive morphological study of the head of both a long-snouted seahorse (*H. reidi*) and a pipefish with an extremely elongate snout (*Doryrhamphus dactyliophorus*), compared to several syngnathids with both short and intermediate snout lengths (*H. zosterae, H. abdominalis, Corythoichthys intestinalis* and *D. melanopleura*), confirmed the previous results. Also, a few specialized muscle, tendon and ligament configurations are discovered, such as the sternohyoideus muscle, which is very well developed in seahorses, the protractor hyoidei muscle that is enclosed by the mandibulo-hyoid ligament in some syngnathids and the long, rod-shaped sesamoid bone in the epaxial tendons of several pipefishes. These observations seem to reveal different power generating strategies during pivot feeding, favouring storage and release of elastic energy in the epaxial and hypaxial tendons over plain muscle force in pipefishes and *vice versa* in seahorses. Although the syngnathid musculoskeletal structure consists of some elements shared by all representatives, there are also notable morphological differences among species. However, only a few of these differences could be related to variation in relative snout length.

The morphological variation within the family is quantified in chapter four by means of a geometric morphometric analysis carried out on a large number of syngnathid representatives. Through this method, it is established that the most important differences between the pipefish and seahorse head morphology are related to changes in snout and head dimension, position of the pectoral girdle and height of the opercular bone. This variation is likely associated with the head-body axis (body in line or at an angle with the head) and with the feeding

kinematics (long snout with little head rotation or short snout with large rotation). Due to the high degree of specialization in the feeding apparatus of Syngnathidae, a small deviation of the movements of or interactions between the elements in the head, might result in reduced functional performance. This leads to the hypothesis that each species of the family is characterized by limited intraspecific morphological variation. Morphological variation within species with a long snout, which are regarded as being more specialized compared to short-snouted species, will be diminished. The preliminary results of this study confirm our expectations. Finally, it was investigated whether juvenile seahorses (*H. reidi*) still undergo important ontogenetic transformations after leaving the pouch. Gradual shifts in shape, like the dorsoventral narrowing of the snout and head and the reorientation of the preopercular bone, characterize juvenile development. However, the period of major developmental changes seems to have taken place in the pouch.

In the fifth chapter, some functional aspects of the specialized feeding apparatus are addressed.
The first part of this research was carried out in collaboration with Gert Roos and Sam van Wassenbergh (University of Antwerp) and it evaluates a previously described planar four-bar mechanism (Muller, 1987) that couples hyoid rotation to neurocranial elevation. Both the morphological description of all linkages and joints involved in the system, as the kinematical recordings of a feeding strike in a seahorse (*H. reidi*), demonstrate the incredible specializations of the trophical system. Not only does the syngnathid pivot feeding differs from suction feeding in a general teleost in terms of velocity (prey capture takes less than 6 ms), but also in sequence of movements; the expansion phase starts with hyoid rotation and not with mouth opening as is usually the case (*i.e.* rostrocaudal wave). Besides that, the results provide clear proof for the coupling between hyoid and neurocranium. However, a discrepancy is discovered between the predicted movements (based on four-bar modelling) and the observed movements (based on video recordings). This is most likely due to modelling the bar that consists of the urohyal bone together with the sternohyoideus muscle, as constant in length, whereas it shortens due to muscle contraction.

The second part of this chapter explores where in the skull most mechanical stress is exerted as a consequence of the large pressure differences during feeding. This was done by means of a finite element analysis on the modelled skulls of three seahorse and three pipefish species with various relative snout length (*H. reidi, H. abdominalis, H. zosterae, D. dactyliophorus, S. rostellatus* and *D. melanopleura*). In accordance with our expectations, in all models (except for D. *dactyliophorus*) peak stress accumulations where observed at the level of articulations and cartilaginous regions in the modelled crania. These concentrations of stress will be much lower in the real skulls since both cartilaginous tissue and articulating elements are thought to resist compressive stress well. A second aim was to analyze whether or not a difference in stress distribution pattern exists between short- and long-snouted species. The prediction was that species with a long snout need to generate larger pressure differences, and hence should be able to withstand higher amounts of stress through certain morphological adaptations. When applying the same pressure to both short- and long-snouted models, the models with a long snout are thought to experience less stress. This hypothesis could not be confirmed by the results, however, the geometry of the bones in the snout (bone thickness, amount of overlap between different bones, *etc.*) has a clear influence on the stress distribution.

In chapter six, the obtained results are discussed in an ontogenetic, functional and evolutionary context, followed by a general conclusion.
First, the remarkable development of Syngnathidae is dealt with. The parental care is long and extensive; the male attaches the eggs and embryos onto its body or keeps them in a sealed pouch, even after hatching. The degree of parental investment increases with increasing complexity of the brood area. Even the most basal syngnathids protect the young against predation and some more derived species osmoregulate, nourish and aerate the young as well. Due to the prolongation of the brood period, onset of exogenous feeding is delayed and more time for development of the young is available. Hence, newly born syngnathids are almost fully developed (the larval phase and related metamorphosis are absent or occur in the pouch) and juveniles are able to capture prey by means of pivot

feeding. In sum, it can be stated that the far-reaching parental care probably has aided in the evolution of the specialized syngnathid head morphology.

The second part of the discussion highlights the functioning of the syngnathid feeding system. The most important structural and functional modifications in comparison with the trophic apparatus of a generalized teleost are repeated. Next, a detailed description of the movements and activity of all separate elements in the head during feeding intake is given. Finally, the advantages and disadvantages related to snout elongation are listed. From this it was deduced that the morphological variation associated with snout dimension present in the family, is probably the result of a trade-off. To optimize head rotation performance, a long snout is favoured, whereas a short snout is beneficial for improving suction capacity. This might account for the large morphological diversity seen within Syngnathidae.

Part three considers the results in a phylogenetic and evolutionary framework. First, arguments for comparison of the syngnathid head with the head of the three-spined stickleback (*Gasterosteus aculeatus*), even though they might not be sister taxa, are provided. Then, the evolutionary trends that might have led to the seahorse morphology (*i.e.* the prehensile tail, tilted head and vertical body posture) are described. The genus *Idiotropiscis* (pygmy pipehorses) is regarded as the extant transition from pipefishes to seahorses. Divergence between seahorses and pipehorses is thought to have benefitted from the increase of habitats dominated by seagrasses, which provide better protection to organisms with an upright body axis. In addition, biomechanics of pivot feeding might have played a role in the evolution towards seahorses. The tilted head-body axis likely promotes head rotation and the grasping tail allows stretching of the body in the direction of the prey. The anterior directed movement of the mouth reduces the time needed to reach the prey. Hence, the selective advantage of snout elongation, which is thought to similarly minimize time to reach prey, is reduced in seahorses. The absence of extremely long-snouted seahorses could thus be explained.

Finally, these findings are concisely recapitulated in the general conclusion.

7.2. SAMENVATTING

Dit doctoraatsproefschrift behandelt de evolutie van de gespecialiseerde kopmorfologie in Syngnathidae, een familie binnen de beenvissen waartoe zeenaalden, zeepaardjes, zeedraken en 'pipehorses' behoren. Een gedetailleerde morfologische beschrijving van het voedselopnameapparaat bij enkele syngnathe vertegenwoordigers vormt de kern van dit onderzoek. Daarnaast worden andere aspecten zoals morfologische variatie binnen de familie, werking van het trofisch systeem en mechanische belasting tijdens de voedselopname uitvoerig bestudeerd. De volgende samenvatting geeft een duidelijk overzicht van de belangrijkste resultaten en conclusies per hoofdstuk en biedt een antwoord op de onderzoeksvragen zoals geformuleerd in hoofdstuk 1.3.2.

In het eerste hoofdstuk worden enkele algemene begrippen zoals 'evolutie', 'natuurlijke selectie' en 'specialisatie' toegelicht. Daarop volgt een inleiding tot de biologie van Syngnathidae, waarbij de taxonomische positie, voortplanting, complexe broedzorg en uitwendige morfologie aan bod komen. Vervolgens wordt de wetenschappelijke probleemstelling geschetst. Het voedselopname-appararaat is in deze familie extreem gespecialiseerd. Alle vertegenwoordigers hebben een buisvormige snuit met kleine, eindstandige kaken. De lengte en diameter van de snuit is echter variabel over verschillende soorten. Voedselopname ('pivot feeding') gebeurt door middel van koprotatie waardoor de snuittip naar de prooi gebracht wordt, gevolgd door een volumetoename in de buccale holte. Deze expansie creëert een onderdruk waardoor een waterstroom in de richting van de mond ontstaat. Het vangen van een prooi gebeurt heel snel (minder dan 6 ms), maar voedselopname met behulp van een lange, smalle snuit houdt ook een aantal hydrodynamische beperkingen in (zoals een hoge weerstand bij het zuigen van water door een dunne buis en een groot inertiemoment tijdens rotatie van een kop met lange snuit). Deze paradox maakt het voedselopname-apparaat bij Sygnathidae tot een zeer interessant onderzoeksobject. De doelstelling van dit doctoraatsonderzoek is dan ook het ontrafelen van het evolutionaire patroon dat aan de basis ligt van deze extreme morfologische en functionele specialisatie.

Hoofdstuk twee geeft een overzicht van het bestudeerde materiaal en de toegepaste methodes. Eerst wordt een opsomming gegeven van de gekozen soorten met vermelding van de herkomst van de specimens en waarvoor ze gebruikt werden. In een tweede deel worden de technieken die doorheen het onderzoek toegepast werden, uitgebreid uitgelegd. Gedetailleerde protocols voor het ophelderen en kleuren van specimens en voor het maken van histologische coupes worden gegeven, alsook de gehanteerde methode bij het meten, uitvoeren van dissecties, nemen van CT-scans en maken van grafische 3D-reconstructies. Iets meer aandacht wordt besteed aan de geometrisch morfometrische en de eindige elementen (finite element) analyses. Tenslotte volgt in de laatste paragraaf een verduidelijking van een aantal controversiële begrippen.

Het derde hoofdstuk handelt over de morfologie van het voedselopname-apparaat bij Syngnathidae en is onderverdeeld in twee delen.
In het eerste deel wordt de bouw van het cranium van een zeenaald (*Syngnathus rostellatus*) en van een zeepaard (*Hippocampus capensis*) in een evolutieve context geplaatst door vergelijking met de kopmorfologie van een stekelbaars (*Gasterosteus aculeatus*). Ook de morfologie van de juveniele kop rond het tijdstip van vrijkomen uit de buidel, komt aan bod. De snuitverlenging van de kraakbenige schedel situeert zich ter hoogte van de ethmoid regio en de ethmoidplaat, het hyosymplecticum en het basihyale zijn verlengd. In de juvenielen zijn alle craniale beenderen, met uitzondering van de circumorbitalia en enkele operculaire beenderen, al gevormd, zij het enkel als een zeer dun laagje. Deze grote gelijkenis met de adulte kop is waarschijnlijk te wijten aan de lange broedperiode en uitgebreide ouderlijke zorg. Hierdoor kan het vrijlaten van de jongen uit de buidel uitgesteld worden tot ze een vergevorderd ontwikkelingsstadium bereikt hebben. Verder tonen de resultaten aan dat de adulte snuit gevormd wordt door een verlenging van het vomer, mesethmoid, quadratum, metapterygoid, symplecticum en preoperculare. Enkele morfologische aspecten die als evolutionaire adaptaties aan de gespecialiseerde voedselopname kunnen beschouwd worden, zijn de gereduceerde en tandloze maxillaire beenderen, de stevige verbinding tussen de verschillende beenderen van de onderkaak, het robuuste kieuwdeksel en het zadelvormig gewricht tussen interhyale en ceratohyale posterior.

In het tweede deel van dit hoofdstuk ligt de nadruk op het effect van snuitverlenging binnen de familie, zowel op osteologisch als myologisch vlak. Een gedetailleerde morfologische studie van de kop van zowel een lang-snuitige zeepaard (*H. reidi*) als een zeenaald met extreem lange snuit (*Doryrhamphys dactyliophorus*), in vergelijking met een aantal syngnathen met korte en intermediaire snuit (*H. zosterae, H. abdominalis, Corythoichthys intestinalis* en *D. melanopleura*), bevestigt de resultaten uit het voorgaande deel. Bovendien worden enkele gespecialiseerde spier-, pees- en ligamentconfiguraties aan het licht gebracht. Zo is de sternohyoideus spier heel goed ontwikkeld bij zeepaardjes, wordt de protractor hyoidei spier bij enkele syngnathen omgeven door het mandibulo-hyoid ligament en wordt in de epaxiale pezen van een aantal zeenaalden een lang, staafvormig sesamoid been gevonden. Deze waarnemingen suggereren de aanwezigheid van verschillende vermogen versterkende strategieën voor koprotatie tijdens de voedselopname. Het vrijlaten van elastische energie, opgeslagen in de epaxiale en hypaxiale pezen, lijkt begunstigd in zeenaalden terwijl spierkracht verkozen wordt in zeepaardjes. Hoewel het syngnathe musculoskeletale systeem uit een aantal elementen bestaat die gedeeld worden door alle vertegenwoordigers, zijn er dus toch een aantal opmerkelijke morfologische verschillen tussen soorten. Slechts weinig van deze verschillen kunnen echter gerelateerd worden aan variatie in relatieve snuitlengte.

Aansluitend bij het voorgaande, wordt in hoofdstuk vier de morfologische variatie binnen de familie gekwantificeerd door middel van een geometrisch morfometrische analyse bij een groot aantal syngnathe vertegenwoordigers. Via deze methode kan vastgesteld worden dat de belangrijkste verschillen in kopmorfologie tussen zeenaalden en zeepaardjes gerelaterd zijn aan veranderingen in snuit- en kopdimensie, de positie van de pectorale vin en de hoogte van het kieuwdeksel. Deze variatie heeft waarschijnlijk te maken met de oriëntatie van de lichaamsas ten opzichte van de kop (lichaam in het verlengde of onder een hoek met de kop) en aan de kinematica van de voedselopname (lange snuit en beperkte koprotatie of korte snuit en veel rotatie). Gezien de hoge graad van specialisatie in het voedselopname-apparaat bij Syngnathidae zou een kleine afwijking in de interactie tussen de verschillende elementen in de kop al tot een verminderde prestatie kunnen leiden. Dit doet vermoeden dat elke soort binnen

de familie gekenmerkt wordt door een beperkte intraspecifieke morfologische variatie. Vooral de morfologische plasticiteit van soorten met een lange snuit, die als meer gespecialiseerd beschouwd worden dan kort-snuitige soorten, zal gereduceerd zijn. De preliminaire resultaten van deze studie bevestigen onze verwachtingen. Tenslotte wordt onderzocht of er nog belangrijke ontogenetische transformaties optreden bij juveniele zeepaardjes (*H. reidi*) na het vrijkomen uit de buidel. Graduele vormverschuivingen, zoals het dorsoventraal vernauwen van de snuit en kop en de heroriëntatie van het preoperculair been, kenmerken de juveniele ontwikkeling. Maar, de periode van ingrijpende veranderingen lijkt reeds doorlopen te zijn in de buidel.

In het vijfde hoofdstuk komen enkele functionele aspecten van het gespecialiseerde voedselopname-apparaat aan bod.
Het eerste deelonderzoek werd uitgevoerd in samenwerking met Gert Roos en Sam van Wassenbergh (Universiteit Antwerpen) en evalueert een eerder beschreven planair vierstangensysteem (Muller, 1987) dat rotatie van het hyoid koppelt aan neurocraniale elevatie. Zowel de morfologische beschrijving van alle stangen en gewrichten betrokken bij het systeem, als de kinematische opnames van de voedselopname bij een zeepaardje (*H. reidi*) tonen de ongelooflijke specialisatie van het trofisch apparaat aan. Niet alleen verschilt de syngnathe 'pivot feeding' van zuigvoeding bij een gegeneralizeerde teleost in snelheid (duur van een prooiopname is minder dan 6 ms), maar ook de volgorde van beweging is anders. De expansiefase begint met hyoidrotatie en niet met mondopening zoals gebruikelijk (rostrocaudale golf). Bovendien leveren de resultaten een duidelijk bewijs voor de koppeling tussen hyoid en neurocranium. Er wordt echter een discrepantie tussen de voorspelde bewegingen (op basis van het vierstangenmodel) en de waargenomen bewegingen (op basis van de video-opnames) aangetoond. Dit is hoogst waarschijnlijk te wijten aan het modelleren van de stang bestaande uit het urohyale en de sternohyoideus spier als onveranderlijk in lengte, terwijl deze verkort bij spiercontractie.
In het tweede deel wordt onderzocht waar in de schedel de meeste mechanische stress optreedt als gevolg van de grote drukveranderingen tijdens de voedselopname. Hiervoor wordt een eindige elementen analyse uitgevoerd op de gemodelleerde schedels van drie zeepaard- en drie zeenaaldsoorten met

variërende relatieve snuitlengte (*H. reidi, H. abdominalis, H. zosterae, D. dactyliophorus, S. rostellatus* en *D. melanopleura*). In overeenstemming met de verwachtingen (uitgezonderd in D. *dactyliophorus*) worden stresspieken waargenomen ter hoogte van articulaties en kraakbenige zones in de gemodelleerde schedels. Deze concentraties aan stress zullen in de werkelijke schedels veel lager liggen aangezien zowel kraakbeen als articulerende elementen verondersteld worden stress goed te weerstaan. Een tweede doel is nagaan of er een verschil is in stressdistributiepatroon tussen kort- en langsnuitige soorten. De hypothese is dat soorten met een lange snuit grotere drukverschillen moeten creeëren, hogere stress moeten kunnen weerstaan en dus bepaalde morfologische adaptaties zullen hebben die dit toelaten. Wanneer kort- en langsnuitige modellen blootgesteld worden aan eenzelfde druk, zullen de modellen met een lange snuit de minste stress ervaren. Deze hypothese wordt niet bevestigd door de resultaten, maar de geometrie van de beenderen in de snuit (dikte van het been, mate van overlap tussen de beenderen, enz.) heeft een duidelijke invloed op de stress distributie.

In hoofdstuk zes worden de behaalde resultaten bediscussieerd in een ontogenetische, functionele en evolutionaire context, gevolgd door een algemene conclusie.

Ten eerste komt de bijzondere ontwikkeling bij Syngnathidae aan bod. De broedzorg duurt lang en is complex; het mannetje hecht de eitjes en embryos aan het lichaam vast of bewaart ze in een afgesloten buidel, zelfs nadat ze uit het ei gekomen zijn. De mate van ouderlijke investering neemt toe met toenemende complexiteit van de broedstructuur. Zelfs de meest basale syngnathen bieden de jongen bescherming tegen predatie, meer geëvolueerde soorten zorgen ook voor osmoregulatie, voeding en zuurstoftoevoer. Door de verlenging van de broedperiode wordt de start van exogene voedselopname uitgesteld en is er meer tijd voor de ontwikkeling van de jongen. Pasgeboren syngnathen zijn dan ook bijna volledig ontwikkeld (de larvale fase en bijhorende metamorfose zijn afwezig of vinden plaats in de buidel) en juvenielen kunnen zelfstandig prooien vangen door middel van de speciale 'pivot feeding'. Samenvattend kan gesteld worden dat de ingrijpende broedzorg waarschijnlijk de evolutie van de gespecialiseerde syngnathe kopmorfologie in de hand heeft gewerkt.

In het tweede deel van de discussie wordt de nadruk gelegd op de werking van de syngnathe kop. De belangrijkste structurele en functionele modificaties in vergelijking met het trofische apparaat van een gegeneraliseerde teleost worden herhaald. Daarna volgt een gedetailleerde beschrijving van de beweging van en interactie tussen de afzonderlijke elementen in de kop tijdens de voedselopname. Tenslotte worden de voor- en nadelen gerelateerd aan snuitverlenging opgesomd. Hieruit blijkt dat de morfologische variatie in termen van snuitdimensie in de familie waarschijnlijk het gevolg is van een trade-off. Voor de optimalisatie van koprotatie is een lange snuit voordelig, terwijl voor het genereren van een grote zuigkracht een korte snuit gunstiger is. De grote morfologische diversiteit binnen de Syngnathidae zou zo verklaard kunnen worden.

Het derde deel behandelt de resultaten in een fylogenetisch en evolutionair kader. Er wordt eerst kort beargumenteerd waarom vergelijking van de syngnathe kop met die van de driedoornige stekelbaars (*Gasterosteus aculeatus*) nog steeds nuttig is, ook als ze niet elkaars zustertaxa blijken te zijn. Vervolgens worden de evolutionaire trends besproken die tot de zeepaardmorfologie (d.w.z. de grijpstaart, de gekantelde kop en de verticale lichaamshouding) zouden hebben kunnen leiden. Het genus *Idiotropiscis* ('pygmy pipehorses') wordt beschouwd als de nog levende transitievorm tussen zeenaalden en zeepaardjes. De divergentie van pipehorses en zeepaarden zou bevorderd zijn door de opmars van zeegrashabitats die meer bescherming bieden aan organismen met een rechte lichaamsas. Ook de biomechanica van de voedselopname zou een rol gespeeld kunnen hebben in de evolutie van zeepaardjes. De kanteling van de kop ten opzichte van de lichaamsas zou koprotatie kunnen bevoordelen en de grijpstaart laat een strekking van het lichaam in de richting van de prooi toe. Deze voorwaartse beweging van de mond zou de tijd die nodig is om de prooi te bereiken reduceren, wat precies het effect van snuitverlenging is. Als een grote koprotatie in combinatie met een voorwaartse beweging in de richting van de prooi hetzelfde selectief voordeel biedt als een lange snuit, zou dat een verklaring kunnen zijn voor het ontbreken van zeepaardjes met uitzonderlijk lange snuit.

Tenslotte worden deze bevindingen kort en bondig samengevat in de algemene conclusie.

8 References

ADAMS DC, ROHLF FJ, SLICE DE. 2004. Geometric morphometrics: Ten years of progress following the 'revolution'. Italian Journal of Zoology 71:5-16.

ADRIAENS D, HERREL A. 2009. Functional consequences of extreme morphologies in the craniate trophic system. Physiological and Biochemical Zoology 82:1-6.

ADRIAENS D, VERRAES W. 1998. Ontogeny of the osteocranium in the African catfish, *Clarias gariepinus* (Burchell, 1822) (Siluriformes: Clariidae): Ossification sequence as a response to functional demands. Journal of Morphology 235:183-237.

AERTS P. 1991. Hyoid morphology and movements relative to abducing forces during feeding in Astatotilapia elegans (Teleostei: Cichlidae). Journal of Morphology 208:323-345.

AERTS P. 1998. Vertical jumping in *Galago senegalensis*: The quest for an obligate mechanical power amplifier. Philosophical Transactions of the Royal Society of London, Biological Sciences 353:1607-1620.

AERTS P, VERRAES W. 1984. Theoretical analysis of a planar four-bar linkage in the teleostean skull: The use of mathematics in biomechanics. Annales de la Société Royal Zoologique de Belgique 114:273–290.

AERTS P, VERRAES W. 1987. Do inertial effects explain the maximal rotation of the maxilla in the rainbow trout (*Salmo gairdneri*) during feeding? Annales de la Société royale zoologique de Belgique 117:221-235.

ALEXANDER RMCN. 1966. The functions and mechanisms of the protrusible upper jaws of two species of cyprinid fish. Journal of Zoology (London) 149:288-296.

ALEXANDER RMCN. 1967a. The functions and mechanisms of the protrusible

upper jaws of some acanthopterygian fish. Journal of Zoology (London) 151:43-64.

ALEXANDER RMCN. 1967b. Mechanisms of the jaws of some atheriniform fish. Journal of Zoology (London) 151:233-255.

ALEXANDER RMCN. 1967c. Functional design in fishes. Hutchinson University Library, London. p. 160.

ALEXANDER RMCN. 1969. Mechanics of the feeding action of a cyprinid fish. Journal of Zoology (London) 159:1-15.

ALEXANDER RMCN, BENNET-CLARK HC. 1977. Storage of elastic strain energy in muscle and other tissues. Nature 265:114-117.

ANKER GCH. 1974. Morphology and kinetics of the head of the stickleback, *Gasterosteus aculeatus*. Transactions of the Zoological Society of London 32:311-416.

ANKER GCH. 1989. The morphology of joints and ligaments of a generalized *Halpochromis* species: *H. elegans* Trawavas 1933 (Teleostei, Cichlidae). III. The hyoid and the branchiostegal apparatus, the branchial apparatus and the shoulder girdle apparatus. Netherlands Journal of Zoology 39:1-40.

ARRATIA G, SCHULTZE HP. 1990. The urohyal: Development and homology within osteichthyans. Journal of Morphology 203:247-282.

ARRATIA G, SCHULTZE HP. 1991. Palatoquadrate and its ossifications: Development and homology within osteichthyans. Journal of Morphology 208:1-81.

AZZARELLO MY. 1990. A comparative study of the developmental osteology of *Syngnathus scovelli* and *Hippocampus zosterae* (Pisces: Syngnathidae) and its phylogenetic implications. Evolutionary Monographs 12:1-90.

BALON EK. 1975. Terminology of intervals in fish development. Journal of Fisheries Research Board of Canada 32:1663-1670.

BALON EK. 1979. The theory of saltation and its application in the ontogeny of fishes: steps and thresholds. Environmental Biology of Fishes 4:97-101.

BALON EK. 1984. Reflections on some decisive events in the early life of fishes. Transactions of the American Fisheries Society 113:178-185.

BALON EK. 1986. Types of feeding in the ontogeny of fishes and the life-history model. Environmental Biology of Fishes 16:11-24.

BAYLIS JR. 1981. The evolution of parental care in fishes, with reference to Darwin's rule of male sexual selection. Environmental Biology of Fishes 6:223-251.

BENKMAN CW. 1987. Crossbill foraging behavior, bill structure, and patterns of food profitability. The Wilson Bulletin 99:351-368.

BENKMAN CW. 1993. Adaptation to single resources and the evolution of crossbill (*Loxia*) diversity. Ecological Monographs 63:305-325.

BERGERT BA, WAINWRIGHT PC. 1997. Morphology and kinematics of prey capture in the syngnathid fishes *Hippocampus erectus* and *Syngnathus floridae*. Marine Biology 127:563-570.

BISHOP KL, WAINWRIGHT PC, HOLZMAN R. 2008. Anterior-to-posterior wave of buccal expansion in suction feeding fishes is critical for optimizing fluid flow velocity profile. Journal of the Royal Society Interface 5:1309-1316.

BLOODWORTH B, MARSHALL CD. 2005. Feeding kinematics of *Kogia* and *Tursiops* (Odontoceti: Cetacea): characterization of suction and ram feeding. The Journal of Experimental Biology 208:3721–3730.

BOCK WJ. 2003. Ecological aspects of the evolutionary processes. Zoological Science 20:279-289.

BOCK WJ, SHEAR RC. 1972. A staining method for gross dissection of vertebrate muscles. Anatomischer Anzeiger 130:222-227.

BRANCH GM. 1966. Contributions to the functional morphology of fishes. Part III. The feeding mechanism of *Syngnathus acus* Linnaeus. Zoologica Africana 2:69-89.

BRITZ R, JOHNSON D. 2002. "Paradox lost": Skeletal ontogeny of *Indostomus paradoxus* and its significance for the phylogenetic relationships of the Indostomidae (Teleostei, Gasterosteiformes). American Museum Novitates 3383:2-42.

BRUNER E, BARTOLINO V. 2008. Morphological variation in the seahorse vertebral system. International Journal of Morphology 26:247-262.

CARCUPINO M, BALDACCI A, MAZZINI M, FRANZOI P. 2002. Functional significance of the male brood pouch in the reproductive strategies of pipefishes and seahorses: A morphological and ultrastructural comparative study on three anatomically different pouches. Journal of Fish Biology 61:1465-1480.

CARROLL AM, WAINWRIGHT PC. 2003. Functional morphology of prey capture in the sturgeon, *Scaphirhynchus albus*. Journal of Morphology 256:270–284.

CARROLL AM, WAINWRIGHT PC, HUSKEY SH, COLLAR DC, TURINGAN RG. 2004. Morphology predicts suction feeding performance in centrarchid fishes. The Journal of Experimental Biology 207:3873-3881.

CASEY SP, HALL HJ, STANLEY HF, VINCENT ACJ. 2004. The origin and evolution of seahorses (genus *Hippocampus*): A phylogenetic study using cytochrome *b* gene of mitochondrial DNA. Molecular Phylogenetics and Evolution 30:261-272.

CASTRO ALD, DINIZ AD, MARTINS IZ, VENDEL AL, DE OLIVEIRA TPR, ROSA IMD. 2008. Assessing diet composition of seahorses in the wild using a non destructive method: *Hippocampus reidi* (Teleostei: Syngnathidae) as a study-case. Neotropical Ichthyology 6:637-644.

CHEN W, BONILLO C, LECOINTRE G. 2003. Repeatability of clades as a criterion of reliability: A case study for molecular phylogeny of Acanthomorpha (Teleostei) with larger number of taxa. Molecular Phylogenetics and Evolution 26:262-288.

CHOO CK, LIEW HC. 2006. Morphological development and allometric growth patterns in juvenile seahorse. Journal of Fish Biology 69:426-445.

COLSON DJ, PATEK SN, BRAINERD EL, LEWIS SM. 1998. Sound production during feeding in *Hippocampus* seahorses (Syngnathidae). Environmental Biology of Fishes 51:221-229.

CONSI TR, SEIFERT PA, TRIANTAFYLLOU MS, EDELMAN ER. 2001. The dorsal fin engine of the seahorse (*Hippocampus* sp.). Journal of Morphology 248:80-97.

COOK A. 1996. Ontogeny of feeding morphology and kinematics in juvenile fishes: A case study of the cottid fish *Clinocottus analis*. The Journal of Experimental Biology 199:1961-1971.

COUGHLIN DJ. 1994. Suction prey capture by clownfish larvae (*Amphiprion perideraion*). Copeia 1:242-246.

CURREY JD. 1999. The design of mineralised hard tissues for their mechanical functions. The Journal of Experimental Biology 202:3285-3294.

CURREY JD. 2010. Mechanical properties and adaptations of some less familiar bony tissues. Journal of the Mechanical Behavior of Biomedical Materials 3:357-372.

CURTIS JMR, VINCENT ACJ. 2005. Distribution of sympatric seahorse species along a gradient of habitat complexity in a seagrass-dominated community. Marine Ecology Progress Series 291:81-91.

DAGET J. 1964. Le crâne des téléostéens. Mémoires du Muséum d'Histoire Naturelle Serie A. Zoologie 31:163-341.

DARWIN C. 1859. On the origin of species by means of natural selection, or preservation of favored races in the struggle for life. John Murray: London (reprint edition 1998: Wordsworth Editions Limited, Herfordshire. p. 392.

DAWSON CE. 1978. *Syngnathus parvicarinatus* a new Australian pipefish, with notes on *S. sauvagei* (Whitley) and *Leptonotus caretta* (Klunzinger). Copeia 2:288-293.

DAWSON CE. 1983. Western Atlantic occurrence of the genus *Minyichthys* (Pisces: Syngnathidae), with a description of *M. inusitatus* n. sp. Copeia 3:774-776.

DE BEER GR. 1937. The development of the vertebrate skull. University Press, Oxford. p. 552.

DE LUSSANET MHE, MULLER M. 2007. The smaller your mouth, the longer your snout: Predicting the snout length of *Syngnathus acus*, *Centriscus scutatus* and other pipette feeders. Journal of the Royal Society Interface 4:561-573.

DEAN MN. 2003. Suction feeding in the pipid frog, *Hymenochirus boettgeri*: Kinematic and behavioral considerations. Copeia 4:879–886.

DELARIVA RL, AGOSTINHO AA. 2001. Relationship between morphology and diets of six neotropical loricariids. Journal of Fish Biology 58:832-847.

DETTAI A, LECOINTRE G. 2005. Further support for the clades obtained by multiple molecular phylogenies in the acanthomorph bush. Comptus Rendus Biologies 328:674-689.

DHANYA S, RAJAGOPAL S, AJMAL KHAN S, BALASUBRAMANIAN T. 2005. Embryonic development in alligator pipefish, *Syngnathoides biaculeatus* (Bloch, 1785). Current Science 88:178-181.

DOBZHANSKY T. 1973. Nothing in biology makes sense except in the light of evolution. American Biology Teacher 35:125-129.

DROST MR. 1987. Relation between aiming and catch success in larval fishes. Canadian Journal of Fisheries and Aquatic Sciences 44:304-315.

DROST MR, MULLER M, OSSE JWM. 1988. A quantitative hydrodynamic model of suction feeing in larval fishes: The role of frictional forces. Proceedings of the Royal Society of London Series B Biological Sciences 234:263-281.

DROZDOV AL, KORNIENKO ES, KRASNOLUTSKY. 1997. Reproduction and development of *Syngnathus acusimilis*. Russian Journal of Marine Biology 23:265-268.

DUMONT ER, PICCIRILLO J, GROSSE IR. 2005. Finite-element analysis of biting behavior and bone stress in the facial skeletons of bats. The Anatomical Record Part A 283A:319-330.

DUMONT ER, GROSSE IR, SLATER GJ. 2009. Requirements for comparing the performance of finite element models of biological structures. Journal of Theoretical Biology 256:96-103.

EDELAAR P, POSTMA E, KNOPS P, PHILLIPS R. 2005. No support for a genetic basis of mandible crossing direction in crossbills (*Loxia* spp.). The Auk 122:1-7.

ELWOOD JRL, CUNDALL D. 1994. Morphology and behavior of the feeding apparatus in *Cryptobranchus alleganiensis* (Caudata). Journal of Morphology 220:47–70.

EMERSON SB, BRAMBLE DM. 1993. Scaling, allometry, and skull design. In: Hanken J, Hall BK, editors. The skull volume 3: Functional and evolutionary mechanisms. The University of Chicago Press, Chicago. pp. 384-421.

ERICKSON GM, CATANESE J, KEAVENY TM. 2002. Evolution of the biomechanical material properties of the femur. Anatomical Record 268:115-124.

FAUSTINO M, POWER DM. 2001. Osteological development of the viscerocranial skeleton in sea bream: Alternative ossification strategies in teleost fish. Journal of Fish Biology 58:537-572.

FELÍCIO AKC, ROSA IL, SOUTO A, FREITAS RHA. 2006. Feeding behavior of the longsnout seahorse *Hippocampus reidi* Ginsburg, 1933. Journal of Ethology 24:219–225.

FERRY-GRAHAM LA, WAINWRIGHT PC, BELLWOOD DR. 2001a. Prey capture in long-jawed butterflyfishes (Chaetodontidae): The functional basis of novel feeding habits. Journal of Experimental Marine Biology and Ecology 256:167–184.

FERRY-GRAHAM LA, WAINWRIGHT PC, HULSEY CD, BELLWOOD DR. 2001b. Evolution and mechanics of long jaws in butterflyfishes (Family Chaetodontidae). Journal of Morphology 248:120–143.

FERRY-GRAHAM LA, BOLNICK DI, WAINWRIGHT PC. 2002. Using functional morphology to examine the ecology and evolution of specialization. Integrative and Comparative Biology 42:265-277.

FLYNN AJ, RITZ DA. 1999. Effect of habitat complexity and predatory style on the capture of fish feeding on aggregated prey. Journal of the Marine Biology Association of the United Kingdom 79:487-494.

FOOTE M. 1993. Contributions of individual taxa to overall morphological disparity. Paleobiology 19:403-419.

FOSTER SJ, VINCENT ACJ. 2004. Life history and ecology of seahorses: Implications for conservation and management. Journal of Fish Biology 64:1-61.

FRANZOI P, MACCAGNANI R, ROSSI R, CECCHERELLI VU. 1993. Life cycles and feeding habits of Syngnathus taenionotus and S. abaster (Pisces, Syngnathidae) in a brackish bay of the Po river delta (Adriatic Sea). Marine Ecology Progress Series 97:71-81.

FROESE R, PAULY D. 2011. Fishbase. World Wide Web electronic publication. Version 05/2010. www.fishbase.org. Downloaded on 23 August 2010.

GEERINCKX T, ADRIAENS D. 2007. Ontogeny of the intermandibular and hyoid musculature in the suckermouth armoured catfish *Ancistrus cf. triradiatus* (Loricariidae, Siluriformes). Animal Biology 57:339–357.

GEERINCKX T, BRUNAIN M, ADRIAENS D. 2005. Development of the chondrocranium in the suckermouth armored catfish *Ancistrus* cf. *triradiatus* (Loricariidae, Siluriformes). Journal of Morphology 266:331-355.

GEERINCKX T, BRUNAIN M, ADRIAENS D. 2007. Development of the osteocranium in the suckermouth armored catfish *Ancistrus* cf. *triradiatus* (Loricariidae, Siluriformes. Journal of Morphology 268:254-274.

GEFFEN AJ, VAN DER VEER HW, NASH RDM. 2007. The cost of metamorphosis in flatfishes. Journal of Sea Research 58:35-45.

GERKING SD. 1994. Feeding ecology of fish. Academic Press, California. p. 416.

GIBB AC. 1995. Kinematics of prey capture in a flatfish, *Pleuronichthys verticalis*. Journal of Experimental Biology 198, 1173-1183.

GIBB AC. 1997. Do flatfish feed like other fishes? A comparative study of percomorph prey-capture kinematics. The Journal of Experimental Biology 200:2841–2859.

GIBB AC, FERRY-GRAHAM LA. 2005. Cranial movements during suction feeding in teleost fishes: Are they modified to enhance suction production? Zoology 108:141–153.

GOFFREDO S, PICCINETTI C, ZACCANTI F. 2004. Volunteers in marine conservation monitoring: A study of the distribution of seahorses carried out in collaboration with recreational scuba divers. Conservation Biology 18:1492-1503.

GOODWIN NB, BALSHINE-EARN S, REYNOLDS JD. 1998. Evolutionary transitions in parental care in cichlid fish. Proceedings of the Royal Society of London Series B Biological Sciences 265:2265-2272.

GOSLINE WA. 1967. Reduction in branchiostegal ray number. Copeia 1:237-239.

GOSLINE WA. 1977. The structure and function of the dermal pectoral girdle in bony fishes with particular reference to ostariophysines. Journal of Zoology (London) 183, 329-338.

GOSLINE WA. 1981. The evolution of the premaxillary protrusion system in some teleostean fish groups. Journal of Zoology (London) 193:11-23.

GREGORY WK. 1933. Fish skull: A study of the evolution of natural mechanisms. Transactions of the American Philosophical Society 32:75-481.

GROBECKER DB, PIETSCH TW. 1979. High-speed cinematographic evidence for ultrafast feeding in antennariid anglerfishes. Science 205:1161–1162.

HALE ME. 1996. Functional morphology of ventral tail bending and prehensile abilities of the seahorse, *Hippocampus kuda*. Journal of Morphology 227:51-65.

HALL BK. 2005. Bones and cartilage: Developmental and evolutionary skeletal biology. Elsevier Academic Press, London, p. 760.

HAMMER Ø, HARPER DAT, RYAN PD. 2001. PAST: Paleontological Statistics software package for education and data analysis. Palaeontologia Electronica 4. p.9.

HARRINGTON RWJR. 1955. The osteocranium of the American cyprinid fish, *Notropis bifrenatus*, with an annotated synonymy of teleost skull bones. Copeia 4:267-291.

HELFMAN GS, COLLETTE BB, FACEY DE, BOWEN BW. 2009. The diversity of fishes 2nd edition. Biology, evolution, and ecology. Wiley-Blackwell, Chichester. p. 720.

HERALD ES. 1959. From pipefish to seahorse: A study of phylogenetic relationships. Proceedings of the California Academy of Sciences 29:465-473.

HERNANDEZ LP, BIRD NC, STAAB KL. 2007. Using zebrafish to investigate cypriniform evolutionary novelties: functional development and evolutionary diversification of the kinethmoid. Journal of Experimental Zoology (Mol Dev Evol) 308B:625-641.

HERNANDEZ LP, GIBB AG, FERRY-GRAHAM L. 2009. Trophic apparatus in cyprinodontiform fishes: Functional specializations for picking and scraping behaviors. Journal of Morphology 270:645-661.

HERRING SW. 1993. Epigenetic and functional influences on skull growth. In: Hanken J, Hall BK, editors. The skull volume 1: Development. The University of Chicago Press, Chicago, pp. 153-206.

HERRING SW, TENG S. 2000. Strain in the braincase and its sutures during function. American Journal of Physical Anthropology 112:575-593.

HOLLIDAY JA, STEPPAN SJ. 2004. Evolution of hypercarnivory: The effect of specialization on morphological and taxonomic diversity. Paleobiology 30:108-128.

HORTON JM, SUMMERS AP. 2009. The material properties of acellular bone in a teleost fish. The Journal of Experimental Biology 212:1413-1420.

HUNT VON HERBING I, KEATING K. 2003. Temperature-induced changes in viscosity and its effects on swimming speed in larval haddock. In: Browman HI, Skiftesvik AB, editors. The Big Fish Bang. Proceedings of the 26the Annual Larval Fish Conference. Institute of Marine Research, Bergen. pp. 23-34.

HUNT VON HERBING I, MIYAKE T, HALL BK, BOUTILIER RG. 1996a. Ontogeny of feeding and respiration in larval Atlantic cod *Gadus morhua* (Teleostei, Gadiformes): I. Morphology. Journal of Morphology 227:15-35.

HUNT VON HERBING I, MIYAKE T, HALL BK, BOUTILIER RG. 1996b. Ontogeny of feeding and respiration in larval Atlantic cod *Gadus morhua* (Teleostei, Gadiformes): II. Function. Journal of Morphology 227:37-50.

HUSKEY S, QUINTERO R. 2006. Why the long face? Prey capture in trumpetfishes. Integrative and Comparative Biology 46:E65-E65.

HUYSENTRUYT F. 2008. Early development of *Corydoras aeneus* (Siluriformes, Callichthyidae): A case study for understanding the evolutionary basis of loricarioid ontogenetic patterning. Unpublished Doctoral Thesis. Ghent University.

HUYSENTRUYT F, GEERINCKX T, BRUNAIN M, ADRIAENS D. 2011. Development of the osteocranium in *Corydoras aeneus* (Gill, 1858) (Callichthyidae, Siluriformes). Journal of Morphology.

IUCN. 2010. IUCN Red List of Threatened Species. World Wide Web electronic publication. Version 2010.4. www.iucnredlist.org. Downloaded on 15 December 2010.

JAMIESON BGM. 1991. Fish evolution and systematic: Evidence from spermatozoa. With a survey of lophophorate, echinoderm and protochordate sperm and an account of gamete cryopreservation. Cambridge University Press, Cambridge. p. 319.

JOHNSON GD, PATTERSON C. 1993. Percomorph phylogeny: A survey of acanthomorphs and a new proposal. Bulletin of Marine Science 52:554-626.

JOHNSON GD, PAXTON JR, SUTTON TT, SATOH TP, SADO T, NISHIDA M, MIYA M. 2009. Deep-sea mystery solved: astonishing larval transformations and extreme sexual dimorphism unite three fish families. Biology Letters 5:235-239.

JUNGERSEN HFE. 1910. Ichthyotomical contributions. II. The structure of the Aulostomidae, Syngnathidae and Solenostomidae. Det Kongelige Danske Videnskabernes Selskabs Skrifter 8:267-364.

KADAM KM. 1958. The development of the chondrocranium in the sea-horse, *Hippocampus* (Lophobranchii). Zoological Journal of the Linnean Society 43:557-573.

KADAM KM. 1961. The development of the skull in *Nerophis* (Lophobranchii). Acta Zoologica 42:257-298.

KANOU K, KOHNO H. 2001. Early life history of a seahorse, *Hippocampus mohnikei*, in Tokyo Bay, Japan. Ichtyological Research 48:361-368.

KARINA A, FELICIO C, ROSA IL, SOUTO A, FREITAS RHA. 2006. Feeding behavior of the longsnout seahorse *Hippocampus reidi* Ginsburg, 1933. Journal of Ethology 24:219-225.

KAWAHARA R, MIYA M, MABUCHI K, LAVOUÉ S, INOUE JG, SATOH TP, KAWAGUCHI A, NISHIDA M. 2008. Interrelationships of the 11 gasterosteiform families (sticklebacks, pipefishes, and their relatives): A new perspective based on whole mitogenome sequences from 75 higher teleosts. Molecular

Phylogenetics and Evolution 46:224-236.

KEIVANY Y, NELSON JS. 2006. Interrelationships of Gasterosteiformes (Actinopterygii, Percomorpha). Journal of Ichthyology 46:S84-S96.

KENDRICK AJ, HYNDES GA. 2003. Patterns in the abundance and size-distribution of syngnathid fishes among habitats in a seagrass-dominated marine environment. Estuarine, Coastal and Shelf Science 57:631–640.

KENDRICK AJ, HYNDES GA. 2005. Variations in the dietary compositions of morphologically diverse syngnathid fishes. Environmental Biology of Fishes 72:415-427.

KINDRED JE. 1921. The chondrocranium of *Syngnathus fuscus*. Journal of Morphology 35:425-456.

KINDRED JE. 1924. An intermediate stage in the development of the skull of *Syngnathus fuscus*. American Journal of Anatomy 33:421-447.

KITSOS MS, TZOMOS T, ANAGNOSTOPOULOU L, KOUKOURAS A. 2008. Diet composition of the seahorses, *Hippocampus guttulatus* Cuvier, 1829 and *Hippocampus hippocampus* (L., 1758) (Teleostei, Syngnathidae) in the Aegean Sea. Journal of Fish Biology 72:1259-1267.

KOLDEWEY HJ, MARTIN-SMITH KM. 2010. A global review of seahorse aquaculture. Aquaculture 302:131-152.

KOLM N, AHNESJÖ I. 2005. Do egg size and parental care coevolve in fishes? Journal of Fish Biology 66:1499-1515.

KORNIENKO ES. 2001. Reproduction and development in some genera of pipefish and seahorses of the family Syngnathidae. Russian Journal of Marine Biology 27:515-526.

KUITER RH. 2003. Seahorses, pipefishes and their relatives. A comprehensive guide to Syngnathiformes revised edition. TMC Publishing, Chorleywood. p. 237.

KUITER RH. 2004. A new pygmy pipehorse (Pisces: Syngnathidae: *Idiotropiscis*) from eastern Australia. Records of the Australian Museum 56:163-165.

KUTSCHERA U, NIKLAS KJ. 2004. The modern theory of biological evolution: an expanded synthesis. Naturwissenschaften 91:255-276.

KVARNEMO C, SIMMONS LW. 2004. Testes investment and spawning mode in pipefishes and seahorses (Syngnathidae). Biological Journal of the Linnean Society 83:369-376.

KVARNEMO C, MOORE GI, JONES AG, NELSON WS, AVISE JC. 2000. Monogamous pair bonds and mate switching in the western Australian seahorse *Hippocampus subelongatus*. Journal of Evolutionary Biology 13:882-888.

LARSEN PS, MADSEN CV, RIISGÅRD. 2008. Effect of temperature and viscosity on

swimming velocity of the copepod *Acartia tonsa*, brine shrimp *Artemia salina* and rotifer *Brachionus plicatilis*. Aquatic Biology 4:47-54.

LAUDER GV, LIEM KF. 1983. The evolution and interrelationships of the actinopterygian fishes. Bulletin of The Museum of Comparative Zoology 150:95-197.

LAUDER GV. 1979. Feeding mechanics in primitive teleosts and in the halecomorph fish *Amia calva*. Journal of Zoology (London) 187:543-578.

LAUDER GV. 1980a. Evolution of the feeding mechanism in primitive actinopterygian fishes: A functional anatomical analysis of *Polypterus*, *Lepisosteus* and *Amia*. Journal of Morphology 163:283-317.

LAUDER GV. 1980b. The suction feeding mechanism in sunfishes (*Lepomis*): An experimental analysis. The Journal of Experimental Biology 88:49-72.

LAUDER GV. 1983. Food capture. In: Webb PW, Weihs D, editors. Fish Biomechanics. Praeger Publishers, New York. pp. 280-311.

LAUDER GV. 1985. Aquatic feeding in lower vertebrates. In: Hildebrand M, Bramble DM, Liem KF, Wake DB, editors. Functional vertebrate morphology. The Belknap Press, Cambridge. pp. 210-229.

LAUDER GV, NORTON SF. 1980. Asymmetrical muscle activity during feeding in the gar, *Lepisosteus oculatus*. Journal of Experimental Biology 84:17-32.

LAWRENCE E. 2005. Henderson's dictionary of biology 13th edition. Pearson Education Limited, Essex. p. 748.

LEKANDER B. 1949. The sensory line system and the canal bones in the head of some Ostariophysi. Acta Zoologica 30:1-131.

LIEBERMAN DE, DEVLIN MJ, PEARSON OM. 2001. Articular area responses to mechanical loading: Effects of exercise, age and skeletal location. American Journal of Physical Anthropology 116:266-277.

LIEM KF. 1991. A functional approach to the development of the head of teleosts: Implications on constructional morphology and constraints. In: Schmidt-Kittler N, Vogel K, editors. Constructional Morphology and Evolution. Springer-Verlag, Berlin. pp. 231-249.

LIEM KF, STEWART DJ. 1976. Evolution of the scale-eating cichlid fishes of Lake Tanganyika: A generic revision with a description of a new species. Bulletin Museum of Comparative Zoology 147:319-350.

LINNAEUS C. 1766. Systema naturae per regna tria naturae, secundum classes, ordines, genera, species, cum characteribus, differentiis, synonymis, locis. Tomus 1 (Regnum animale). Editio duodecima, reformata. Laurentii Salvii, Holmiae. p. 532.

LINTON JR, SOLOFF BL. 1964. The physiology of the brood pouch of the male sea

horse Hippocampus erectus. Bulletin of Marine Science of the Gulf and Caribbean 14:45-61.

LOURIE SA, PRITCHARD JC, CASEY SP, TRUONG SK, HALL HJ, VINCENT ACJ. 1999a. The taxonomy of Vietnam's exploited seahorses (family Syngnathidae). Biological Journal of the Linnean Society 66:231-256.

LOURIE SA, VINCENT ACJ, HALL HJ. 1999b. Seahorses. An identification guide to the world's species and their conservation. Project Seahorse, London. p. 214.

LOURIE SA, FOSTER SJ, COOPER EWT, VINCENT ACJ. 2004. A guide to the identification of seahorses. Project Seahorse and TRAFFIC North America. University of British Columbia and World Wildlife Fund, Washington DC. p. 114.

LOURIE SA, GREEN DM, VINCENT ACJ. 2005. Dispersal, habitat differences, and comparative phylogeography of Southeast Asian seahorses (Syngnathidae : *Hippocampus*). Molecular Ecology 14:1073-1094.

MARKEY MJ, MARSHALL CR. 2007. Linking form and function of the fibrous joints in the skull: A new quantification scheme for cranial sutures using the extant fish *Polypterus endlicherii*. Journal of Morphology 268:89-102.

MARKEY MJ, MAIN RP, MARSHALL CR. 2006. *In vivo* cranial suture function and suture morphology in the extant fish *Polypterus*: implications for inferring skull function in living and fossil fish. The Journal of Experimental Biology 209:2085-2102.

MASSCHAELE BC, CNUDDE V, DIERICK M, JACOBS P, VAN HOOREBEKE L, VLASSENBROECK J. 2007. UGCT: New X-ray radiography and tomography facility. Nuclear Instruments & Methods in Physics Research Section A: Accelerators, Spectrometers, Detectors and Associated Equipment 580:266-269.

MAYR E. 1996. What is a species and what is not? Philosophy of Science 63:262-277.

MCALLISTER DE. 1968. The evolution of branchiostegals and associated opercular, gular, and hyoid bones and the classification of teleostome fishes, living and fossil. Bulletin of the National Museum of Canada (Biological Series) 221:1-239.

MCGONNELL IM. 2001. The evolution of the pectoral girdle. Journal of Anatomy 199:189-194.

MCHENRY CR, CLAUSEN PD, DANIEL WJT, MEERS MB, PENDHARKAR A. 2006. Biomechanics of the rostrum in crocodilians: A comparative analysis using finite-element modeling. The Anatomical Record Part A 288A:827-849.

MCMURRICH JPMA. 1883. On the osteology and development of *Syngnathus peckianus* (Storer). The Quarterly Journal of Microscopical Science 23:623-

650.

MIYA M, TAKESHIMA H, ENDO H, ISHIGURO NB, INOUE JG, MUKAI T, SATOH TP, YAMAGUCHI M, KAWAGUCHI A, MABUCHI K, SHIRAI SM, NISHIDA M. 2003. Major patterns of higher teleostean phylogenies: A new perspective based on 100 complete mitochondrial DNA sequences. Molecular Phylogenetics and Evolution 26:121-138.

MIYA M, SATOH TP, NISHIDA M. 2005. The phylogenetic position of toadfishes (order Batrachoidiformes) in the higher ray-finned fish as inferred from partitioned Bayesian analysis of 102 whole mitochondrial genome sequences. Biological Journal of the Linnean Society 85:289-306.

MONTEIRO NM, ALMADA VC, VIEIRA MN. 2003. Early life history of the pipefish *Nerophis lumbriciformis* (Pisces: Syngnathidae). Journal of the Marine Biological Association of the United Kingdom 83:1179-1182.

MOTTA PJ. 1984. Mechanics and function of jaw protrusion in teleost fishes: A review. Copeia 1:1-18.

MULLER M. 1987. Optimization principles applied to the mechanisms of neurocranium levation and mouth bottom depression in bony fishes (Halecostomi). Journal of Theoretical Biology 126:343-368.

MULLER M, OSSE JWM. 1984. Hydrodynamics of suction feeding in fish. Transactions of the Zoological Society of London 37:51-135.

MURUGAN A, DHANYA S, RAJAGOPAL S, BALASUBRAMANIAN T. 2008. Seahorses and pipefishes of the Tamil Nadu coast. Current Science 95:253-260.

NALLA RK, KINNEY JH, RITCHIE RO. 2003. Mechanistic failure criteria for the failure of human cortical bone. Nature Materials 2:164–168.

NAPLES VL. 1999. Morphology, evolution and function of feeding in the giant anteater (*Myrmecophaga tridactyla*). Journal of Zoology London 249:19-41.

NELSON GJ. 1969. Infraorbital bones and their bearing on the phylogeny and geography of osteoglossomorph fishes. American Museum Novitates 2394:1-37.

NELSON JS. 2006. Fishes of the world 4th edition. John Wiley & Sons, New Jersey. p. 601.

OLIVEIRA F, ERZINI K, GONÇALVES JMS. 2007. Feeding habits of the deep-snouted pipefish *Syngnathus typhle* in a temperate coastal lagoon. Estuarine, Coastal and Shelf Science 72:337-347.

OSSE JWM, MULLER M. 1980. A model of suction feeding in teleost fishes with some implications for ventilation. In: Ali MA, editor. Environmental physiology of fishes. Plenum Publishing Corporation, New York. pp. 335-352.

OTTEN E. 1982. The development of a mouth-opening mechanism in a generalized

Haplochromis species: *H. elegans* Trewavas 1933 (Pisces, Chichlidae). Netherlands Journal of Zoology 32:31-48.

PALMA J, ANDRADE JP. 2002. Morphological study of *Diplodus sargus*, *Diplodus puntazzo*, and *Lithognathus mormyrus* (Sparidae) in the Eastern Atlantic and Mediterranean Sea. Fisheries Research 57:1-8.

PARENTI LR, SONG J. 1996. Phylogenetic significance of the pectoral-pelvic fin association in acanthomorph fishes: A reassessment using comparative neuroanatomy. In: Stiassny MLJ, Parenti LR, Johnson GD, editors. Interrelationships of fishes. Academic Press, California. pp. 427-444.

PATTERSON C. 1977. Cartilage bones, dermal bones and membrane bones, or the exoskeleton *versus* the endoskeleton. In: Andrews SM, Miles RS, Walker AD, editors. Problems in Vertebrate Evolution. Academic Press, London. pp. 77-121.

PATTERSON C. 1993. An overview of the early fossil record of Acanthomorphs. Bulletin of Marine Science 52:29-59.

PAYNE MF, RIPPINGALE RJ, LONGMORE RB. 1998. Growth and survival of juvenile pipefish (*Stigmatopora argus*) fed live copepods with high and low HUFA content. Aquaculture 167:237-245.

PHAM TCHI MI, KORNIENKO ES, DROZDOV AL. 1998. Embryonic and larval development of the seahorse *Hippocampus kuda*. Russian Journal of Marine Biology 24:325-329.

PETERSON J, DECHOW PC. 2003. Material properties of the human cranial vault and zygoma. The Anatomical Record Part A 274A:785-797.

POORTENAAR CW, WOODS CMC, JAMES JP, GIAMBARTOLOMEI FM, LOKMAN PM. 2004. Reproductive biology of female big-bellied seahorses. Journal of Fish Biology 64:717-725.

RALSTON KR, WAINWRIGHT PC. 1997. Functional consequences of trophic specialization in pufferfish. Functional Ecology 11:43-52.

RAYFIELD EJ. 2005. Using finite-element analysis to investigate suture morphology: A case study using large carnivorous dinosaurs. The Anatomical Record Part A 283A:349-365.

REIRIZ L, NICIEZA AG, BRAÑA F. 1998. Prey selection by experienced and naive juvenile Atlantic salmon. Journal of Fish Biology 53:100-114.

RENO HW. 1966. The infraorbital canal, its lateral-line ossicles and neuromasts, in the minnows *Notropis volucellus* and *N. buchanani*. Copeia 3:403-413.

REYSERHOVE L. 2008. Liggen morfologische transformaties in het cranium van larvale zeepaardjes (*Hippocampus reidi*) aan de basis van de mortaliteitspiek in hun ontwikkeling? Unpublished Bachelor Thesis. Ghent University.

RICHMOND BG, WRIGHT BW, GROSSE I, DECHOW PC, ROSS CF, SPENCER MA, STRAIT DS. 2005. Finite element analysis in functional morphology. The Anatomical Record Part A 283A:259-274.

RIDLEY M. 1993. Evolution. Oxford: Blackwell Scientific Publications. p. 670.

RIDLEY M. 2003. Evolution. Oxford University Press, Oxford. p. 472.

RIPLEY JL, FORAN CM. 2009. Direct evidence for embryonic uptake of paternally-derived nutrients in two pipefishes (Syngnathidae: *Syngnathus* spp.). Journal of Comparative Physiology B-Biochemical Systemic and Environmental Physiology 179:325-333.

ROHLF FJ. 2003. TpsSmall: Thin Plate Spline Small Variation (version 1.20). Stony Brook University, New York.

ROHLF FJ. 2009. TpsRegr: Thin Plate Spline Regression (version 1.39). Stony Brook University, New York.

ROHLF FJ. 2010a. TpsUtil: Thin Plate Spline Utility (version 1.46). Stony Brook University, New York.

ROHLF FJ. 2010b. TpsDig2: Thin Plate Spline Digitise (version 2.16). Stony Brook University, New York.

ROHLF FJ. 2010c. TpsRelw: Thin Plate Spline Relative Warps Analysis (version 1.49). Stony Brook University, New York.

ROJO AL. 1991. Dictionary of evolutionary fish osteology. CRC Press, Boca Raton. p. 273.

ROOS G. 2010. Specializations of extreme head morphology: A detailed functional morphological study of feeding in seahorses and pipefishes (Syngnathidae). Unpublished Doctoral Thesis. University of Antwerp.

ROOS G, VAN WASSENBERGH S, HERREL A, AERTS P. 2009. Kinematics of suction feeding in the seahorse *Hippocampus reidi*. The Journal of Experimental Biology 212:3490-3498.

ROOS G, VAN WASSENBERGH S, HERREL A, ADRIAENS D, AERTS P. 2010. Snout allometry in seahorses: Insights on optimization of pivot feeding performance during ontogeny. The Journal of Experimental Biology 213:2184-2193.

ROOS G, VAN WASSENBERGH S, AERTS P, HERREL A, ADRIAENS D. 2011. Effects of snout dimensions on the hydrodynamics of suction feeding in juvenile and adult seahorses. Journal of Theoretical Biology 269:307-317.

ROOS G, VAN WASSENBERGH S, AERTS P, HERREL A, ADRIAENS D. submitted a. Why the long face? A comparative study of feeding kinematics of two pipefish with different snout lengths. Journal of Fish Biology.

ROOS G, LEYSEN H, VAN WASSENBERGH S, AERTS P, HERREL A, ADRIAENS D. submitted b. Locking the pivot-feeding mechanism in Syngnathidae: The role of snout adduction. Animal Biology.

ROSE CS, REISS JO. 1993. Metamorphosis and the vertebrate skull: Ontogenetic patterns and development mechanisms. In: Hanken J, Hall BK, editors. The skull volume 1: Development. The University of Chicago Press, Chicago. pp. 289-346.

ROSS CF. 2005. Finite element analysis in vertebrate biomechanics. The Anatomical Record Part A 283A:253-258.

RYDER JA. 1881. A contribution to the development and morphology of the lophobranchiates (*Hippocampus antiquorum*, the sea-horse). Bulletin of the United States Fish Commission 1882:191-199.

RYER CH, ORTH RJ. 1987. Feeding ecology of the northern pipefish, *Syngnathus fuscus*, in a seagrass community of the lower Chesapeake Bay. Estuaries 10:330-336.

SALZBURGER W, MACK T, VERHEYEN E, MEYER A. 2005. Out of Tanganyika: Genesis, explosive speciation, key-innovations and phylogeography of the haplochromine cichlid fishes. BMC Evolutionary Biology 5:17.

SANDERS JG, CRIBBS JE, FIENBERG HG, HULBURD GC, KATZ LS, PALUMBI SR. 2008. The tip of the tail: Molecular identification of seahorses for sale in apothecary shops and curio stores in California. Conservation Genetics 9:65-71.

SANDERSON, S. L. 1991. Functional stereotypy and feeding performance correlated in a trophic specialist. Functional Ecology 5:795-803.

SANFORD CPJ, WAINWRIGHT PC. 2002. Use of sonomicrometry demonstrates the link between prey capture kinematics and suction pressure in largemouth bass. The Journal of Experimental Biology 205:3445-3457.

SANFORD CPJ, DAY S, KINOW N. 2009. The role of mouth shape on the hydrodynamics of suction feeding in fishes. Integrative and Comparative Biology 49 (suppl.1):e149.

SARIN VK, ERICKSON GM, GIORI NJ, BERGMAN AG, CARTER DR. 1999. Coincident development of sesamoid bones and clues to their evolution. Anatomical Record 257:174-180.

SASAKI K, TANAKA Y, TAKATA Y. 2006. Cranial morphology of *Ateleopus japonicus* (Ateleopodidae, Ateleopodiformes), with a discussion on metamorphic mouth migration and lampridiform affinities. Ichthyological Research 53:254-263.

SCALES H. 2010. Advances in the ecology, biogeography and conservation of seahorses (genus *Hippocampus*). Progress in Physical Geography 34:443-458.

SCHULTZE HP. 2008. Nomenclature and homologization of cranial bones in actinopterygians. In: Arratia G, Schultze HP, Wilson WVH, editors. Mesozoic fishes 4 - Homology and phylogeny. Verlag Dr. Friederich Pfeil., München. pp. 23-48.

SHEETS HD. 2000a. CoordGen6f: Integrated Morphometrics Package Coordinate Generating Utility. Canisius College, Buffalo, New York, http://www3.canisius.edu/~sheets/morphsoft.html.

SHEETS HD. 2000b. TwoGroup6h: Integrated Morphometrics Package. Canisius College, Buffalo, New York, http://www3.canisius.edu/~sheets/morphsoft.html.

SILVA K, MONTEIRO NM, ALMADA VC, VIEIRA MN. 2006. Early life history of *Syngnathus abaster*. Journal of Fish Biology 68:80-86.

SMITH WML. 2010. Promoting resolution of the percomorph bush: A reply to Mooi and Gill. Copeia 3:520-524.

SMITH WML, WHEELER WC. 2004. Polyphyly of the mail-cheeked fishes (Teleostei: Scorpaeniformes): Evidence from the mitochondrial and nuclear sequence data. Molecular Phylogenetics and Evolution 32:627-646.

SMITH WML, CRAIG MT. 2007. Casting the percomorph net widely: The importance of broad taxonomic sampling in the search for the placement of serranid and percid fishes. Copeia 1:35-55.

SPRINGER VG, ORRELL TM. 2004. Appendix: Phylogenetic analysis of 147 families of acanthomorph fishes based on dorsal gill-arch muscles and skeleton. Bulletin of the Biological Society of Washington 11:237–260.

STARCK D. 1979. Der Schultergürtel der Fische. In: Starck D, editors. Vergleichende Anatomie der Wirbeltiere. Springer-Verlag, Berlin. pp. 467-472.

STEWART TA, ALBERTSON RC. 2010. Evolution of a unique predatory feeding apparatus: functional anatomy, development and a genetic locus for jaw laterality in Lake Tanganyika scale-eating cichlids. BMC Biology 8:11.

STIASSNY MLJ. 1996. Basal ctenosquamate relationships and the interrelationships of the myctophiform (Scopelomorph) fishes. In: Stiassny MLJ, Parenti LR, Johnson GD, editors. *Interrelationships of fishes*. Academic Press, San Diego. pp. 405-426.

STÖLTING KN, WILSON AB. 2007. Male pregnancy in seahorses and pipefish: Beyond the mammalian model. BioEssays 29:884-896.

STORERO LP, GONZÁLEZ RA. 2009. Prey selectivity and trophic behavior of the Patagonian seahorse, *Hippocampus patagonicus*, in captivity. Journal of the World Aquaculture Society 40:394-401.

SVANBÄCK R, WAINWRIGHT PC, FERRY-GRAHAM LA. 2002. Linking cranial kinematics, buccal pressure, and suction feeding performance in largemouth bass. Physiological and Biochemical Zoology 75:532–543.

SWINNERTON HH. 1902. A contribution to the morphology of the teleostean head skeleton, based upon a study of developing skull of the three-spined stickleback (*Gasterosteus aculeatus*). Quarterly Journal of Microscopical Sciences 45:503-597.

TAKAHASHI R, MORIWAKI T, HORI M. 2007. Foraging behaviour and functional morphology of two scale-eating cichlids from Lake Tanganyika. Journal of Fish Biology 70:1458-1469.

TAKATA J, SASAKI K. 2005. Branchial structures in the Gasterosteiformes, with special reference to myology and phylogenetic implications. Ichthyological Research 52:33-49.

TAYLOR WR, VAN DYKE GC. 1985. Revised procedures for staining and clearing small fishes and other vertebrates for bone and cartilage study. Cybium 9:107-119.

TCHERNAVIN VV. 1953. The feeding mechanisms of a deep sea fish. British Museum (Natural History), London. p.101.

TEIXEIRA RL, MUSICK JA. 1995. Trophic ecology of 2 congeneric pipefishes (Syngnathidae) of the lower York River, Virginia. Environmental Biology of Fishes 43:295-309.

TESCH FW. 2003. The eel 3rd edition. Blackwell Science, Oxford. p.408.

TESKE PR, BEHEREGARAY LB. 2009. Evolution of seahorses' upright position was linked to Oligocene expansion of seagrass habitats. Biology Letters 5:521-523.

TESKE PR, CHERRY MI, MATTHEE CA. 2003. Population genetics of the endangered Knysna seahorse, *Hippocampus capensis*. Molecular Ecology 12:1703-1715.

TESKE PR, CHERRY MI, MATTHEE CA. 2004. The evolutionary history of seahorses (Syngnathidae: *Hippocampus*): Molecular data suggest a West Pacific origin and two invasions of the Atlantic Ocean. Molecular Phylogenetics and Evolution 30:273-286.

TESKE PR, HAMILTON H, PALSBØLL PJ, CHOO CK, GABR H, LOURIE SA, SANTOS M, SREEPADA A, CHERRY MI, MATTHEE CA. 2005. Molecular evidence for long-distance colonization in an Indo-Pacific seahorse lineage. Marine Ecology Progress Series 286:249-260.

THIELEMANS A. 2007. Studie naar het musculo-skeletale apparaat bij een larvaal Kaaps zeepaardje (*Hippocampus capensis*) aan de hand van een grafische 3D-reconstructie. Unpublished Bachelor Thesis. Ghent University.

TILNEY RL, HECHT T. 1993. Early ontogeny of *Galeichthys feliceps* from the south east coast of South Africa. Journal of Fish Biology 43:183-212.

TIPTON K, BELL SS. 1988. Foraging patterns of two syngnathid fishes: Importance of harpacticoid copepods. Marine Ecology Progress Series 47:31-43.

VAN DAMME J, AERTS P. 1997. Kinematics and functional morphology of aquatic feeding in Australian snake-necked turtles (Pleurodira; *Chelodina*). Journal of Morphology 233:113–125.

VAN GINNEKEN VJT, MAES GE. 2005. The European eel (*Anguilla anguilla*, Linnaeus), its lifecycle, evolution and reproduction: a literature review. Reviews of Fish Biology and Fisheries 15:367-398.

VAN WASSENBERGH S, HERREL A, ADRIAENS D, AERTS P. 2005. A test of mouth-opening and hyoid-depression mechanisms during prey capture in a catfish using high-speed cineradiography. The Journal of Experimental Biology 208: 4627-4639.

VAN WASSENBERGH S, HERREL A, ADRIAENS D, AERTS P. 2006a. Modulation and variability of prey capture kinematics in clariid catfishes. Journal of Experimental Zoology 305A:559–569.

VAN WASSENBERGH S, AERTS P, HERREL A. 2006b. Hydrodynamic modelling of aquatic suction performance and intra-oral pressures: limitations for comparative studies. Journal of the Royal Society Interface 3:507-514.

VAN WASSENBERGH S, STROTHER JA, FLAMMANG B, FERRY-GRAHAM LA, AERTS P. 2008. Extremely fast prey capture in pipefish is powered by elastic recoil. Journal of the Royal Society Interface 5:285-296.

VAN WASSENBERGH S, ROOS G, GENBRUGGE A, LEYSEN H, AERTS P, ADRIAENS D, HERREL A. 2009. Suction is kids play: Extremely fast suction in newborn seahorses. Biology Letters 5:200-203.

VAN WASSENBERGH S, ROOS G, FERRY L. 2011. An adaptive explanation for the horse-like shape of seahorses. Nature Communications 2.

VERRAES W. 1977. Postembryonic ontogeny and functional anatomy of the ligamentum mandibulo-hyoideum and the ligamentum interoperculo-mandibulare, with notes on the opercular bones and some other cranial elements in *Salmo gairdneri* Richardson, 1836 (Teleostei: Salmonidae). Journal of Morphology 151:111-119.

VINCENT ACJ, SADLER LM. 1995. Faithful pair bonds in wild seahorses, *Hippocampus whitei*. Animal Behaviour 50:1557-1569.

VINCENT ACJ, GILES BG. 2003. Correlates of reproductive success in a wild population of *Hippocampus whitei*. Journal of Fish Biology 63:344-355.

VINCENT ACJ, BERGLUND A, AHNESJÖ I. 1995. Reproductive ecology of five pipefish species in one eelgrass meadow. Environmental Biology of Fishes

44:347-361.

VIZZINI S, MAZZOLA M. 2004. The trophic structure of the pipefish community (Pisces: Syngnathidae) from a western Mediterranean seagrass meadow based on stable isotope analysis. Estuaries 27:325-333.

VLASSENBROECK J, DIERICK M, MASSCHAELE B, CNUDDE V, VAN HOOREBEKE L, JACOBS P. 2007. Software tools for quantification of X-ray microtomography at the UGCT. Nuclear Instruments & Methods in Physics Research Section A: Accelerators, Spectrometers, Detectors and Associated Equipment 580:442-445.

WALLACE AR. 1889. Darwinism: An exposition of the theory of natural selection. With some of its applications. MacMillian, London. p. 494.

WARBURTON K. 2003. Learning of foraging skills by fish. Fish and Fisheries 4:203-215.

WEBB PW, WEIHS D. 1986. Functional locomotor morphology of early life history stages in fishes. Transactions of the American Fisheries Society 115:115-127.

WERNER EE, GILLIAM JF. 1984. The ontogenetic niche and species interactions in size-structured populations. Annual Review of Ecology, Evolution and Systematics 15:393-425.

WESTNEAT MW. 1990. Feeding mechanics of teleost fishes (Labridae; Perciformes): A test of four-bar linkage models. Journal of Morphology 205:269-295.

WESTNEAT MW. 2004. Evolution of levers and linkages in the feeding mechanisms of fishes. Integrative and Comparative Biology 44:378-389.

WESTNEAT MW, WAINWRIGHT PC. 1989. Feeding mechanism of *Epibulus insidator* (Labridae; Teleostei): evolution of a novel functional system. Journal of Morphology 202:129-150.

WILEY EO, JOHNSON DG. 2010. A teleost classification based on monophyletic groups. In: Nelson JS, Schultze HP, Wilson MVH, editors. Origin and phylogenetic interrelationships of teleosts. Honoring Gloria Arratia. Verlag Dr. Friedrich Pfeil, München. pp. 123-182.

WILGA CD, MOTTA PJ, SANFORD CP. 2007. Evolution and ecology of feeding in elasmobranchs. Integrative and Comparative Biology 47: 55–69.

WILSON NG, ROUSE GW. 2010. Convergent camouflage and the non-monophyly of 'seadragons' (Syngnathidae: Teleostei): Suggestions for a revised taxonomy of syngnathids. Zoologica Scripta 39:551-558.

WILSON AB, ORR JW. submitted. The evolutionary origins of syngnathid fishes. Journal of Fish Biology.

WILSON AB, VINCENT A, AHNESJÖ I, MEYER A. 2001. Male pregnancy in seahorses

and pipefishes (family Syngnathidae): Rapid diversification of paternal brood pouch morphology inferred from a molecular phylogeny. The Journal of Heredity 92:159-166.

WILSON AB, AHNESJÖ I, VINCENT ACJ, MEYER A. 2003. The dynamics of male brooding, mating patterns, and sex roles in pipefishes and seahorses (family Syngnathidae). Evolution 57:1374-1386.

WINTERBOTTOM R. 1974. A descriptive synonymy of the striated muscles of the Teleostei. Proceedings of the Academy of Natural Sciences of Philadelphia 125:225-317.

WOODS CMC. 2003. Growth and survival of the juvenile seahorse *Hippocampus abdominalis* reared on live, frozen and artificial foods. Aquaculture 220:287-298.

ZACK TI, CLAVERIE T, PATEK SN. 2009. Elastic energy storage in the mantis shrimp's fast predatory strike. The Journal of Experimental Biology 212:4002-4009.

ŽALOHAR J, HITIJ T, KRIŽNAR M. 2009. Two new species of seahorses (Syngnathidae, *Hippocampus*) from the Middle Miocene (Sarmatian) Coprolitic Horizon in Tunjice Hills, Slovenia : The oldest fossil record of seahorses. Annales de Paléontologie 92:71-96.

ZELDITCH ML, SWIDERSKI DL, SHEETS HD, FINK WL. 2004. Geometric morphometrics for biologists: A primer. Elsevier Academic Press, London p. 443.

Publication list

ROOS G, LEYSEN H, VAN WASSENBERGH S, HERREL A, JACOBS P, DIERICK M, AERTS P, ADRIAENS D. 2009. Linking morphology and motion: A test of a four-bar mechanism in seahorses. Physiological and Biochemical Zoology 82(1):7-19.

VAN WASSENBERGH S, ROOS G, GENBRUGGE A, LEYSEN H, AERTS P, ADRIAENS D, HERREL A. 2009. Suction is kids play: Fast suction in newborn seahorses. Biology Letters 5:200-203.

LEYSEN H, JOUK P, BRUNAIN M, CHRISTIAENS J, ADRIAENS A. 2010. Cranial architecture of tube-snouted Gasterosteiformes (*Syngnathus rostellatus* and *Hippocampus capensis*). Journal of Morphology 271(3):255-270.

LEYSEN H, CHRISTIAENS J, DE KEGEL B, BOONE MN, VAN HOOREBEKE L, ADRIAENS D. in press. Musculoskeletal structure of the feeding system and implications of snout elongation in *Hippocampus reidi* and *Dunckerocampus dactyliophorus*. Journal of Fish Biology,

ROOS G, LEYSEN H, VAN WASSENBERGH S, AERTS P, HERREL A, ADRIAENS D. submitted. Locking the pivot-feeding mechanism in Syngnathidae: The role of snout adduction. Animal Biology.

LEYSEN H, ROOS G, ADRIAENS D. submitted. Morphological variation in pipefish and seahorse head shape in relation to snout length and developmental growth. Journal of Morphology.

LEYSEN H, DUMONT ER, BRABANT L, VAN HOOREBEKE L, ADRIAENS D. submitted. Dealing with stress in the feeding apparatus of seahorses and pipefishes. Zoological Journal of the Linnean Society.

Universiteit Gent
Faculteit Wetenschappen
Vakgroep Biologie
Evolutionaire Morfologie van Vertebraten

EVOLUTIONARY MORPHOLOGY OF THE EXTREMELY SPECIALIZED FEEDING APPARATUS IN SEAHORSES AND PIPEFISHES (SYNGNATHIDAE)

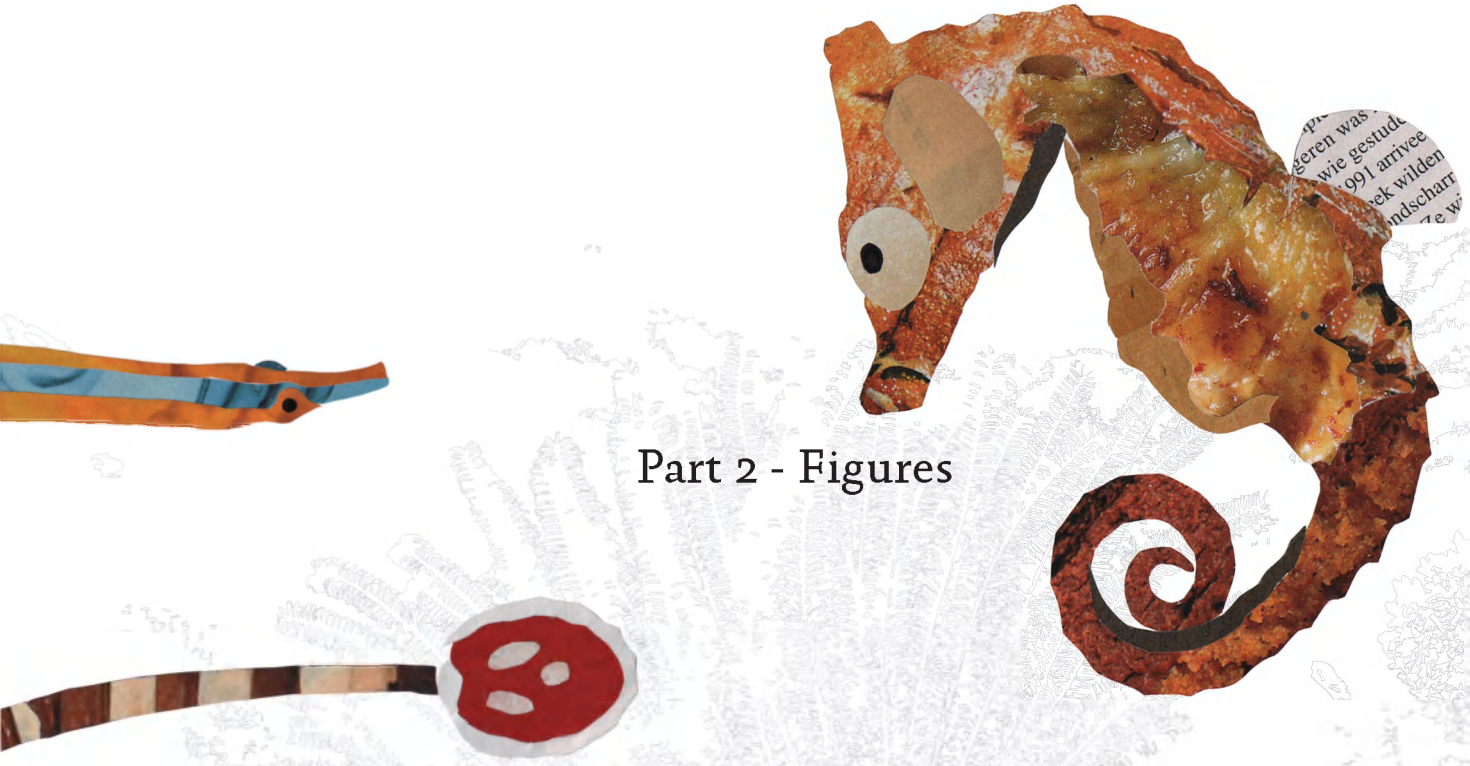

Part 2 - Figures

Heleen Leysen

Thesis submitted to obtain the degree of Doctor in Sciences (Biology)

Academiejaar 2010-2011

Proefschrift voorgedragen tot het bekomen van de graad van Doctor in de Wetenschappen (Biologie)

Rector: Prof. Dr. Paul van Cauwenberge
Decaan: Prof. Dr. Herwig Dejonghe
Promotor: Prof. Dr. Dominique Adriaens

EVOLUTIONARY MORPHOLOGY OF THE EXTREMELY SPECIALIZED FEEDING APPARATUS IN SEAHORSES AND PIPEFISHES (SYNGNATHIDAE)

Part 2 - Figures

Heleen Leysen

Thesis submitted to obtain the degree of Doctor in Sciences (Biology)

Academiejaar 2010-2011

Proefschrift voorgedragen tot het bekomen van de graad van Doctor in de Wetenschappen (Biologie)

Rector: Prof. Dr. Paul van Cauwenberge
Decaan: Prof. Dr. Herwig Dejonghe
Promotor: Prof. Dr. Dominique Adriaens

Table of contents

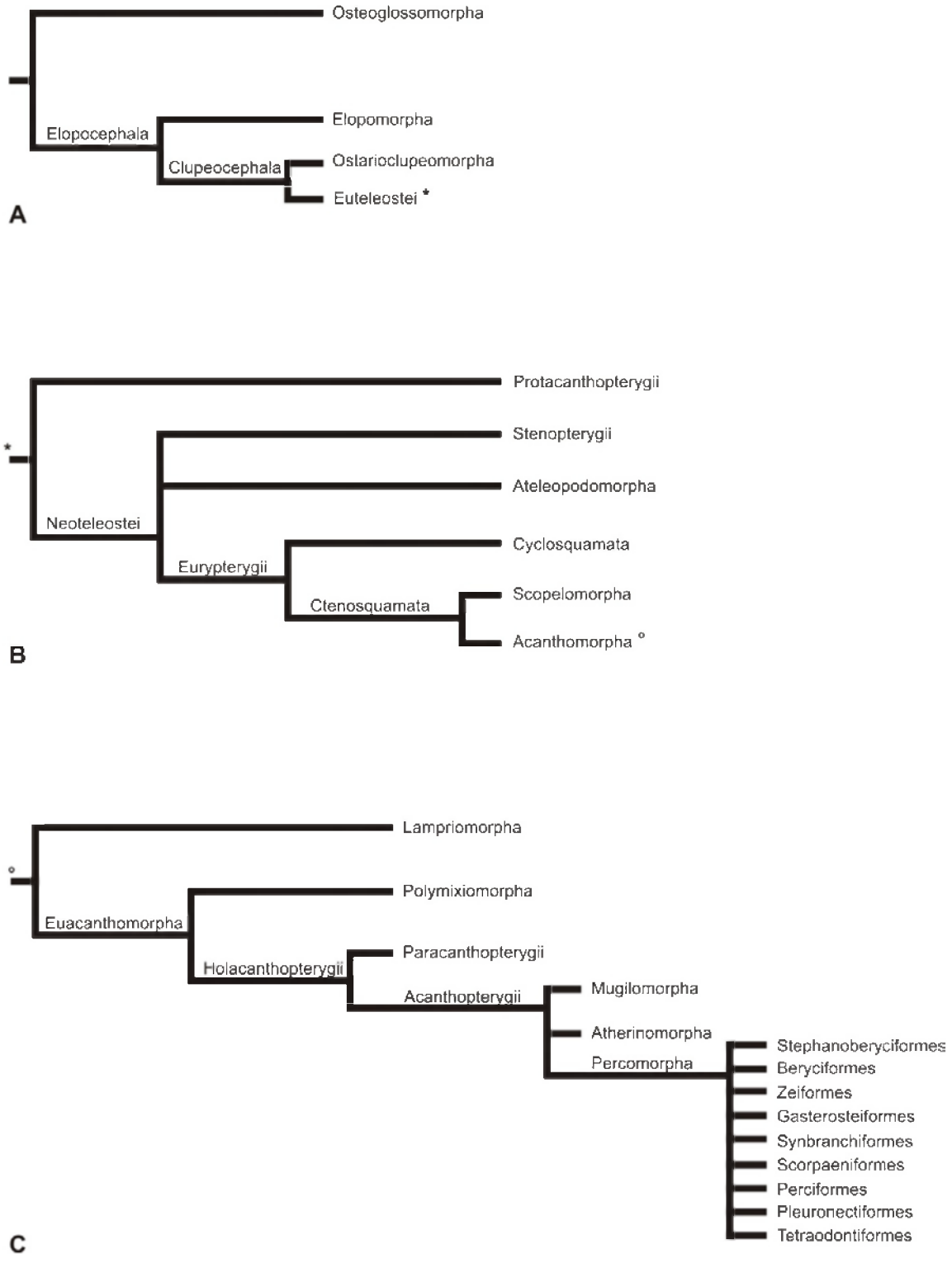

Fig. 1.1 – Phylogenetic relationships of **A** Teleostei; **B** Euteleostei; **C** Acanthomorpha (Nelson, 2006).

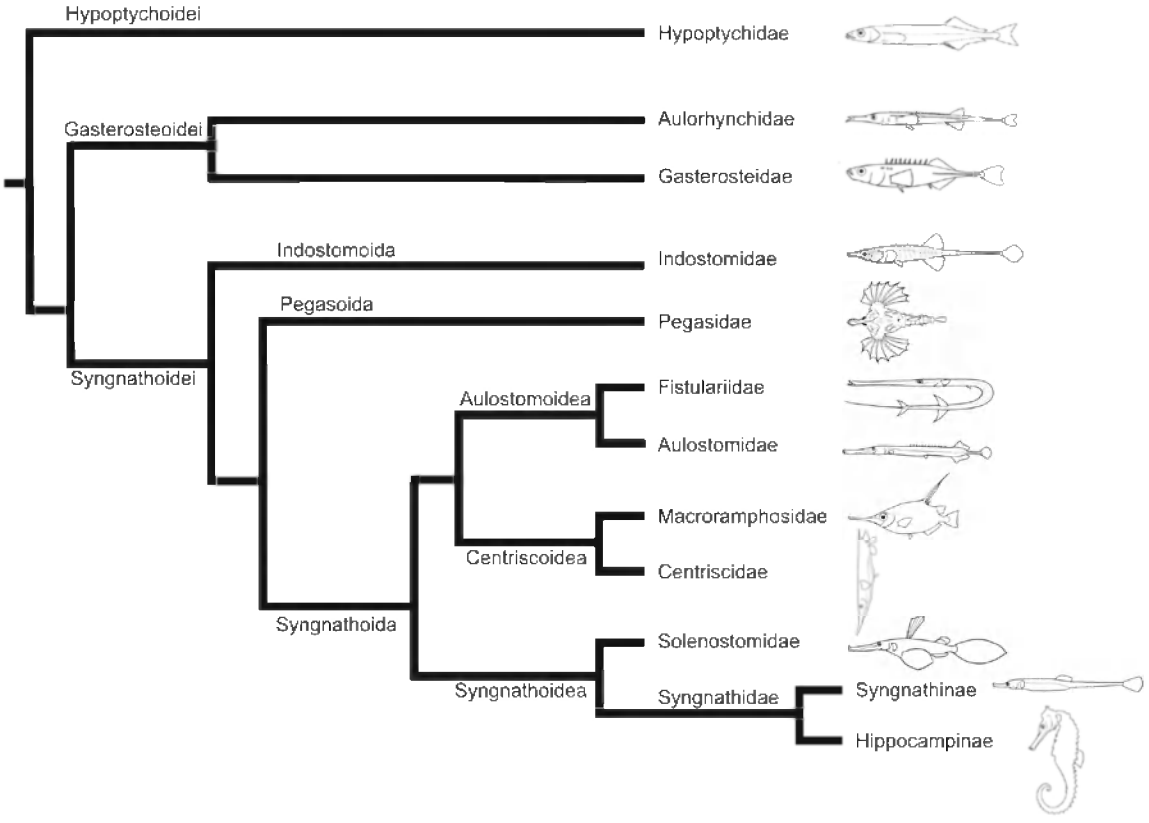

Fig. 1.2 – Phylogenetic relationships of Gasterosteiformes (Keivany & Nelson, 2006). Note the division into three suborders: Hypoptychoidei, Gasterosteoidei and Syngnathoidei. (All pictures from Nelson (2006) except for Hypoptychidae from FishBase (Froese & Pauly, 2010)).

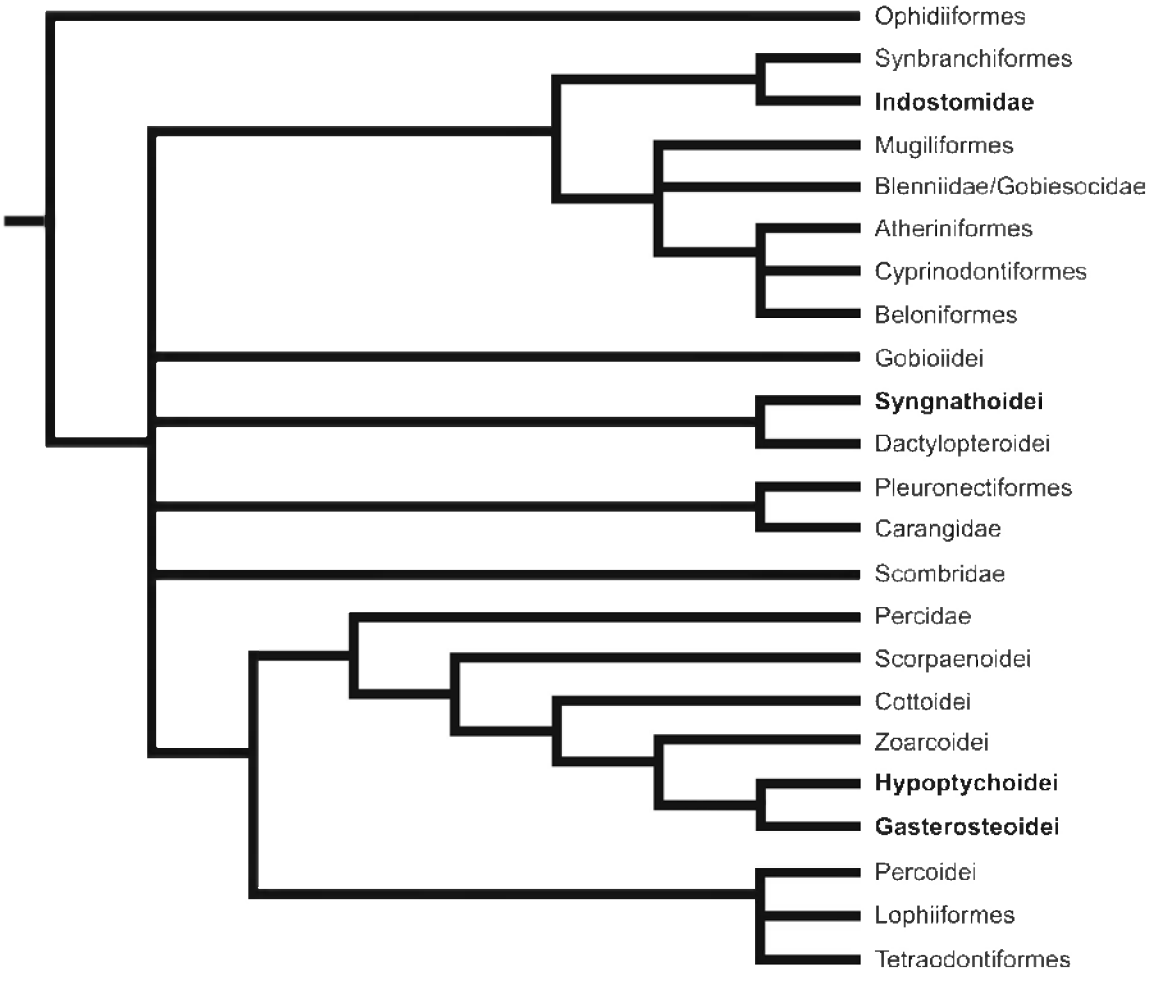

Fig. 1.3 – Molecular phylogeny of Percomorpha proposed by Kawahara *et al.* (2008). The clades belonging to the order Gasterosteiformes *sensu* Keivany & Nelson (2006) are in bold.

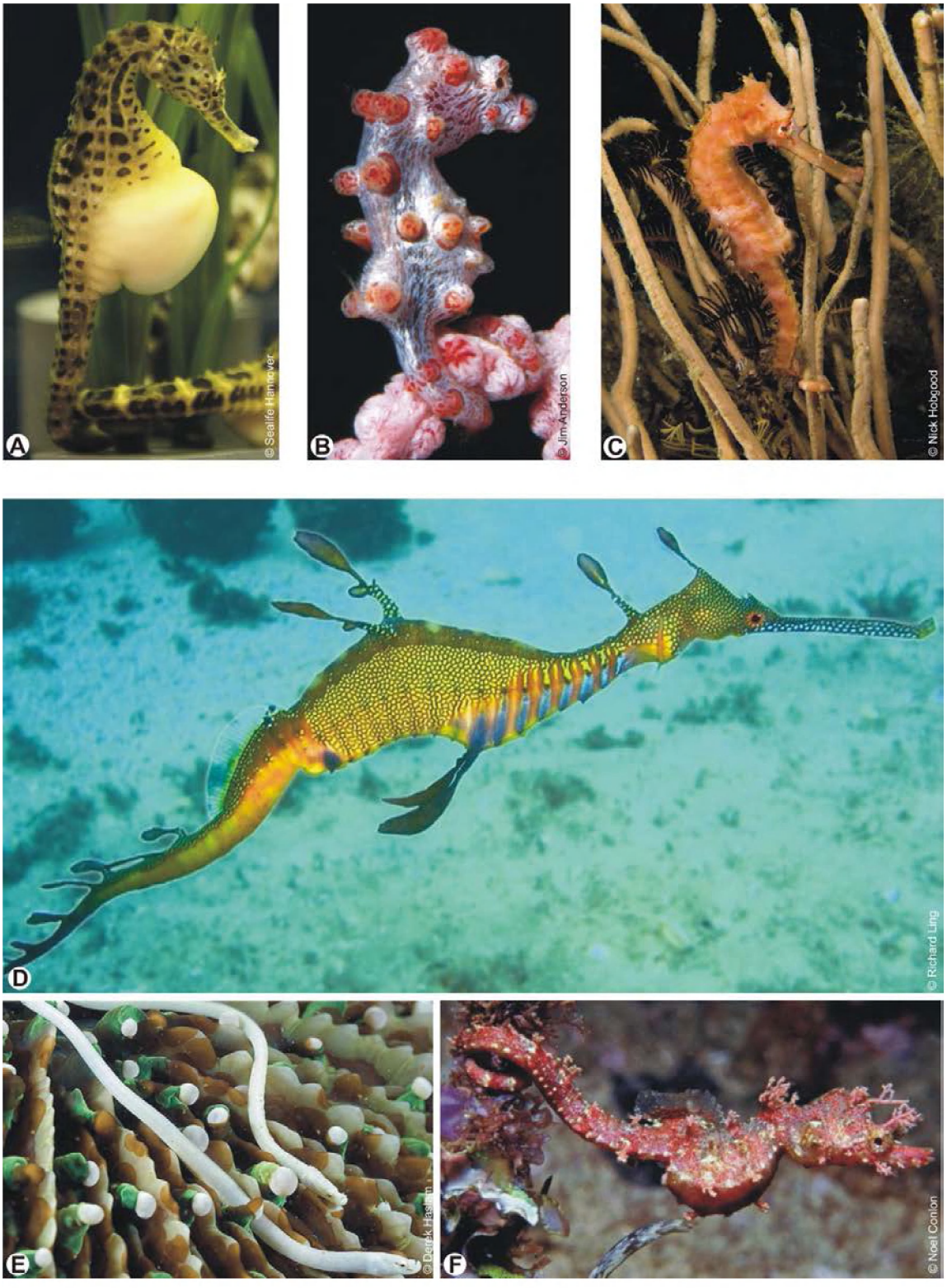

Fig. 1.4 – Some species of the family Syngnathidae (A-C subfamily Hippocampinae, D-F subfamily Syngnathinae) showing the morphological diversity. **A** *Hippocampus abdominalis*; **B** *H. bargibanti*; **C** *H. histrix*; **D** *Phyllopteryx taeniolatus*; **E** *Siokunichthys nigrolineatus*; **F** *Idiotropiscis lumnitzeri*.

Fig. 1.5 – Legend


unprotected eggs


individual egg compartments


rudimentary pouch with plates and/or skin-folds


enclosed pouch (semi-inverted)


enclosed pouch (inverted)


enclosed pouch (everted)


fully enclosed pouch

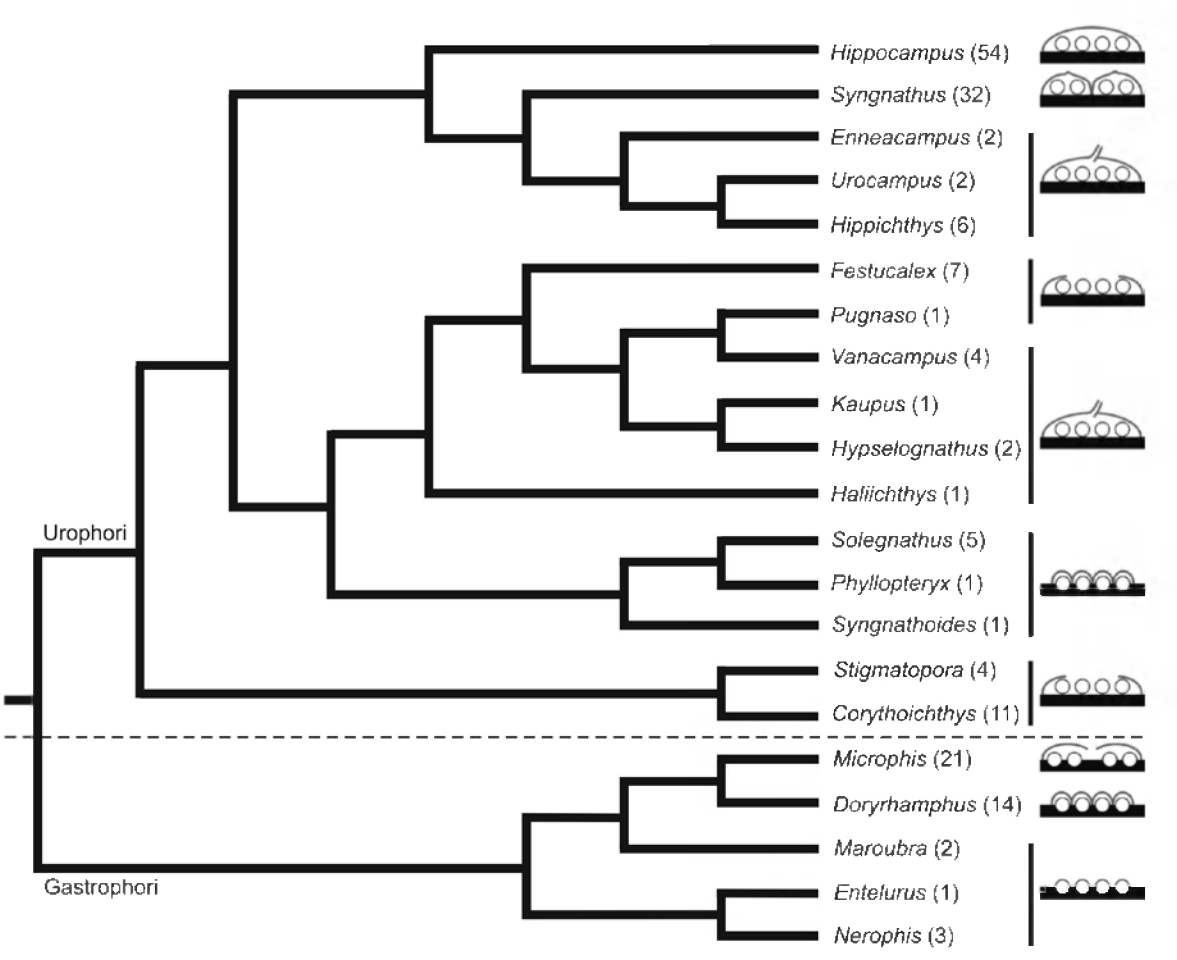

Fig. 1.5 – Phylogenetic relationships of some syngnathid genera with schematic cross sections through the male brood pouch showing the increase in pouch enclosure. Figures between brackets indicate the number of species considered valid according to Fishbase (Froese & Pauly, 2011). Genera below the dashed line are abdominal brooders (Gastrophori), genera above the line are tail brooders (Urophori). The genus *Hippocampus* belongs to the subfamily Hippocampinae, all other genera are part of the subfamily Syngnathinae. Modified from Wilson & Orr (submitted), based on complete cytochrome *b* and partial 12S rDNA and 16S rDNA sequence data.

Fig. 1.6 – Legend

h	hyoid
n	neurocranium-suspensorium complex
pg	pectoral girdle
u	urohyal bone and sternohyoideus muscle
v	vertebral column
P	connection between the neurocranium and vertebral column
Q	connection between the pectoral girdle and the neurocranium
m-epax	epaxial muscle
m-hypax	hypaxial muscle
m-st	sternohyoideus muscle

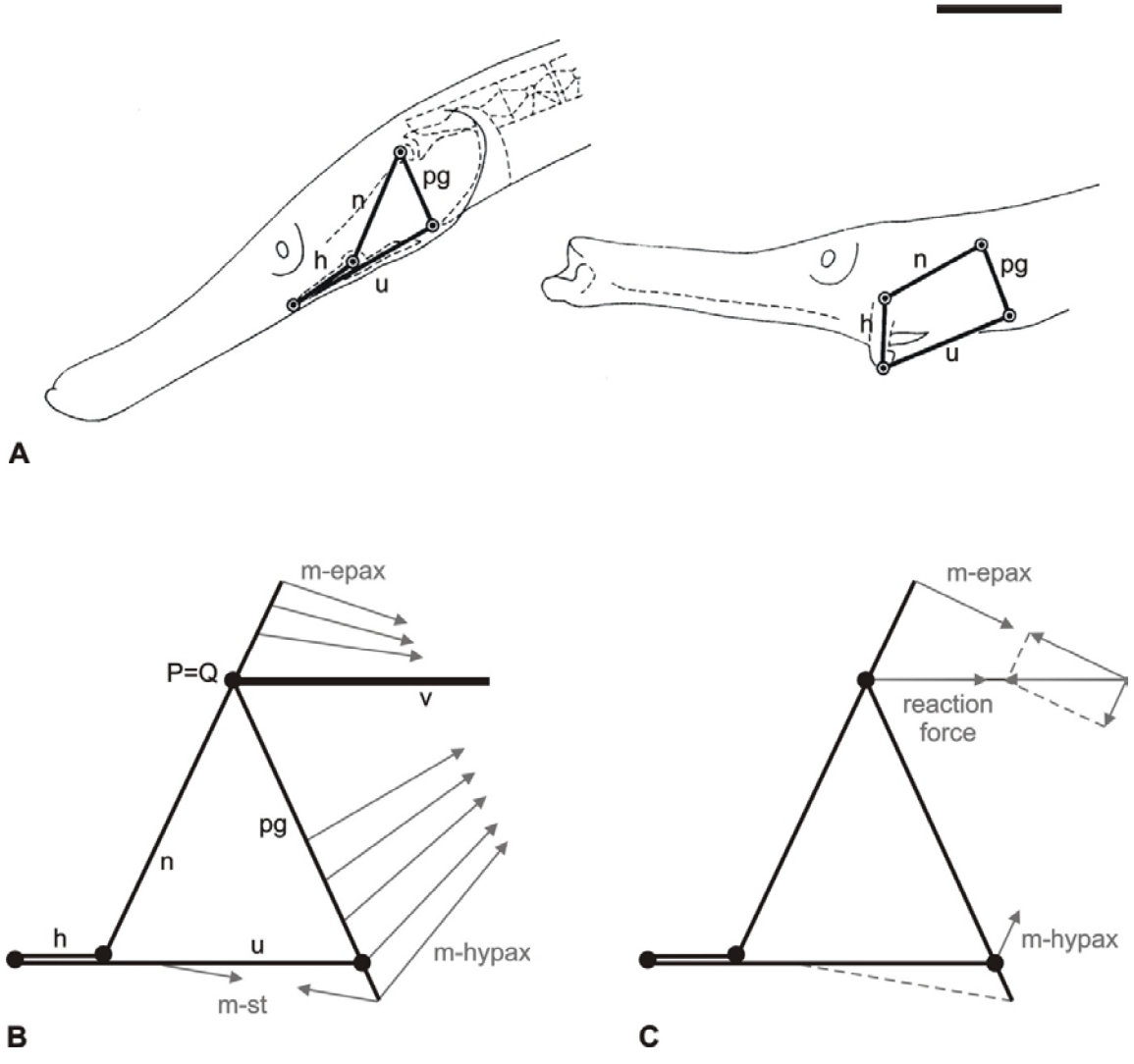

Fig. 1.6 – The planar four-bar chain as described by Muller (1987). The system is stressed by the epaxial and hypaxial muscles whereas the sternohyoideus muscle is thought to act as a trigger thus initiating fast head and hyoid movements. **A** Head of *Entelurus aequoreus* in rest (left) and expanded (right) situation; **B** Diagram of the bars, joints and muscles of the four-bar system; **C** Schematic drawing of the resultant forces. Scale bar = 5 mm.

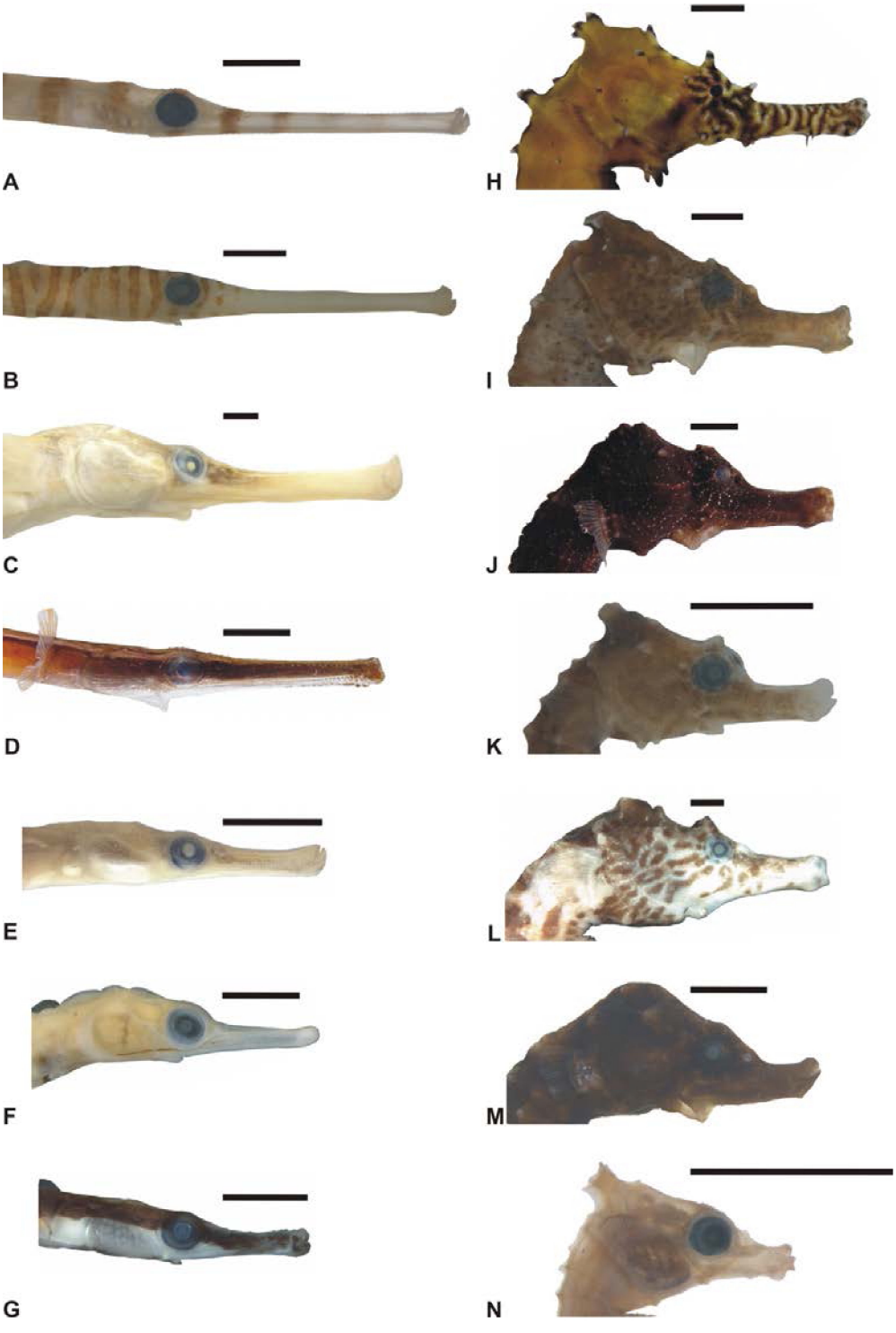

Fig. 2.1 – Right lateral side of the heads of the 14 syngnathid species studied. Pictures of fixed specimens scaled based on braincase length and sorted according to snout length (A-G pipefishes, H-N seahorses). **A** *Doryrhamphus dactyliophorus;* **B** *Dunckerocampus pessuliferus;* **C** *Syngnathus acus;* **D** *Doryrhamphus janssi;* **E** *Syngnathus rostellatus;* **F** *Corythoichthys intestinalis;* **G** *Doryrhamphus melanopleura;* **H** *Hippocampus barbouri;* **I** *Hippocampus kuda;* **J** *Hippocampus reidi;* **K** *Hippocampus breviceps;* **L** *Hippocampus abdominalis;* **M** *Hippocampus capensis;* **N** *Hippocampus zosterae.* Scale bar = 5 mm.

Fig. 2.2 – Legend

HL	head length; from tip of upper jaw to base of cleithral curvature
SL	standard length; between tip of snout and base of caudal fin
SnL	snout length; between tip of upper jaw and caudal margin of nostril
TaL	tail length; from mid-point of last trunk ring to tail tip
TrL	trunk length; from base of cleithral curvature to mid-point of last trunk ring

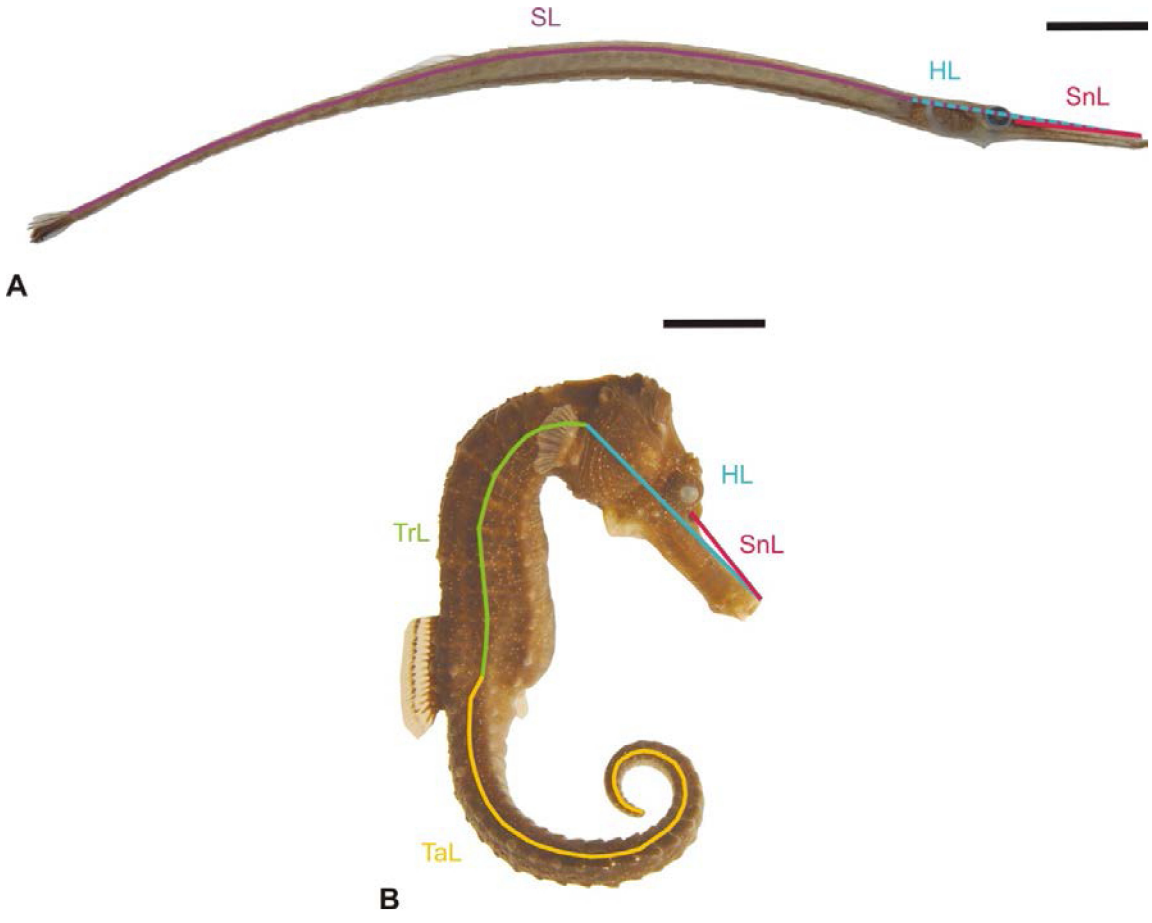

Fig. 2.2 – Measurements as performed on **A** a pipefish (*Microphis brachyurus aculeatus*), and **B** a seahorse (*Hippocampus reidi*). See text for a definition of the lengths. Scale bar = 10 mm.

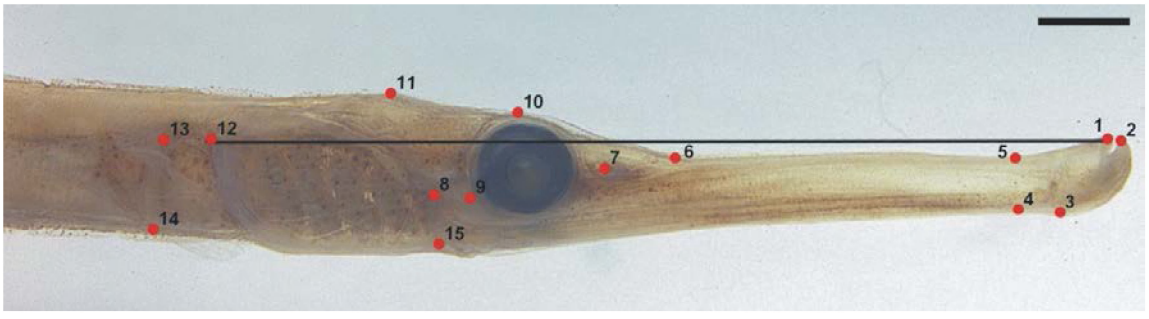

Fig. 2.3 – Right lateral side of the head of a *Microphis brachyurus aculeatus* specimen showing the 15 landmarks used for the geometric morphometrical analysis. The thin black line, connecting landmark 1 with landmark 12, measures head length and was used to define landmarks 10 and 11. See text for an anatomical description of the landmarks. Scale bar = 2 mm.

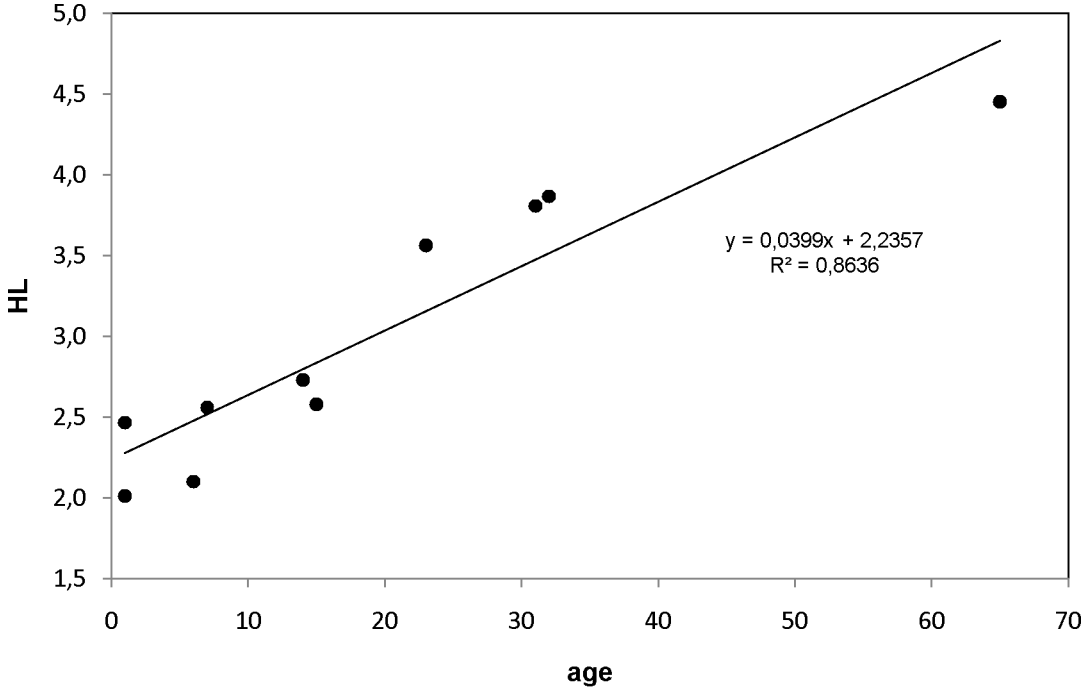

Fig. 2.4 – Relation between age and head length (HL) of ten *Hippocampus reidi* juveniles with linear regression trendline and equation. Correlation coefficient is 0.93.

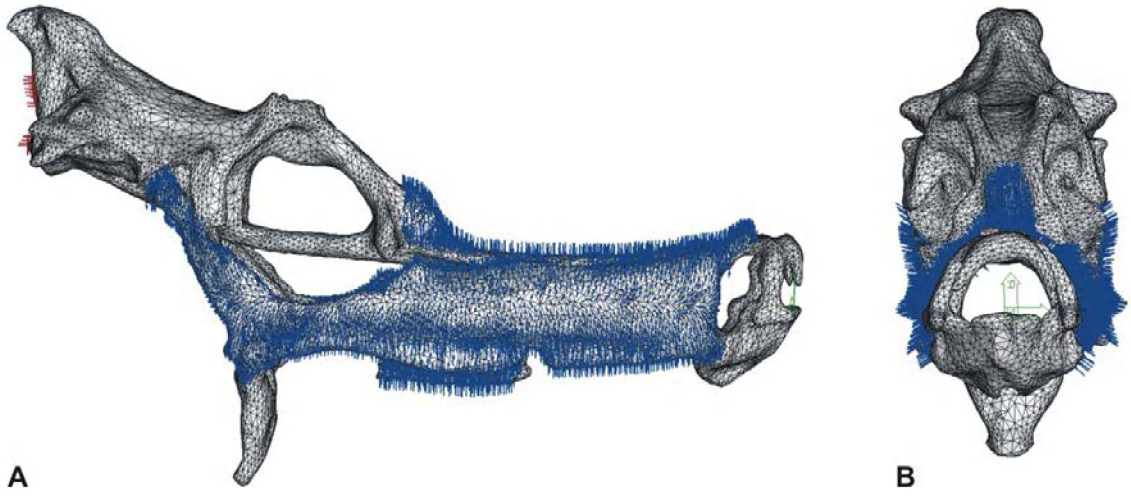

Fig. 2.5 – *Hippocampus reidi* model for the finite element analysis showing the applied pressure (blue), the constraints at the occipital part of the skull (red) and the cylindrical coordinate system with the origin at the tip of the snout (green). **A** right lateral view; **B** rostral view.

Fig. 3.1 – Legend

bh	basihyal cartilage
ch	ceratohyal cartilage
c-Meck	Meckel's cartilage
c-rost	rostral cartilage
et-p	ethmoid plate
fn-hyp	fenestra hypophysea
f-on	orbitonasal foramen
hh	hypohyal cartilage
hs	hyosymplectic cartilage
ih	interhyal cartilage
lm-on	orbitonasal lamina
ot-cap	otic capsule
p-p	palatine part of palatoquadrate cartilage
p-q	pterygoquadrate part of palatoquadrate cartilage
pl-oc	pila occipitalis
s-in	internasal septum
tn-m	taeniae marginalis
tn-t-m-p	taeniae tecti medialis posterior
tr-c	trabecula communis
tt-p	tectum posterius
tt-syn	tectum synoticum

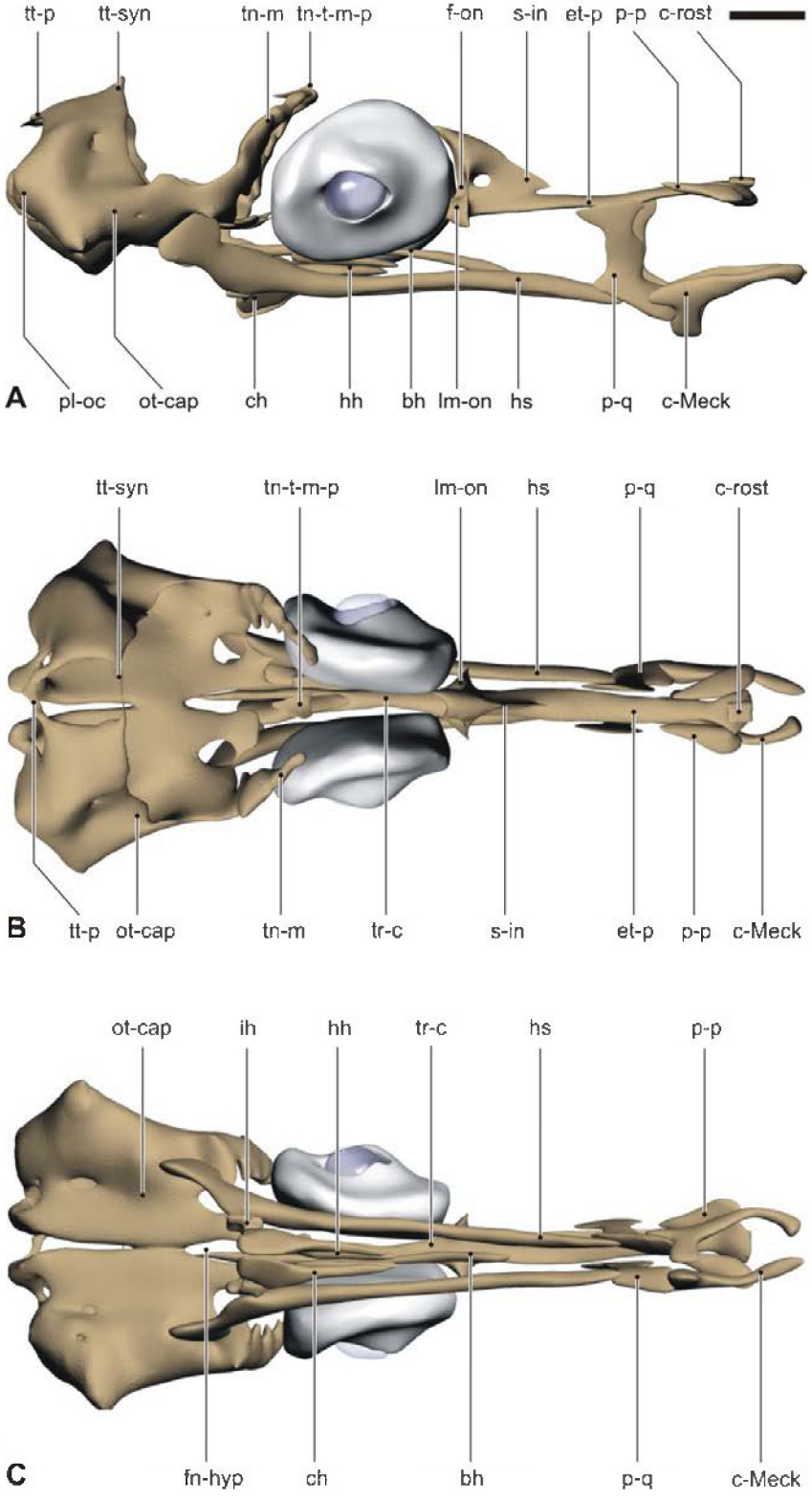

Fig. 3.1 – 3D-reconstruction of the juvenile chondrocranium of *Syngnathus rostellatus* (13.1 mm SL) based on histological sections. **A** lateral view of the right side; **B** dorsal view; **C** ventral view. Scale bar = 0.2 mm.

Fig. 3.2 – Legend

bh	basihyal cartilage
c-Meck	Meckel's cartilage
ch	ceratohyal cartilage
et-p	ethmoid plate
hh	hypohyal cartilage
hs	hyosymplectic cartilage
ih	interhyal cartilage
lm-on	orbitonasal lamina
o-ang	anguloarticular bone
o-apal	autopalatine bone
o-bh	basihyal bone
o-ch	ceratohyal bone
o-den	dentary bone
o-ecp	ectopterygoid bone
o-hh	hypohyal bone
o-hm	hyomandibular bone
o-ih	interhyal bone
o-meth	mesethmoid bone
o-mp	metapterygoid bone
o-mx	maxillary bone
o-par	parietal bone
o-para	parasphenoid bone
o-pop	preopercular bone
o-q	quadrate bone
o-rart	retroarticular bone
o-sym	symplectic bone
ot-cap	otic capsule
p-p	palatine part of palatoquadrate cartilage
p-q	pterygoquadrate part of palatoquadrate cartilage
s-in	internasal septum.

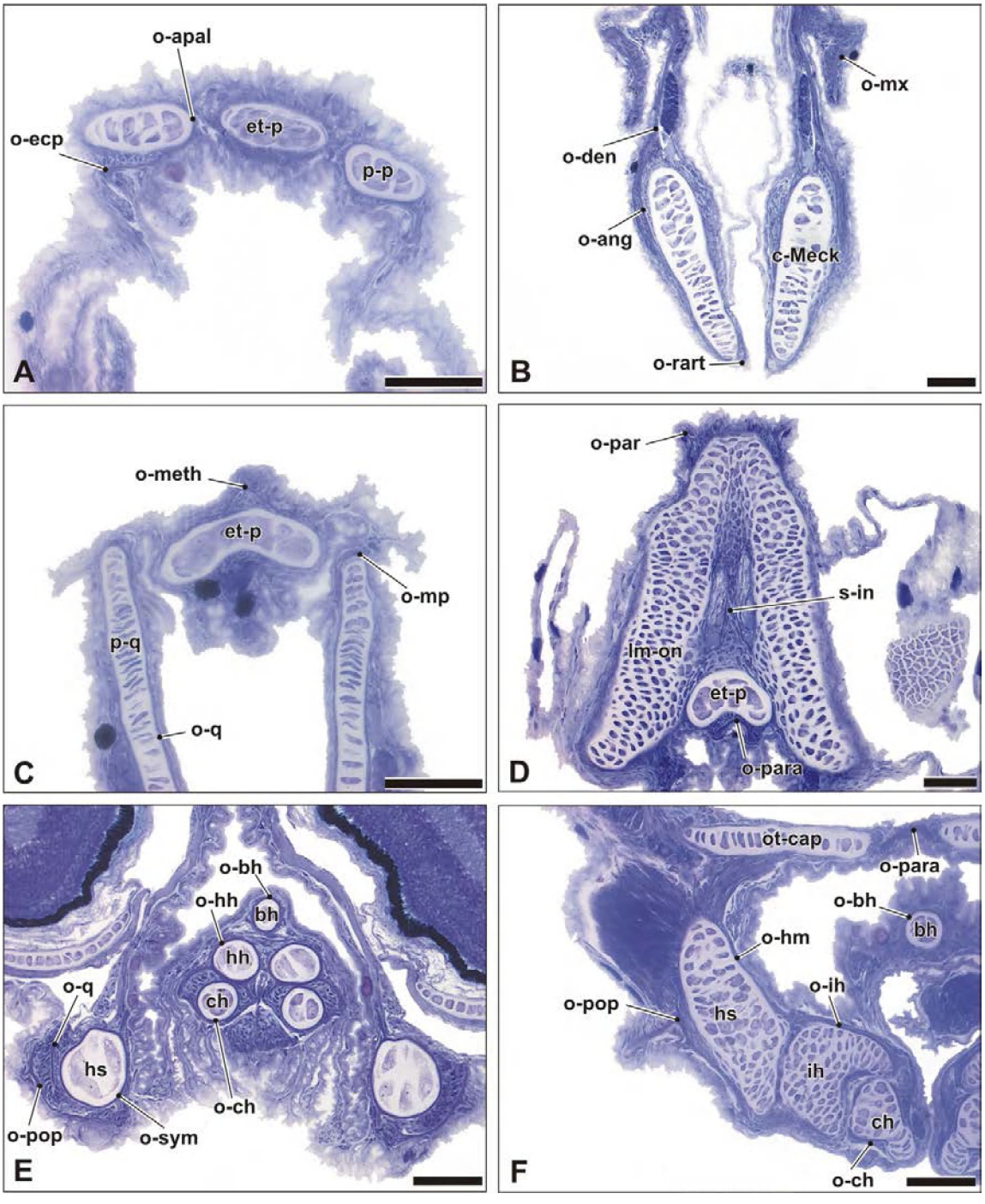

Fig. 3.2 – Histological cross sections of the juvenile cranium of *Syngnathus rostellatus* (13.1 mm SL). **A** dorsorostral part of the snout at the level of the autopalatine bone; **B** lower jaw; **C** dorsal part of ethmoid region; **D** internasal region; **E** hyoid; **F** right hyoid-suspensorium articulation. Scale bars = 50 µm.

Fig. 3.3 – Legend

bh	basihyal cartilage
c-Meck	Meckel's cartilage
c-rost	rostral cartilage
ch	ceratohyal cartilage
cp-a	anterior copula
et-p	ethmoid plate
hh	hypohyal cartilage
hs	hyosymplectic cartilage
ih	interhyal cartilage
lm-on	orbitonasal lamina
ot-cap	otic capsule
p-p	palatine part of palatoquadrate cartilage
p-q	pterygoquadrate part of palatoquadrate cartilage
pl-oc	pila occipitalis
r-s-pt	spheno-pterotic ridge
s-in	internasal septum
tn-m	taenia marginalis
tn-t-m-p	taenia tecti medialis posterior
tr-c	trabecula communis
tt-syn	tectum synoticum.

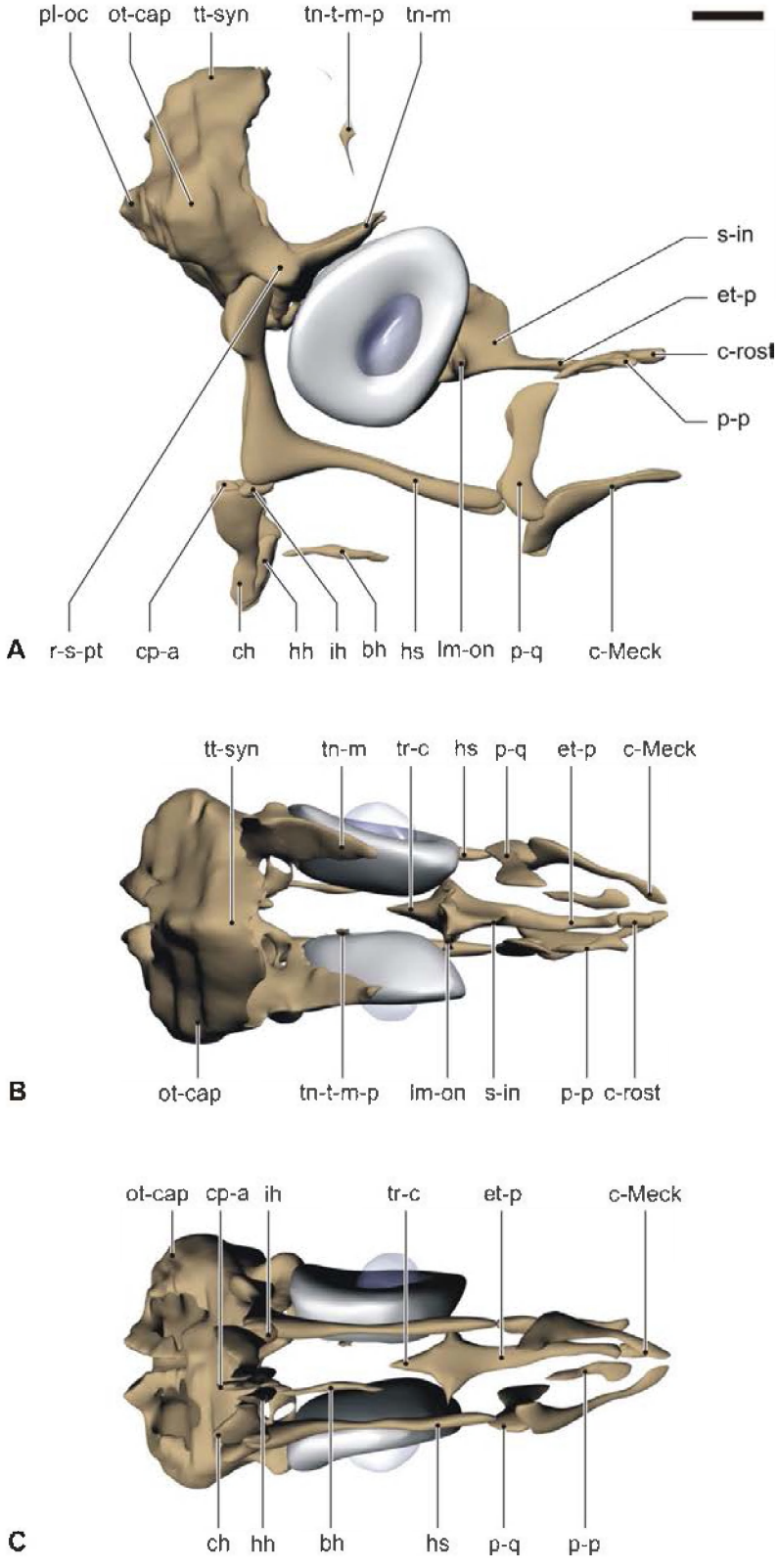

Fig. 3.3 – 3D-reconstruction of the juvenile chondrocranium of *Hippocampus capensis* (12.8 mm SL), with hyoid depressed, based on histological sections. **A** lateral view of the right side; **B** dorsal view; **C** ventral view. Scale bar = 0.2 mm.

Fig. 3.4 – Legend

bh	basihyal cartilage
c-Meck	Meckel's cartilage
ch	ceratohyal cartilage
et-p	ethmoid plate
hh	hypohyal cartilage
hs	hyosymplectic cartilage
ih	interhyal cartilage
lm-on	orbitonasal lamina
o-ang	anguloarticular bone
o-apal	autopalatine bone
o-ch-p	posterior ceratohyal bone
o-ecp	ectopterygoid bone
o-hh	hypohyal bone
o-hm	hyomandibular bone
o-ih	interhyal bone
o-leth	lateral ethmoid bone
o-meth	mesethmoid bone
o-mp	metapterygoid bone
o-par	parietal bone
o-para	parasphenoid bone
o-pop	preopercular bone
o-q	quadrate bone
o-rart	retroarticular bone
o-sym	symplectic bone
o-vm	vomeral bone
p-p	palatine part of palatoquadrate cartilage
p-q	pterygoquadrate part of palatoquadrate cartilage
s-in	internasal septum

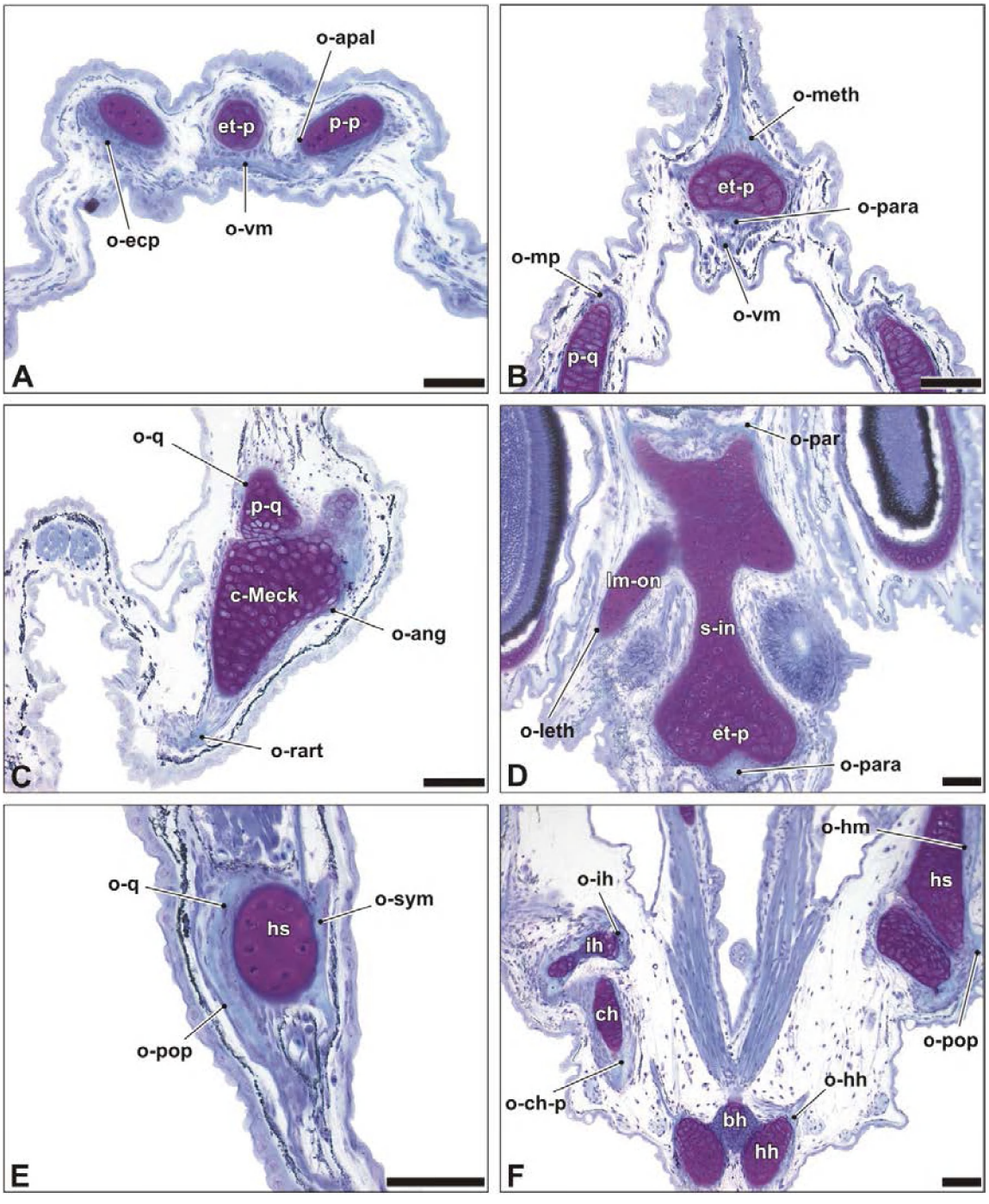

Fig. 3.4 – Histological cross sections of the juvenile cranium of *Hippocampus capensis* (12.8 mm SL). **A** dorsorostral part of the snout at the level of the autopalatine bone; **B** dorsal part of ethmoid region; **C** left lower jaw; **D** internasal region; **E** part of right suspensorium; **F** hyoid-suspensorium articulation. Scale bars = 50 µm.

Fig. 3.5 – Legend

c-rost	rostral cartilage
o-ang	anguloarticular bone
o-ant-lac	antorbitolacrimal bone
o-apal	autopalatine bone
o-ch-a	anterior ceratohyal bone
o-ch-p	posterior ceratohyal bone
o-cl	cleithrum
o-den	dentary bone
o-ecp	ectopterygoid bone
o-hm	hyomandibular bone
o-ih	interhyal bone
o-io-II	second infraorbital bone
o-iop	interopercular bone
o-leth	lateral ethmoid bone
o-meth	mesethmoid bone
o-mp	metapterygoid bone
o-mx	maxillary bone
o-op	opercular bone
o-par	parietal bone
o-para	parasphenoid bone
o-pop	preopercular bone
o-postp	postparietal bone
o-postt	posttemporal bone
o-prmx	premaxillary bone
o-pt	pterotic bone
o-q	quadrate bone
o-rart	retroarticular bone
o-soc	supraoccipital bone
o-sph	sphenotic bone
o-spop	suprapreopercular bone
o-sym	symplectic bone
o-uh	urohyal bone
o-vm	vomeral bone
r-br	branchiostegal ray

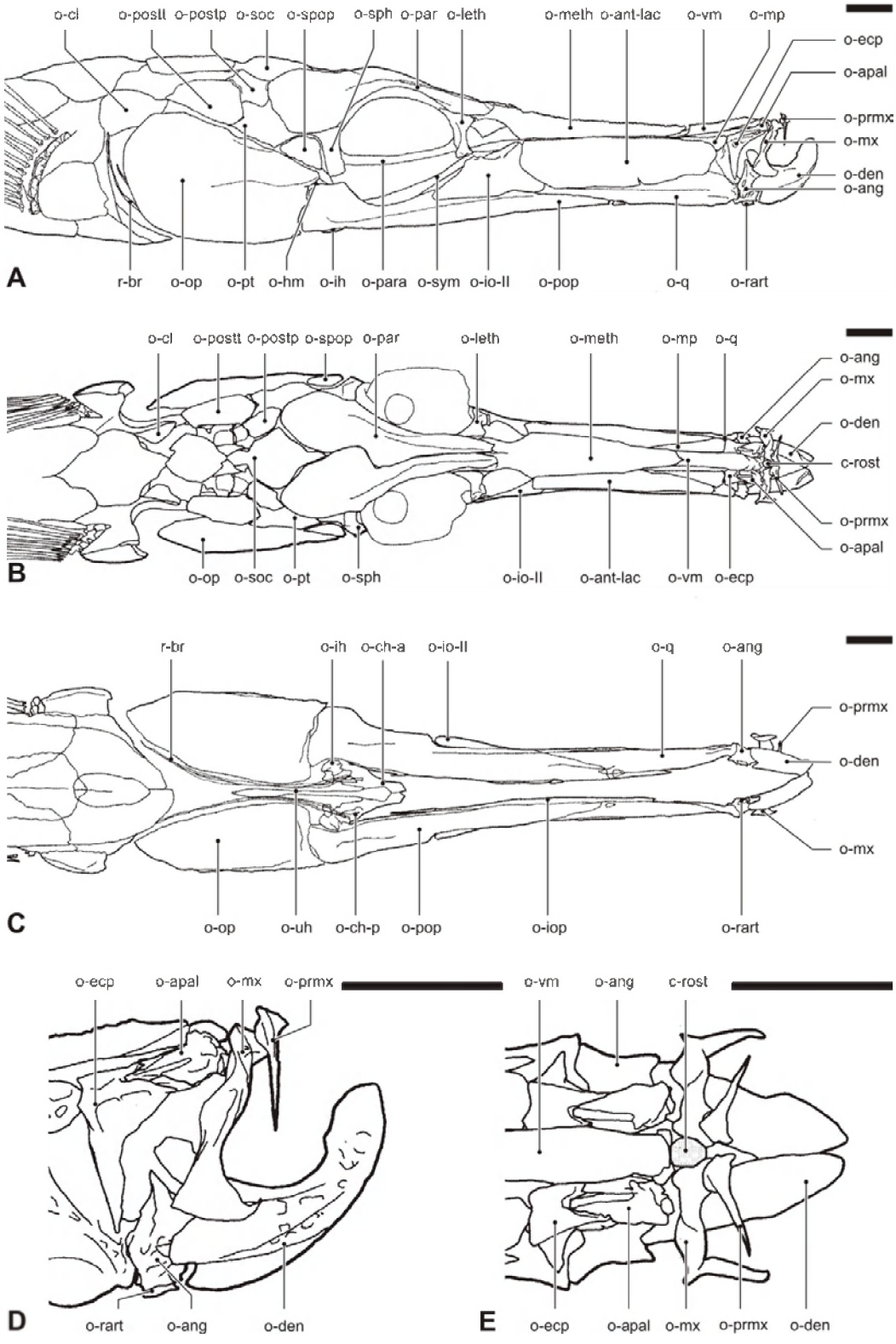

Fig. 3.5 – Adult osteocranium of *Syngnathus rostellatus* (111.1 mm SL). **A** lateral view of the right side; **B** dorsal view; **C** ventral view; **D** lateral view of snout tip; **E** dorsal view of snout tip. Scale bars = 1 mm.

Fig. 3.6 – Legend

c-rost	rostral cartilage
cr	corona
o-ang	anguloarticular bone
o-ant	antorbital bone
o-apal	autopalatine bone
o-ch-a	anterior ceratohyal bone
o-ch-p	posterior ceratohyal bone
o-cl	cleithrum
o-den	dentary bone
o-ecp	ectopterygoid bone
o-epoc	epioccipital bone
o-hm	hyomandibular bone
o-ih	interhyal bone
o-io-II	second infraorbital bone
o-iop	interopercular bone
o-leth	lateral ethmoid bone
o-lac	lacrimal bone
o-meth	mesethmoid bone
o-mp	metapterygoid bone
o-mx	maxillary bone
o-op	opercular bone
o-par	parietal bone
o-para	parasphenoid bone
o-pop	preopercular bone
o-postt	posttemporal bone
o-prmx	premaxillary bone
o-pt	pterotic bone
o-q	quadrate bone
o-rart	retroarticular bone
o-soc	supraoccipital bone
o-sop	subopercular bone
o-sph	sphenotic bone
o-sym	symplectic bone
o-uh	urohyal bone
o-vm	vomeral bone
r-br	branchiostegal ray

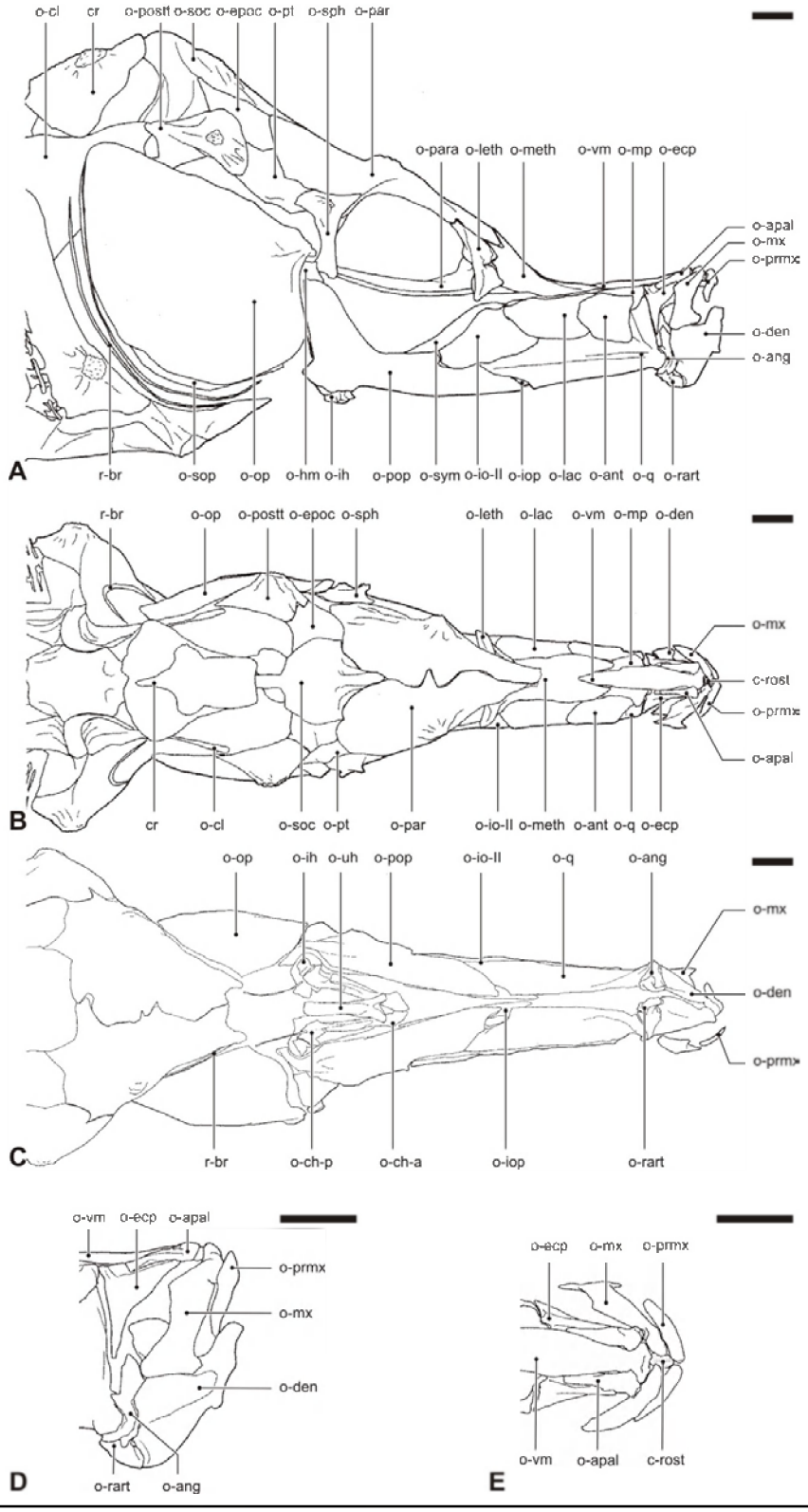

Fig. 3.6 – Adult osteocranium of *Hippocampus capensis* (96.1 mm SL). **A** lateral view of the right side; **B** dorsal view; **C** ventral view; **D** lateral view of snout tip; **E** dorsal view of snout tip. Scale bars = 1 mm.

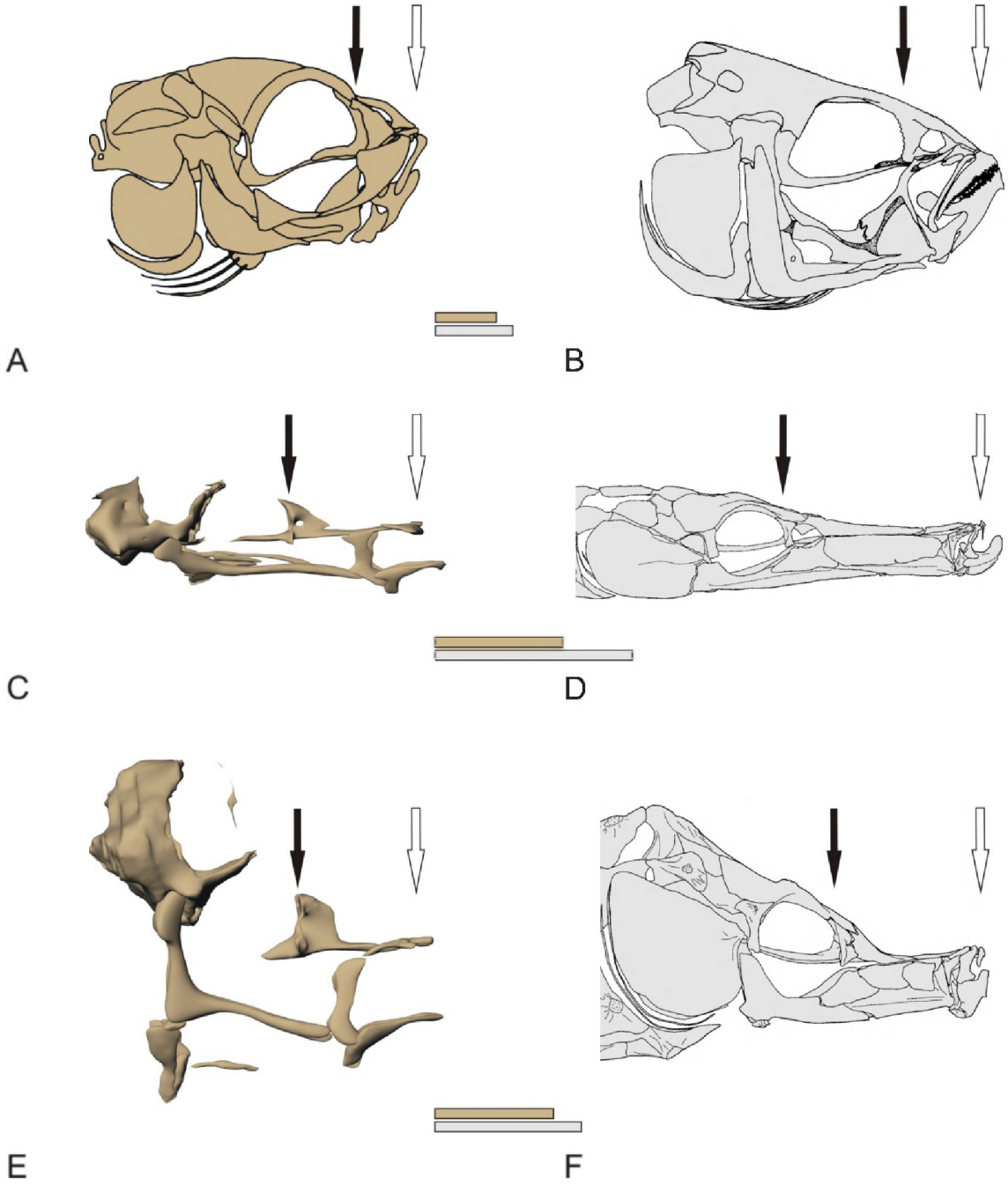

Fig. 3.7 – Crania, scaled to same head length (from front of ethmoid plate (juveniles) or vomeral bone (adults) to back of occipital region), of juveniles (beige) and adults (grey). **A** juvenile *Gasterosteus aculeatus* (16.0 mm SL) (after Swinnerton, 1902); **B** adult *G. aculeatus* (SL not mentioned) (after Anker, 1974); **C** juvenile chondrocranium *Syngnathus rostellatus* (13.1 mm SL); **D** adult *S. rostellatus* (111.1 mm SL); **E** juvenile chondrocranium *Hippocampus capensis* (12.8 mm SL); **F** adult *H. capensis* (96.1 mm SL). Black arrows indicate rostral border of orbita, white arrows indicate front of the autopalatine bone. Area in between the arrows corresponds to the ethmoid region. Bars show length of ethmoid region relative to head length of juveniles (beige) and adults (grey). Note the elongation in both syngnathid species.

Fig. 3.8 – Legend

cr	corona
c-rost	rostral cartilage
l-ch-uh	ceratohyal-urohyal ligament
l-iop-h	interoperculo-hyoid ligament
l-mnd-h	mandibulo-hyoid ligament
l-mnd-iop	mandibulo-interopercular ligament
m-A2	second bundle of the adductor mandibulae muscle complex
m-aap	adductor arcus palatini muscle
m-epax	epaxial muscle
m-h-abd	abductor hyohyoideus muscle
m-im	intermandibularis muscle
m-lap	levator arcus palatini muscle
m-pr-h	protractor hyoidei muscle
m-st	sternohyoideus muscle
o-ang	anguloarticular bone
o-ant	antorbital bone
o-apal	autopalatine bone
o-ch-a	anterior ceratohyal bone
o-ch-p	posterior ceratohyal bone
o-cl	cleithrum
o-den	dentary bone
o-ecp	ectopterygoid bone
o-epoc	epioccipital bone
o-exoc	exoccipital bone
o-hm	hyomandibular bone
o-ih	interhyal bone
o-io-II	second infraorbital bone
o-iop	interopercular bone
o-lac	lacrimal bone
o-leth	lateral ethmoid bone
o-meth	mesethmoid bone
o-mp	metapterygoid bone
o-mx	maxillary bone
o-op	opercular bone
o-par	parietal bone
o-para	parasphenoid bone
o-pop	preopercular bone
o-postt	posttemporal bone
o-prmx	premaxillary bone
o-pt	pterotic bone
o-q	quadrate bone
o-rart	retroarticular bone
o-soc	supraoccipital bone
o-sop	subopercular bone
o-sph	sphenotic bone
o-uh	urohyal bone
o-vm	vomeral bone
r-br	branchiostegal ray
t-epax	epaxial tendon
t-pr-h	protractor hyoidei tendon
t-st	sternohyoideus tendon

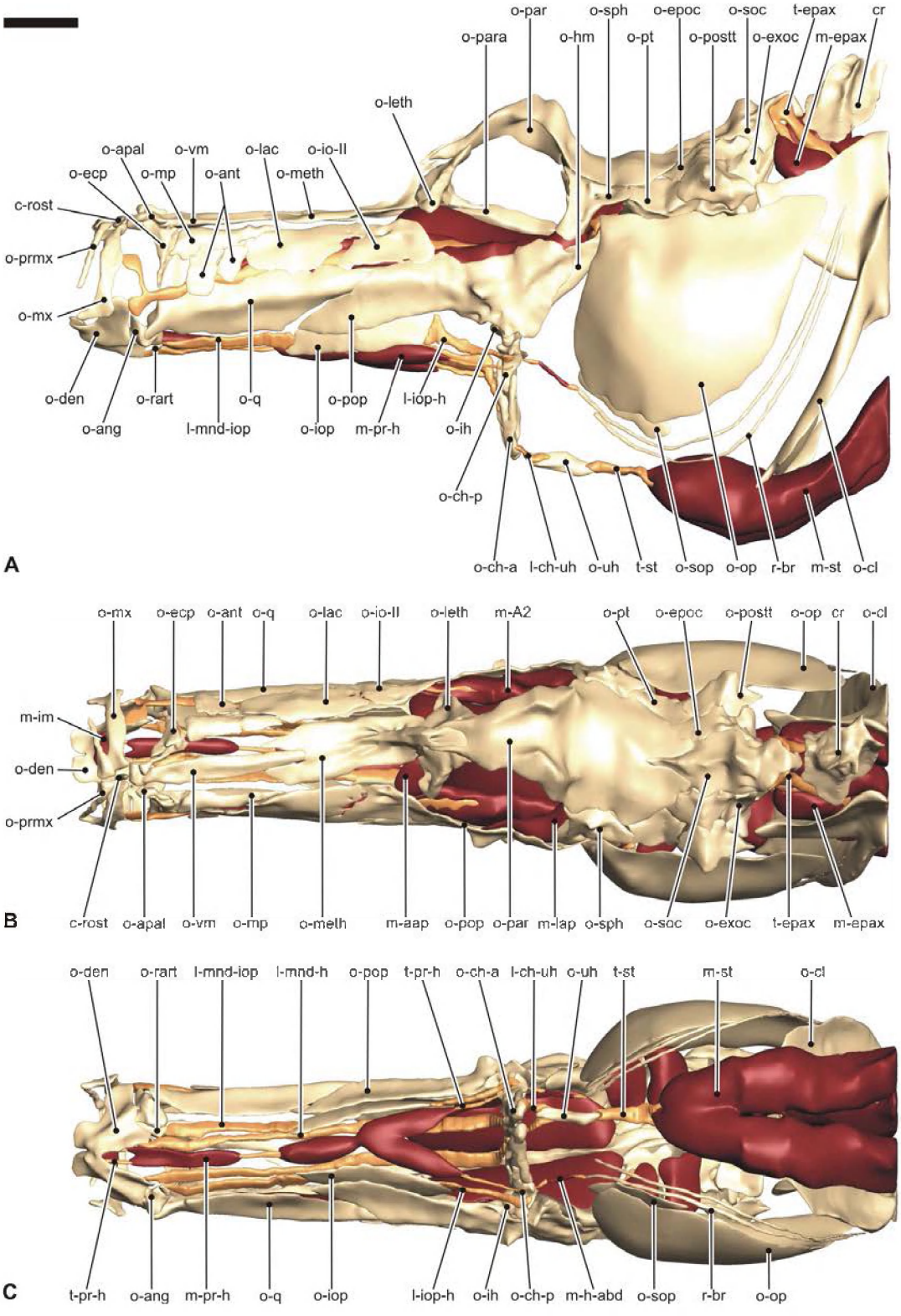

Fig. 3.8 – 3D-reconstruction of the cranium of *Hippocampus reidi* (103.5 mm SL) based on histological sections. **A** lateral view of the left side; **B** dorsal view; **C** ventral view. Beige indicates bone, khaki indicates cartilage, orange indicates tendon and ligament, red indicates muscle. Scale bar = 2 mm.

Fig. 3.9 – Legend

c-rost	rostral cartilage
l-ch-uh	ceratohyal-urohyal ligament
l-iop-h	interoperculo-hyoid ligament
l-mnd-h	mandibulo-hyoid ligament
l-mnd-iop	mandibulo-interopercular ligament
m-A1	first bundle of the adductor mandibulae muscle complex
m-A2	second bundle of the adductor mandibulae muscle complex
m-A3	third bundle of the adductor mandibulae muscle complex
m-aap	adductor arcus palatini muscle
m-add-op	adductor operculi muscle
m-dod	dilatator operculi dorsalis muscle
m-epax	epaxial muscle
m-h-abd	abductor hyohyoideus muscle
m-lap	levator arcus palatini muscle
m-l-op	levator operculi muscle
m-pr-h	protractor hyoidei muscle
m-s-c	supracarinalis muscle
m-st	sternohyoideus muscle
o-ang	anguloarticular bone
o-ant	antorbital bone
o-apal	autopalatine bone
o-boc	basioccipital bone
o-ch-a	anterior ceratohyal bone
o-ch-p	posterior ceratohyal bone
o-den	dentary bone
o-ecp	ectopterygoid bone
o-hm	hyomandibular bone
o-iop	interopercular bone
o-mp	metapterygoid bone
o-mx	maxillary bone
o-prmx	premaxillary bone
o-pt	pterotic bone
o-q	quadrate bone
o-rart	retroarticular bone
o-soc	supraoccipital bone
o-sym	symplectic bone
o-uh	urohyal bone
o-vm	vomeral bone
pr-c	coronoid process
r-br	branchiostegal ray
t-A	adductor mandibulae muscle complex tendon
t-epax	epaxial tendon
t-pr-h	protractor hyoidei tendon
t-st	sternohyoideus tendon

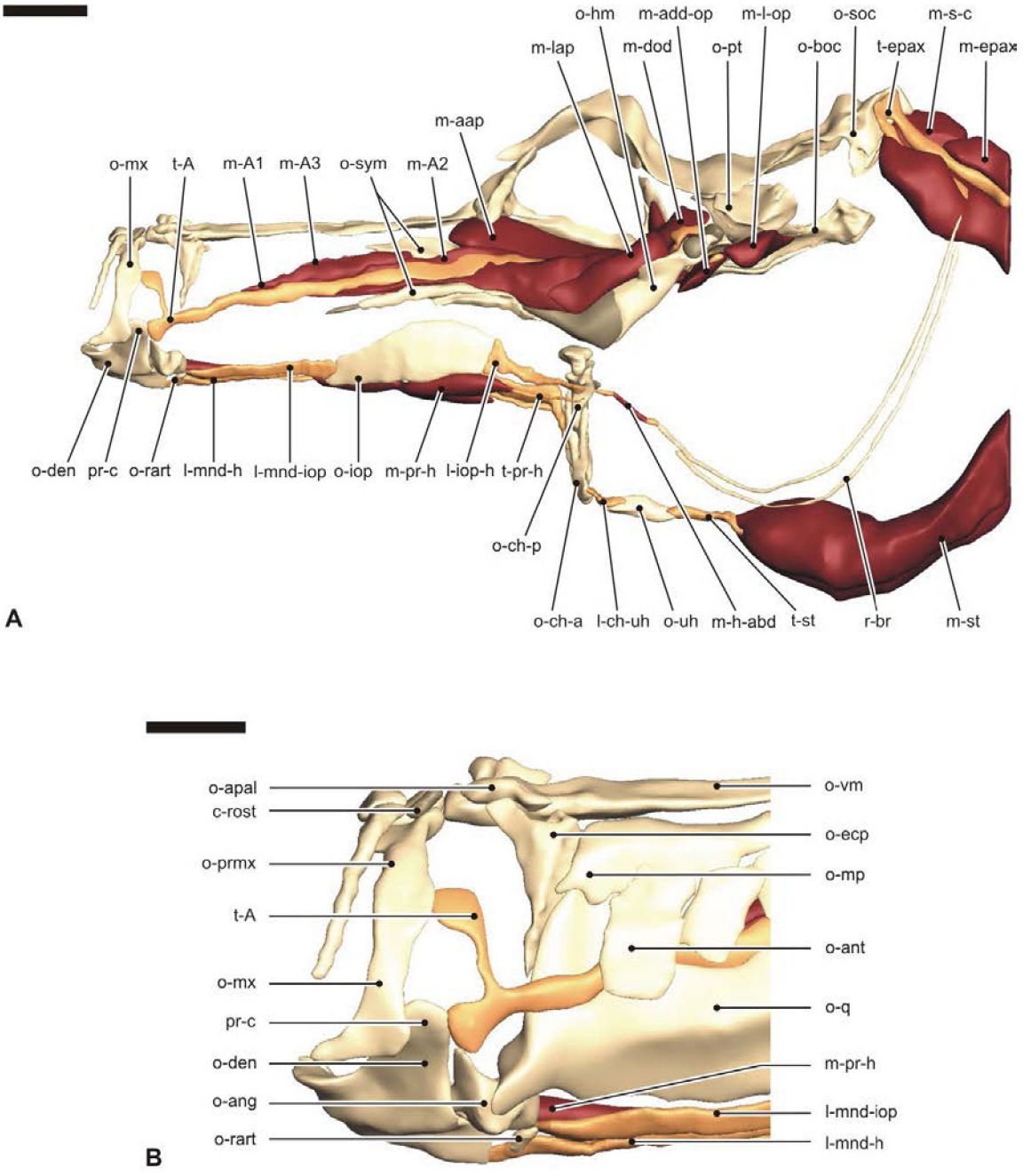

Fig. 3.9 – 3D-reconstruction of the cranium of *Hippocampus reidi* (103.5 mm SL) based on histological sections. **A** lateral view of the left side with several bones removed to show muscles underneath; **B** lateral view of the left side of the snout tip. Beige indicates bone, khaki indicates cartilage, orange indicates tendon and ligament, red indicates muscle. Scale bar A = 2 mm; scale bar B = 1 mm.

Fig. 3.10 – Legend

l-mnd-h	mandibulo-hyoid ligament
m-epax	epaxial muscle
m-pr-h	protractor hyoidei muscle
m-s-c	supracarinalis muscle
m-st	sternohyoideus muscle
o-ant	antorbital bone
o-epax	sesamoid bone in epaxial tendon
o-io-II	second infraorbital bone
o-iop	interopercular bone
o-mp	metapterygoid bone
o-pop	preopercular bone
o-para	parasphenoid bone
o-q	quadrate bone
o-soc	supraoccipital bone
o-vm	vomeral bone
t-A	adductor mandibulae muscle complex tendon
t-epax	epaxial tendon
t-st	sternohyoideus tendon

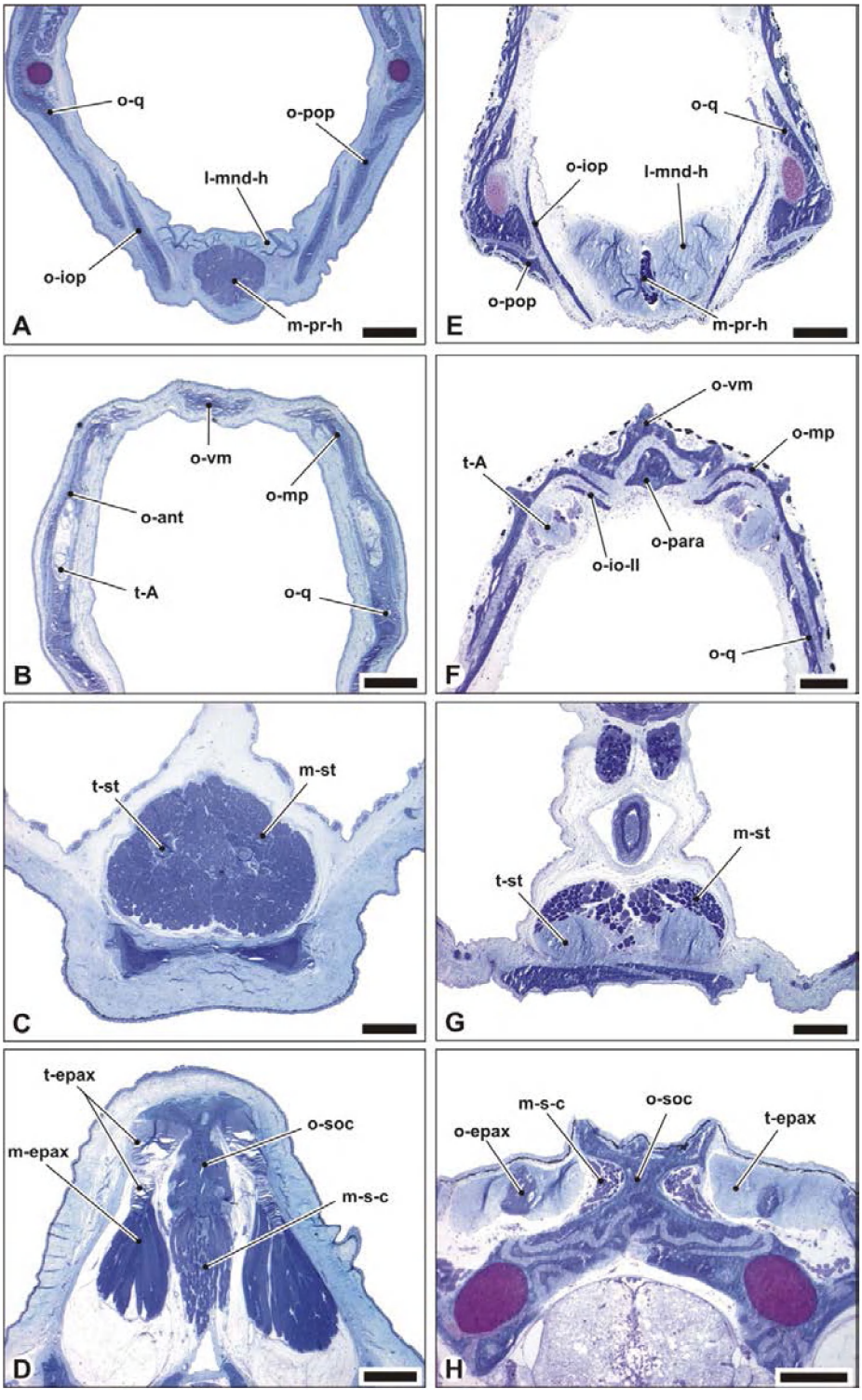

Fig. 3.10 – Histological cross sections of the cranium of *Hippocampus reidi* (103.5 mm SL) (A-D) and *Doryrhamphus dactyliophorus* (91.2 mm SL) (E-H) stained with toluidine blue. **A**,**E** the nasal region showing the mandibulo-hyoid ligament and the protractor hyoidei muscle organisation; **B**,**F** the snout rostrally with the adductor mandibulae tendon; **C**,**G** the sternohyoideus muscle and its tendon; **D**,**H** the occipital region with the supraoccipital bone and its associated tendons and muscles, note the sesamoid bone in *D. dactyliophorus*. Scale bars A-D = 500 µm; E-H = 200 µm.

Fig. 3.11 – Legend

c-rost	rostral cartilage
l-epax	epaxial ligament
l-iop-h	interoperculo-hyoid ligament
l-mnd-h	mandibulo-hyoid ligament
l-mnd-iop	mandibulo-interopercular ligament
l-prim	primordial ligament
m-A2	second bundle of the adductor mandibulae muscle complex
m-aap	adductor arcus palatini muscle
m-dod	dilatator operculi dorsalis muscle
m-epax	epaxial muscle
m-h-abd	abductor hyohyoideus muscle
m-im	intermandibularis muscle
m-lap	levator arcus palatini muscle
m-pr-h	protractor hyoidei muscle
m-s-c	supracarinalis muscle
m-st	sternohyoideus muscle
o-ang	anguloarticular bone
o-apal	autopalatine bone
o-bh	basihyal bone
o-ch-a	anterior ceratohyal bone
o-ch-p	posterior ceratohyal bone
o-cl	cleithrum
o-den	dentary bone
o-ecp	ectopterygoid bone
o-epax	sesamoid bone in epaxial tendon
o-epoc	epioccipital bone
o-ih	interhyal bone
o-io-II	second infraorbital bone
o-iop	interopercular bone
o-lac	lacrimal bone
o-leth	lateral ethmoid bone
o-meth	mesethmoid bone
o-mp	metapterygoid bone
o-mx	maxillary bone
o-op	opercular bone
o-par	parietal bone
o-para	parasphenoid bone
o-pop	preopercular bone
o-postt	posttemporal bone
o-prmx	premaxillary bone
o-pt	pterotic bone
o-q	quadrate bone
o-rart	retroarticular bone
o-soc	supraoccipital bone
o-sop	subopercular bone
o-sph	sphenotic bone
o-spop	suprapreopercular bone
o-sym	symplectic bone
o-uh	urohyal bone
o-vm	vomeral bone
r-br	branchiostegal ray
t-epax	epaxial tendon
t-h-abd	hyohyoideus abductor tendon
t-pr-h	protractor hyoidei tendon
t-st	sternohyoideus tendon

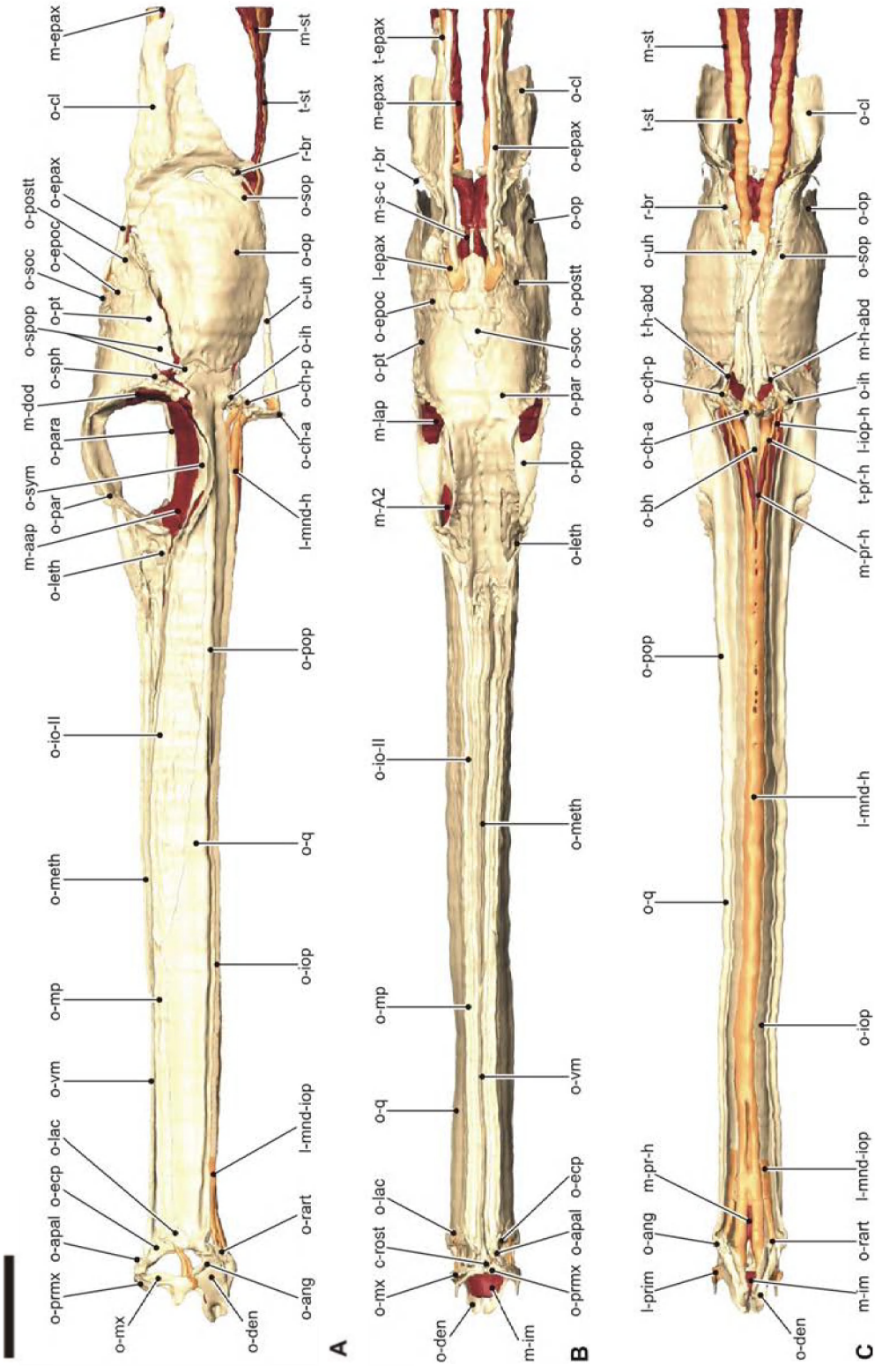

Fig. 3.11 – 3D-reconstruction of the cranium of *Doryrhamphus dactyliophorus* (91.2 mm SL) based on histological sections. **A** lateral view of the left side; **B** dorsal view; **C** ventral view. Beige indicates bone, khaki indicates cartilage, orange indicates tendon and ligament, red indicates muscle. Scale bar = 2 mm.

Fig. 3.12 – Legend

l-ch-uh	ceratohyal-urohyal ligament
l-epax	epaxial ligament
l-iop-h	interoperculo-hyoid ligament
l-mnd-h	mandibulo-hyoid ligament
l-mnd-iop	mandibulo-interopercular ligament
l-prim	primordial ligament
m-A2	second bundle of the adductor mandibulae muscle complex
m-A3	third bundle of the adductor mandibulae muscle complex
m-aap	adductor arcus palatini muscle
m-add-op	adductor operculi muscle
m-dod	dilatator operculi dorsalis muscle
m-dov	dilatator operculi ventralis muscle
m-epax	epaxial muscle
m-h-abd	abductor hyohyoideus muscle
m-lap	levator arcus palatini muscle
m-pr-h	protractor hyoidei muscle
m-s-c	supracarinalis muscle
m-st	sternohyoideus muscle
o-ang	anguloarticular bone
o-apal	autopalatine bone
o-boc	basioccipital bone
o-ch-p	posterior ceratohyal bone
o-den	dentary bone
o-ecp	ectopterygoid bone
o-epax	sesamoid bone in epaxial tendon
o-hm	hyomandibular bone
o-iop	interopercular bone
o-lac	lacrimal bone
o-mp	metapterygoid bone
o-mx	maxillary bone
o-prmx	premaxillary bone
o-pt	pterotic bone
o-q	quadrate bone
o-rart	retroarticular bone
o-soc	supraoccipital bone
o-sym	symplectic bone
o-uh	urohyal bone
o-vm	vomeral bone
pr-c	coronoid process
r-br	branchiostegal ray
t-A2	second tendon of the adductor mandibulae muscle complex
t-A3	third tendon of the adductor mandibulae muscle complex
t-epax	epaxial tendon
t-pr-h	protractor hyoidei tendon
t-st	sternohyoideus tendon

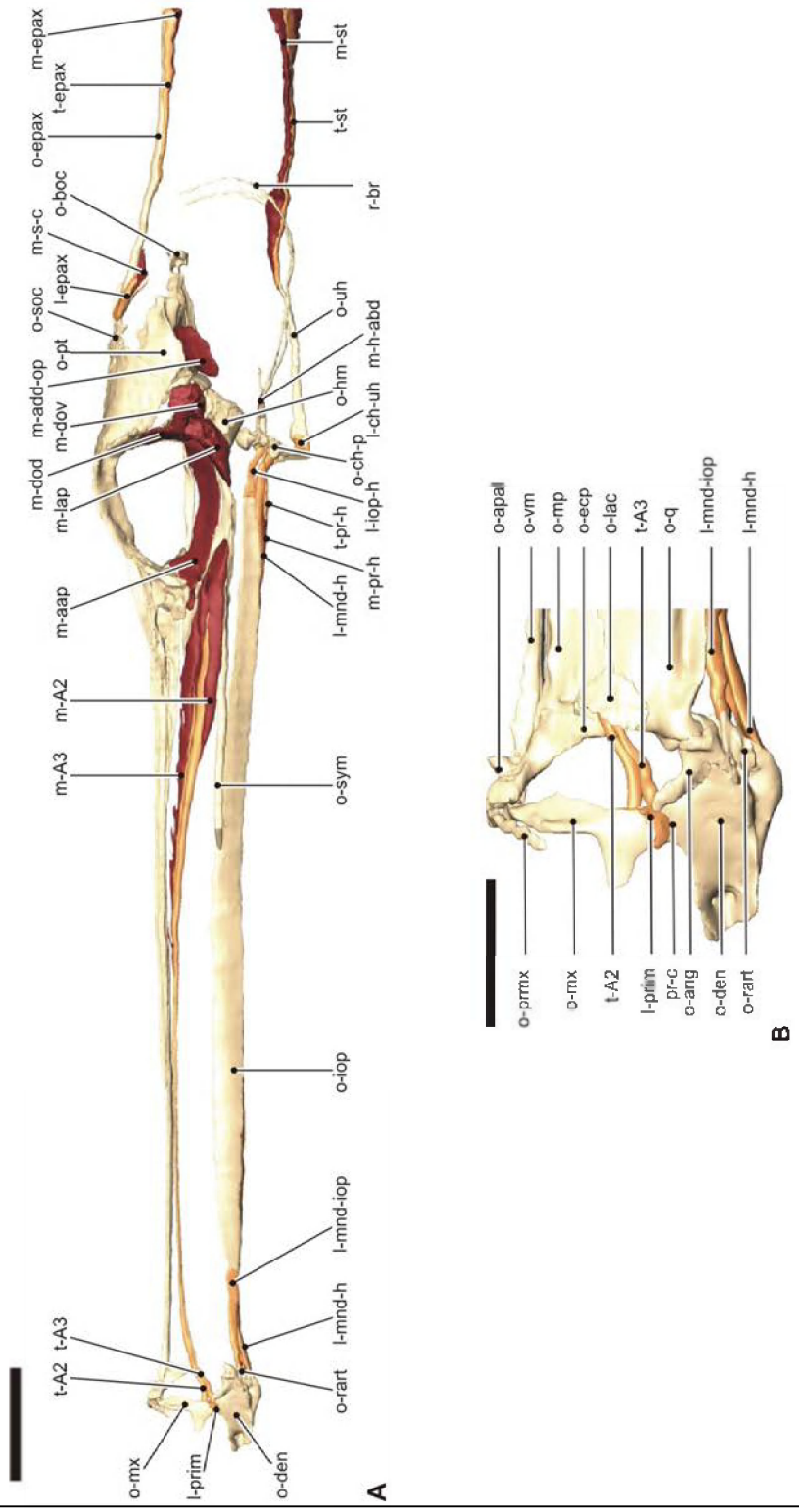

Fig. 3.12 – 3D-reconstruction of the cranium of *Doryrhamphus dactyliophorus* (91.2 mm SL) based on histological sections. **A** lateral view of the left side with several bones removed to show muscles underneath; **B** lateral view of the left side of the snout tip. Beige indicates bone, khaki indicates cartilage, orange indicates tendon and ligament, red indicates muscle. Scale bar A = 2 mm; scale bar B = 1 mm.

Fig. 3.13 – Legend

cr	corona
o-ang	anguloarticular bone
o-ch-a	anterior ceratohyal bone
o-den	dentary bone
o-ecp	ectopterygoid bone
o-epax	sesamoid bone in epaxial tendon
o-ih	interhyal bone
o-iop	interopercular bone
o-meth	mesethmoid bone
o-mx	maxillary bone
o-op	opercular bone
o-par	parietal bone
o-para	parasphenoid bone
o-pop	preopercular bone
o-q	quadrate bone
o-soc	supraoccipital bone
o-sph	sphenotic bone
o-sym	symplectic bone
o-uh	urohyal bone
o-vm	vomeral bone

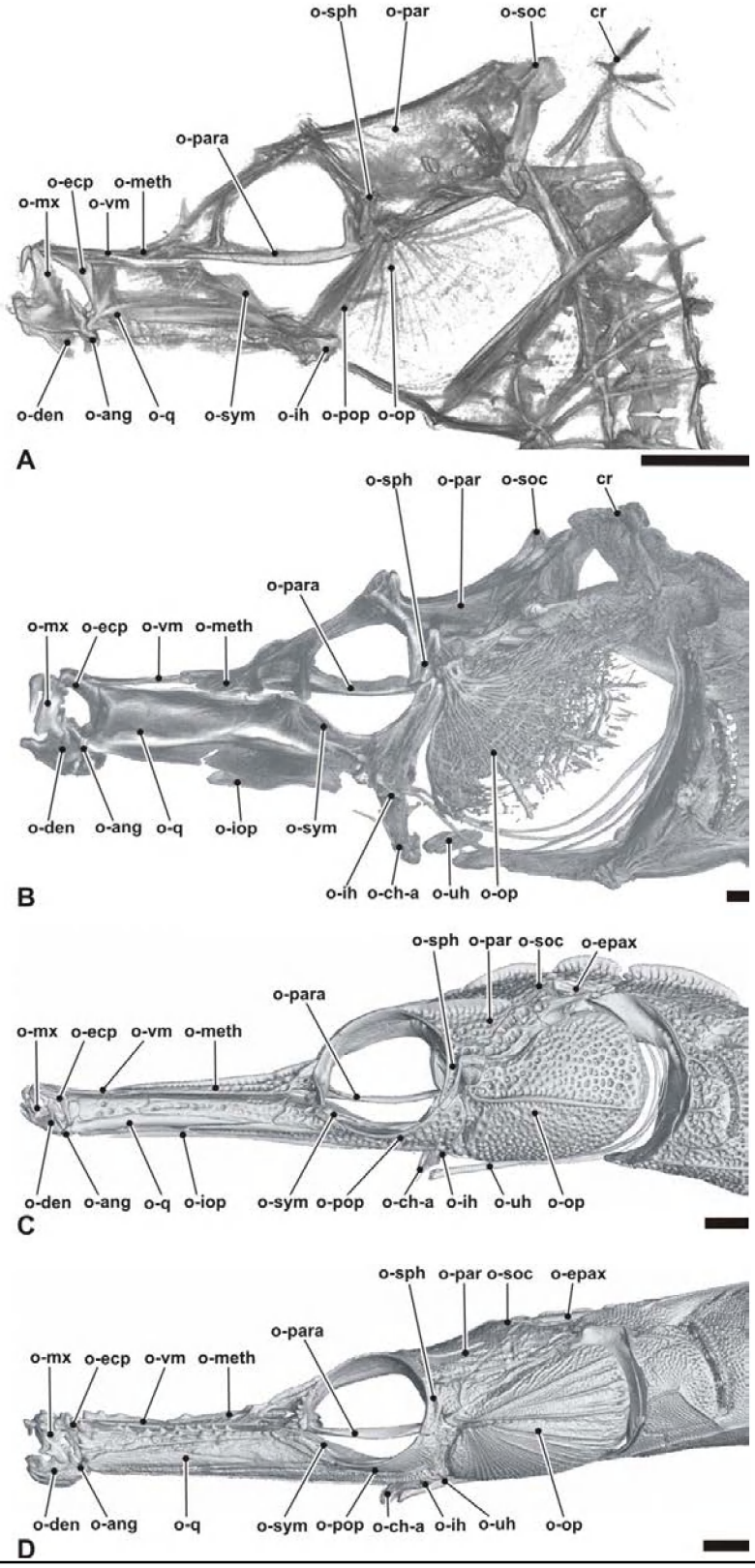

Fig. 3.13 – 3D-reconstructions of the osteocranium based on CT-data in lateral view of **A** *Hippocampus zosterae* (29.0 mm SL); **B** *Hippocampus abdominalis* (222.7 mm SL); **C** *Corythoichthys intestinalis* (120.2 mm SL); **D** *Doryrhamphus melanopleura* (56.5 mm SL). Scale bars = 1 mm.

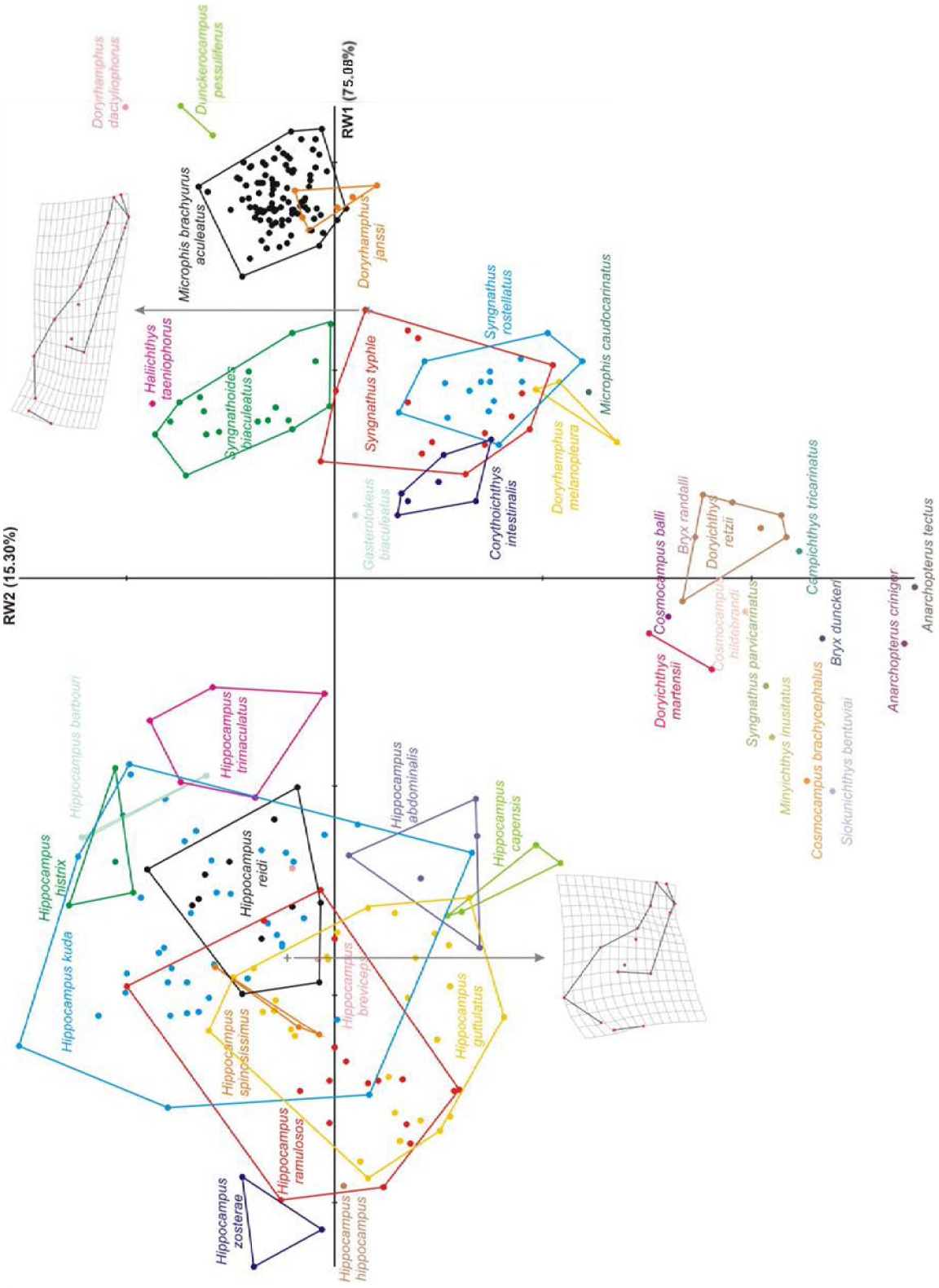

Fig. 4.1 – Scatter plot of relative warp 1 and relative warp 2, together explaining 90.38% of the total shape variation. The position of the mean subfamily configuration is depicted by a '+' (right for pipefishes, left for seahorse) and the corresponding deformation grids with respect to the consensus are illustrated.

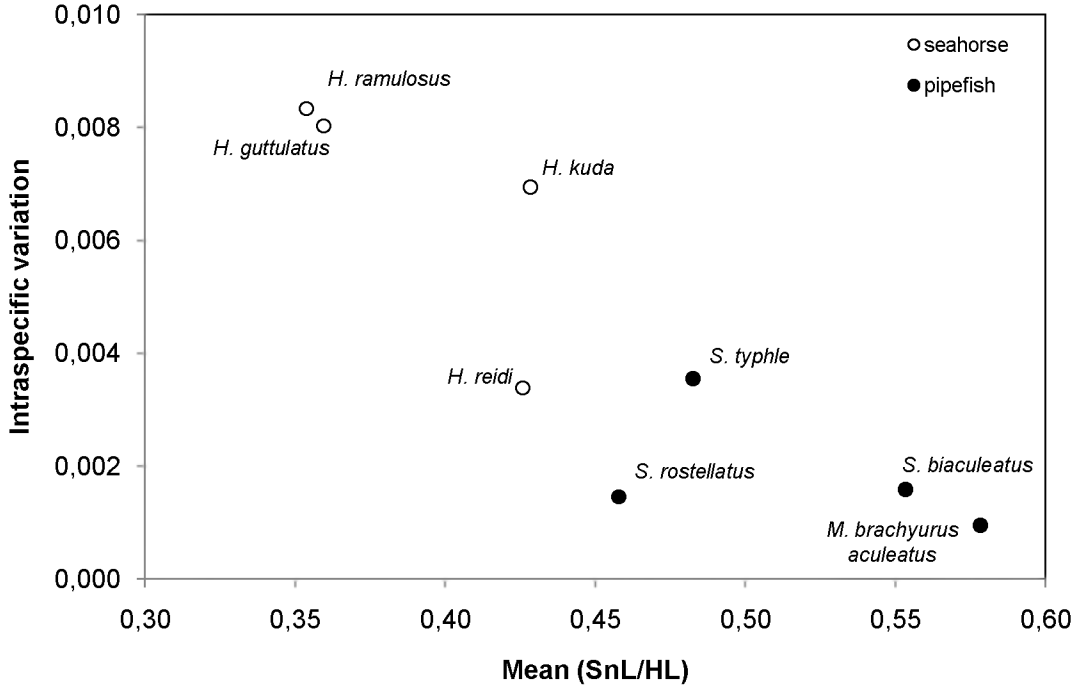

Fig. 4.2 – Scatter plot of the mean relative snout length versus the intraspecific shape variation of four pipefish species (black dots) and four seahorse species (white dots). HL, head length; SnL, snout length.

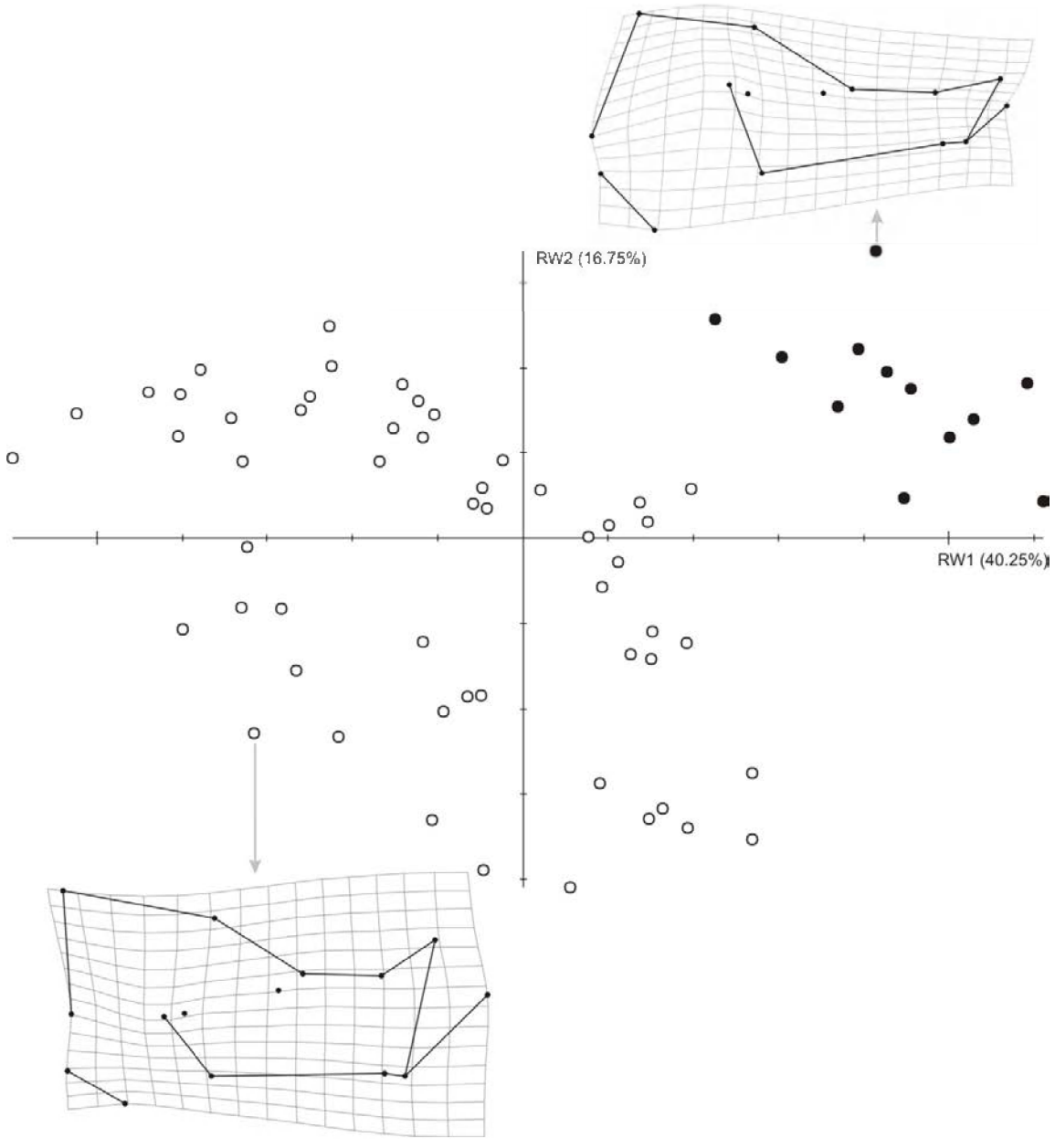

Fig. 4.3 – Scatter plot of relative warp 1 and relative warp 2 of the ontogenetic series of *Hippocampus reidi*, together explaining 57% of the total shape variation. Black dots represent adults, white dots are juveniles. The deformation grids of two specimens, a one day old (below) and an adult (above), are visualized.

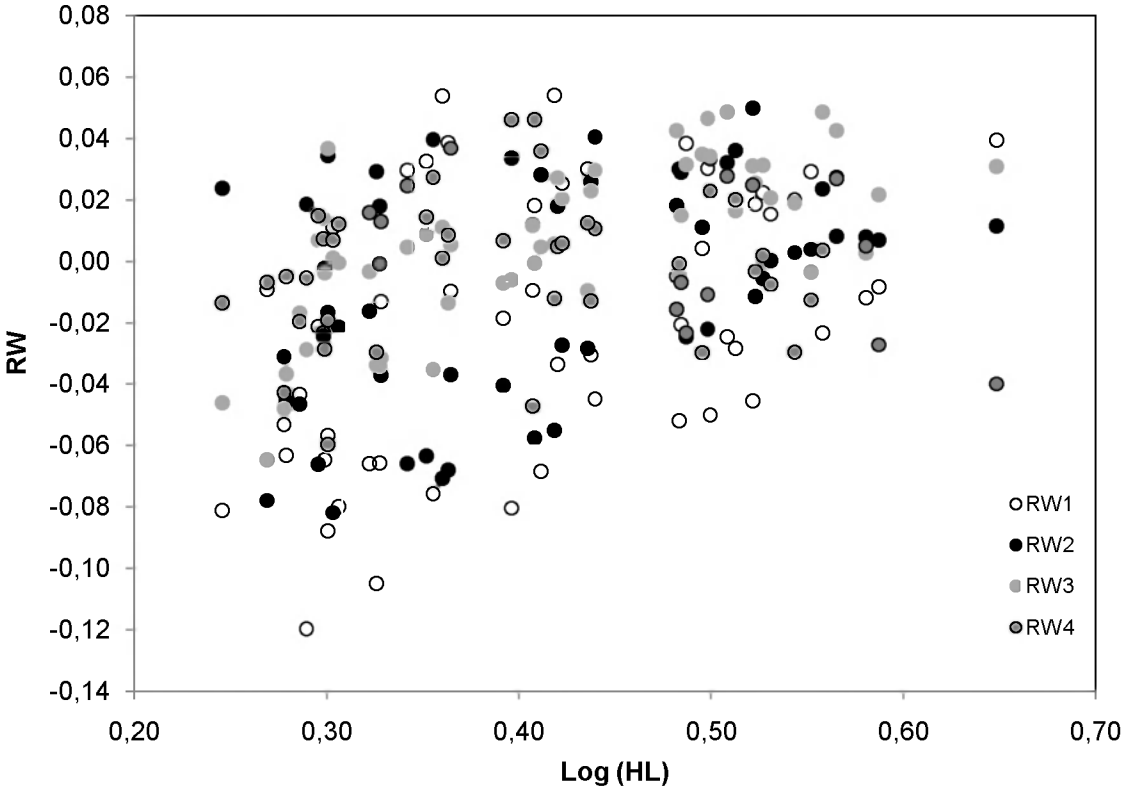

Fig. 4.4 – Growth curve of *Hippocampus reidi* juveniles, with log head length (Log (HL)) as a proxy for age and the relative warp (RW) scores representing head shape changes. No clear trend could be observed.

Fig. 5.1 – Legend

hs	hyosymplectic cartilage
l-ch-uh	ceratohyal-urohyal ligament
l-iop-h	interoperculo-hyoid ligament
l-mnd-h	mandibulo-hyoid ligament
l-mnd-iop	mandibulo-interopercular ligament
m-im-p	posterior intermandibularis part of protractor hyoidei muscle
m-int-a	anterior interhyoideus part of protractor hyoidei muscle
m-st	sternohyoideus muscle
o-ch-a	anterior ceratohyal bone
o-ch-p	posterior ceratohyal bone
o-cl	cleithrum
o-corb	circumorbital bones
o-den	dentary bone
o-ecp	ectopterygoid bone
o-hm	hyomandibular bone
o-ih	interhyal bone
o-iop	interopercular bone
o-mp	metapterygoid bone
o-mx	maxillary bone
o-op	opercular bone
o-pop	preopercular bone
o-prmx	premaxillary bone
o-q	quadrate bone
o-sym	symplectic bone
o-uh	urohyal bone
o-vm	vomeral bone
t-int-a	tendon of anterior interhyoideus part of protractor hyoidei muscle
t-st	sternohyoideus tendon

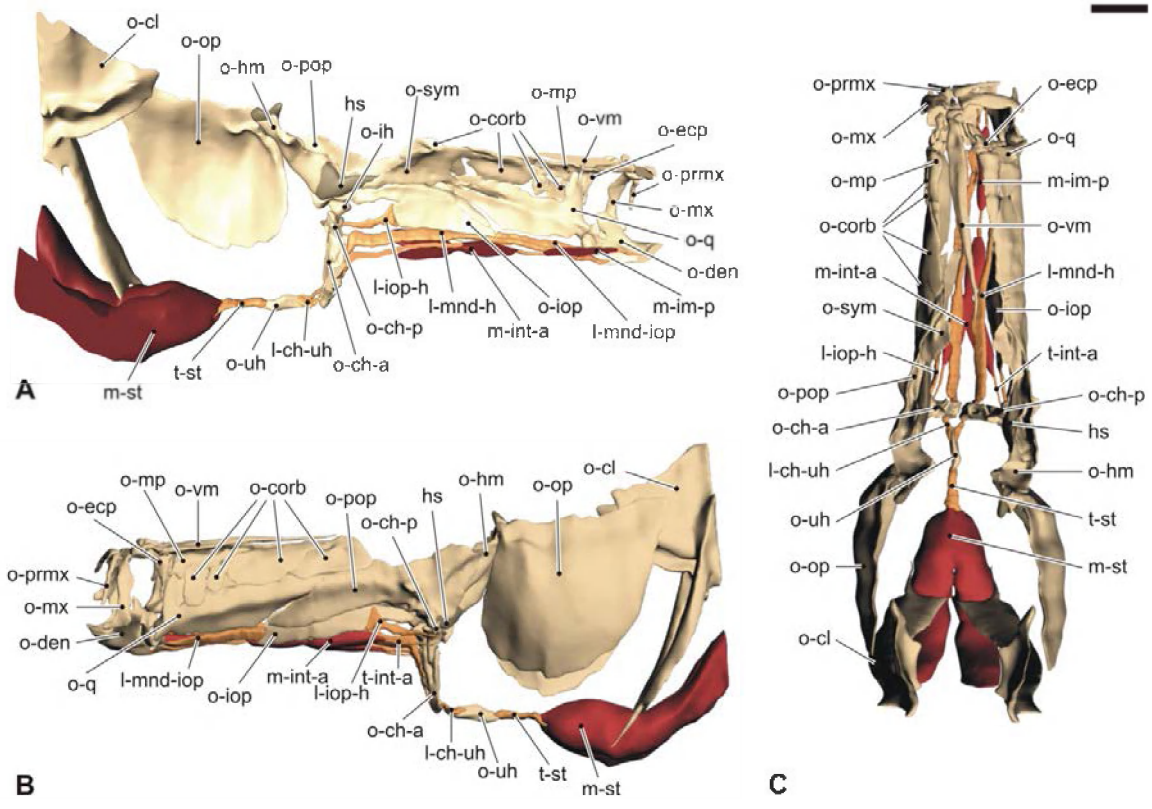

Fig. 5.1 – Graphic 3D-reconstruction of the skull of *Hippocampus reidi* based on histological sections (neurocranium and several muscles and ligaments not reconstructed for clarity). **A** medial view of left side; **B** lateral view of left side; **C** dorsal view. Beige indicates bone, khaki indicates cartilage, orange indicates tendon and ligament, red indicates muscle. Scale bar = 2 mm.

Fig. 5.2 – Legend

1	tip of the nose spine, just anterior of the eye
2	tip of the snout posterior to the maxillary bones
3	symphysis of the ceratohyal bones
4	distal tip of the ventrolateral spine on the pectoral girdle
5	tip of the process on the second nuchal plate
6	proximal tip of the premaxillary bone
7	distal tip of the dentary bone
8	distinct point on the prey
p	centre of the interhyal bone
q	rotation point of neurocranium with vertebral column-pectoral girdle complex
r	mediorostral landmark on the cleithrum
s	symphysis of the ceratohyal bones

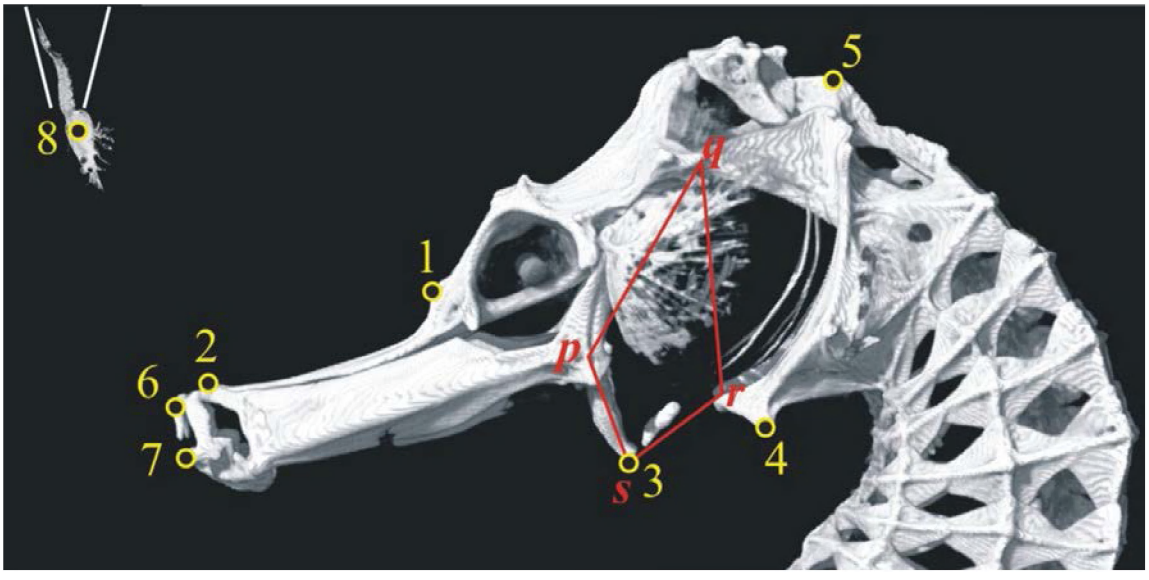

Fig. 5.2 – Graphic 3D-reconstruction of the skull of *Hippocampus reidi* based on CT-data, representing the digitized landmarks (yellow) and the calculated four-bar system (red).

Fig. 5.3 – Legend

1	mandibulo-quadrate articulation
2	mandibular symphysis
3	premaxillary symphysis
4	rostral tip of the vomeral bone
5	distal tip of the nose spine
6	articulation between the supraoccipital bone and the corona
7	distal tip of the dorsocaudal process on the corona
8	distal tip of the process on the second nuchal plate
9	articulation between the neurocranium and the first vertebra (not illustrated)
10	articulation between the neurocranium and the pectoral girdle
11	distal tip of the ventrolateral spine on the pectoral girdle
12	tip of the angle formed by the horizontal and vertical arm of the pectoral girdle
13	rostral point of the pectoral complex
14	caudal tip of the urohyal bone
15	symphysis of the ceratohyal bones
16	articulation between posterior ceratohyal and interhyal bones
17	articulation between interhyal and preopercular bones
cr	corona
np-II	second nuchal plate
o-ch-a	anterior ceratohyal bone
o-cl	cleithrum
o-den	dentary bone
o-hm	hyomandibular bone
o-iop	interopercular bone
o-leth	lateral ethmoid bone
o-meth	mesethmoid bone
o-mx	maxillary bone
o-par	parietal bone
o-para	parasphenoid bone
o-pop	preopercular bone
o-postt	posttemporal bone
o-prmx	premaxillary bone
o-q	quadrate bone
o-soc	supraoccipital bone
o-sph	sphenotic bone
o-uh	urohyal bone
o-vm	vomeral bone
v1	first vertebra

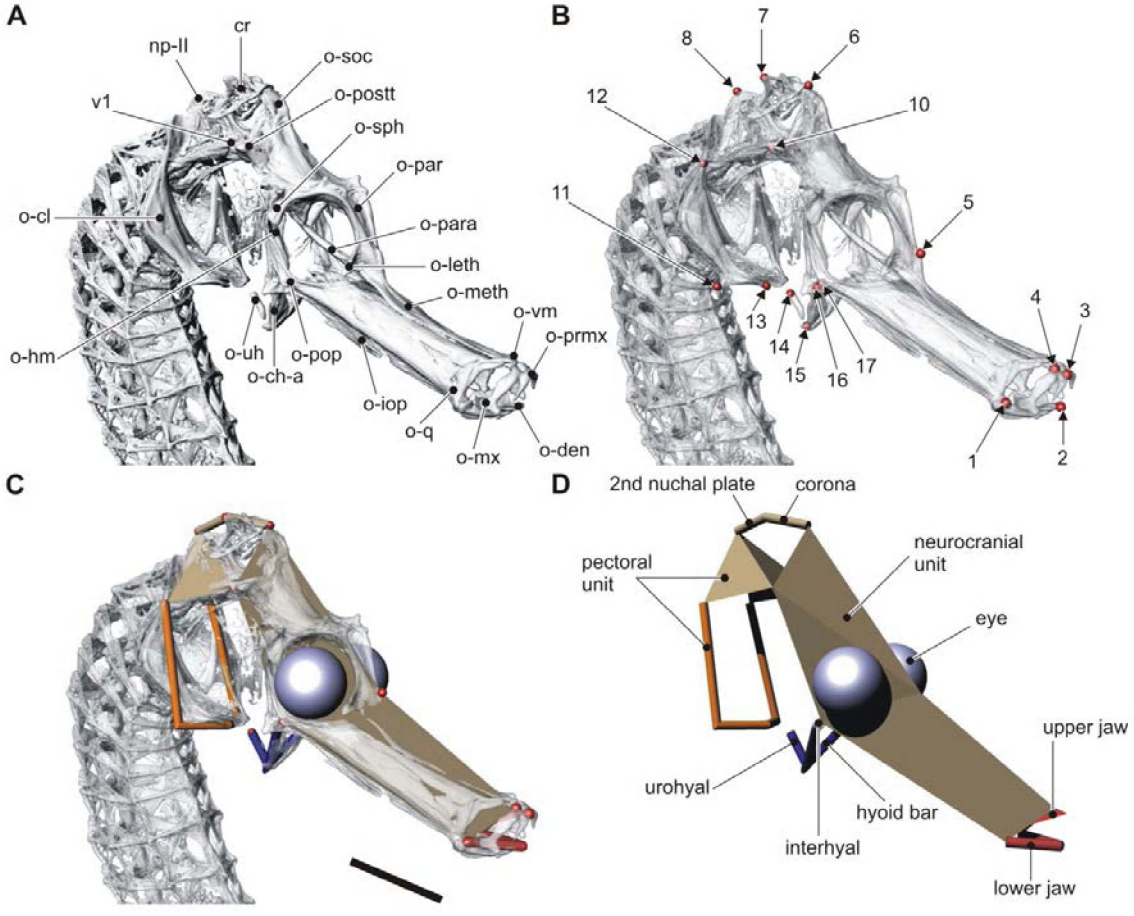

Fig. 5.3 – Skull morphology of adult *Hippocampus reidi* and 3D-model. **A** 3D-reconstruction of the skull based on CT-data; **B** 3D-reconstruction indicating the position of the landmarks used constructing the model (point 9 not illustrated); **C** model drawn based on the landmarks and superimposed on a 3D-reconstruction; **D** model used for visualizing mechanical units and the changes in relative position during feeding strike. Scale bar = 5 mm.

Fig. 5.4 – Legend

af-ih	articulation facet of interhyal bone with preopercular bone
ch	ceratohyal cartilage
l-ch-uh	ceratohyal-urohyal ligament
lh-ch-p	lateral head of posterior ceratohyal bone
lh-ih	lateral head of interhyal bone
l-iop-h	interoperculo-hyoid ligament
l-mnd-h	mandibulo-hyoid ligament
mh-ih	medial head of interhyal bone
m-int-a	anterior interhyoideus part of protractor hyoidei muscle
o-ch-a	anterior ceratohyal bone
o-ch-p	posterior ceratohyal bone
o-ih	interhyal bone
o-iop	interopercular bone
o-pop	preopercular bone
o-uh	urohyal bone
t-int-a	tendon of anterior interhyoideus part of protractor hyoidei muscle
vh-ch-p	ventral head of posterior ceratohyal bone

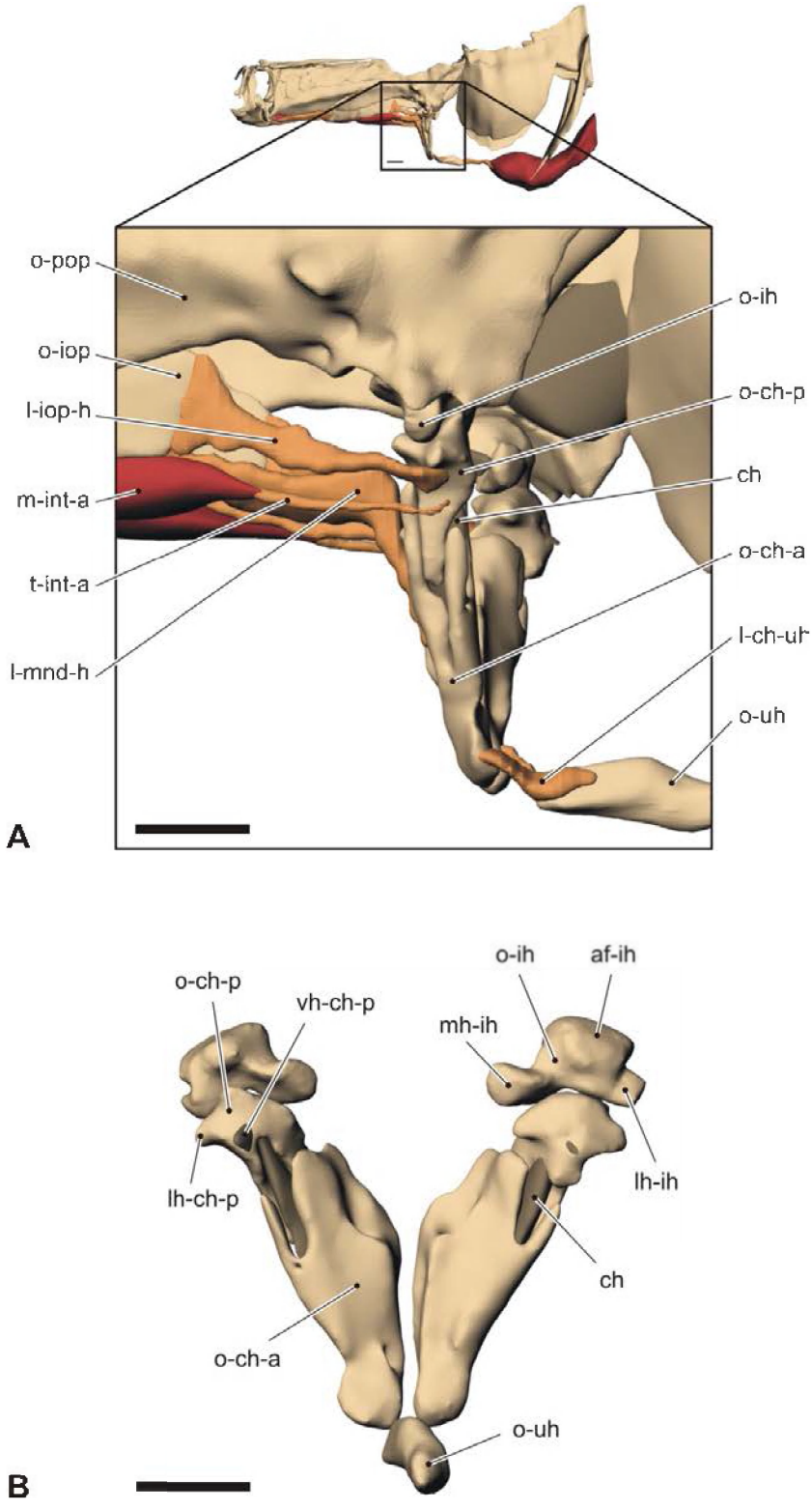

Fig. 5.4 – Detail of the 3D-reconstruction of the retracted hyoid complex in *Hippocampus reidi* based on histological sections (some ligaments not reconstructed for clarity). **A** lateral view of left side; **B** caudal view (other structures not reconstructed). Beige indicates bone, khaki indicates cartilage, orange indicates tendon and ligament, red indicates muscle. Scale bars = 1 mm.

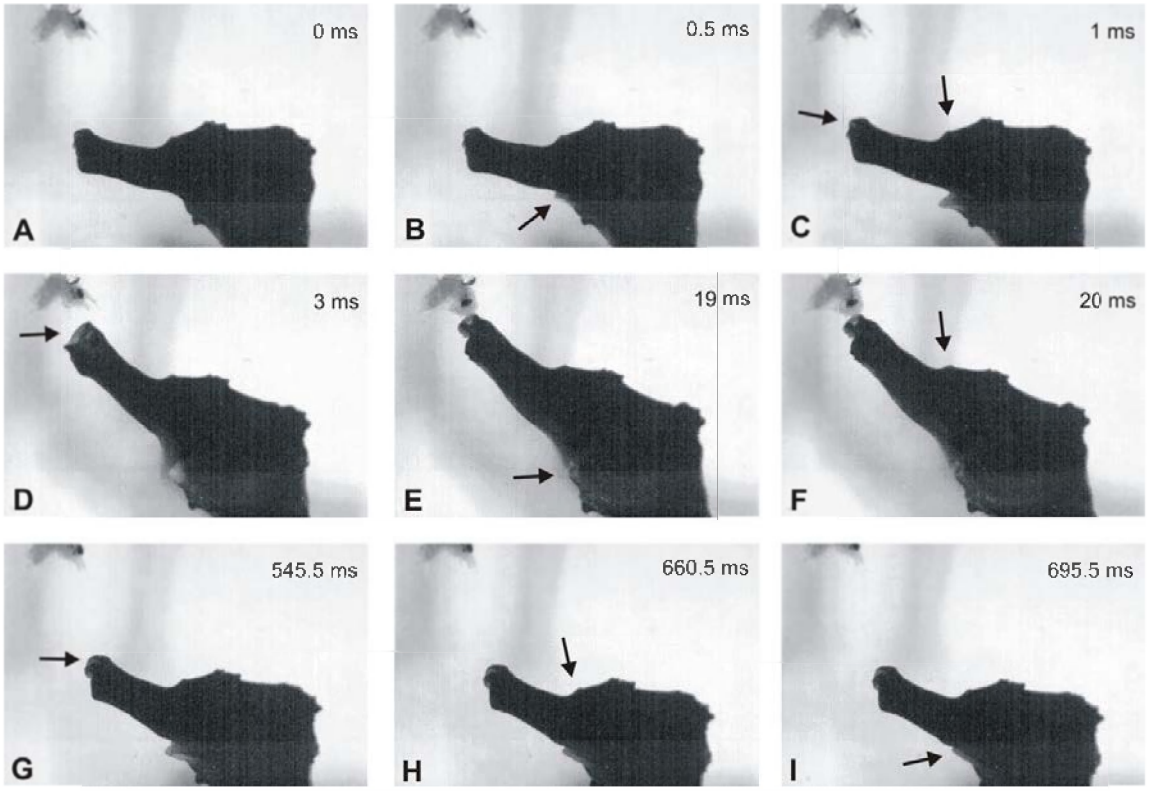

Fig. 5.5 – Example of a (failed) feeding sequence of *Hippocampus reidi* feeding on a mysid shrimp in upper left corner. Important events are indicated by an arrow. **A** image of one frame before the first visible movement; **B** onset of hyoid rotation; **C** onset of cranial rotation and mouth opening; **D** mouth reaches maximal opening; **E** hyoid reaches maximal rotation; **F** neurocranium reaches maximal rotation; **G** mouth fully closed; H neurocranium restored to its original position; I hyoid fully protracted.

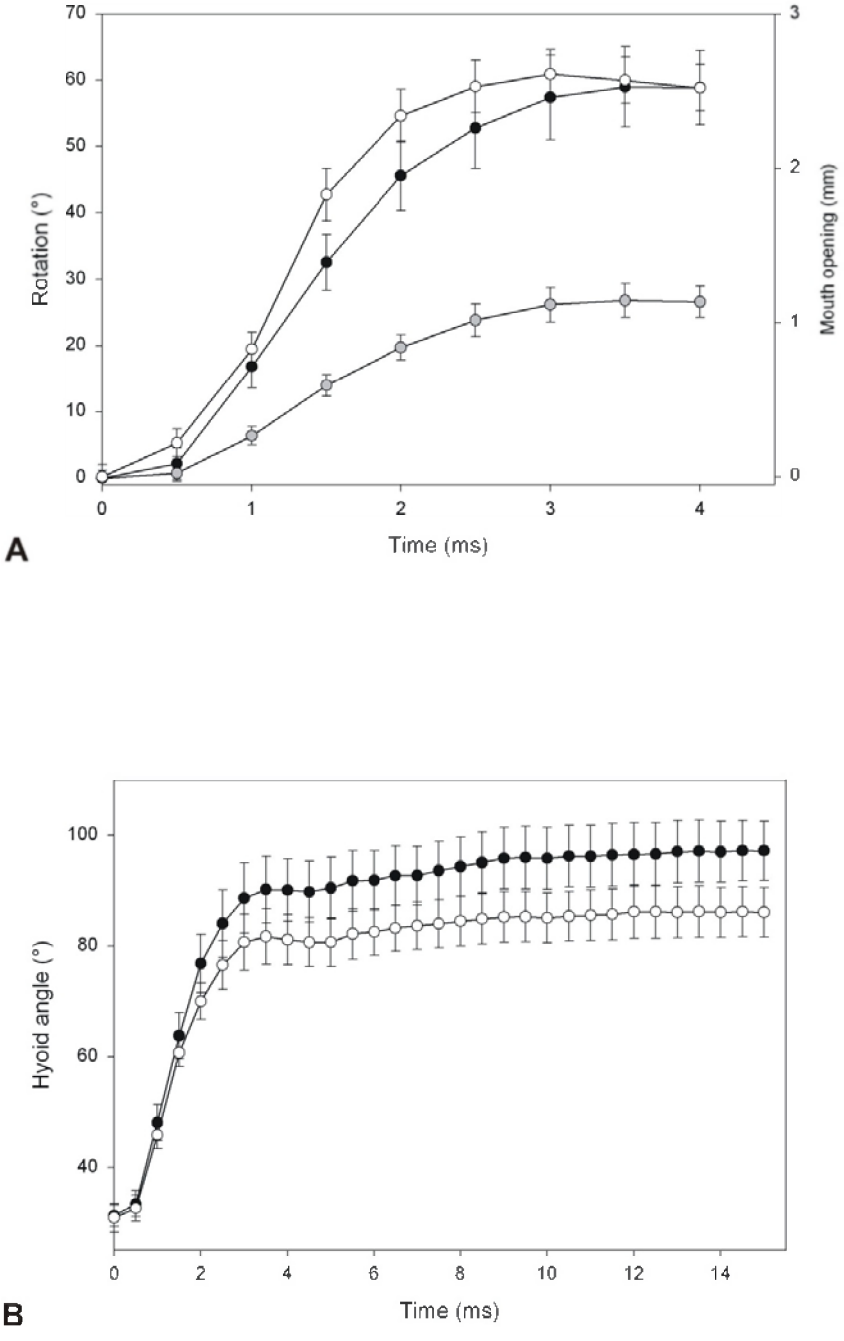

Fig. 5.6 – **A** Time averaged kinematic profiles (N = 14) of the mean hyoid rotation (black dots), the mean neurocranial rotation (gray dots) and the mean mouth opening (white dots) of all 14 sequences. Time = 0 ms was consequently defined for each sequence as the frame before the first visible movement. Prey capture occurs on average 5.5 ms after the onset of hyoid rotation. **B** Comparison of the average measured hyoid angle (black dots) and the average hyoid angle predicted by the four-bar model (white dots; N = 14). In the first 1.5 ms the graphs do not

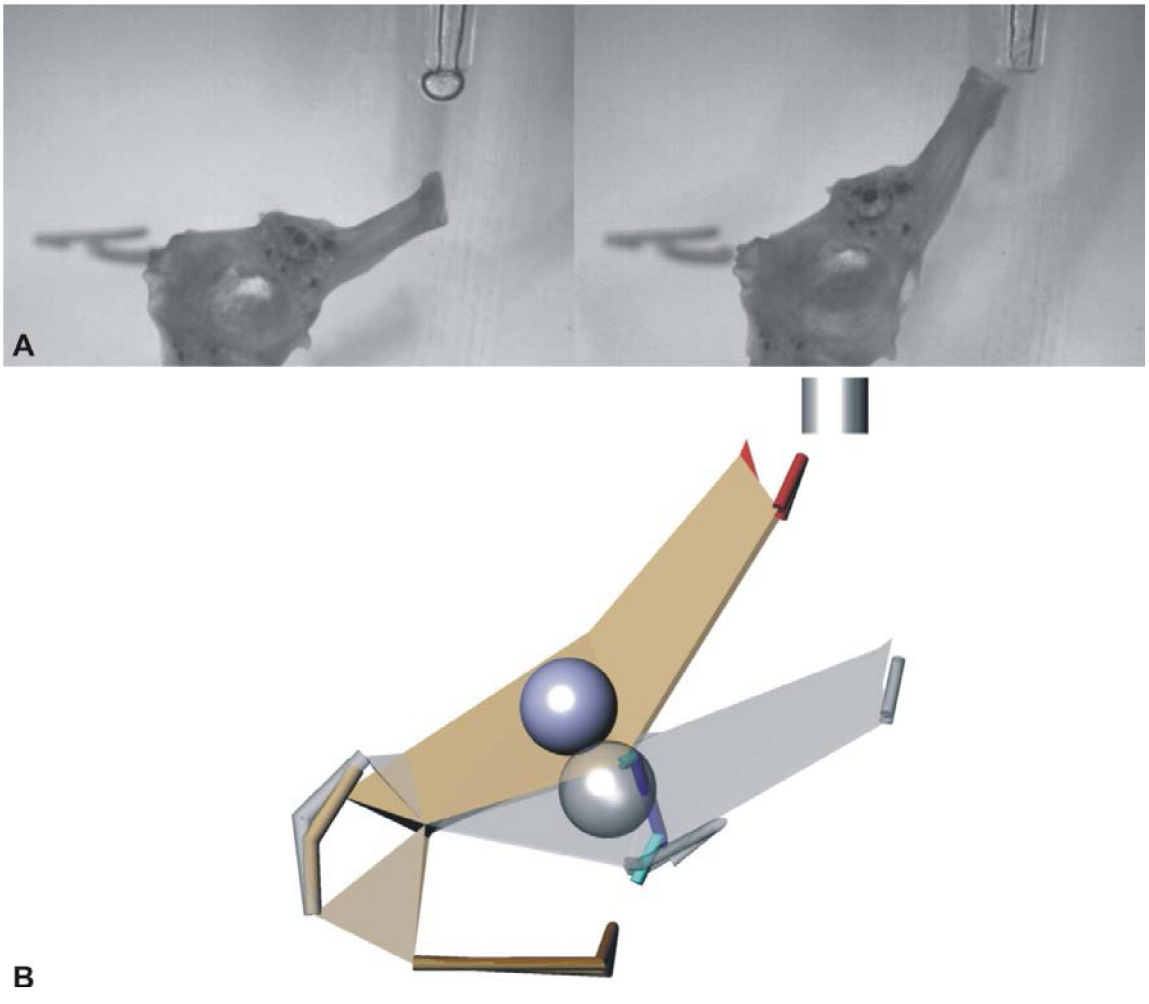

Fig. 5.7 – Model showing extensive neurocranial elevation on *Hippocampus reidi*. **A** video frames used for positioning the components of the model at the onset of neurocranial elevation (left) and at maximal elevation (right). **B** model at the onset of elevation and the position of the skull at maximal elevation, superimposed and aligned based on the position of the pectoral girdle.

Fig. 5.8 – Legend

o-apal	autopalatine bone
o-boc	basioccipital bone
o-den	dentary bone
o-hm	hyomandibular bone
o-iop	interopercular bone
o-leth	lateral ethmoid bone
o-meth	mesethmoid bone
o-mx	maxillary bone
o-para	parasphenoid bone
o-par	parietal bone
o-pop	preopercular bone
o-postt	posttemporal bone
o-prmx	premaxillary bone
o-soc	supraoccipital bone
o-sph	sphenotic bone
o-vm	vomeral bone

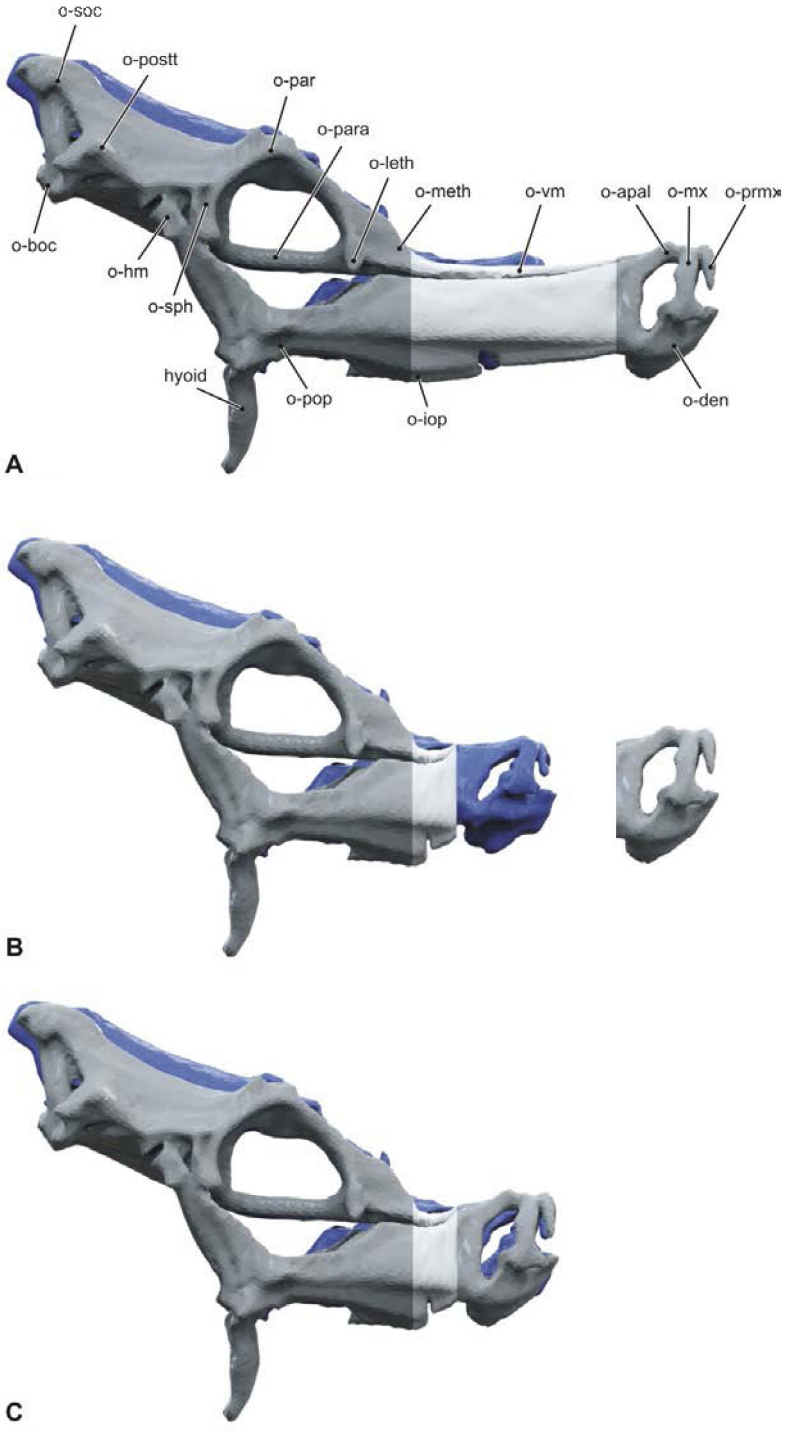

Fig. 5.8 – Construction of the *Hippocampus zosterae* artificial model based on CT-data showing the original *H. zosterae* (blue), the *H. reidi* depressed model being modified (dark grey) and the compressed part of the snout (light grey). Note that the models are scaled based on braincase length. **A** unaltered models of *H. reidi* and *H. zosterae*, with indication of some bones; **B** compression of the snout; **C** attachment of the snout tip and jaws. The compressed snout was then smoothed and simplified until the triangles had the same size as the ones in the rest of the cranium.

Fig. 5.9 – Legend

1	autopalatine-vomeral articulation
2	hyoid
3	lateral wall of the snout
4	mesethmoid-parietal border
5	hyomandibulo-sphenotic joint
6	vomero-mesethmoid transition
7	lower jaw symphysis
8	rostral border of the nostril
9	ventral border of the orbit
10	braincase roof

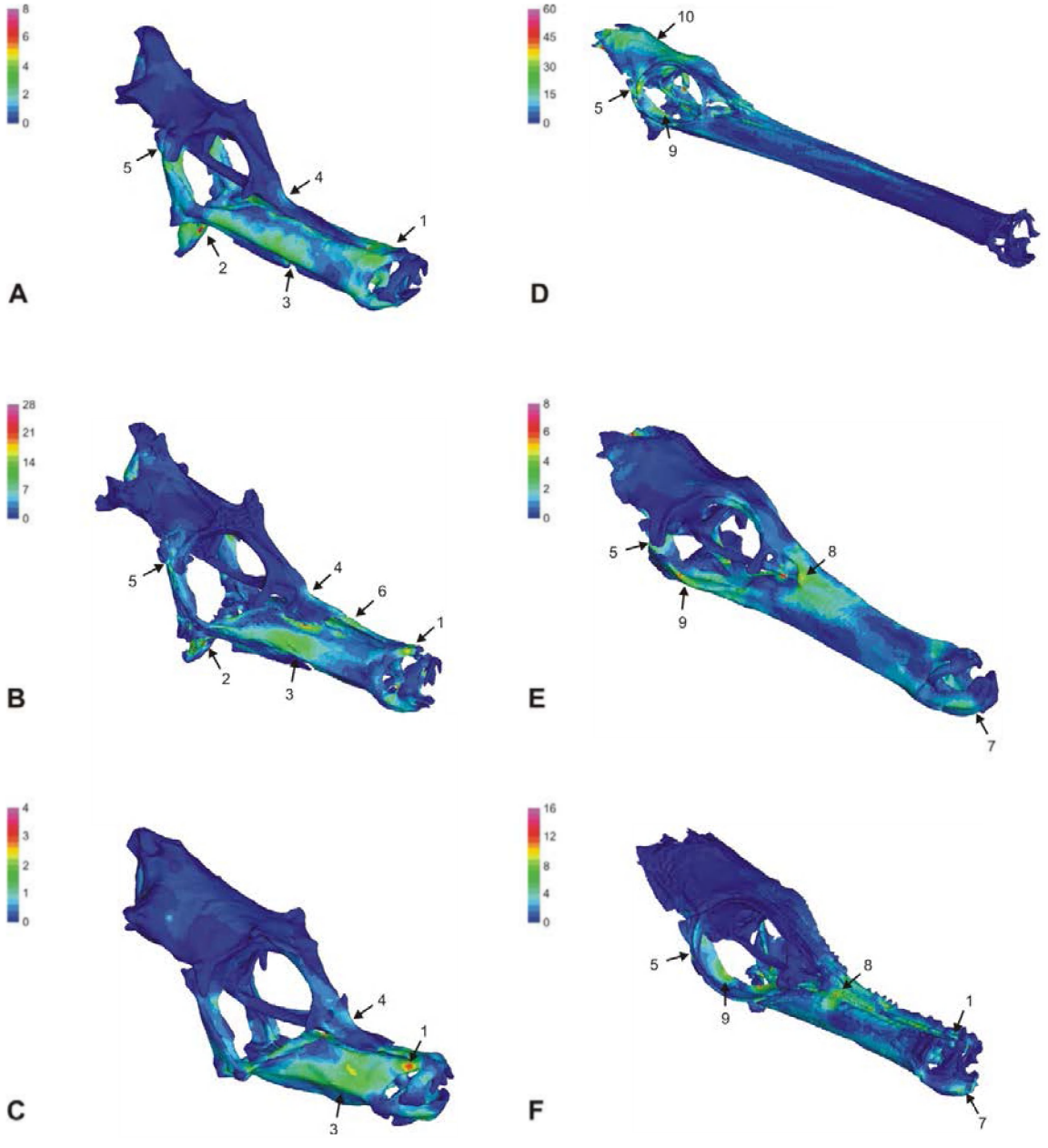

Fig. 5.9 – Von Mises stress distribution pattern in seahorses (A-C) and pipefishes (D-F) with long (A, D), intermediate (B, E) or short (C, F) snout length. **A** *Hippocampus reidi* depressed; **B** *H. abdominalis;* **C** *H. zosterae;* **D** *Doryrhamphus dactyliophorus;* **E** *Syngnathus rostellatus;* **F** *D. melanopleura.* Different color scales are used for each model to facilitate comparison of the stress concentration pattern. Stress values expressed in MPa.

Fig. 5.10 – Legend

1	hyoid symphysis
2	hyomandibulo-sphenotic joint
3	autopalatine-vomeral articulation
4	lower jaw
5	hyoid
6	maxillary bones
7	braincase
8	laterocaudally in the snout
9	laterorostrally in the snout
10	ventrorostral border of the orbit

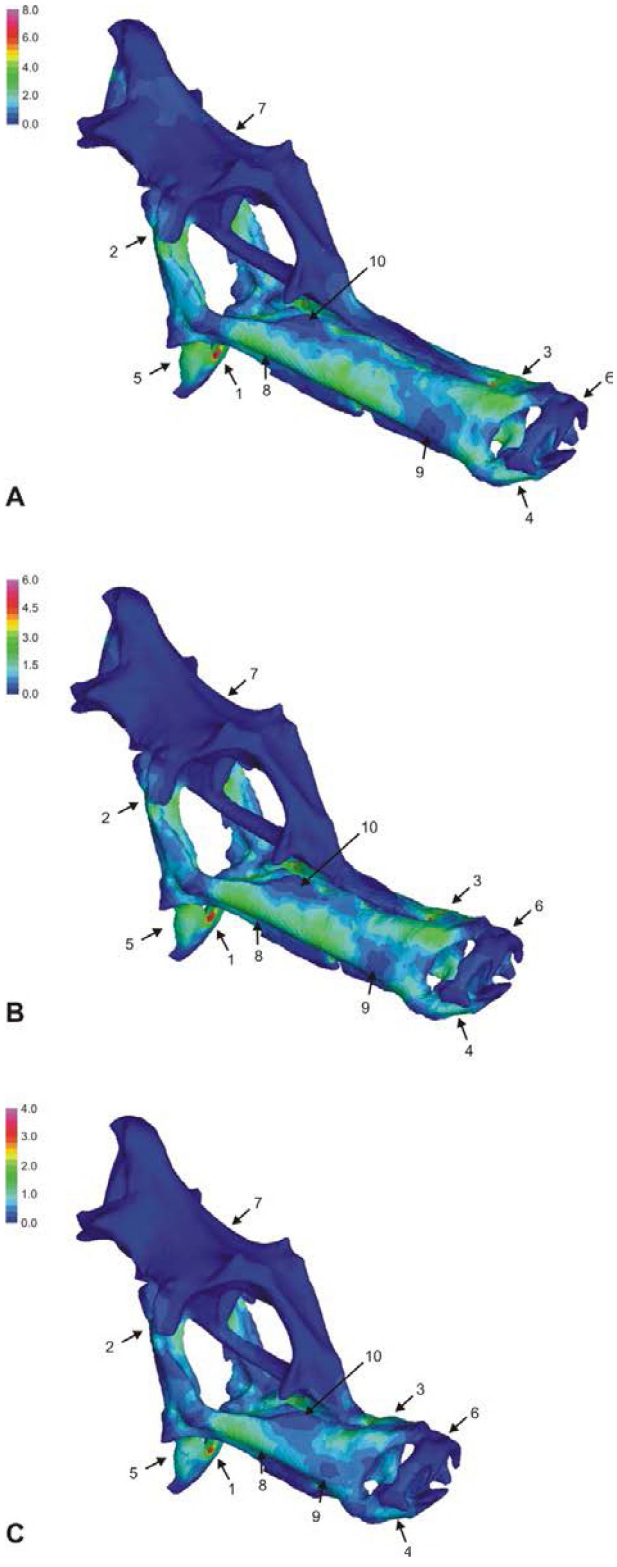

Fig. 5.10 – Von Mises stress distribution pattern in the artificially constructed models based on *Hippocampus reidi* morphology. **A** *H. reidi* depressed model (as in Fig. 5.9A); **B** *H. abdominalis* artificial model; **C** *H. zosterae* artificial model. Stress values expressed in MPa, color scales are different for all models.

Fig. 5.11 – Legend

1 mesethmoid-parietal border
2 laterorostrally in the snout
3 hyoid-suspensorium articulation

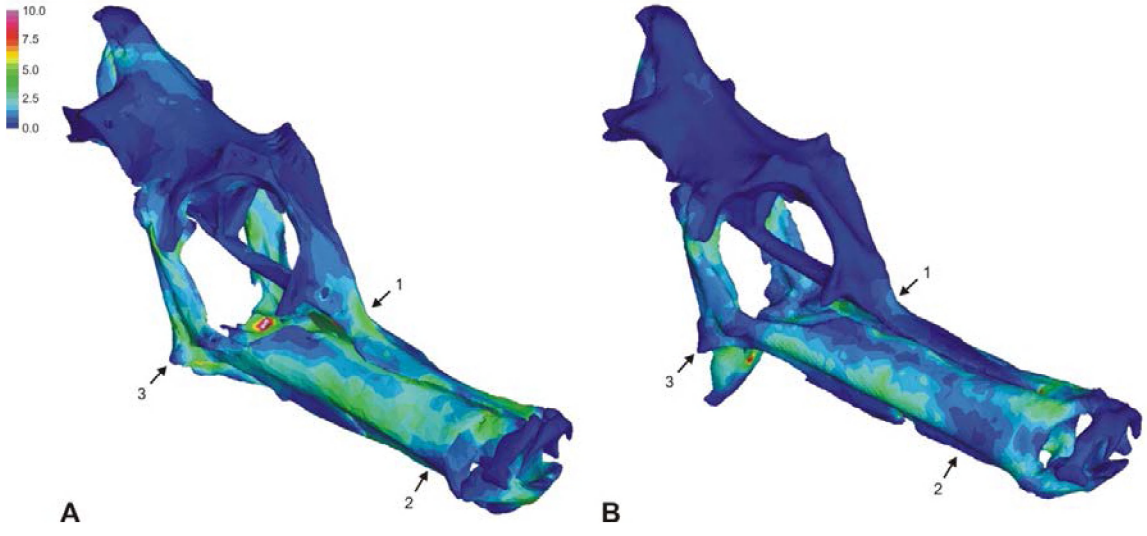

Fig. 5.11 – Von Mises stress distribution pattern in two models of *Hippocampus reidi* showing the effect of the position of the hyoid. **A** *H. reidi* protracted model; **B** *H. reidi* depressed model. Stress values expressed in MPa.